FORGE Benchmark Modelling: Cell, Module and Repository Scale Gas Migration in a Hypothetical Repository

NWMO TR-2014-06 May 2014

Nicola Calder
Geofirma Engineering

nwmo
NUCLEAR WASTE MANAGEMENT ORGANIZATION
SOCIÉTÉ DE GESTION DES DÉCHETS NUCLÉAIRES

Nuclear Waste Management Organization
22 St. Clair Avenue East, 6th Floor
Toronto, Ontario
M4T 2S3
Canada

Tel: 416-934-9814
Web: www.nwmo.ca

FORGE Benchmark Modelling: Cell, Module and Repository Scale Gas Migration in a Hypothetical Repository

NWMO TR-2014-06

May 2014

Nicola Calder
Geofirma Engineering

Document History

Title:	FORGE Benchmark Modelling: Cell, Module and Repository Scale Gas Migration in a Hypothetical Repository		
Report Number:	NWMO TR-2014-06		
Revision:	R000	Date:	May 2014
Geofirma Engineering			
Authored by:	Nicola Calder		
Verified by:	Robert Walsh		
Approved by:	John Avis		
Nuclear Waste Management Organization			
Reviewed by:	Erik Kremer		
Reviewed by:	Helen Leung		
Accepted by:	Paul Gierszewski		

ABSTRACT

Title: **FORGE Benchmark Modelling: Cell, Module and Repository Scale Gas Migration in a Hypothetical Repository**
Report No.: **NWMO TR-2014-06**
Author(s): Nicola Calder
Company: Geofirma Engineering
Date: May 2014

Abstract
The FORGE benchmark modelling examined the transport of gas in a theoretical repository within a simple geology, with the objective of improving the understanding of gas migration modelling at the repository-scale to support performance assessments. Nine different groups with different codes and modelling approaches, including NWMO/Geofirma, contributed to at least one scale of the benchmark modelling exercise. T2GGM, a modified version of TOUGH2 v2.0 with optional gas generation model, was selected as the two-phase flow modelling code.

Three-scales were defined: cell, module and repository scales. A 2D radial model was developed for the cell-scale, and 3D models were developed for the module and repository scales. The greatest challenge in the module and repository scales was the inclusion of small features of the benchmark within a grid of tractable size. To obtain a working model, the interfaces were upscaled with adjacent elements, cells were converted from cylindrical to rectangular shapes of equivalent cross-sectional area, and grid discretization was nested and unstructured.

Within the cell-scale, the flow of gas was mainly advective along the cell EDZ and interface towards the access tunnel, strongly driven by the boundary condition specified at the access tunnel. Despite inclusion of a more permeable interface between the EDZ and sealing materials, the EDZ transported the bulk of gas along the cell due to its greater cross-sectional area. The module-scale also found that free gas migrates along the cells toward the access drift, but only initially. Once pressures in the module begin to equilibrate with the host rock, water and gas flow directions were more complex throughout the module. Module and repository scale results suggest that by 2000 years, bentonite seals are mostly water saturated, limiting the flow of gas through the main drift and out of the repository, even with interfaces surrounding these seals.

As defined in the benchmark, gas generation ceases at 10 000 years. At this time, a maximum gas pressure of 5.7 MPa at the cell scale, 6.7 MPa at the module scale and 7.1 MPa at the repository scale was observed. Modelling was conducted from cell-scale to repository-scale, and consequently boundary conditions defined for the cell and module scale were estimated rather than based on results of the repository-scale. Consequently, results between the three scale are not directly comparable. As well, boundary conditions for the module-scale were found to be incongruous with the behaviour of the module, resulting in some unintended boundary condition effects.

Models were generally found to be insensitive to the presence of an interface, as long as the EDZ is present (i.e., EDZ does not heal). At the cell scale, this lack of sensitivity may be due in part to the low permeability of the plug interface. At the repository scale, removal of the interface resulted in a similar representation of pressures and saturations, with an underestimation of gas and dissolved gas flows (e.g., peak gas flows in the main drift are approximately 4.5 times smaller). However, this lack of sensitivity to an interface at the

repository scale may be limited to this configuration and geology, which resulted in no gas leaving the repository through the engineered barrier system.

Dissolved hydrogen diffusion was identified as another important model parameter. At the cell scale, increasing the diffusion coefficient by a factor of ten resulted in a change in the main gas transport pathway from advective transport towards the access drift to dissolution and diffusion of gas into the host rock. At the repository scale, dissolution and diffusion of gas into the host rock was the only pathway of gas up to surface.

At all three scales, model results compared well to those produced by other modelling groups. The trend in results was typically similar, although there was considerable range in the magnitude of results between groups, particularly for gas and water flows. This range of results is due to the variety of modelling approaches and required model simplifications adopted by the modelling groups, either code-driven or for model tractability purposes.

TABLE OF CONTENTS

LIST OF TABLES

Page

LIST OF FIGURES

Page

1. INTRODUCTION

The FORGE (Fate of Repository Gases) benchmark modelling studies aimed to model gas migration in a repository, with the objective of improving the understanding of gas migration at the repository scale in support of performance assessments. Using a hypothetical repository, modelling studies were divided into three phases:

(1) cell-scale: a single cell within a repository;
(2) module-scale: fifty cells and a single access drift; and
(3) repository-scale: five modules connected to a main drift and a shaft to the ground surface.

Figure 1 illustrates the three scales of the benchmark modelling.

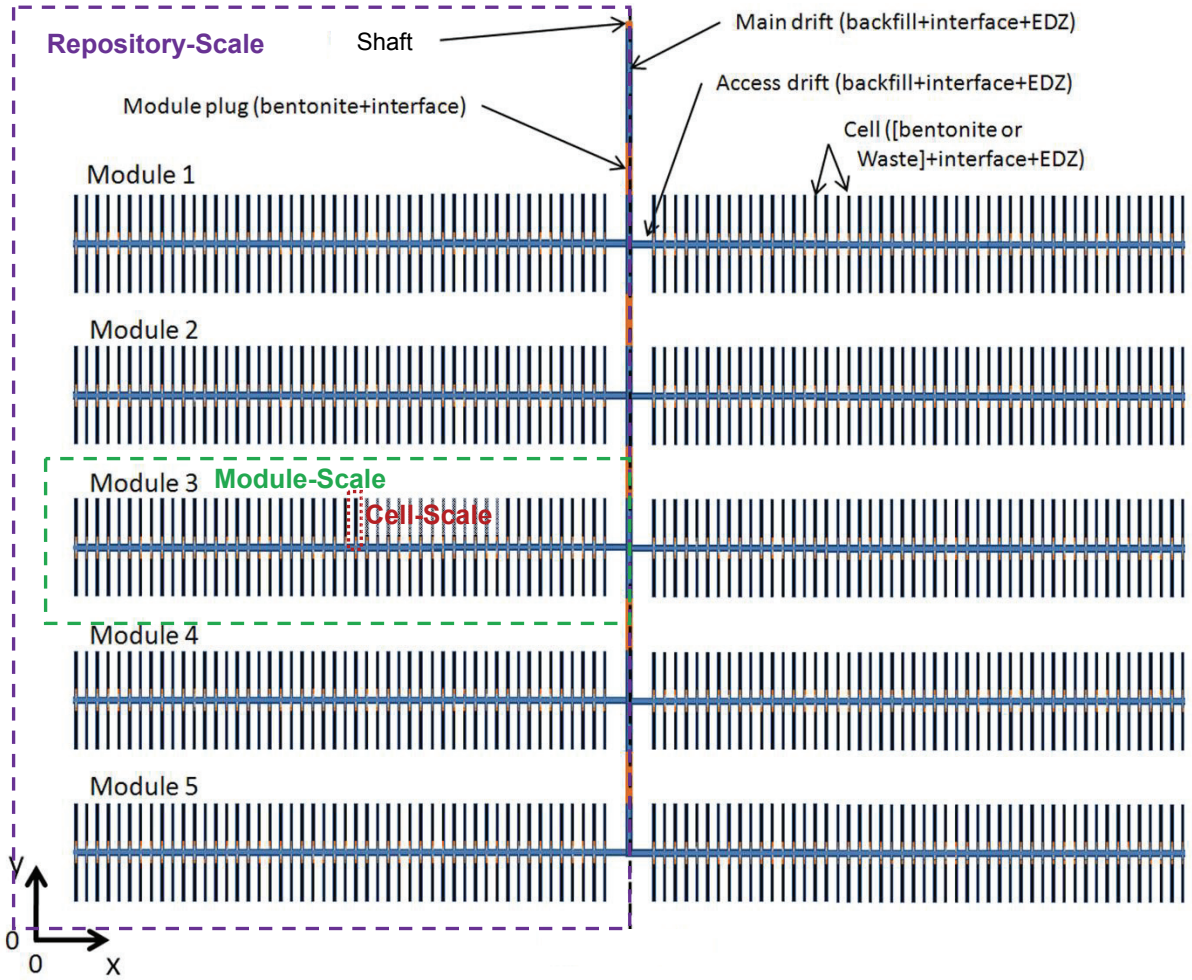

Figure 1: Representation of Cell, Module and Repository Scales

FORGE benchmark modelling (WP1.2) was conducted between 2009 and 2013, with nine groups undertaking these benchmark studies using different codes, detailed in Table 1. The benchmark definition assumes that two-phase flow processes, including both dissolution and diffusion, are sufficient to represent gas flow at the repository scale. Not all groups completed modelling at all three scales.

Table 1: Groups Undertaking FORGE WP1.2 Benchmark Studies

Group	Country	Code*
Geofirma/NWMO	Canada	T2GGM (TOUGH2 derived)
NDA/Quintessa	UK	QPAC
SCK-CEN	Belgium	CODE-BRIGHT 3.0
CEA	France	MPCube**
Andra	France	TOUGH2MP-EOS5
IRSN	France	Diphpom**
CNRS	France	2φICFlow**
LEI	Lithuania	TOUGH2-EOS5 (PetraSim)
ENSI/IFSN	Switzerland	TOUGH2MP-EOS5

*based on Wendling et al. (2014a)
**codes developed internally

The benchmark modelling by Geofirma uses T2GGM v3.1, a modified version of TOUGH2 v2.0 with optional gas generation model GGM (Suckling et al. 2012) and Geofirma modifications (e.g., modified van Genuchten curves and alternate gases to air). The GGM model is turned off for all benchmark modelling. Standard T2GGM was used for cell-scale and module-scale modelling, while T2GGM-MP was used for the repository-scale. Modifications were required to meet benchmark requirements, including addition of time-variable pressure and saturation boundary conditions, and addition of the Mualem gas relative permeability model.

This technical report documents all three scales of benchmark modelling conducted by Geofirma Engineering on behalf of Nuclear Waste Management Organization (NWMO). The report is organized as follows:

- The **Benchmark Description** common to all three scales is presented for context. The detailed benchmarks are provided in Appendixes A, B and C, for the cell, module and repository scales.
- The **Modelling Code** used by Geofirma for the benchmark modelling is described in detail, including modifications to the code.
- The **Modelling Approach** and **Modelling Results** are presented for the cell scale, followed by the module and repository scale. Modelling results at each scale are compared to results available from other groups.
- The **Discussion** section considers modelling issues encountered at all three scales.
- The **Conclusions** section summarizes the main conclusions from all three scales of benchmark modelling.

2. BENCHMARK DESCRIPTION

The benchmark repository is located within an argillite host rock with a permeability of 10^{-20} m^2 and a porosity of 0.15. 75 m above the repository is an aquifer with a permeability of 10^{-15} m^2. Fixed pressure (fully water saturated) boundary conditions exist 75 m below the repository (6 MPa), and at the Y = 0 and Y = 1437 m edges of the aquifer (4 MPa at Y = 0 and 4.5 MPa at Y = 1437 m). See Figure 2. At the repository horizon, hydrostatic water pressure is approximately 5 MPa.

Modelling was developed and conducted from the smallest scale (cell) to the largest scale (repository). Consequently, boundary conditions specified at the cell and module scales were estimated rather than extracted from the repository scale, and each scale is therefore not directly comparable.

Within the repository, each cell is comprised of cylindrical water and gas impermeable waste surrounded by a thin 1 cm interface and 0.5 m of Excavation Damage Zone (EDZ) (Figure 3). A bentonite seal, also surrounded by a thin interface and EDZ (both with a permeability of 5×10^{-18} m^2), separates the cell from the access drift. Rectangular access and main drifts are backfilled, and include interfaces and EDZ surrounding these drifts. 50 m bentonite seals (with interfaces but no EDZ) located in the main drift separate each module. A bentonite seal is also located in the shaft below the aquifer.

The benchmark specified H_2 gas generation at the surface of the waste containers, with the waste containers specified as a no-flow feature. Hydrogen gas generation occurs over the first 10 000 years, at a constant rate of 100 mol of H_2/yr/cell.

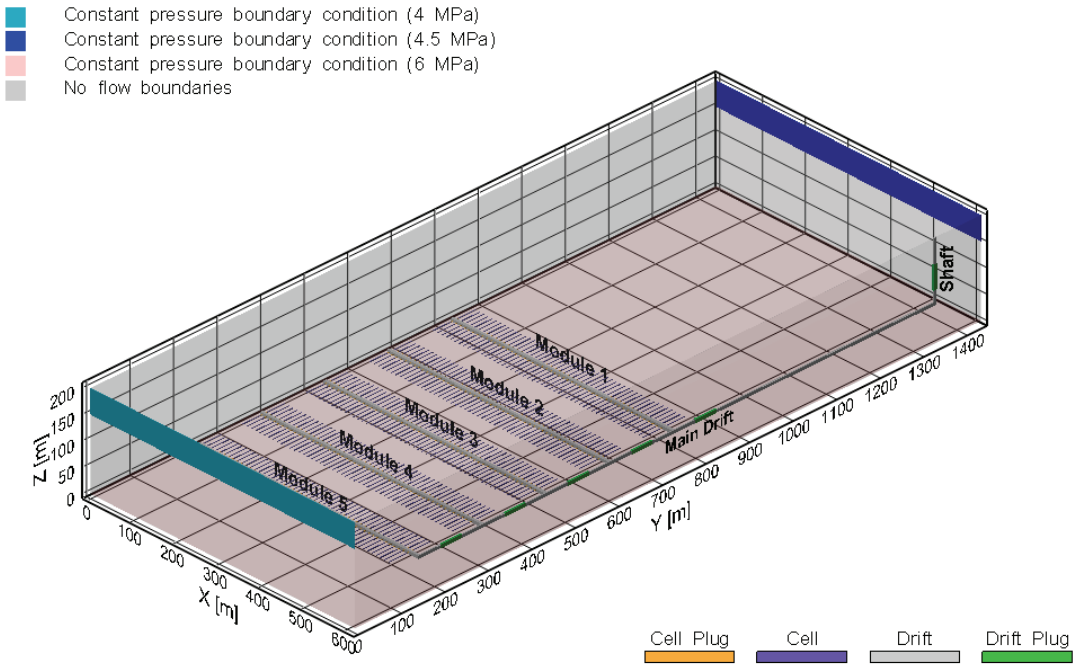

Figure 2: Schematic of the Repository-Scale Domain, With Depiction of Boundary Conditions

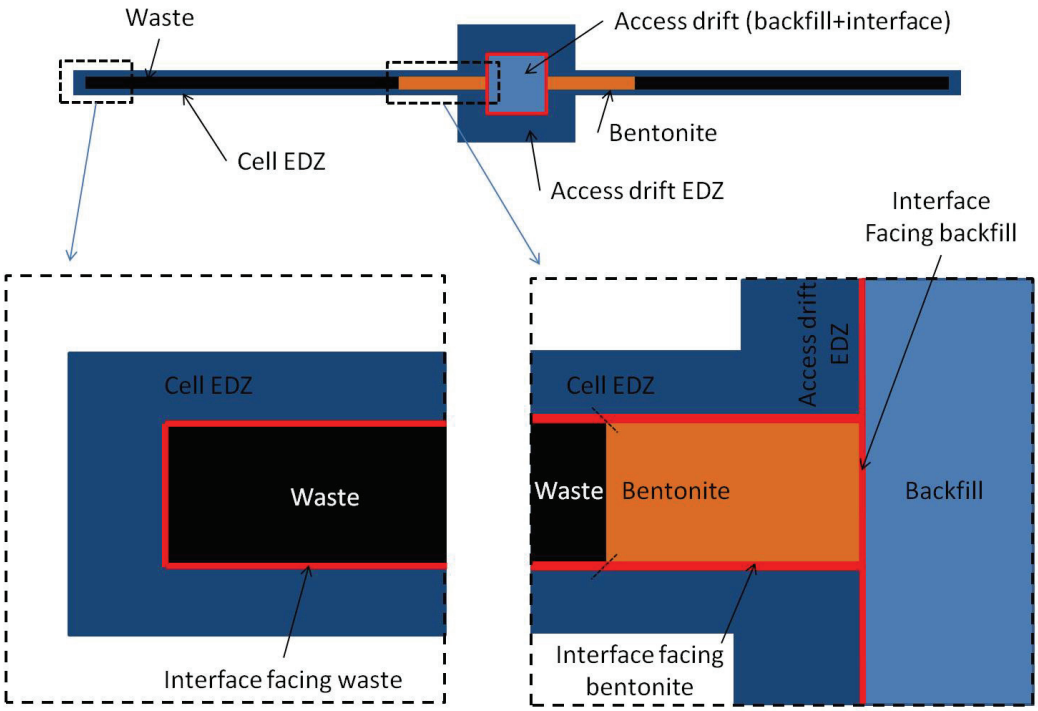

Figure 3: Location of Waste, Interfaces and EDZ Within a Module

3. MODELLING CODE

T2GGM version 3.1 (Suckling et al. 2012), a modified version of TOUGH2 v2.0 with an optional gas generation model, was selected as the two-phase flow modelling code. The gas generation model (GGM) capabilities were turned off. The multi-processor (MP) version of T2GGM was only used at the repository scale. TOUGH2 is a general-purpose numerical simulation program for multi-phase fluid and heat flow in porous and fractured media developed by Lawrence Berkeley National Laboratory (Pruess et al. 1999). The EOS3 equation of state module used in T2GGM simulates the transport of a single separate gas phase in water (note that T2GGM allows for specification of alternate gases to air, the EOS3 default). Thermophysical properties of water are represented by steam-table equations, while the air is treated as ideal gas. Dissolution of air in water is modeled with Henry's law. The phase relationship between gas and liquid is based on a local thermodynamic equilibrium assumption. EOS3 also models the transport of dissolved gas in water by diffusion and advection. Dispersive processes are not modelled.

Several minor modifications were made to the T2GGM code to facilitate the benchmark modelling studies:

- Time-dependent Dirichlet boundary conditions were added based on the implementation within TOUGH2-MP. TOUGH2-MP only allows for time-dependent pressure changes (assuming saturation and temperature remain constant), while this new implementation allows both time-dependent pressure and saturation as required by the benchmark specification.
- A new time-stepping scheme was implemented, based on the scheme used in TOUGH2-MP with minor modifications. This time stepping scheme allows for smaller increases in time step (when the simulation converges within a specified number of iterations) and smaller decreases in time step (when the simulation does not reach convergence within the maximum number of iterations). The scheme also minimizes the occurrence of oscillations between time step increases and decreases (e.g., when a time step decrease results in a time step solving within the specified number of iterations, this causes a subsequent time step increase that cannot be solved, requiring the time step to be decreased etc.) by preventing time step increases for five time steps following a reduction in time step.
- For repository-scale benchmark modelling studies only, the option to use the Mualem relative gas permeability equation as defined in the benchmark was added to T2GGM. Previous cell-scale and module-scale modelling used the Luckner model, which is very similar to the Mualem model. The differences between the Luckner and Mualem models will be explored further in Section 4.1.4.

mView, developed by Geofirma Engineering, was used for pre- and post-processing.

4. CELL-SCALE MODEL

4.1 MODELLING APPROACH

4.1.1 Grid

The benchmark defines the model domain in the negative X and negative Y quadrant, but the models described here are defined in the positive X and positive Y quadrant. X, Y and Z axes are assumed as usually defined, with the Z axis representing the vertical axis. The central axis of the cell is defined along the X axis, with the origin in the middle of the access drift.

A 2D grid was developed, with both radial and rectangular components within the 2D grid. Block volumes and connection areas were calculated by rotating the 2D grid around the X axis, effectively including the full 3D volume of the model domain. Figure 4 shows the overall grid discretization, and Figure 5 shows a detail of the grid discretization near the bentonite plug. The grid has 3391 nodes, with grid refinement around the interface area. The irregular nature of the grid allows for grid refinement only where required.

Originally, a simple 2D radial grid with rectangular discretization was developed. With rectangular discretization, the discretization in the X and Y directions is fixed, resulting in grid refinement in areas where it is not required. Simulations with this grid encountered significant stability issues unless diffusion was removed. The final model grid was developed to alleviate gridding issues resulting from transitions from small to large block sizes, which is exacerbated in a rectangular grid by the fixed X and Y discretizations. It should also be noted that the irregular grid of the final model grid does not strictly adhere to the TOUGH2 integral finite difference requirements; some nodal connections are not perpendicular to the connection area, resulting in shorter connection distances for these connections. The impact of these inaccuracies is expected to be small, and this is confirmed by the comparison of results between the two grids for the no diffusion case, see Figure 6. In this figure, the gas flows that exceed the generation rate are due to gas flowing into the model from the access drift boundary before year 10. Integration of gas flows confirms that the quantities of gas are consistent.

Material properties are defined in Table A-2 of Appendix A.

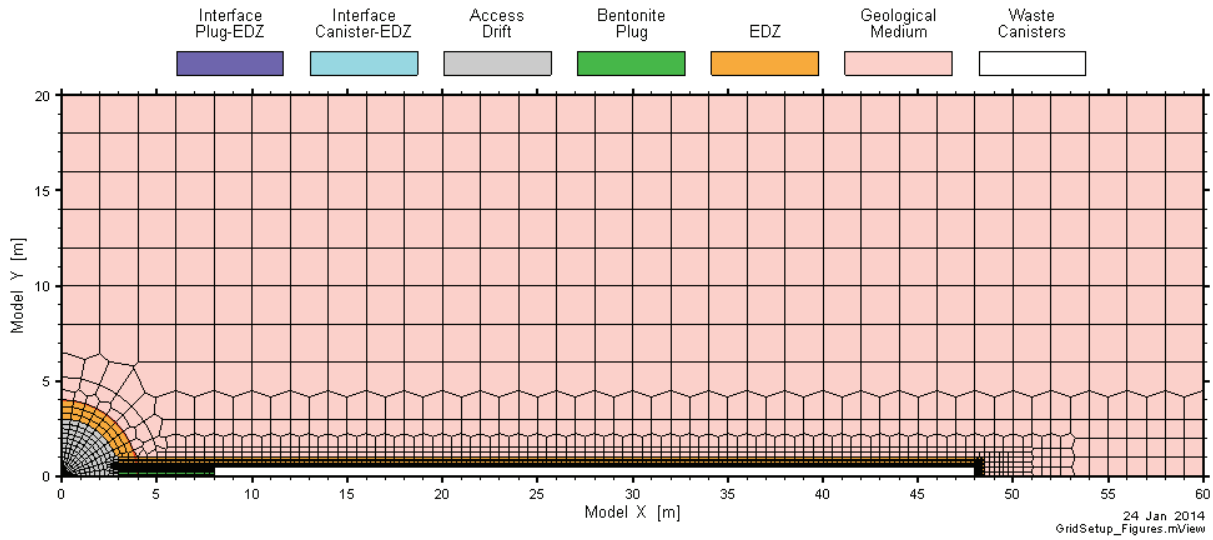

Figure 4: Grid Discretization

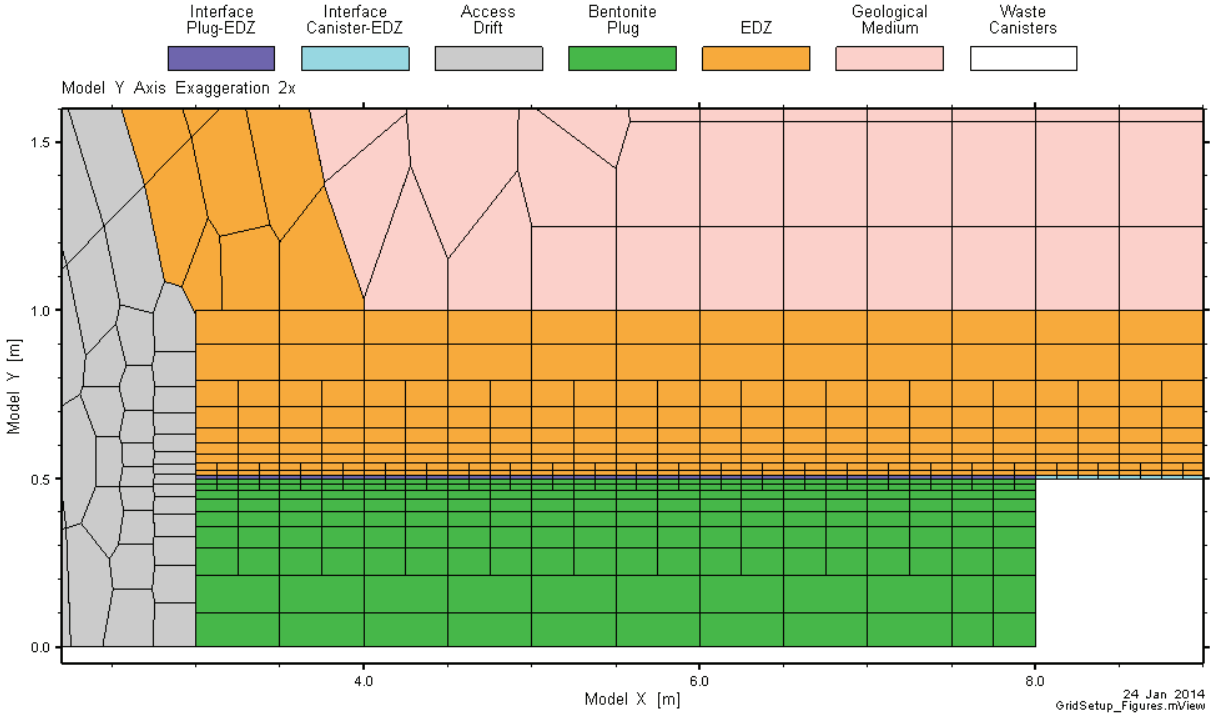

Figure 5: Detail of Grid Discretization Around the Bentonite Plug

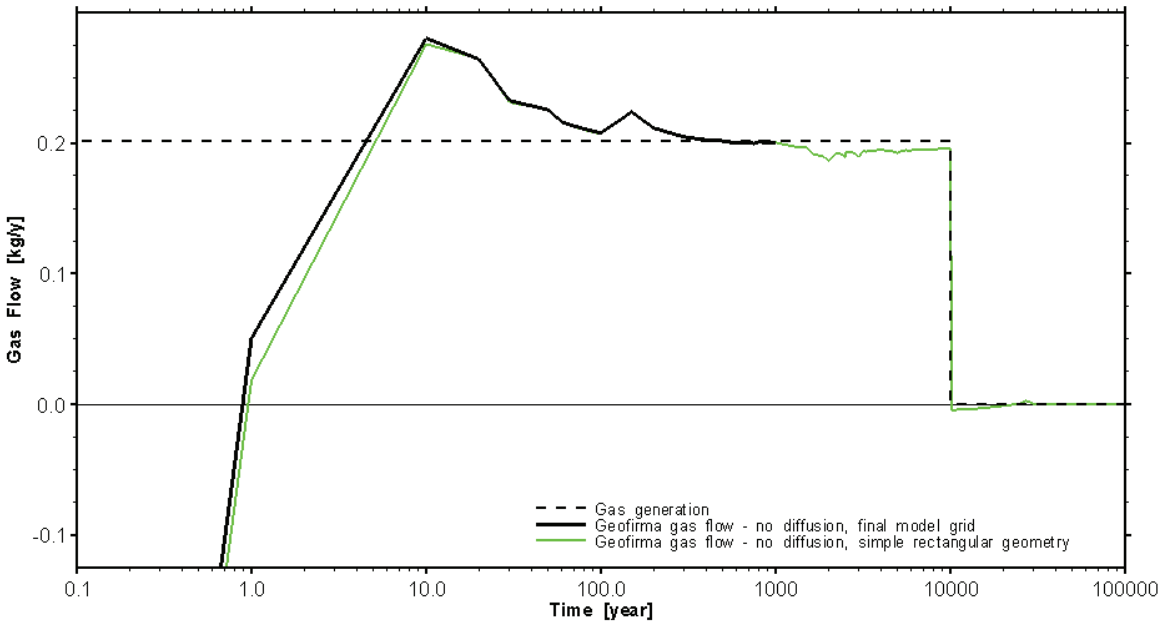

Figure 6: Comparison of Final Model Grid and Simple Rectangular Model Grid Gas Flows Through the Access Drift for the Base Case With No Diffusion

4.1.2 Boundary Conditions and Sources

As the waste containers were not included in the model, gas generation was specified at the nodes immediately adjacent to the waste container, located within the interface between the canister and EDZ and within the bentonite plug nodes adjacent to the waste container. The generation term was proportioned between nodes according to connection area between the generation node and the waste container.

The access drift boundary condition was provided as a water pressure and water saturation curve as a function of time (see Appendix A). As the TOUGH2 inputs require a gas pressure curve, gas pressures were calculated using the van Genuchten parameters for the access drift backfill (see Table A-2 in Appendix A). The resulting gas pressure curve had a few incongruous small bumps which were smoothed out to improve numeric stability.

A constant water pressure boundary of 5 MPa was specified at the outer radius of the domain. A concentration of dissolved gas was also specified at this boundary, equivalent to 0.1 MPa (1 atm) gas pressure.

4.1.3 Initial Conditions

Initial conditions in the host rock and EDZ are 5 MPa water pressure and full water saturation. As in the outer radial boundary condition, dissolved gas concentrations equivalent to 0.1 MPa gas pressure were also specified. In repository features, initial pressure was atmospheric and water saturation was 5% in the interfaces and 70% in the bentonite and backfill.

4.1.4 Deviations from the Benchmark Specification

A limitation of the 2D model geometry is the inaccurate specification of anisotropic permeability for the plug-EDZ interface, EDZ and geologic medium (host rock). In the 2D model grid, all connections are horizontal (in the XY plane), and therefore anisotropic media are represented solely by their horizontal permeability, which is half an order of magnitude greater than the vertical permeability. Results are therefore conservative, resulting in faster radial transport of gas and water away from the cell than would occur in an anisotropic model representation. However, this does not impact transport along the cell in the x-direction, which model results presented below suggest is the primary direction of transport. Due to the small difference in horizontal and vertical permeabilities, the effect of neglecting anisotropy is expected to be small. Many of the other modelling groups also used 2D models, and therefore were unable to represent the anisotropy of the system.

Another deviation from the benchmark is the relative gas permeability model. The benchmark defines the relative gas permeability (k_{rg}) using the Mualem model:

$$\boldsymbol{k_{rg} = (1 - S)^{1/2}(1 - S^{1/m})^{2m}} \qquad \textbf{Equation 1}$$

where:
S is the effective saturation, defined as $S = (S_l - S_{lr})/(1-S_{lr}-S_{gr})$;
S_l is the liquid saturation;
S_{lr} is the residual liquid saturation;
S_{gr} is the residual gas saturation; and
m is a van Genuchten fitting parameter.

However, the modified van Genuchten model option in T2GGM, used in the models presented here, is the Luckner model, identical to the Mualem model except the 1/2 exponent is replaced by a 1/3 exponent:

$$\boldsymbol{k_{rg} = (1 - S)^{1/3}(1 - S^{1/m})^{2m}} \qquad \textbf{Equation 2}$$

A comparison between relative permeability curves (Mualem, Luckner and cubic power models) is shown in Figure 7. The cubic power model is used in a sensitivity case, and the equation provided in Equation 3 (Section 4.2.2.2).

Stability issues were encountered for the final model grid. Stability was improved by adding a residual gas saturation in the EDZ of 10^{-6}, reducing the occurrence of oscillations due to phase generation and disappearance.

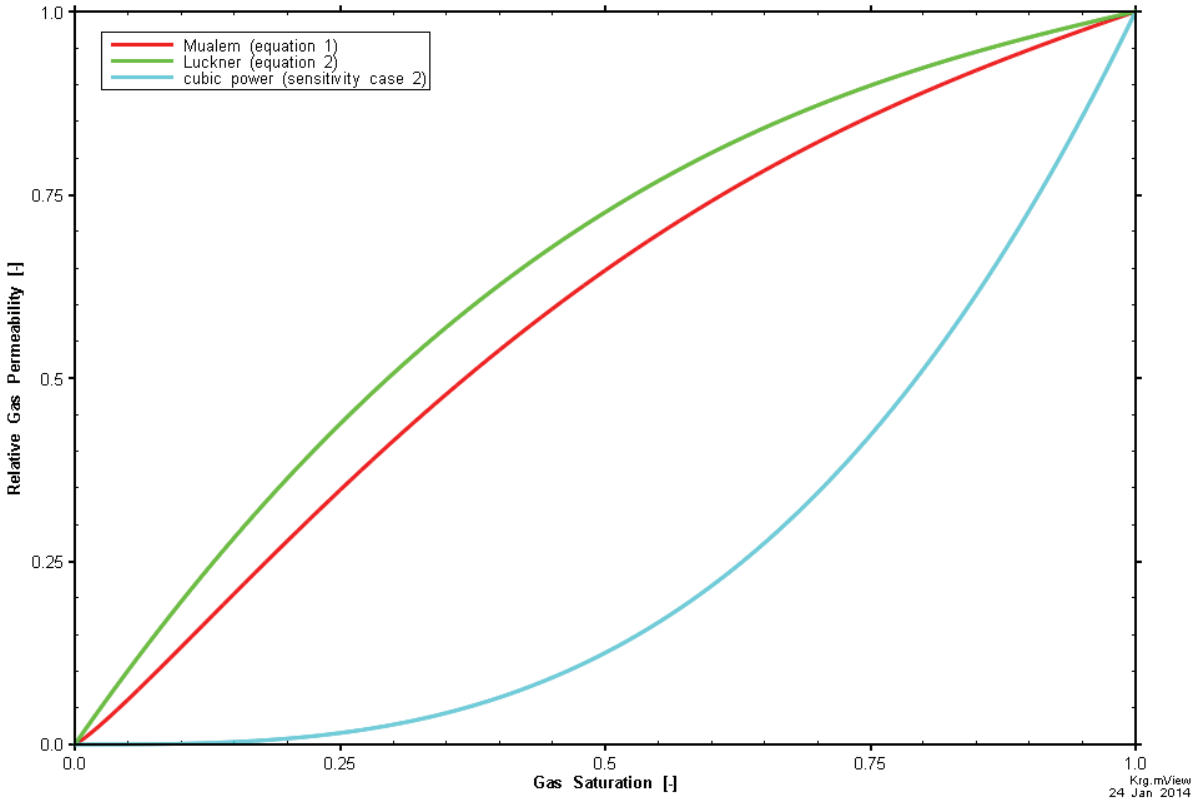

Figure 7: Relative Gas Permeability Curves for the EDZ/Rock (m=1.5) Represented by the Benchmark and T2GGM

4.2 MODELLING RESULTS

4.2.1 Base Case Results

Gas and water pressures are shown for various times in Figure 8 through Figure 13. Gas saturations and dissolved gas mass fractions are shown in Figure 14 through Figure 19. Each plot shows empty space within the canisters, and a ring defining the outer limits of the access drift. Note that for gas pressures, empty space is also shown in areas where gas is not present. Note that some of the contours appear jagged or wavy; this is entirely due to the grid discretization.

By 1 year, gas has migrated out of the interface and into the EDZ surrounding the cell (Figure 14). Gas generated in the cell primarily migrates through the interface and EDZ towards the access drift, and is removed from the access drift boundary condition. Gas also migrates slowly into the host rock, with gas saturations reaching their peak at 10 000 years (the time at which gas injection stopped). See Figure 17. At this time, the interface was almost completely saturated with gas (gas saturation > 0.999, not visible in Figure 17 due to the very small thickness of the interface), the maximum gas saturation in the EDZ was 0.05 and free phase gas is present at very small saturations (less than 0.002) approximately 0.5 to 1 m into the host rock.

The low initial pressures within the cell resulted in reduced pressures in the surrounding host rock. These low pressures are almost dissipated by 10 000 years, at which point gas pressures begin to exceed initial undisturbed water pressures of 5 MPa (Figure 11). The maximum gas pressure reached was 5.7 MPa in the bentonite plug adjacent to the canisters. This maximum occurred at 10 000 years, the time at which gas injection stopped. Water pressures returned to initial undisturbed conditions (5 MPa) by approximately 20 000 years (Figure 12).

Over the course of the simulation, dissolved gas migrates away from the cell into the host rock and towards the access drift. This migration of dissolved gas is diffusion dominated, as water flows towards the cell from the host rock, rather than away from the cell. In the first 100 years, initial dissolved gas is removed from the access drift by the access drift boundary condition and dissolved gas near the cell has not migrated far enough to reach the access drift (Figure 15). By 1000 years, the access drift is full of dissolved gas generated from the cell (Figure 16). At the end of the simulation, dissolved gas continues to migrate towards the access drift, with the greatest concentration of dissolved gas near the access drift boundary condition (Figure 19).

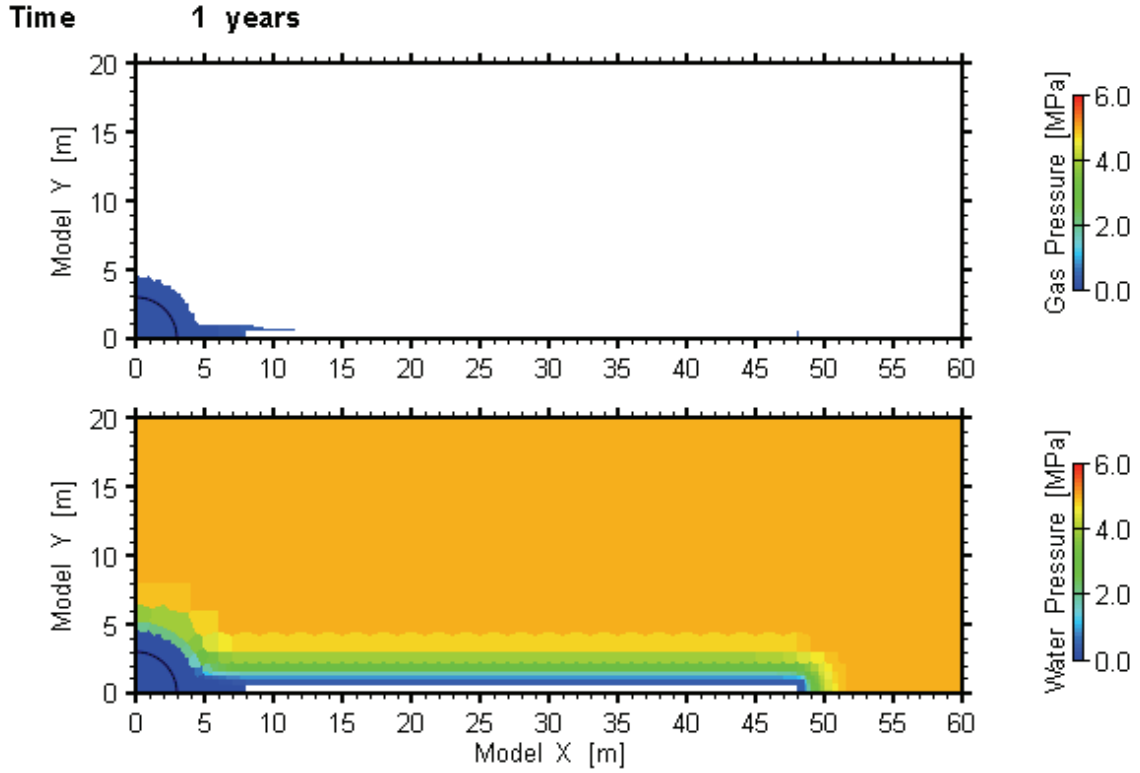

Figure 8: Gas and Water Pressures for the Base Case at 1 Year

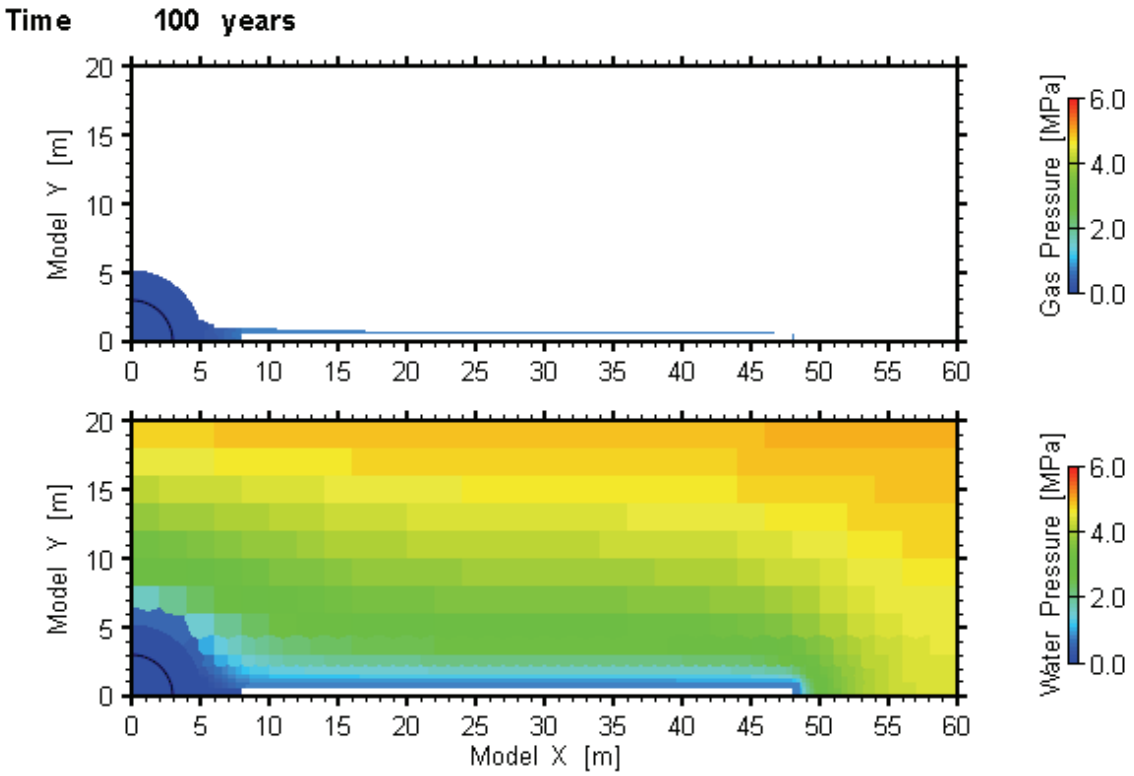

Figure 9: Gas and Water Pressures for the Base Case at 100 Years

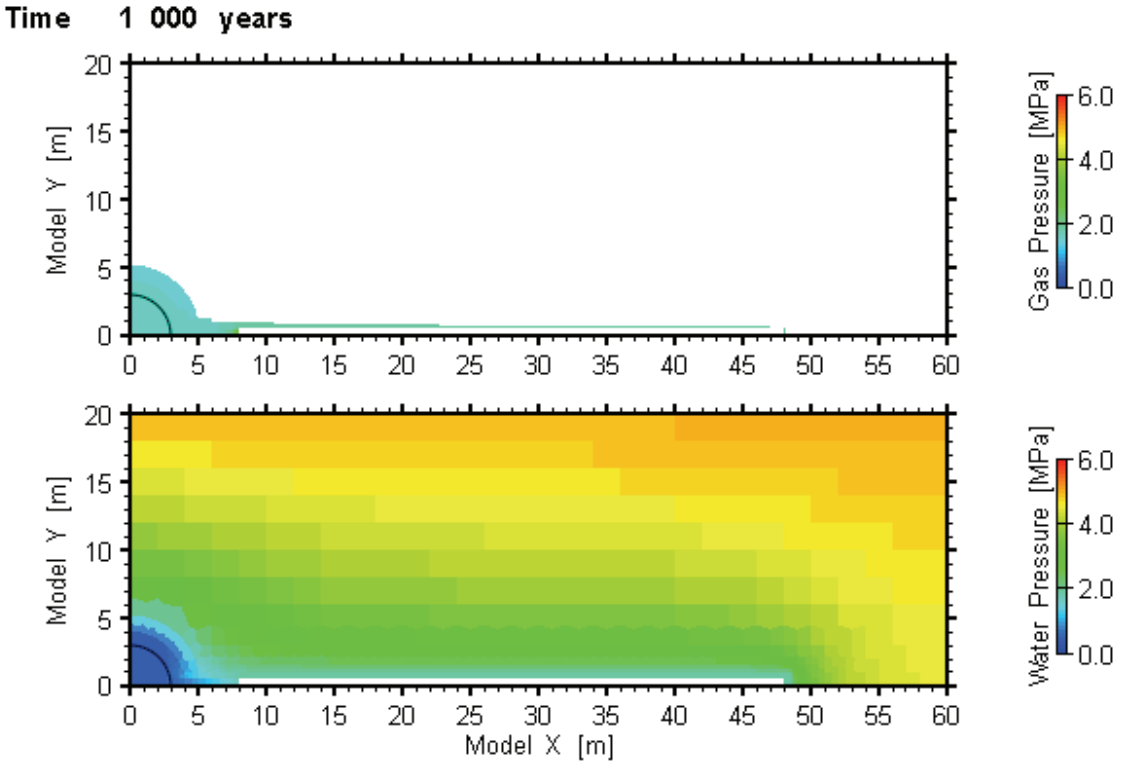

Figure 10: Gas and Water Pressures for the Base Case at 1000 Years

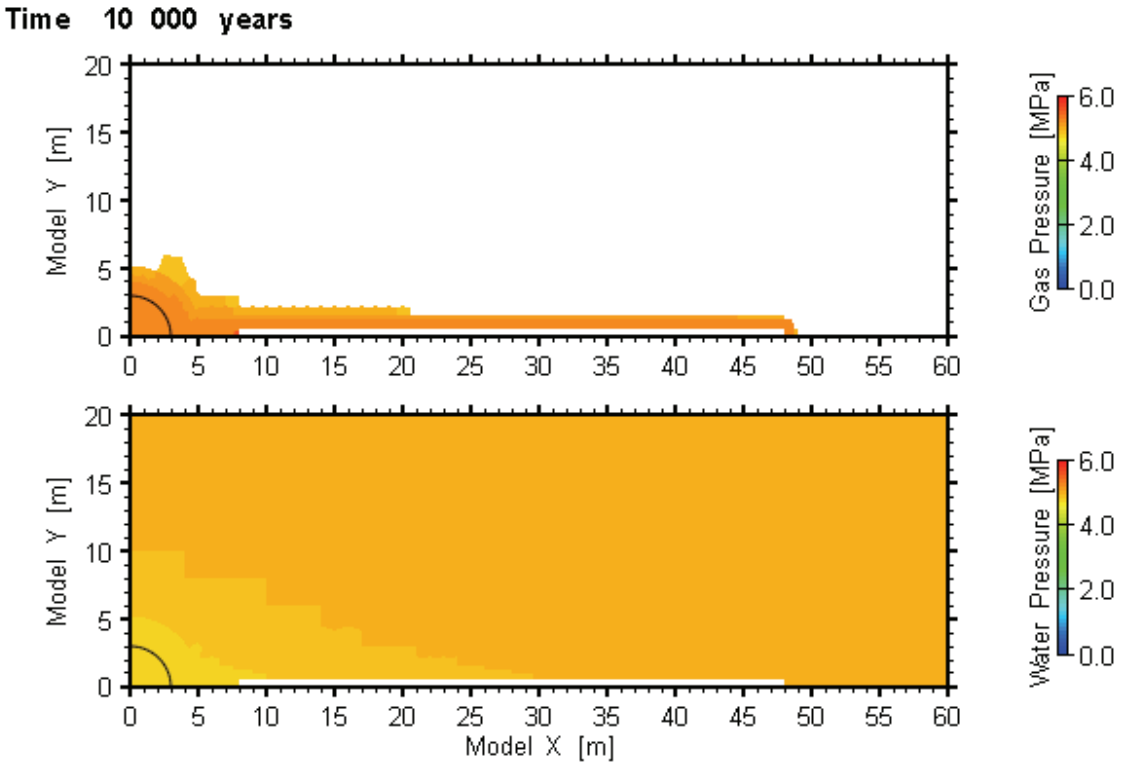

Figure 11: Gas and Water Pressures for the Base Case at 10 000 Years

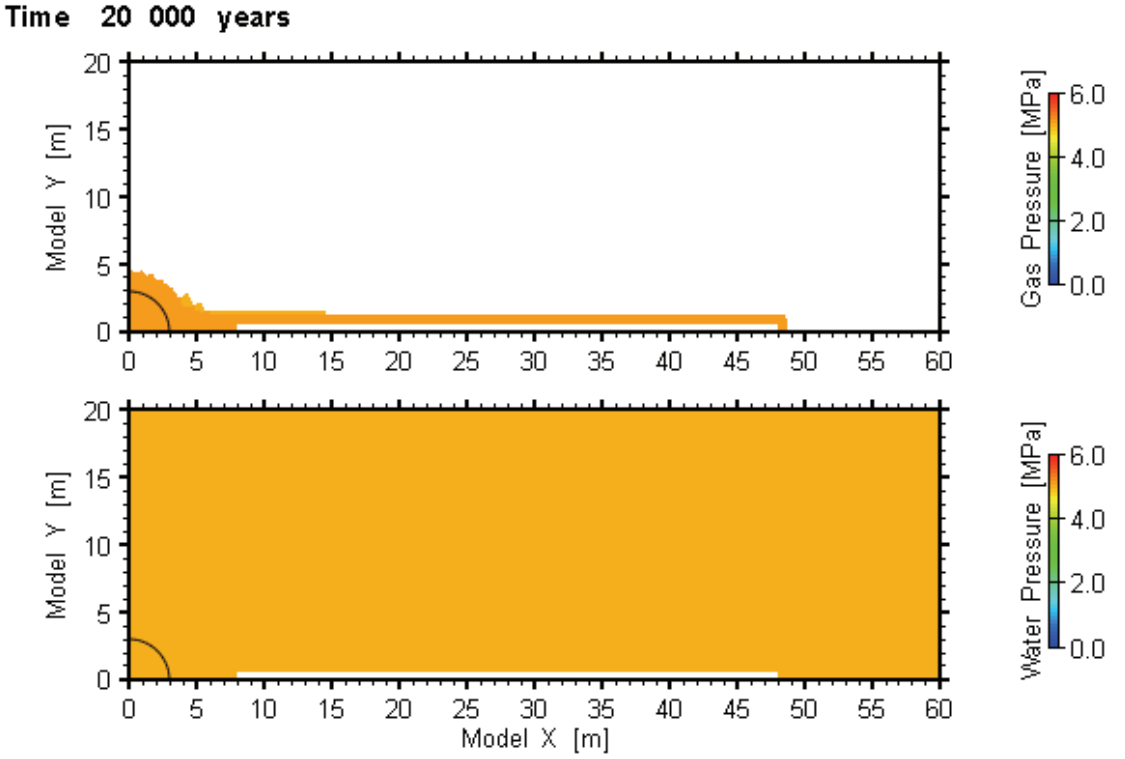

Figure 12: Gas and Water pressures for the Base Case at 20 000 Years

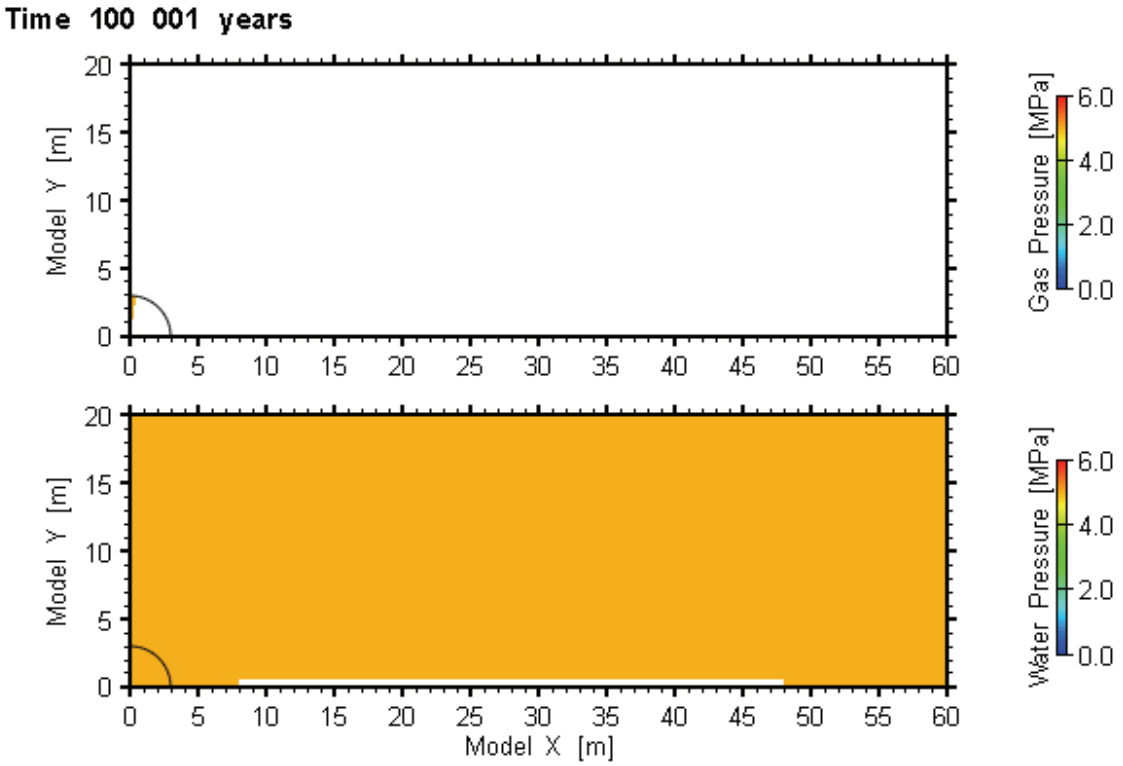

Figure 13: Gas and Water Pressures for the Base Case at 100 000 Years

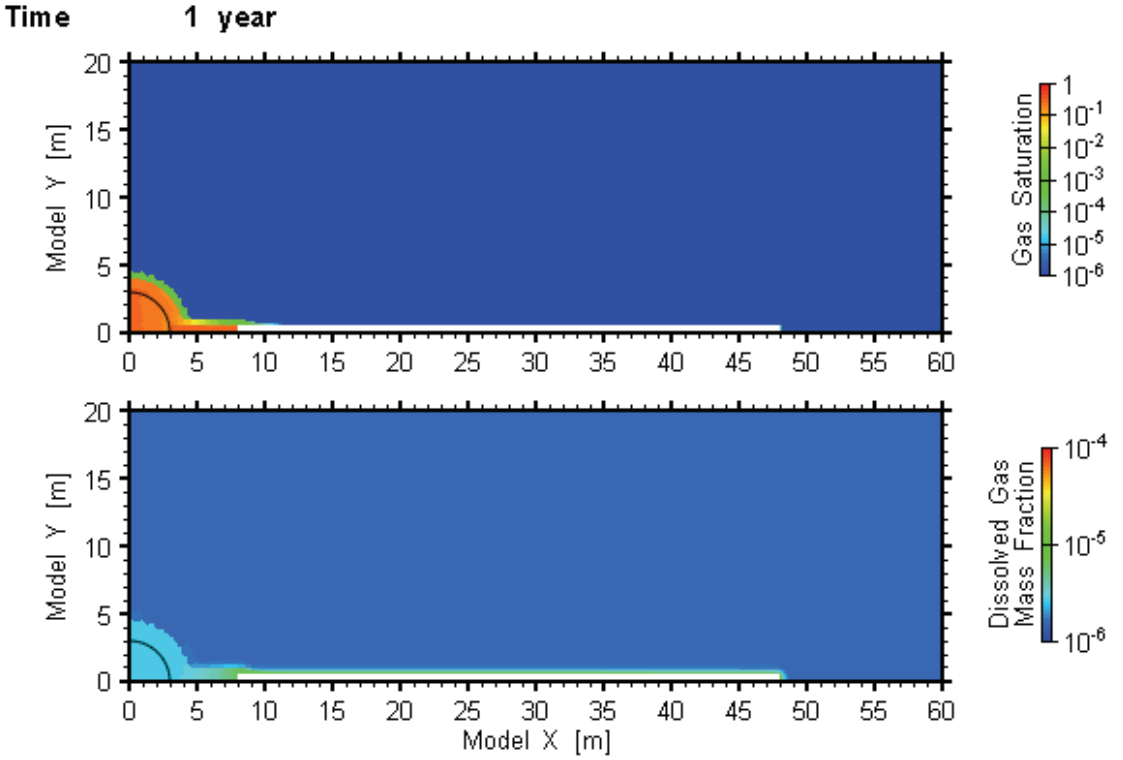

Figure 14: Gas Saturations and Dissolved Gas Mass Fraction at 1 Year

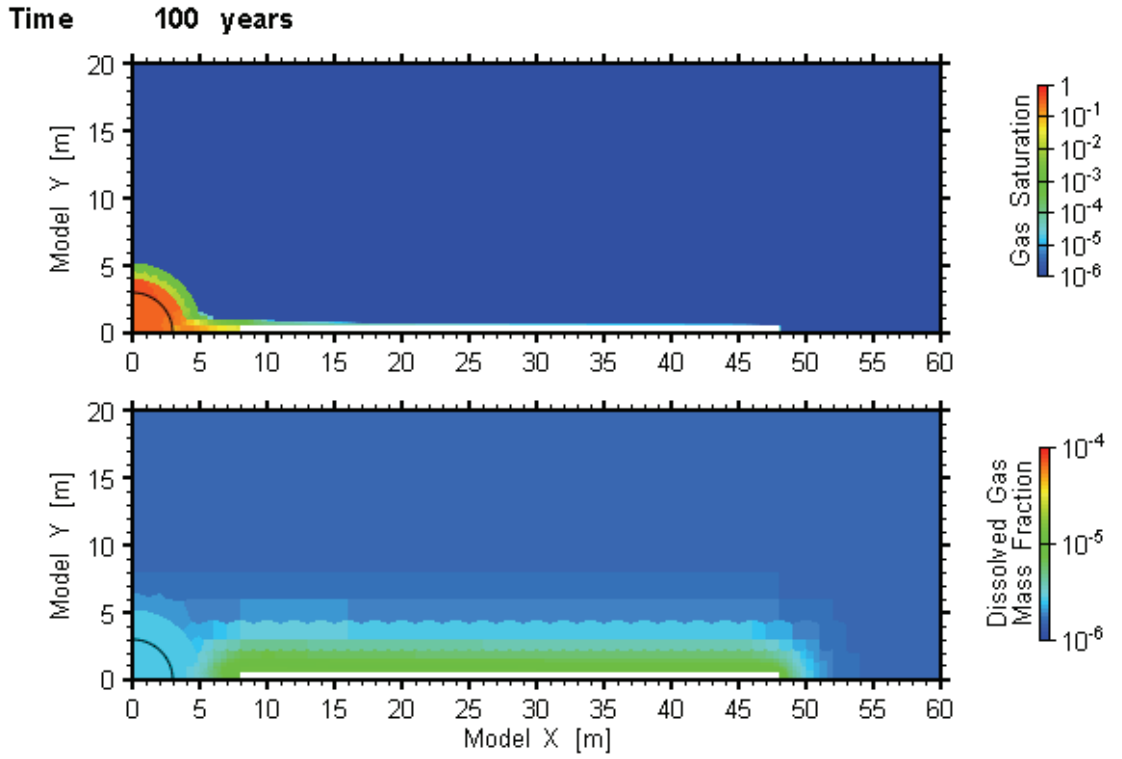

Figure 15: Gas Saturations and Dissolved Gas Mass Fraction at 100 Years

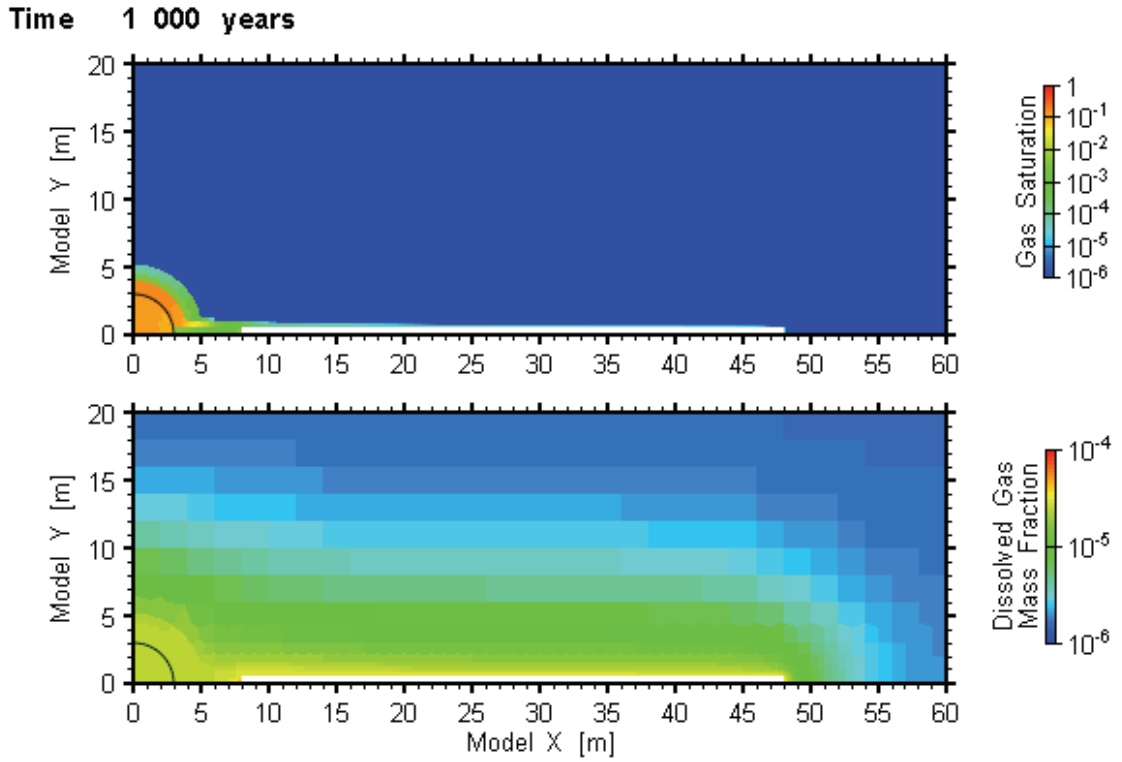

Figure 16: Gas Saturations and Dissolved Gas Mass Fraction at 1 000 Years

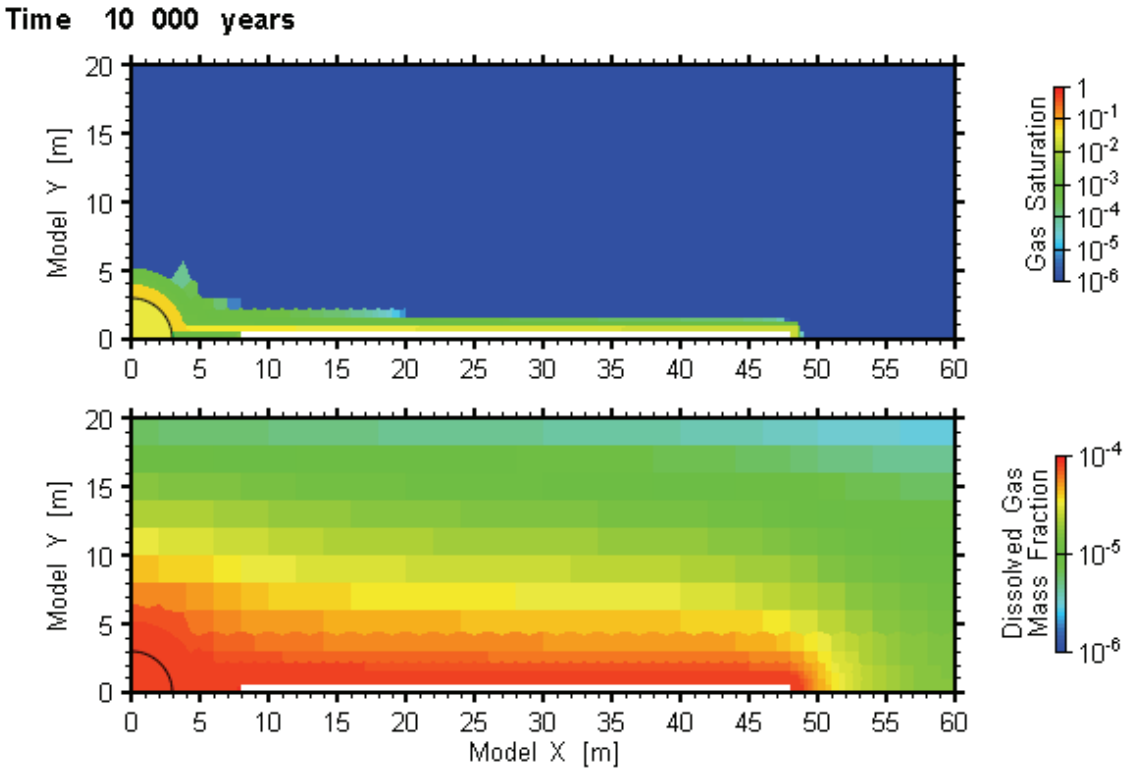

Figure 17: Gas Saturations and Dissolved Gas Mass Fraction at 10 000 Years

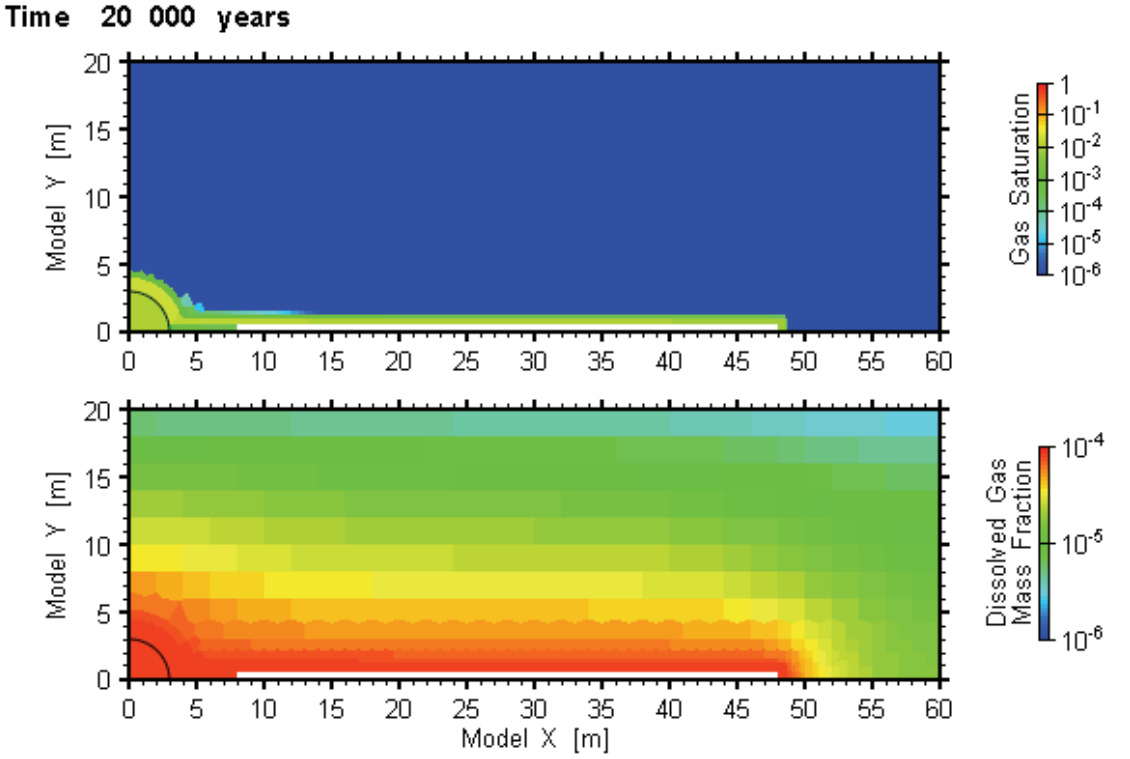

Figure 18: Gas Saturations and Dissolved Gas Mass Fraction at 20 000 Years

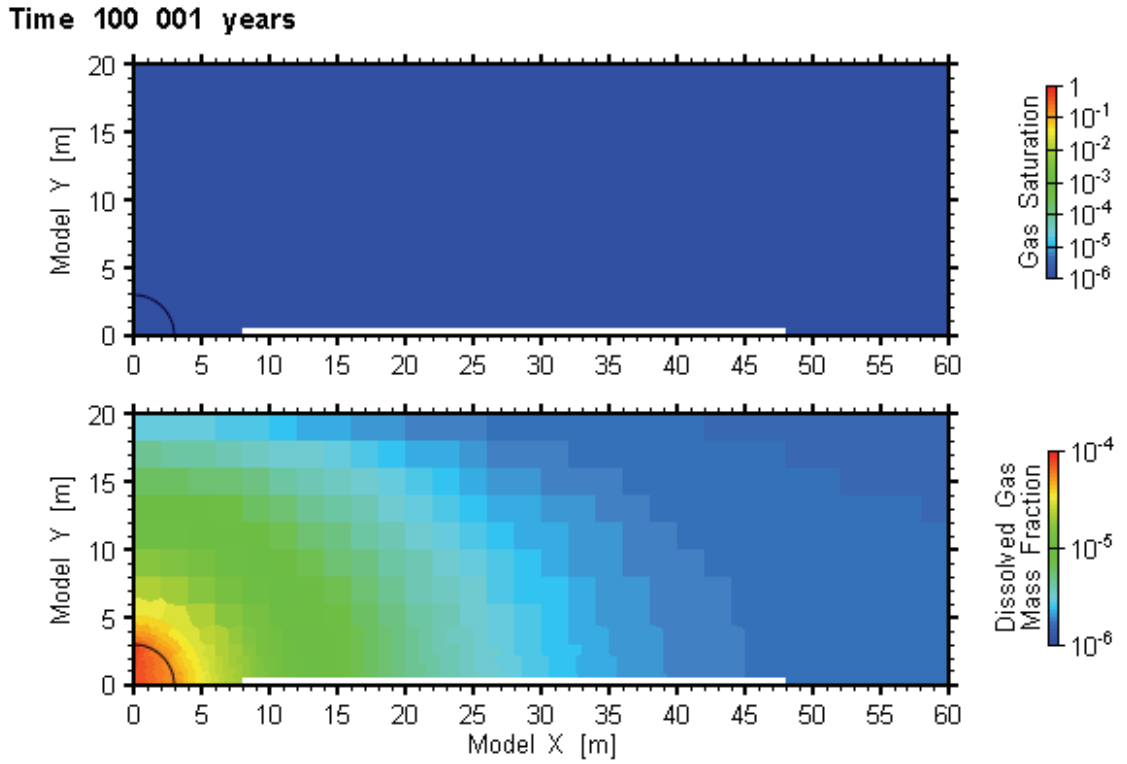

Figure 19: Gas Saturations and Dissolved Gas Mass Fraction at 100 000 Years

Pressure time series at three points are provided in Figure 21 through Figure 23. The locations of these pressure points are shown in Figure 20, highlighted by red circles and lines.

The boundary condition at the access drift clearly dominates behaviour in the system. For the gas pressure curves at Point 4 and Point 5 (Figure 22 and Figure 21), the shape of the curve matches that of the pressure boundary at the access drift. At Point 4, the water pressures become negative between 10 and 1000 years as gas saturations increase. Gas pressures are held low by the pressure boundary at the access drift, and capillary pressures are calculated as a function of saturation. As capillary pressure rises, water pressures lower.

Point 9 also exhibits a drop in water pressure. This is due to the equilibration of low initial pressures within the cell causing water from the host rock to flow into the cell, reducing pressures in the surrounding host rock.

Water pressure at Point 4 increases slightly at 10 000 years, the time at which gas injection stops (Figure 22). This is a result of gas pressures matching the access drift boundary condition, and gas saturations in the interface decreasing very slightly since gas is no longer being generated in the cell (gas saturations at point 4 decrease from 0.999 at 10 000 years to 0.998 at 25 000 years), resulting in lower capillary pressures and consequently higher water pressures. This change in water pressure when gas generation stops is not observed by the other model groups; which suggests that they do not see the very small drop in gas saturation at Point 4. This could be due to a number of differences between models such as grid discretization, differences in Point 4 location, or relative gas permeability models.

Figure 24 shows the gas flow into the access drift, divided into cell components: bentonite plug, interface and EDZ. Positive flow is flow towards the access drift. A short period of negative gas flow (away from the access drift) occurs after 10 000 years, once gas generation ceases. This is a boundary condition effect, as the gas pressures defined at the boundary maintain gas pressures in the cell once gas generation ceases.

It can be seen in Figure 24 that gas flow from the canisters into the access drift is dominated by flow through the EDZ. While the interface is more permeable than the EDZ and contains a greater concentration of gas, the area of the interface is much smaller than the EDZ, resulting in a relatively small amount of flow. Note that the high permeability of the interface allows gas to enter the EDZ with little resistance. The bentonite plug flows are negligible compared to those in the EDZ and interface, due to lower permeabilities and higher gas-entry pressures.

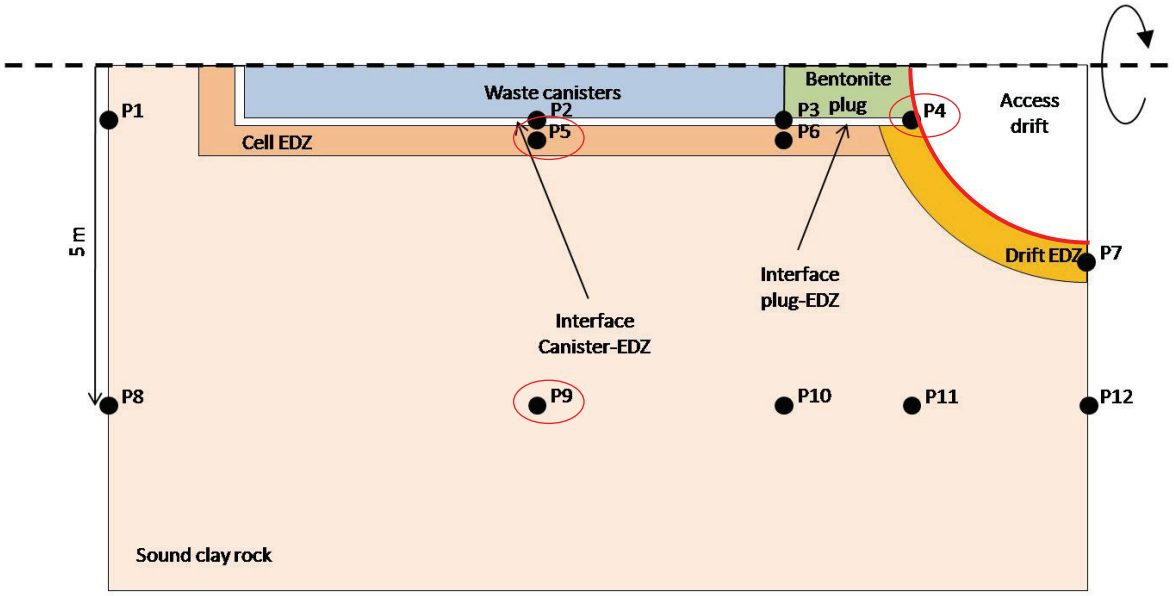

Note: Points 4, 5 and 9 are circled in red, and the interface for the access drift flow is highlighted in red.

Figure 20: Location of Pressure and Flow Time Series

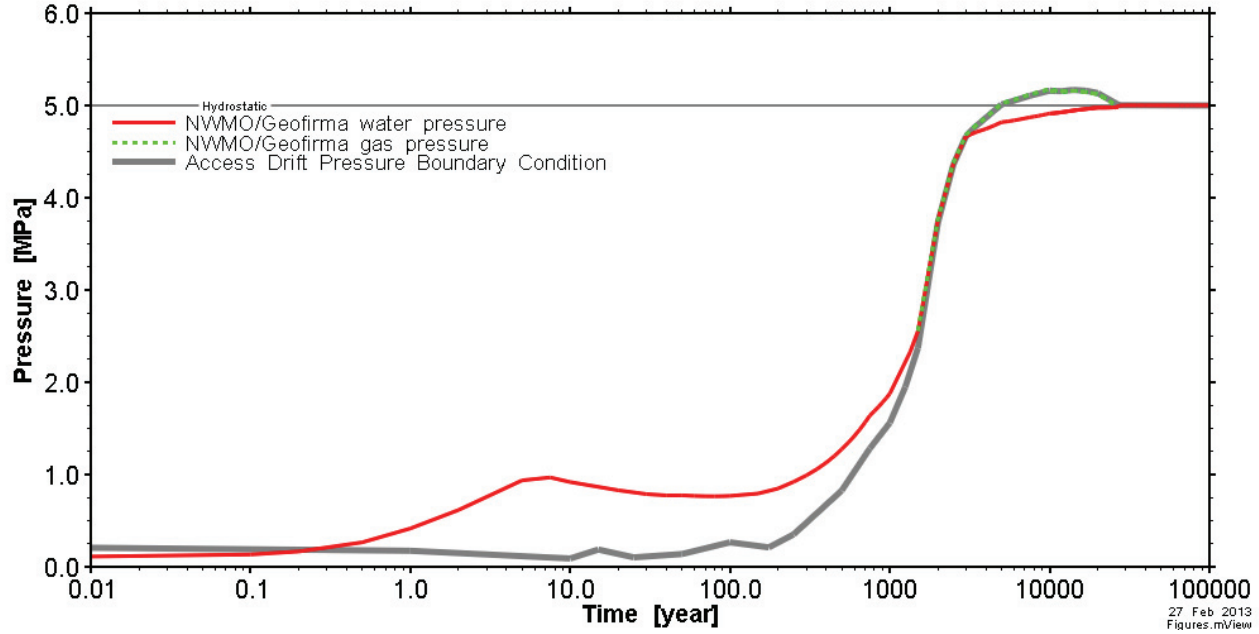

Figure 21: Base Case Water and Gas Pressures at Point 5, Located in the Middle of the EDZ, Half Way Along the Canister

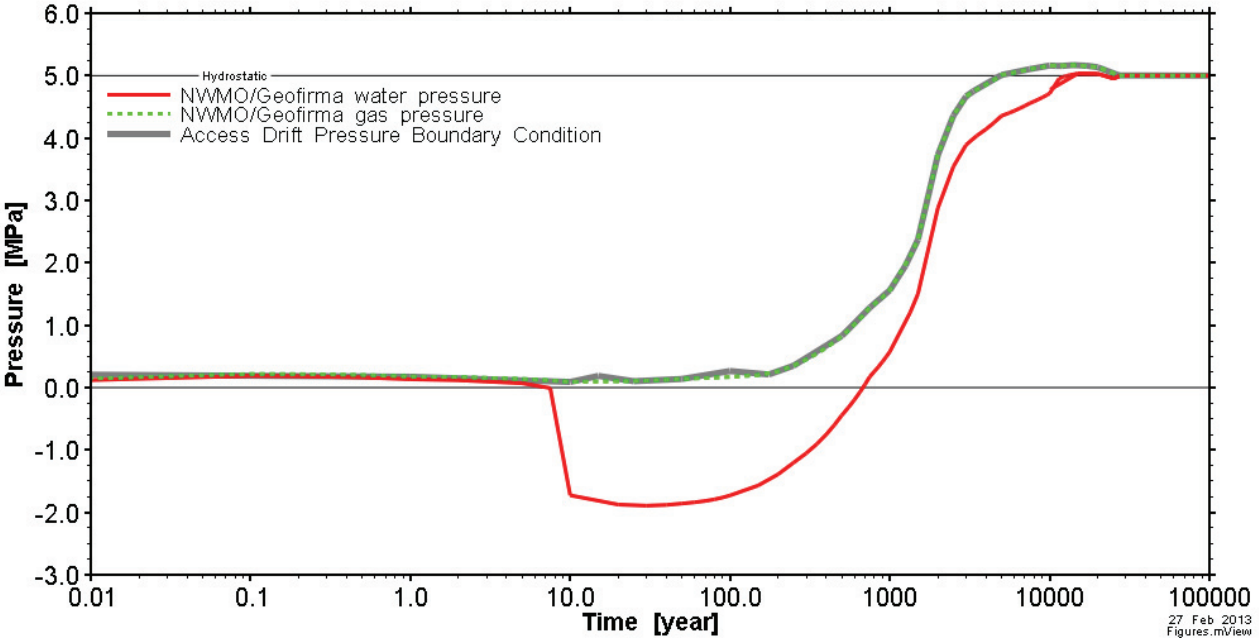

Figure 22: Base Case Water and Gas Pressures at Point 4, Located in the EDZ, at the Intersection of the Access Drift and the Bentonite Plug

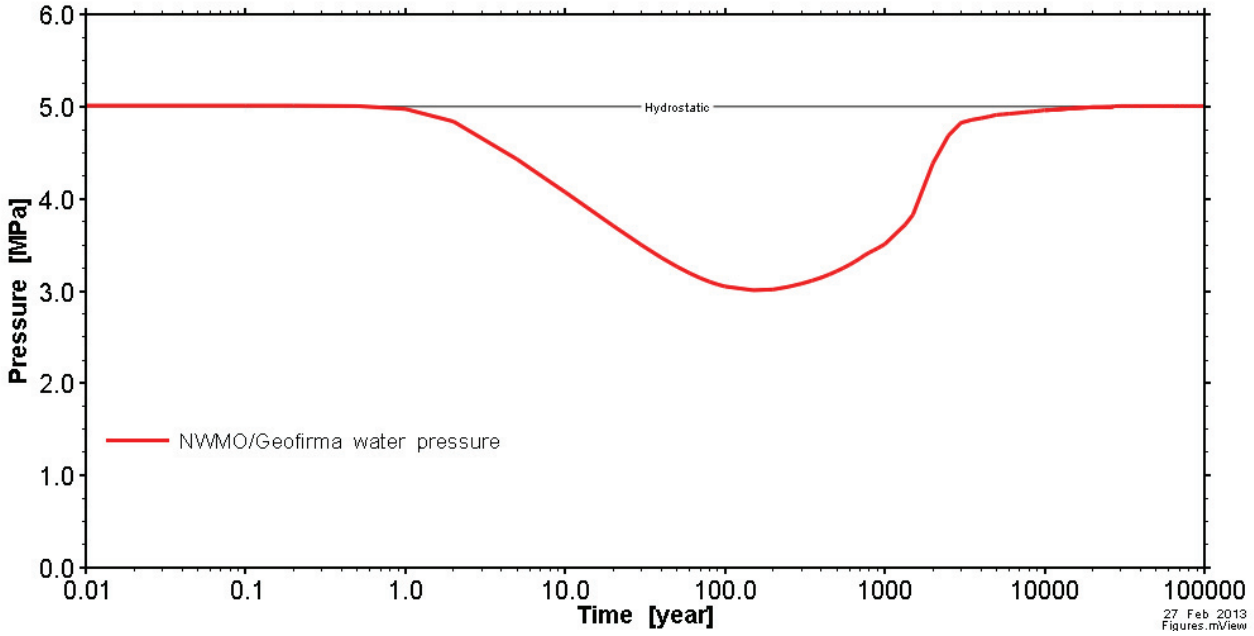

Figure 23: Base Case Water Pressures at Point 9, Located in the Host rock, 5 m Away from the Center of the Cell

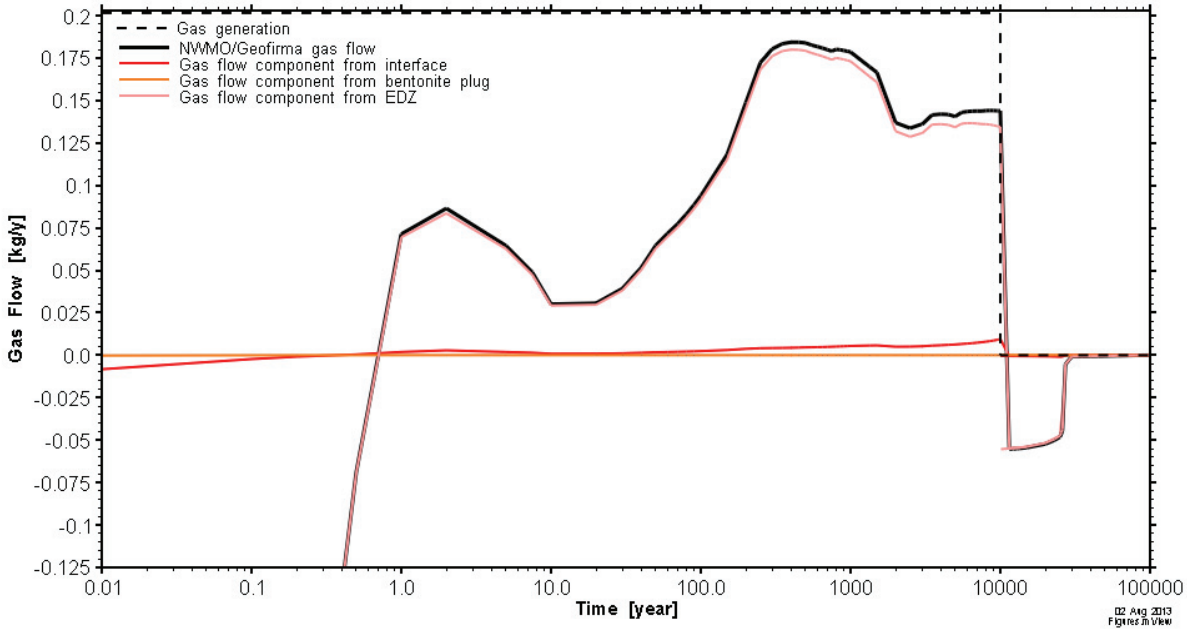

Figure 24: Base Case Gas Flux Into the Access Drift from the EDZ, Interface and Bentonite Plug

4.2.2 Sensitivity Case Results

The benchmark defined three sensitivity cases examining EDZ permeability, altered relative permeability curves, and increased diffusion. Geofirma conducted additional sensitivity cases on the interface, examining a less permeable interface, as well as the impact of no interface and an upscaled interface.

4.2.2.1 Case 1: Self Healing EDZ

In this sensitivity case, the permeability (K) of the EDZ is set equal to that of the host rock (10^{-20} m^2). Results for this case are only shown up to approximately 25 000 years due to numeric instabilities.

Figure 25 shows the gas flows into the access drift for this sensitivity case, compared to the base case. The low permeability of the EDZ resulted in gas flow towards the access drift occurring through the interface rather than the EDZ. Virtually no gas enters the EDZ surrounding the cell. The amount of gas flow is not significantly reduced, but rather simply shifted to flow through the interface. There is a small reduction in the peak gas flow, but the peak occurs for a longer period of time. There is a small amount of gas flow away from the access drift through the EDZ.

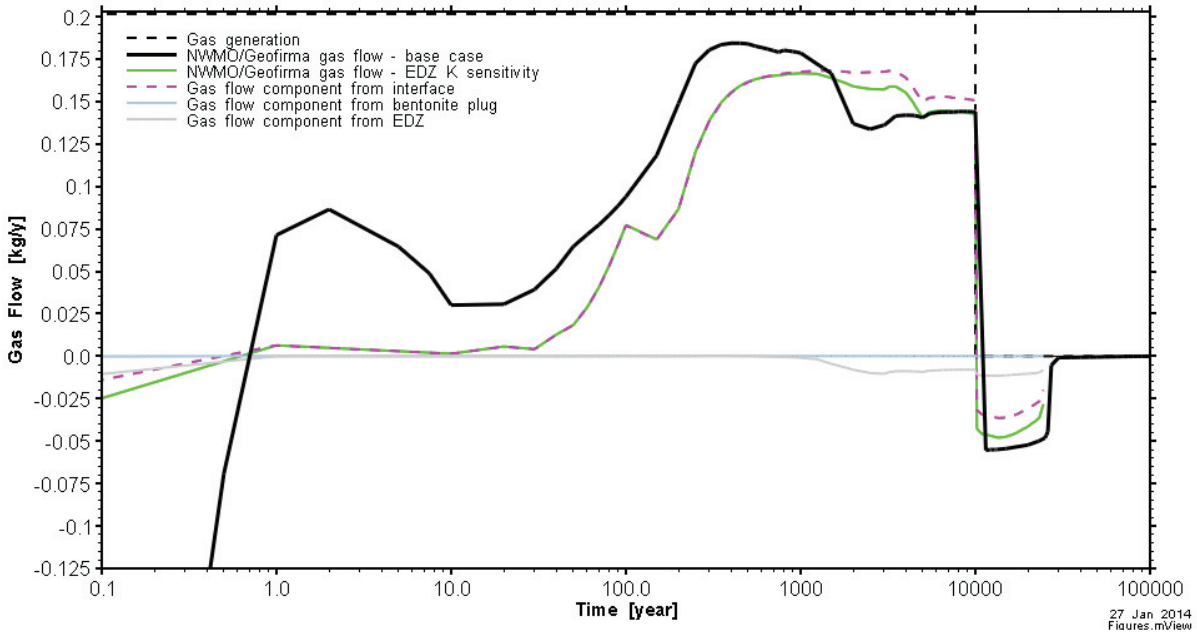

Figure 25: Sensitivity Case 1 (EDZ K Equivalent to Rock K) Gas Flux Into the Access Drift, From the EDZ, Interface and Bentonite Plug

4.2.2.2 Case 2: Altered Relative Permeability Curves

In this case, the relative permeability curve for both the host rock and the EDZ is changed from the van Genuchten relationship to a cubic power relationship (TOUGH2 refers to this relationship as the Verma et al. (1985) relationship):

$$k_{rl} = S_l^3$$

$$\boldsymbol{k_{rg} = S_g^3 = (1 - S_w)^3} \qquad \textbf{Equation 3}$$

where:
k_{rl} is the relative permeability for water (-).

The relative gas permeability curve for this cubic power relationship is shown in Figure 7, compared to the benchmark van Genuchten relative gas permeability curves.

Simulation results are shown up to approximately 2000 years. Numerical issues were encountered with this simulation, particularly at nodes where gas saturation was very small and gas was no longer migrating into the node. While similar numerical difficulties were encountered in other simulations, the very flat relative gas permeability curve at low gas saturations of the cubic power law exacerbated the numerical issues.

Compared to the base case, changing the relative permeability curve had minimal impact on results. Figure 26 shows the gas flow into the access drift. Small differences occur mainly at early times; peak gas flows after 100 years are very close between the two cases.

At early times, the changes in relative gas permeability in the EDZ and host rock resulted in less gas flow to the access drift, and correspondingly resulted in greater flow out of the EDZ and into the host rock (except for a short peak in gas flow in the base case at 1 year), as show in Figure 27.

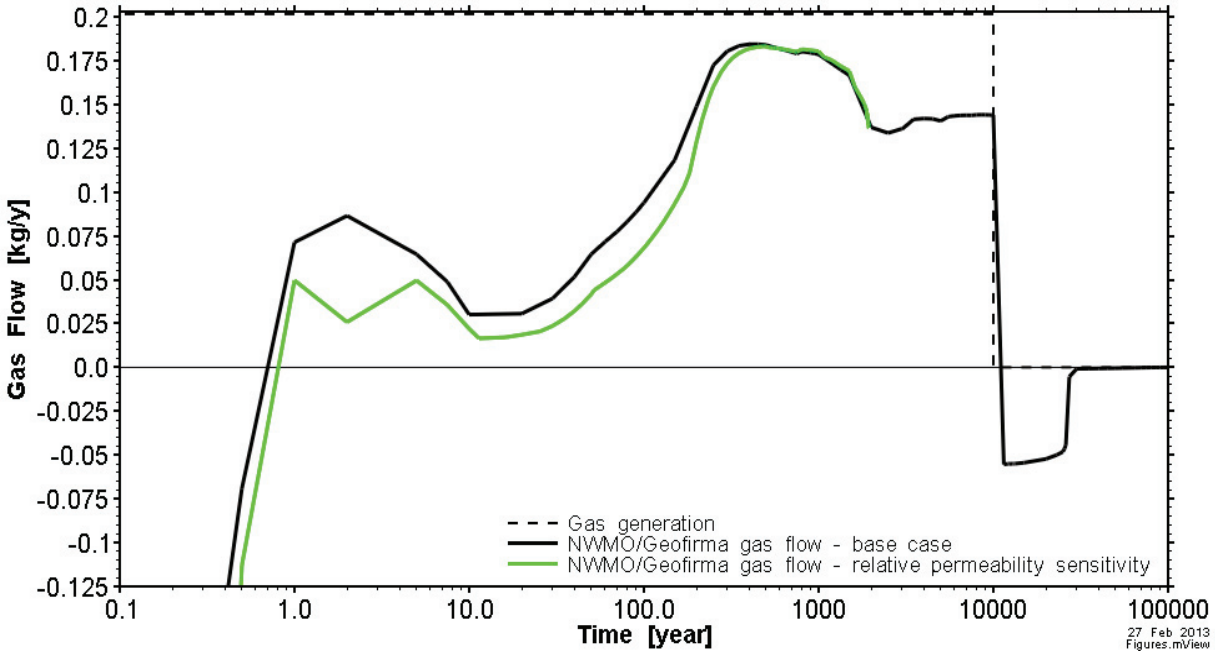

Figure 26: Sensitivity Case 2 (Cubic Power Law Relative Permeability Curve in Host Rock and EDZ) Gas Flow Into the Access Drift

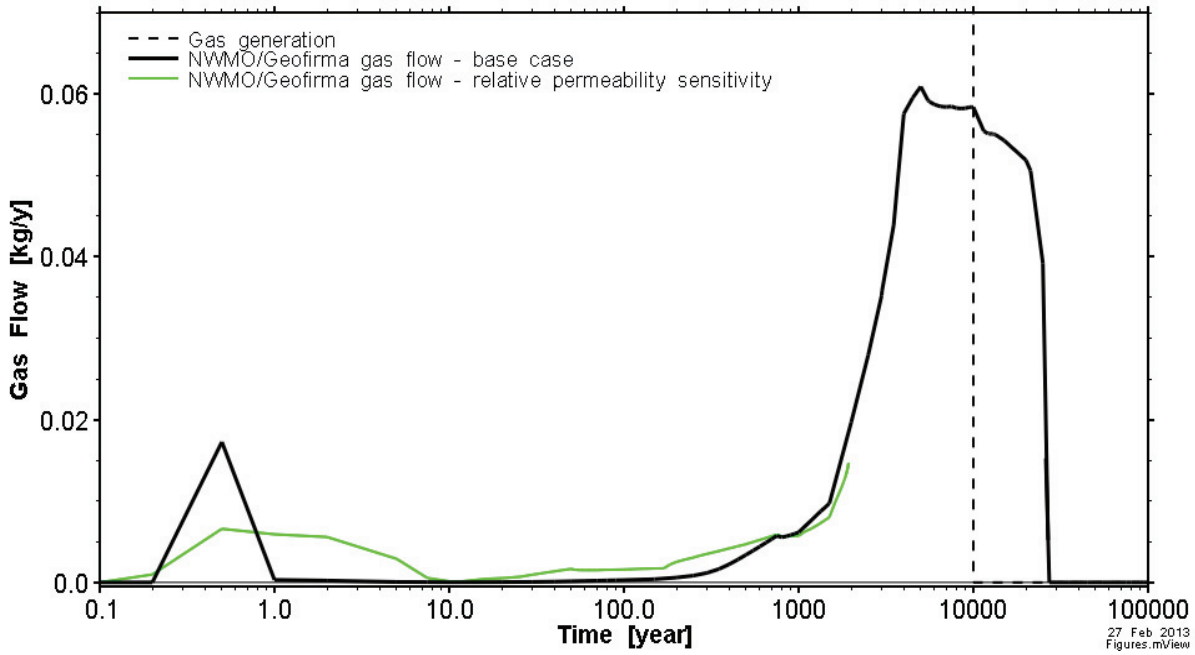

Figure 27: Sensitivity Case 2 (Cubic Power Law Relative Permeability Curve in Host Rock and EDZ) Gas Flow Out of EDZ Surface into Host Rock

4.2.2.3 Case 3: Increased Diffusion in Water

In this sensitivity case, the diffusion coefficient for dissolved hydrogen was increased by a factor of 10. The base case diffusion coefficient is 4.59×10^{-9} m^2/s. Simulation results are shown up to 23 000 years in Figure 28.

Increasing diffusion has a substantial impact on results. A greater amount of dissolved gas migrates away from the cell and into the host rock, resulting in less gas travelling towards the access drift. It should be emphasized that the greater amount of gas migrating away from the cell is dissolved gas, not free phase gas. This greater amount of dissolved gas travelling away from the cell results in greater dissolution of gas near the cell, and consequently the gas phase does not travel as far away from the cell as in the base case. By 10 000 years, the gas phase has only extended between 0.25 and 0.5 m into the host rock (compared to 0.5 and 1 m in the base case).

Greater dissolution also results in lower gas pressures. These lower gas pressures are lower than specified in the access drift boundary condition, resulting in gas entering from the boundary condition into the cell, EDZ and host rock, as shown in Figure 28. As in the base case, almost all gas flow is through the EDZ, not the interface or the bentonite plug. Based on these gas fluxes, this diffusion scenario is not realistic, as the access drift is unlikely to provide gas greater than gas generation in the cells.

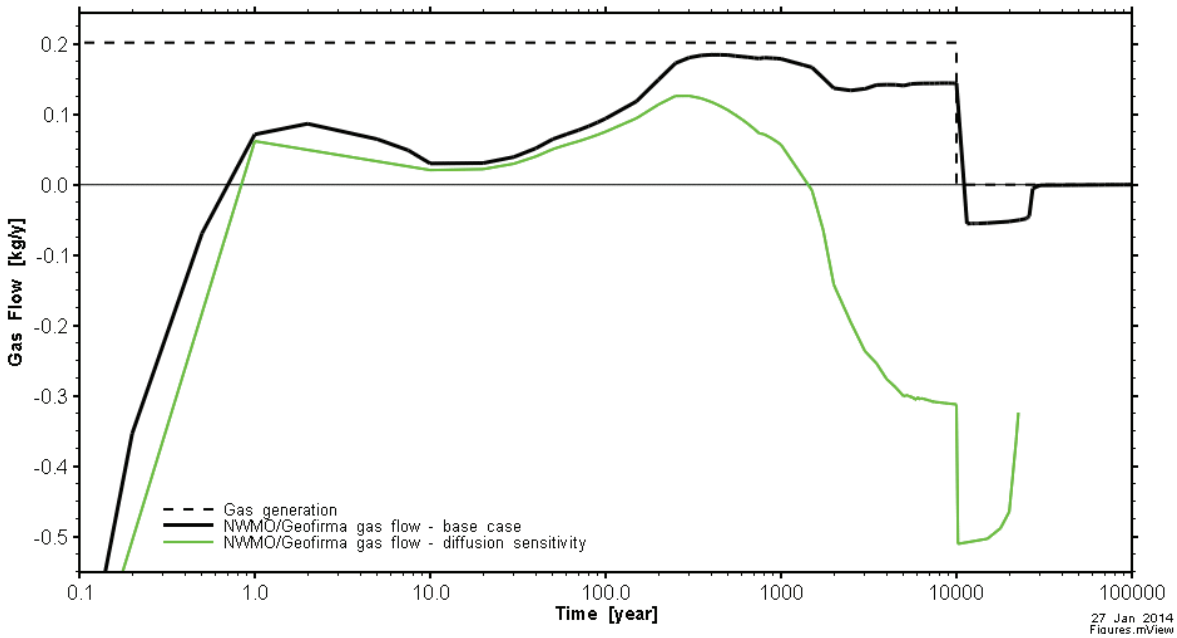

Figure 28: Sensitivity Case 3 (Increased Diffusion Coefficient) Gas Flux Into the Access Drift

4.2.2.4 Less Permeable Interfaces

In this sensitivity case, the permeability of the interface along the canister face is reduced to 10^{-15} m^2 (base case canister interface permeability is 10^{-12} m^2).

Figure 29 shows the gas flow into the access drift compared to the base case. Gas flows through the access drift are very similar to the base case, with flow through the interface reduced to negligible amounts.

The gas flow results of this interface permeability sensitivity case and the EDZ permeability sensitivity case suggest that the interface is only an important feature of the system if the EDZ permeability is small. It is possible that the interface plays a role in distributing the gas out into the EDZ. A sensitivity case that removes the interface entirely, considered in Section 4.2.2.5, will further evaluate the importance of the interface to gas transport at the cell-scale.

Figure 30 compares the gas and water pressures at Point 5 for this less permeable interface sensitivity case to the base case. Point 5 is located in the middle of the EDZ, half way along the canister (Figure 20). Gas pressures for both cases follow the access drift boundary condition.

At 10 years, water pressures at Point 5 (Figure 30) are approximately double the water pressures in the base case; by 1000 years, water pressures are the same as the base case. These high water pressures at early times can be explained by slightly more gas migrating out into the EDZ in the low interface permeability case, instead of migrating along the interface to the access drift. This slightly greater amount of gas will result in slightly lower water pressures near the cell, resulting in a greater gradient of water towards the cell, and a faster resaturation of the EDZ. The effect is small, and once the access drift pressures increase, the effect is negligible. This explanation is confirmed by the gas flow rates through the EDZ to the access drift in Figure 29.

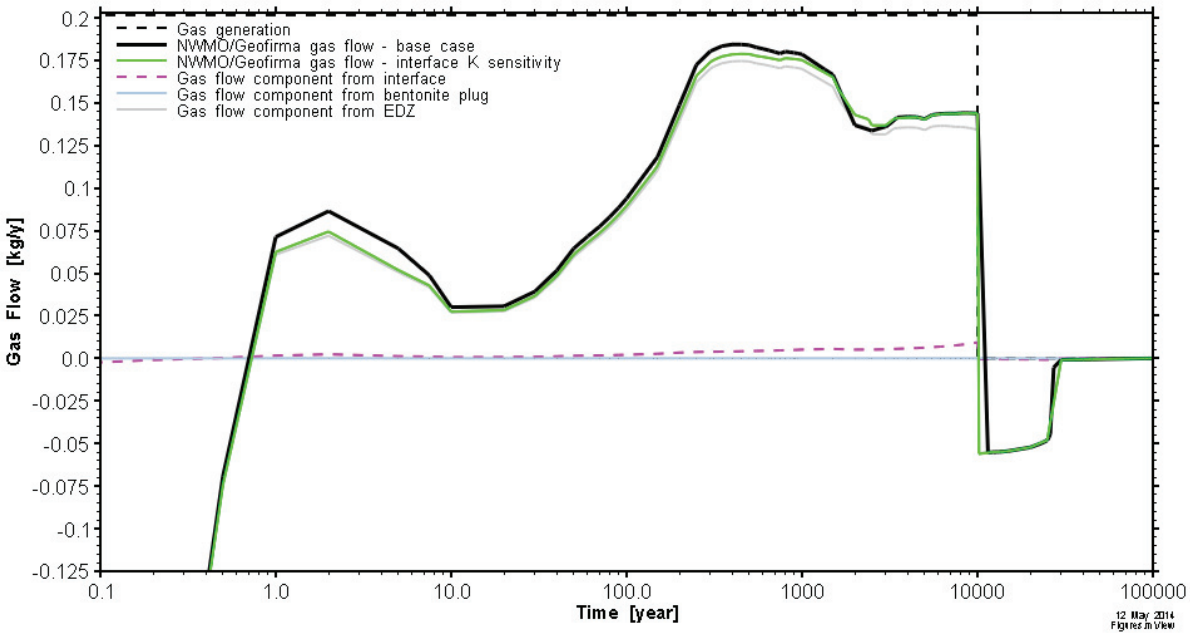

Figure 29: Less Permeable Interface Case (10^{-15} m^2) Gas Flux Into the Access Drift, From the EDZ, Interface and Bentonite Plug

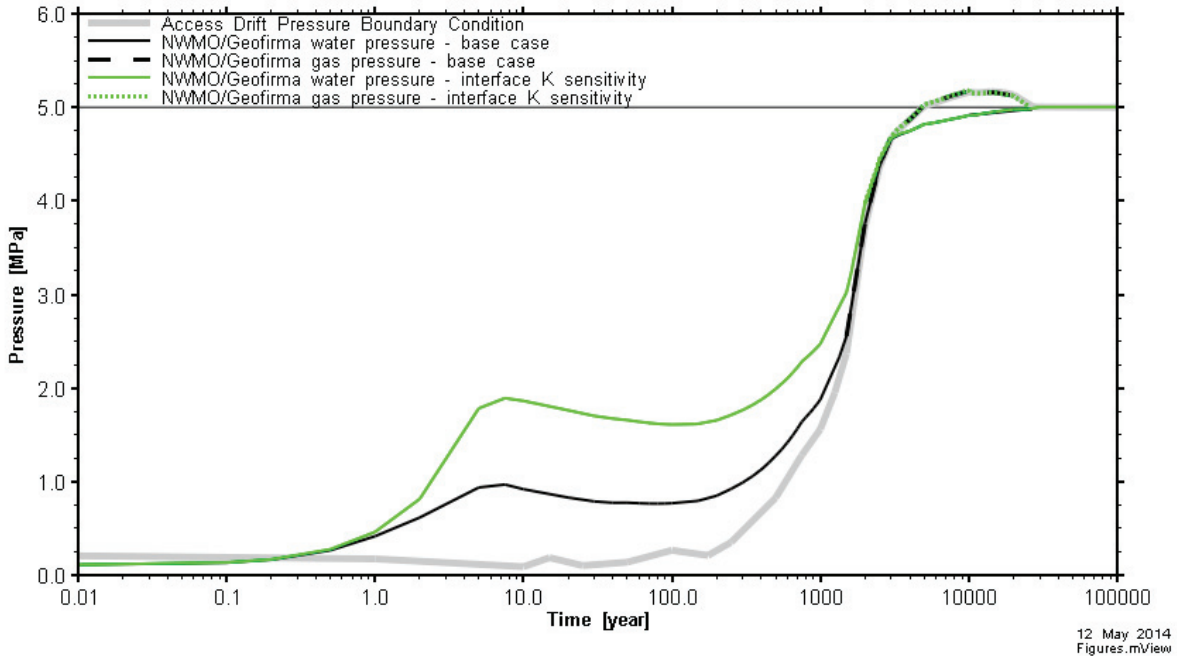

Note: Point 5 is located in the middle of the EDZ, half way along the canister.

Figure 30: Water and Gas Pressures at Point 5 for Less Permeable Interface Case (10^{-15} m^2)

4.2.2.5 No Interface and Upscaled Interface

Two interface sensitivity cases were simulated to help define the impact of potential grid simplifications for the future module and repository scale models:

(1) No interface. The interface (both cell and plug) was removed from the model simulation, and replaced with EDZ. It should be noted that gas is injected directly into the EDZ in this case.
(2) Upscaled interface. The interface (both cell and plug) was combined with the EDZ, effectively forming an inner EDZ 25 cm thick. Upscaled parameters for the inner EDZ and other interface combinations were developed by weighting parameters by the relative volume of the contributing materials. This was the first approach used in the module-scale modelling; a more conventional upscaling scheme was subsequently applied to the module-scale model resulting in little difference in both parameters and results. Initial pressures in the upscaled interface elements are the same as the EDZ.

These cases are compared to the base case. Two metrics were used to compare the differences between these two cases and the base case: gas flow into the access drift and gas flow out of the EDZ and into the host rock. Dissolved gas flows across these surfaces were also examined but differences between the cases were negligible, and consequently results are not presented.

Figure 31 shows the gas flows to the access drift for the base case, compared to the two additional sensitivity cases described above. Removal of the interface entirely had surprisingly little impact on gas flows to the access drift, particularly after 2000 years. However, the upscaled results provide an improved approximation to the reference case results, particularly at early times. Neither case reproduced the peak in gas flow shortly after 1 year, indicating that this peak gas flow is strongly related to the high permeability of the interface.

Figure 32 shows the gas flows out of the EDZ and into the host rock for the base case and the two cases described above. Removal and upscaling of the interface resulted in a marginally greater amount of gas flow out the EDZ into the host rock, at an earlier time. This is perhaps not unexpected, as it corresponds to the slightly smaller flows out of the access drift. Note that the bulk of the gas flow out of the EDZ originates from the EDZ adjacent to the cell, rather than adjacent to the access drift, confirming that gas flows into the host rock are not directly affected by the access drift boundary condition. The small peak in gas flow for the upscaled interface case at 0.5 years is not apparent in either of the other cases due to coarse output discretization in the other cases (only data points at 0.1 and 1 years). This small peak in gas flow is also a result of gas flow out of the EDZ adjacent to the access drift.

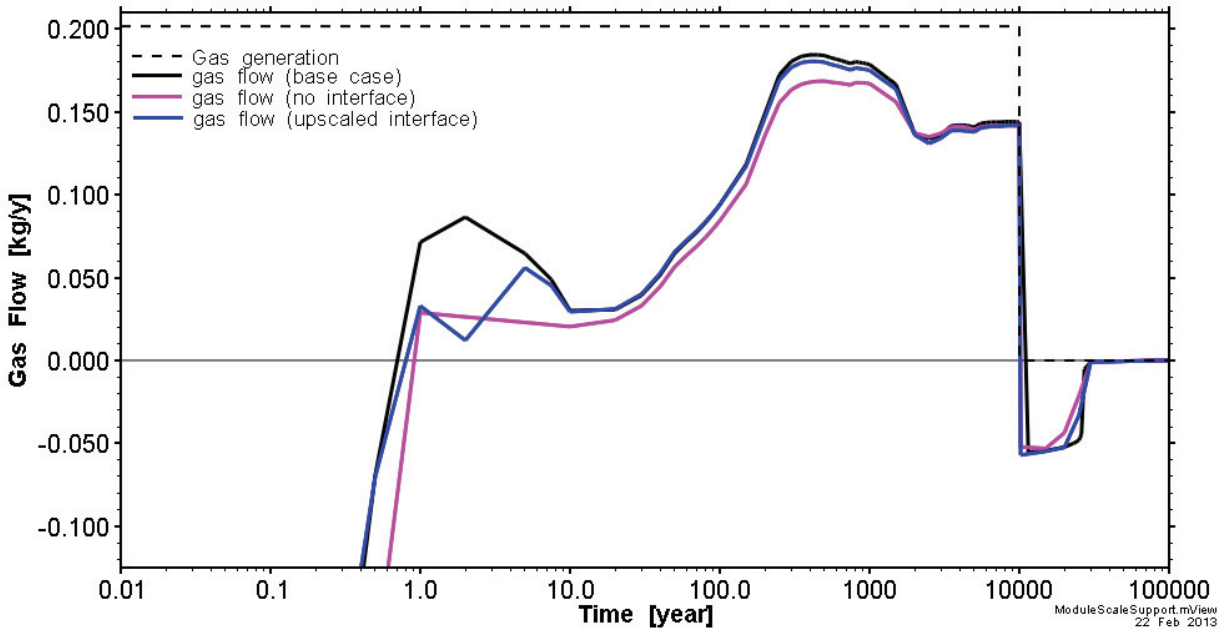

Figure 31: Gas Flows to the Access Drift for the Base Case, No Interface Case and Upscaled Interface Case

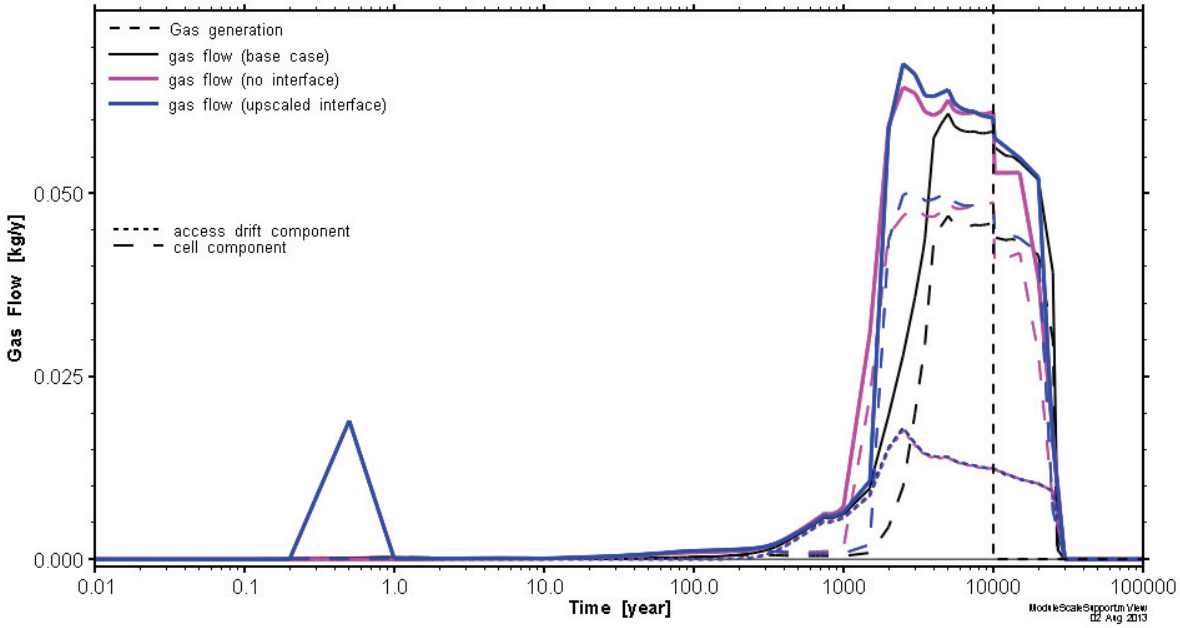

Figure 32: Gas Flows out of the EDZ into the Host Rock for the Base Case, No Interface Case and Upscaled Interface Case

Pressures at Points 4, 5 and 9 were also examined, shown respectively in Figure 33, Figure 34 and Figure 35. Higher initial pressures (5 MPa rather than atmospheric) at Point 5 for the no interface and upscaled interface simulations explain the differences in pressure (Figure 34). Initial pressures are higher in these two cases by definition: the benchmark defines initial pressures of 5 MPa in the EDZ, and atmospheric in the interface. Since the no interface case is only EDZ, and the upscaled interface case is mostly EDZ, initial pressures were assumed to be 5 MPa. At Point 5, pressures for the upscaled interface case are very close to the base case after approximately 10 years. At Point 4, pressures for the upscaled interface case are almost identical to the reference case, reinforcing the importance of the access drift boundary condition for pressure at this point. For the no interface case at Point 4, note that the negative water pressures before 10 years is a result of the location of the point. This point is located within the interface for the other cases (interface has low capillary pressures), and within the EDZ for the no interface case (EDZ has large capillary pressures).

The results of these additional sensitivities suggest that (a) an upscaled interface approach is a slightly more accurate representation of the system than removal of the interface, and (b) the contribution of the interface is relatively small and could potentially be ignored.

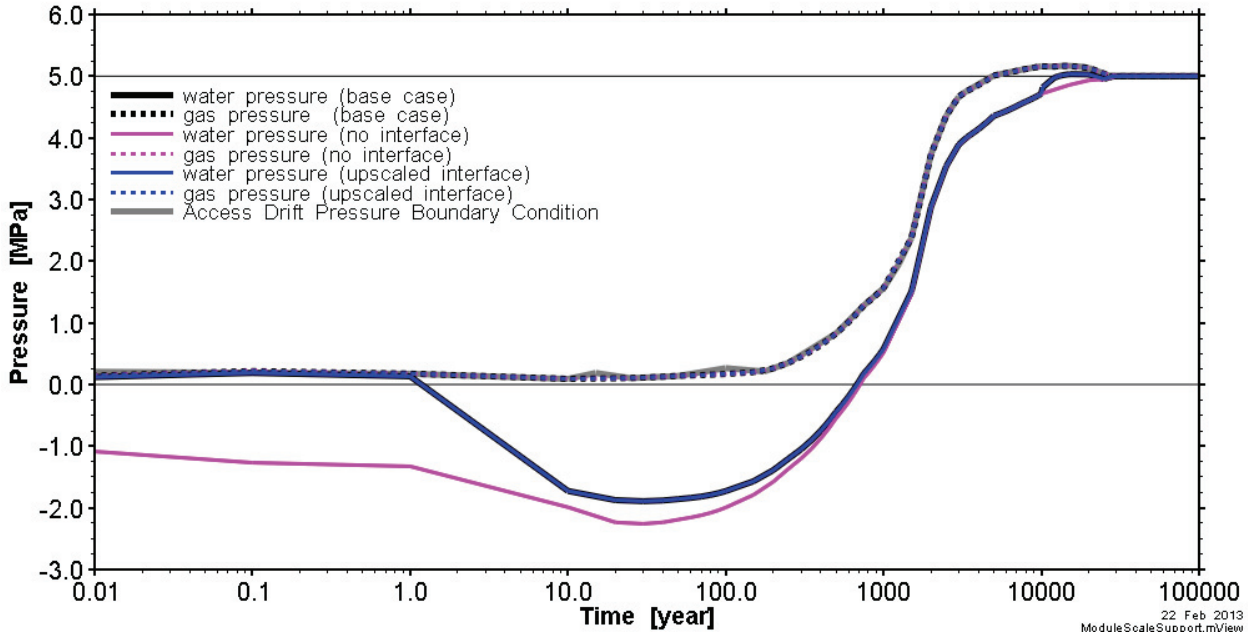

Figure 33: Water and Gas Pressures at Point 4 for the Base Case, No Interface Case and Upscaled Interface Case

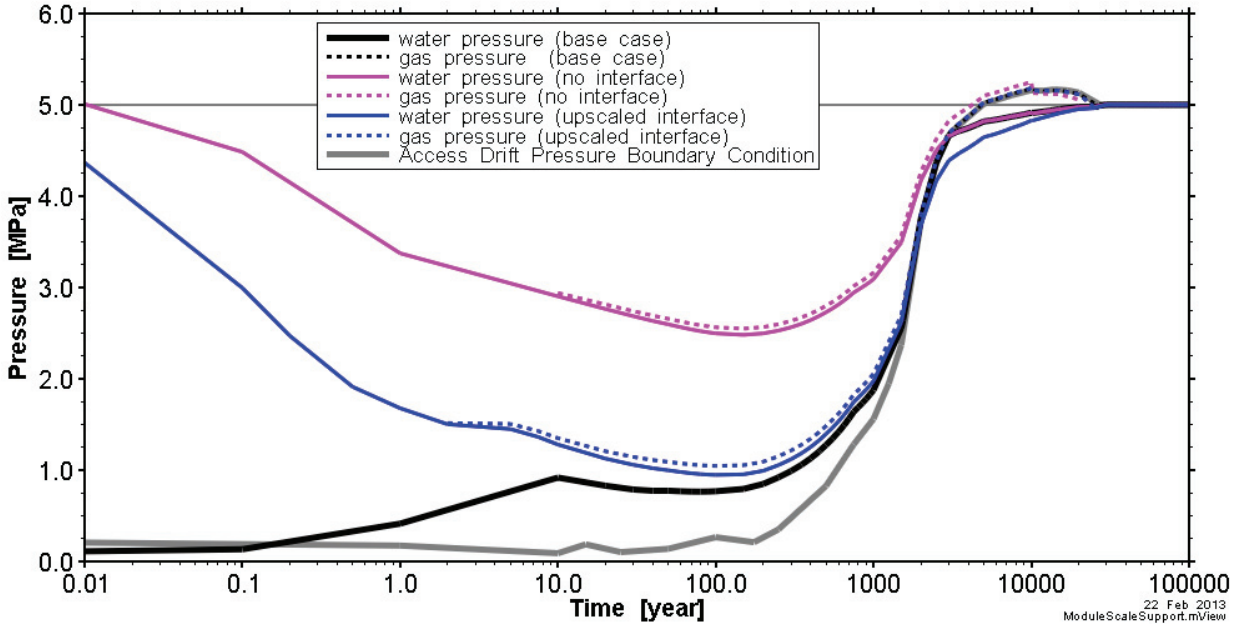

Figure 34: Water and Gas Pressures at Point 5 for the Base Case, No Interface Case and Upscaled Interface Case

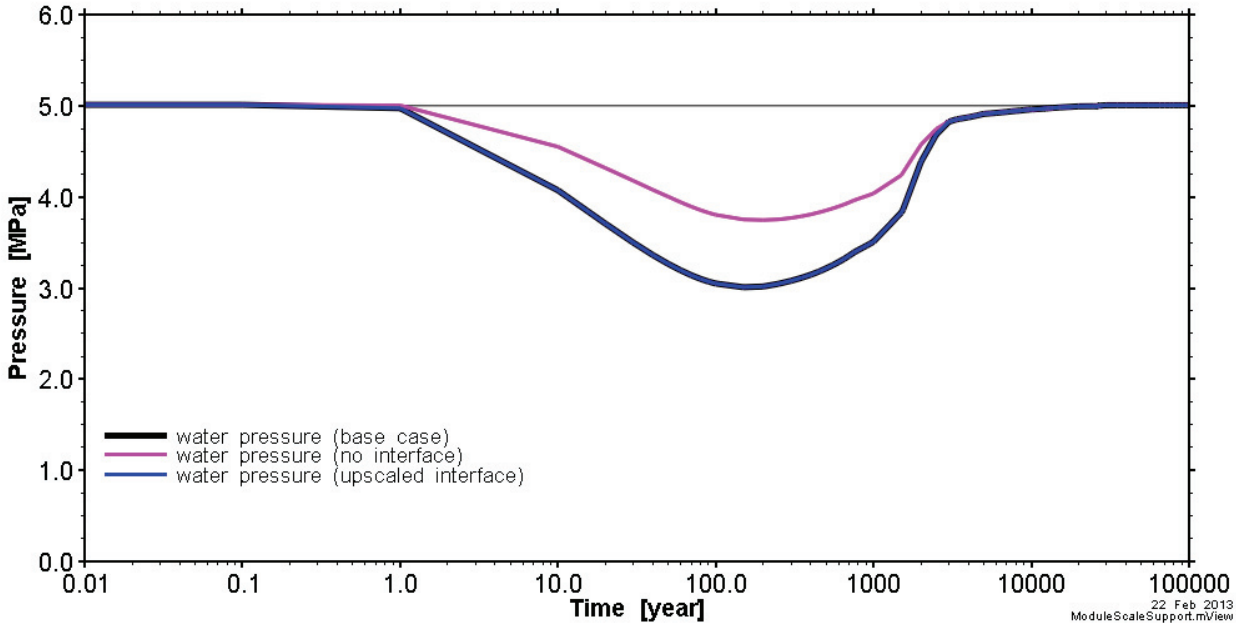

Figure 35: Water Pressures at Point 9 for the Base Case, No Interface Case and Upscaled Interface Case

4.2.3 Comparison of Key Results

A comparison of base case model results with results obtained by other modelling groups is shown in Figure 36 through Figure 39 (Wendling et al. 2014a). The locations of comparison are shown in Figure 20, highlighted by red circles and lines. In general, results compare well. There is a range of results between groups, attributed in part to deviations from the benchmark employed by the different modelling groups. For example, several groups, including Geofirma, ignored the permeability anisotropy of the EDZ and geologic medium due to the constraints of a 2D radial model approach.

In Figure 39, which shows the gas flow into the access drift, Geofirma modelling results show higher gas flows than other modelling groups, excepting LEI and CNRS. The pattern of gas flow is similar to the results presented by Andra and ENSI, with some similarity to the results presented by NDA/Quintessa. In general, the greatest gas flows occur while the access drift boundary condition pressures are low between 100 and 1000 years, and decrease after 1000 years as the boundary condition water pressure increases.

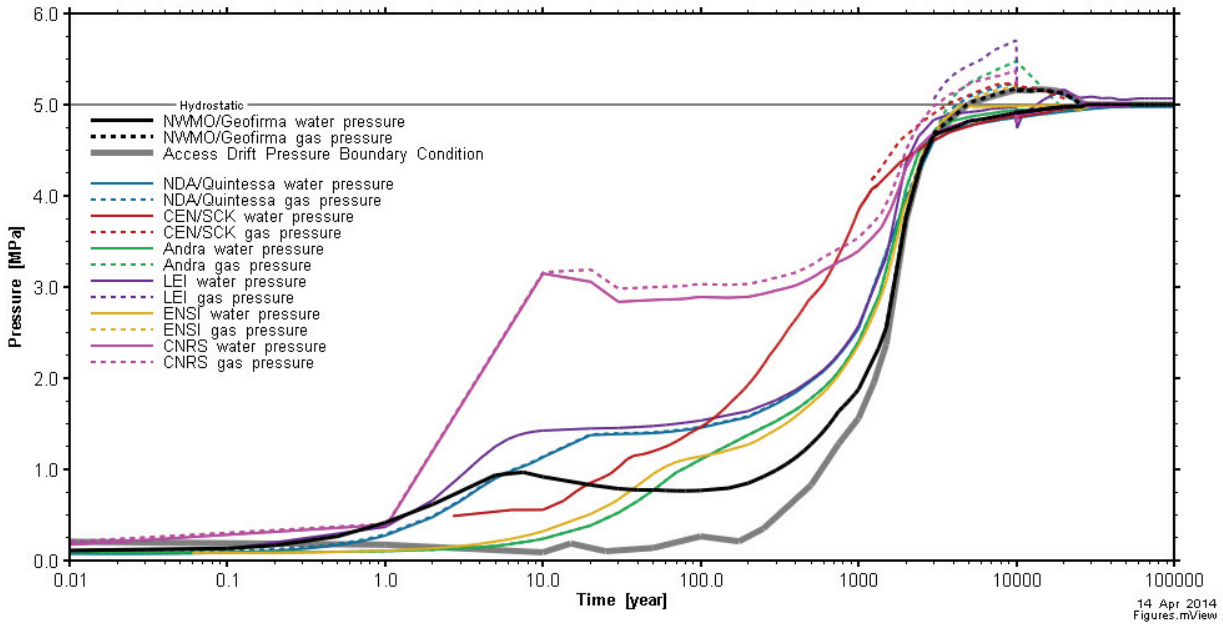

Figure 36: Comparison of FORGE Modelling Results: Base Case Water and Gas Pressures at Point 5, Located in the Middle of the EDZ, Half Way Along the Canister

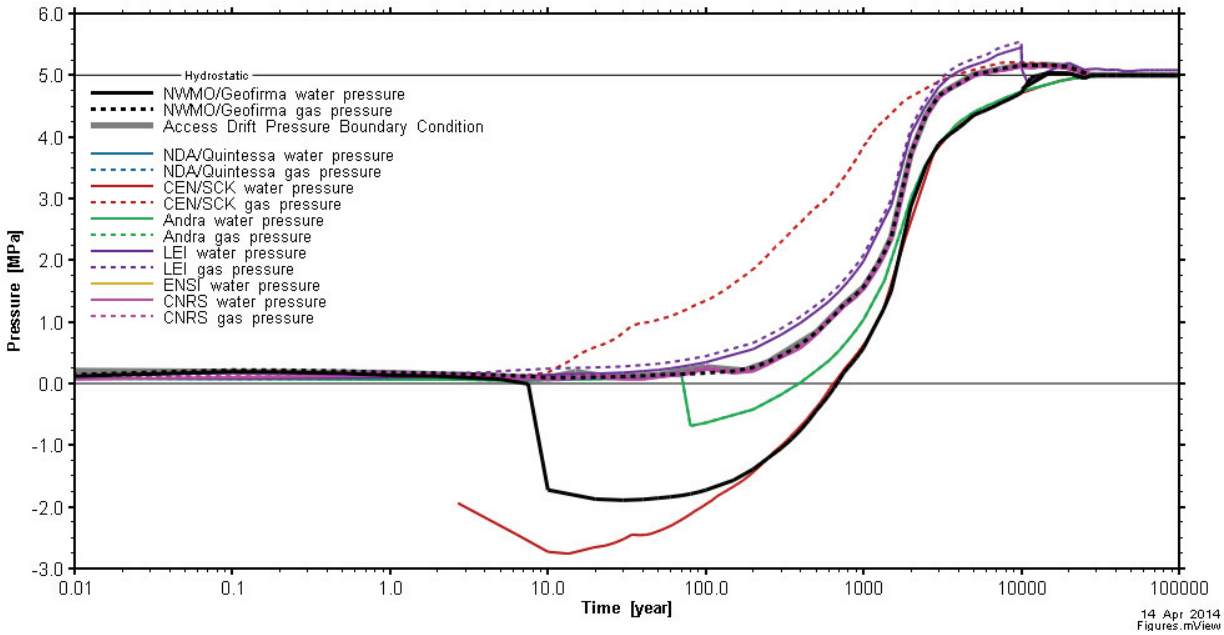

Figure 37: Comparison of FORGE Modelling Results: Base Case Water and Gas Pressures at Point 4, Located in the EDZ, at the Intersection of the Access Drift and the Bentonite Plug

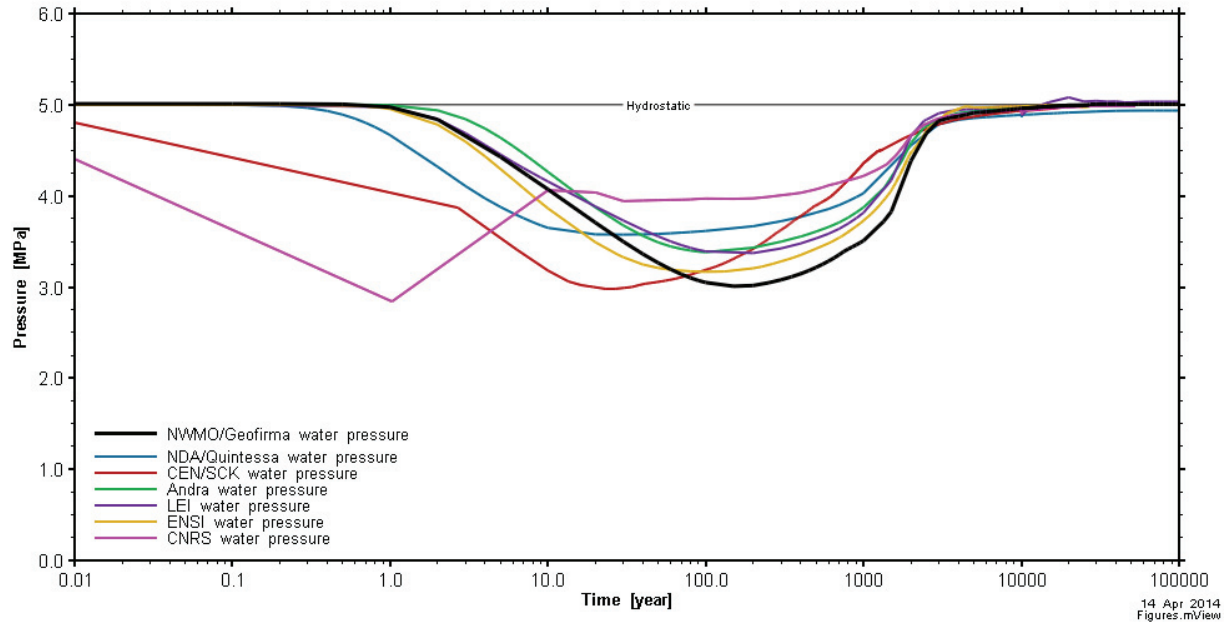

Figure 38: Comparison of FORGE Modelling Results: Base Case Water Pressures at Point 9, Located in the Host Rock, 5 m Away From the Center of the Cell

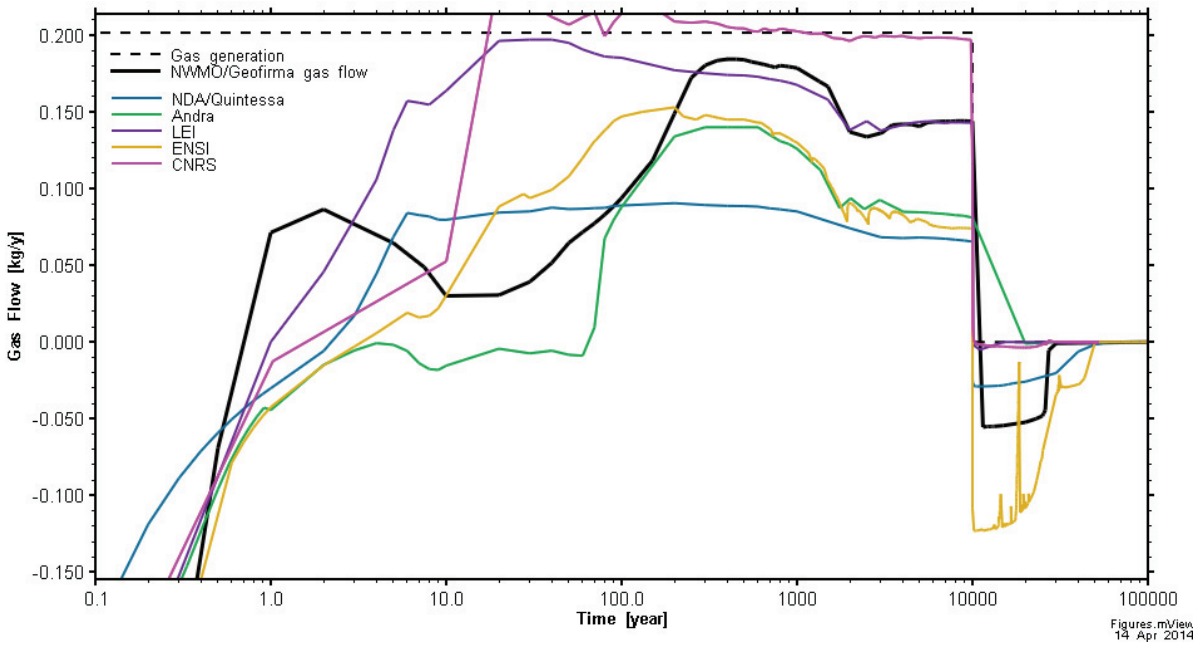

Figure 39: Comparison of FORGE Modelling Results: Base Case Gas Flux Into the Access Drift

4.2.4 Summary

The boundary condition at the access tunnel is a strong driver in this model, ensuring flow along the cell and towards the access drift. During the simulation, pressures in the interface and EDZ develop towards pressures at this boundary condition. At the mid-point of the cell, in the middle of the EDZ (Point 5), pressures match the access drift boundary condition by 2000 years.

Free gas flow occurs mainly in the cell EDZ, due to the greater cross-sectional area for flow compared to the more permeable 1 cm interface. The maximum gas pressure reached was 5.7 MPa in the bentonite plug adjacent to the canisters. This occurred at 10 000 years, the time at which gas injection stopped.

The sensitivity cases demonstrated the following important points about the cell-scale system:

(1) The importance of the EDZ is limited by permeability. Reducing the permeability of the EDZ (to the same as the host rock) shifts gas flow into interface (towards the access drift).

(2) In the presence of a relatively permeable EDZ, the interface has a minor importance. The small size of the interface means that the bulk of the gas flow travels through the EDZ. Decreasing the permeability of the interface, removing the interface or upscaling the interface with the EDZ, has minimal to no impact on results.

(3) Changing the relative gas permeability model to the cubic power relationship resulted in minor differences.

(4) Increasing the diffusion coefficient had a dramatic effect on results. Greater diffusion of dissolved gas away from the canister resulted in greater dissolution of gas near the canister. This reduced the gas pressure, halting free phase gas migration towards the access drift.

5. MODULE-SCALE MODEL

5.1 MODELLING APPROACH

5.1.1 Grid

A 3D grid was developed, representing the entire model domain. Figure 40 shows the model domain, with boundary conditions, cells and drifts.

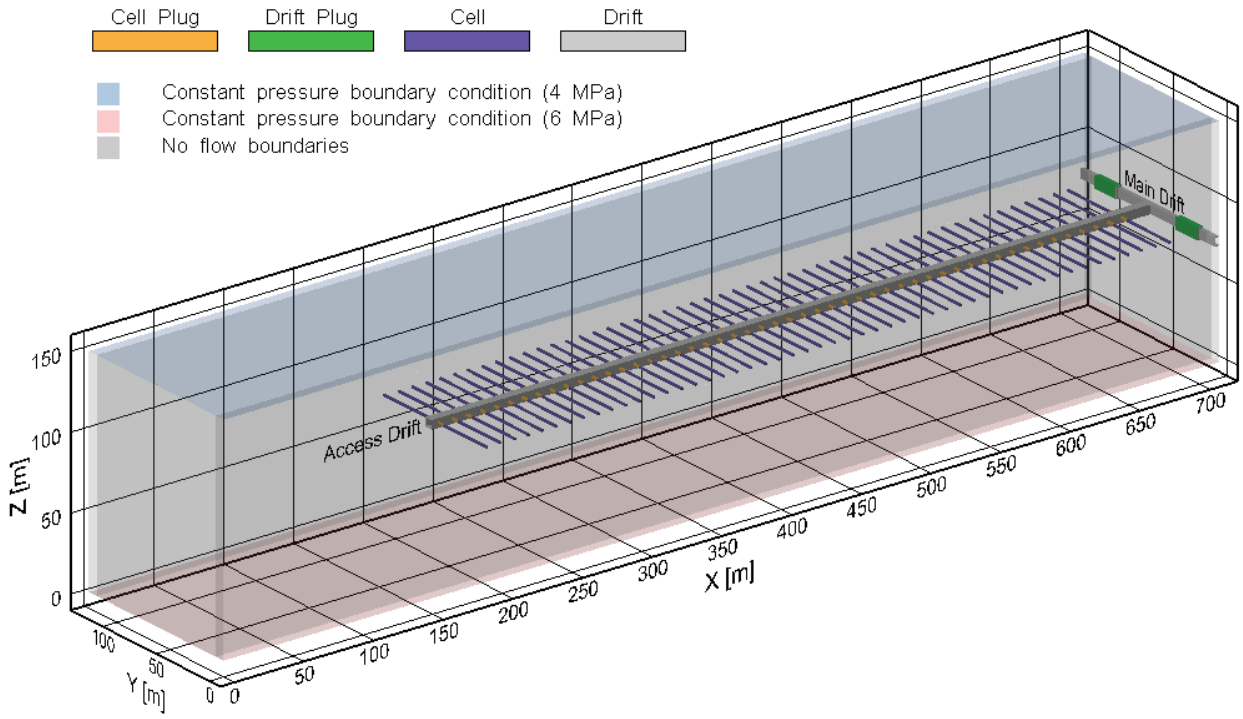

Note: Variable pressure and saturation boundary conditions exist at the upstream (Y= 0) and downstream (Y= 126) ends of the main drift.

Figure 40: 3D Model Domain With Boundary Conditions, Cells and Drifts

The greatest challenge in developing this grid was to obtain sufficient representation of the repository details while maintaining a grid of tractable size. Initial attempts at gridding, which included some simplifications for the very thin interface, produced grids that were much too large for standard TOUGH2. While TOUGH-MP, which allows much larger grids than TOUGH2, was capable of simulating these large grids, the cumbersome size and complexity of these grids resulted in difficulties in isolating problems with the grid and model set-up and these MP simulations were abandoned. Major simplifications were required to develop a tractable grid, and after several iterations, the following simplifications were adopted:

(1) The cells were represented as rectangular in cross-section, with equivalent cross-sectional areas to the circular cells defined in the benchmark. Using rectangular-shaped cells allows for significantly fewer grid elements, producing an overall grid of tractable size. The impact of this grid simplification was not examined.

(2) Interface materials were combined with adjacent materials to provide tractable discretization. The impact of combining the interface with the EDZ was examined with the cell-scale model. However, the cell-scale model was not capable of judging the impact of upscaling the interface in the drifts or drift plug. The details of the interface combinations are as follows:

   a) The interface between the cell canisters and the EDZ was combined with the EDZ. The cell EDZ was divided into two components: (1) an inner EDZ which represents the combination of interface and EDZ, and (2) an outer EDZ which represents the EDZ alone. The inner EDZ of the cells was represented as a single element in the middle of the cell. Block volumes and areas were adjusted to represent the actual volumes and areas of the inner EDZ surrounding the waste. The benchmark specifies the waste canisters as impermeable to gas and water. Figure 41 shows a detailed cross-section of the discretization of a cell.

   b) The interface between the cell plug and the EDZ was combined with the EDZ, as above. Figure 42 shows a detailed cross-section of the discretization of the cell plug.

   c) The interface between the drift backfill and the EDZ was combined with the backfill in a 0.5 m width block on the edges of the drift (both access and main drifts). Figure 43 shows a plan-view of the discretization of the access drift, and Figure 44 shows a plan-view of the discretization of the main drift.

   d) The interface between the main drift plug and the host rock was combined with the bentonite plug, also shown in Figure 44.

(3) EDZ and the interface at the end of the access drift are ignored (the far end from the main drift). This omission is expected to be inconsequential, as gas and water are expected to flow towards the main drift.

(4) The bentonite plugs in the main drift were shifted 5 m towards the access drift, to minimize discretization in the y direction. The length of the bentonite plugs remains unchanged at 20 m. The impact of this change is likely negligible.

The resulting grid has 121 847 nodes and 404 166 connections. This is still a very large grid for TOUGH2, and was terminated at 30 000 years after a run time of five weeks. It should be emphasized that sensitivity of the simulation to the above simplifications were not examined.

It should also be noted that the irregular grid of the final model does not strictly adhere to the TOUGH2 integral finite difference requirements; some nodal connections are not perpendicular to the connection area, resulting in shorter connection distances for these connections. The impact of these inaccuracies is expected to be small, and this has been confirmed at the cell-scale (see Section 4.1.1).

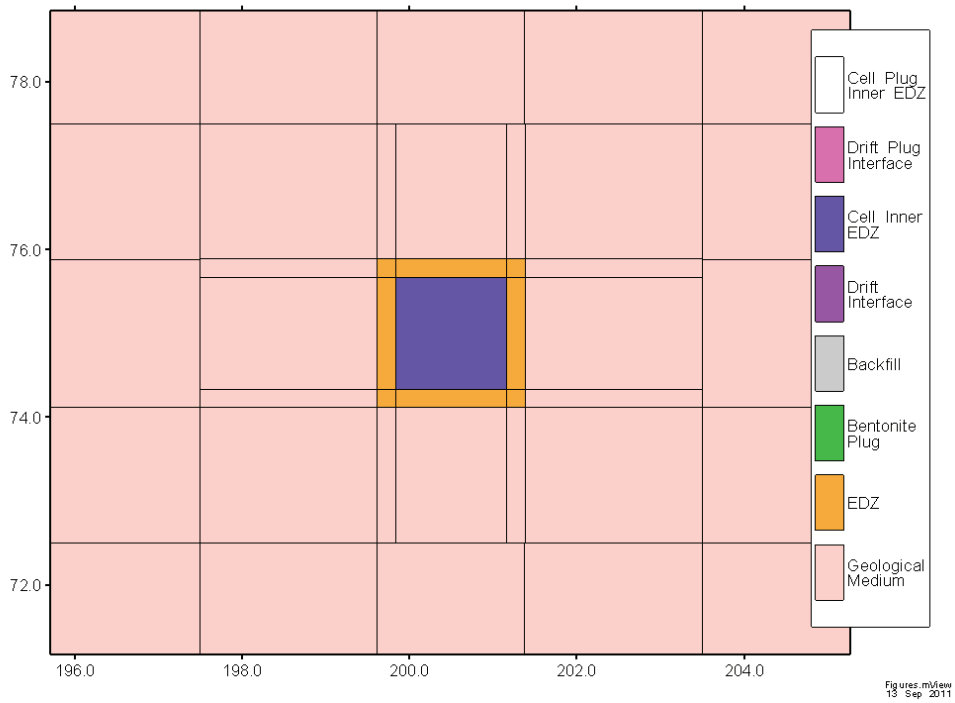

Note: Cell areas and volumes for the inner cell EDZ have been corrected to remove the inactive waste containers, as described in the text.

Figure 41: Grid Discretization Detail: Cross-Section of a Cell

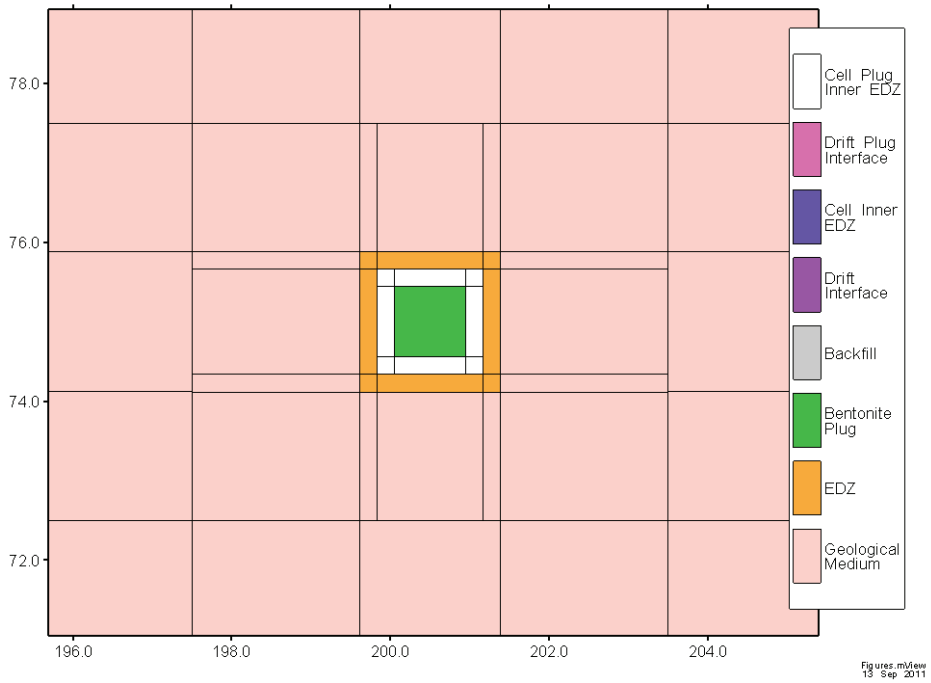

Figure 42: Grid Discretization Detail: Cross-Section of a Cell Plug

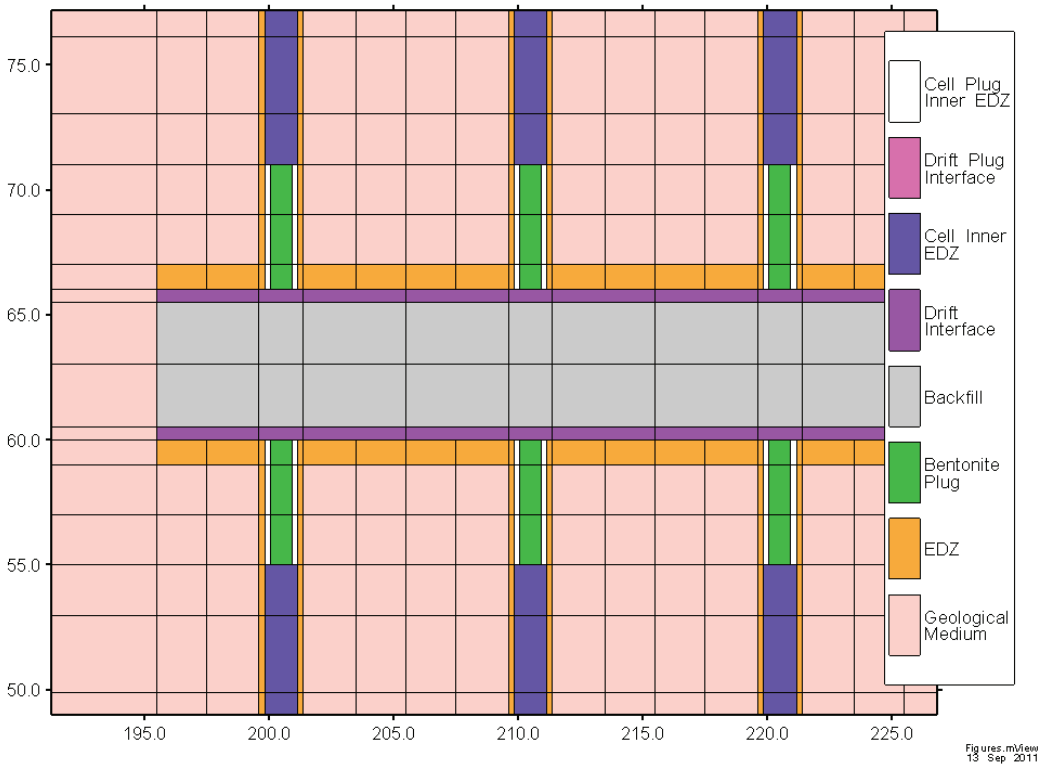

Figure 43: Grid Discretization Detail: Plan View of the Access Drift

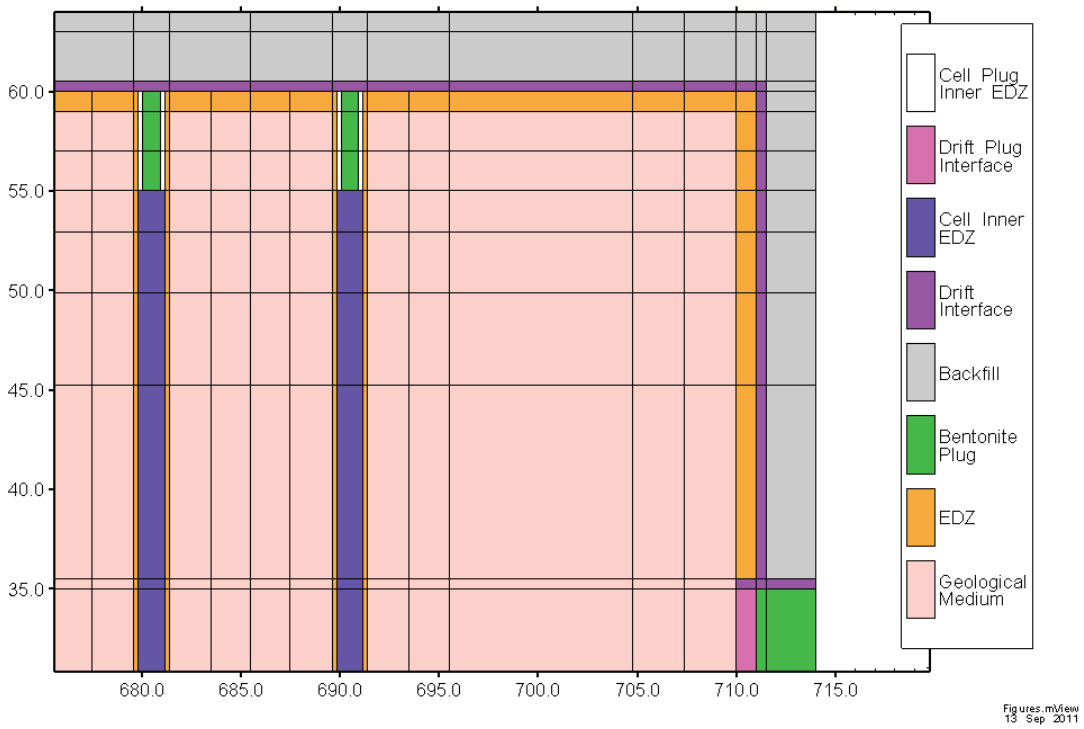

Figure 44: Grid Discretization Detail: Plan View of the Main Drift

5.1.2 Boundary Conditions and Sources

Constant pressure and zero gas saturation boundary conditions are specified on the top and the bottom of the model, at 4 MPa on the top boundary and 6 MPa on the bottom boundary. Variable saturation and pressure boundary conditions are specified at the upstream (Y=0 m) and downstream (Y=126 m) ends of the main drift (see Figures B-10 and B-11 in Appendix B for gas and water pressures at the boundary condition, gas saturations are calculated from the difference in gas and water pressure or capillary pressure). The boundary conditions at the upstream and downstream ends of the main drift are almost identical, with the exception of very slightly greater pressures at the upstream end between 400 and 30 000 years.

As the waste canisters were not included in the model, gas generation was specified at all inner EDZ nodes of the cell (properties a combination of interface and EDZ). The generation term was proportioned between nodes according to the block volume of the generation node.

5.1.3 Initial Conditions

Initial conditions in the host rock and EDZ are linearly interpolated pressures between the top and bottom boundaries, approximately 5 MPa at the repository horizon, and fully water saturated. In repository features, initial gas pressure is atmospheric and water saturation is 5% in the interfaces and 70% in the drift backfill and bentonite plugs. Initial conditions for upscaled materials are presented in the following section.

5.1.4 Deviations from the Benchmark Specification

Several deviations from the benchmark specification are detailed in the gridding section. Upscaled parameters associated with the interface gridding simplifications were developed by weighting parameters by the relative volume of the contributing materials. For example, for the cell inner EDZ, with an interface 1 cm thick and an inner EDZ block 25 cm thick, the porosity (θ) was calculated as follows:

$$\boldsymbol{\theta_{inner\ edz} = \theta_{interface}\frac{0.01}{0.25} + \theta_{edz}\frac{0.24}{0.25}} \qquad \textbf{Equation 4}$$

Log weighting was used for the van Genuchten air-entry pressure parameter, as a simple linear average resulted in a curve with capillary pressures at very high liquid saturations slightly greater than capillary pressures in the EDZ or interface (see Figure 45). This effect is due to the linear weighting of the van Genuchten shape parameter, n, in addition to the air-entry pressure. Using log weighting for the air-entry pressure resolves the issue without much change to the overall shape of the curve, as shown in Figure 45. The van Genuchten capillary pressure function described by the benchmark and used in the modelling is provided below:

$$P_c = -\frac{1}{\alpha}\left[S*^{-1/m} - 1\right]^{1/n} \qquad \textbf{Equation 5}$$

$$S* = \frac{S_l - S_{lr}}{1 - S_{lr}} \qquad \textbf{Equation 6}$$

where:
P_c is the capillary pressure, Pa;
S* is the effective saturation for the capillary pressure relationship (volume ratio);
S_l is the liquid saturation (volume ratio);
S_{lr} is the residual liquid saturation (volume ratio);
m is a van Genuchten fitting parameter (unitless), equivalent to m = 1 – 1/n;
n is a van Genuchten fitting parameter (unitless); and
α is a van Genuchten fitting parameter, Pa-1. $1/\alpha$ is the air-entry pressure parameter.

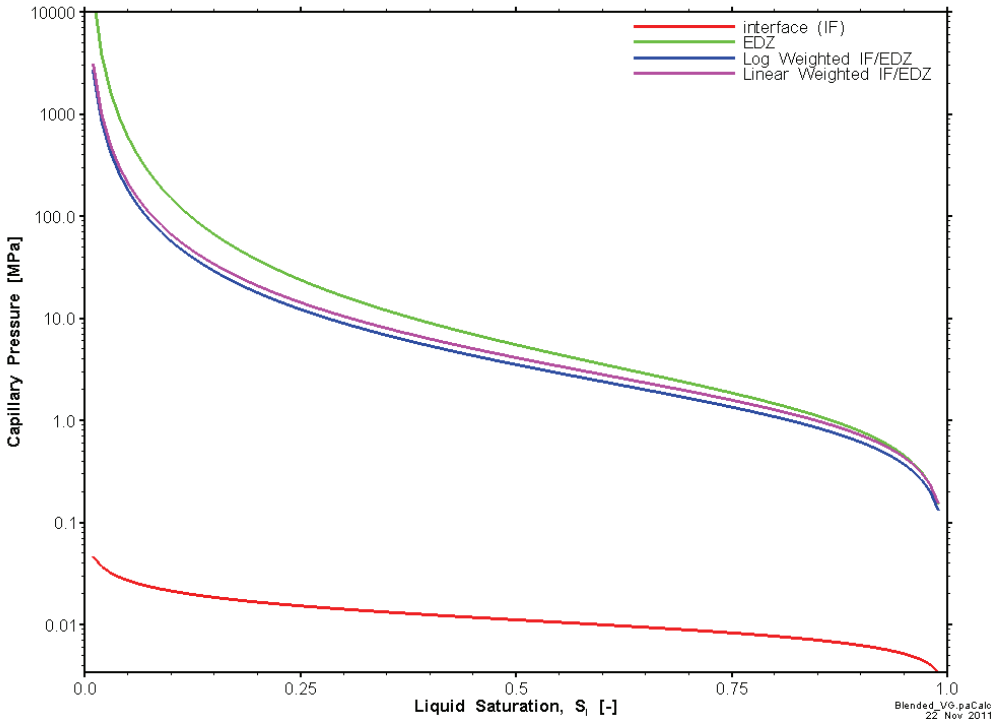

Figure 45: Capillary Pressure Curve for Cell Interface, EDZ and Cell Inner EDZ (Combined Interface and EDZ)

Table 2 provides the final parameters for upscaled interface materials. Table 2 also contains the initial conditions within the upscaled interface materials. These initial conditions are determined in the same manner as the parameters, weighted according to the relative volume of the contributing materials. Note that initial pressure conditions were not weighted: all materials with a partial saturation, including upscaled interface materials, were assigned a gas pressure of 0.1 MPa.

Table 2: Parameters and Initial Conditions for Upscaled Interface Materials

	Permeability [m^2]	Porosity [-]	Pore Compressibility [Pa^{-1}]	Tortuosity [-]	S_{lr} [%]	S_{gr} [%]	n [-]	P_o [Pa]	Initial Water Saturation [%]
Inner cell EDZ	4.0E-14	0.18	1.06E-09	0.28	0	0	1.60	1.23E6	96.2
Inner plug EDZ	5.0E-18	0.16	1.10E-09	0.28	0	0	1.60	1.23E6	96.2
Main Drift Plug Interface	6.0E-20	0.35	8.24E-10	0.06	0	0	1.62	1.49E7	69.35
Drift Interface	6.9E-17	0.40	2.06E-09	0.27	0	0	1.55	1.80E6	68.7

Once the initial case (the base case) was working, an additional case was simulated with more conventional upscaled parameters. This simulation is not presented as the base case as it was less stable, and only completed to 7000 years. These improved upscaled parameters were developed as follows:

- Scalar parameters, such as porosity, were calculated using a volumetric weighting approach, as described above.
- Tensor parameters, such as permeability, used an arithmetic average when component materials were layered parallel to the direction of the tensor and a harmonic average when component materials were layered perpendicular to the direction of the tensor.
- Van Genuchten shape parameter n was held constant (assumes relative permeability in the interface is the same as in the EDZ, backfill or bentonite), while the van Genuchten air entry pressure was calculated using the volumetric weighting approach of a scalar parameter.

The alternative case parameters are provided in Table 3, only for parameters that differ from the base case.

Table 3: Alternative Parameters for Upscaled Interface Materials

	Kx [m^2]	Ky [m^2]	Kz [m^2]	n [-]	P_o [Pa]
Inner cell EDZ	5.2E-18	4.0E-14	5.2E-18	1.5	1.44E+06
Inner plug EDZ	5.0E-18	5.0E-18	5.0E-18	1.5	1.44E+06
Main Drift Plug Interface	1.0E-20	6.0E-20	1.0E-20	1.6	1.58E+07
Drift Interface	6.9E-17	6.9E-17	5.1E-17	1.5	1.96E+06

Another deviation from the benchmark is the relative gas permeability model, as described for the cell-scale model in Section 4.1.4.

5.2 MODELLING RESULTS

5.2.1 Base Case Results

The module-scale model is only complete to approximately 30 000 years. The simulation time step became very small due to numeric instabilities associated with the very small gas saturations disappearing from the system.

Output points and slices presented below correspond to those defined in the benchmark, including:

(1) Evolution of mass flows across surfaces in the cells, access drifts and main drifts as shown in Figure 46, where gas flows are assumed positive for flow along the cell (F-C, flow-cell) towards the access drift, along the access drift (F-D, flow-drift) towards the main drift, or along the main drift (F-P, flow-plug) from the upstream to downstream boundary condition; and
(2) Evolution of water saturation, gas pressure and water pressure at different times along lines as shown in Figure 47 and at specified points as shown in Figure 48.

Note that in the subsequent figures showing gas saturation, white space indicates areas where gas saturations are below the legend threshold of 1E-6, often at zero gas saturation. For figures showing gas pressure, white areas indicate areas where there is no gas phase, and therefore no gas pressure.

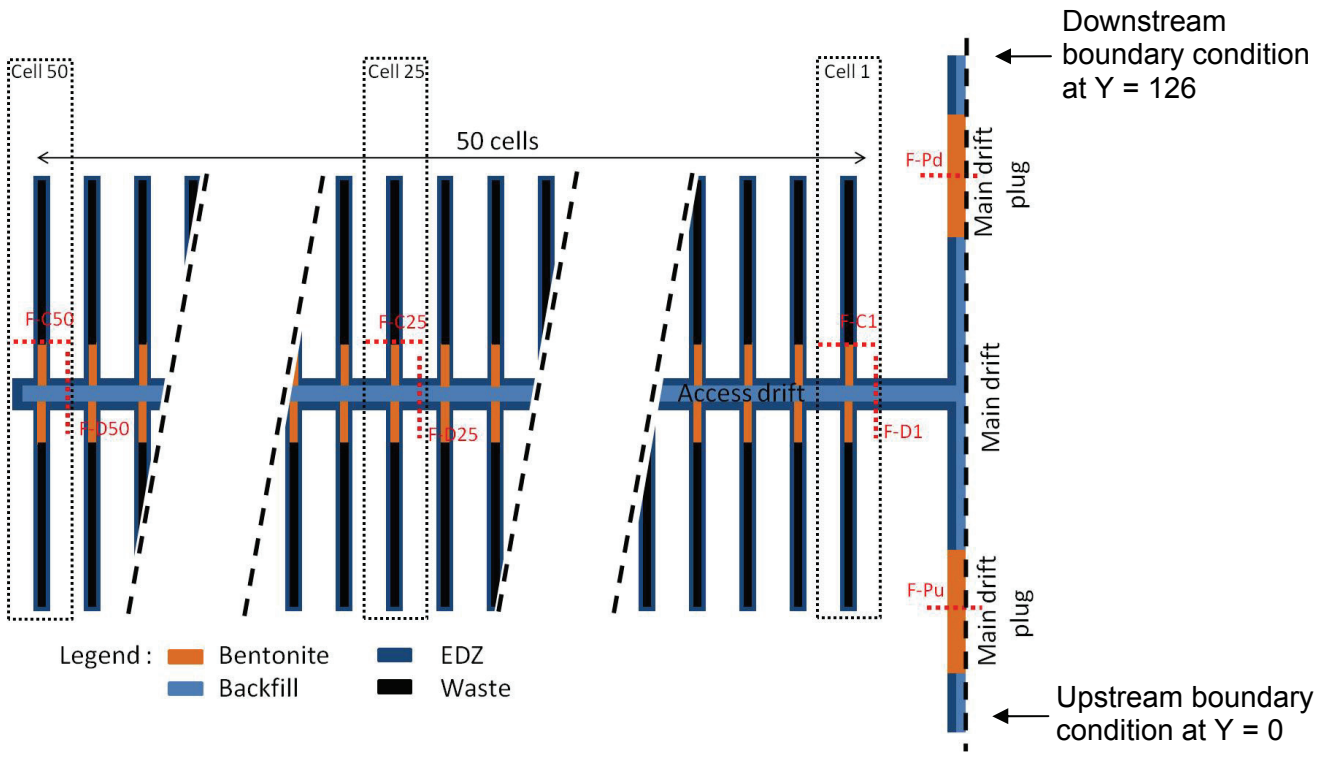

Note: Positive flow denotes flows along the cell (F-C) towards the access drift, along the access drift (F-D) towards the main drift, and along the main drift (F-P) from the upstream to downstream boundary condition. Figure duplicated from benchmark description in Appendix B.

Figure 46: Location of Surfaces at Which Evolution of Mass Flow With Time Is Presented

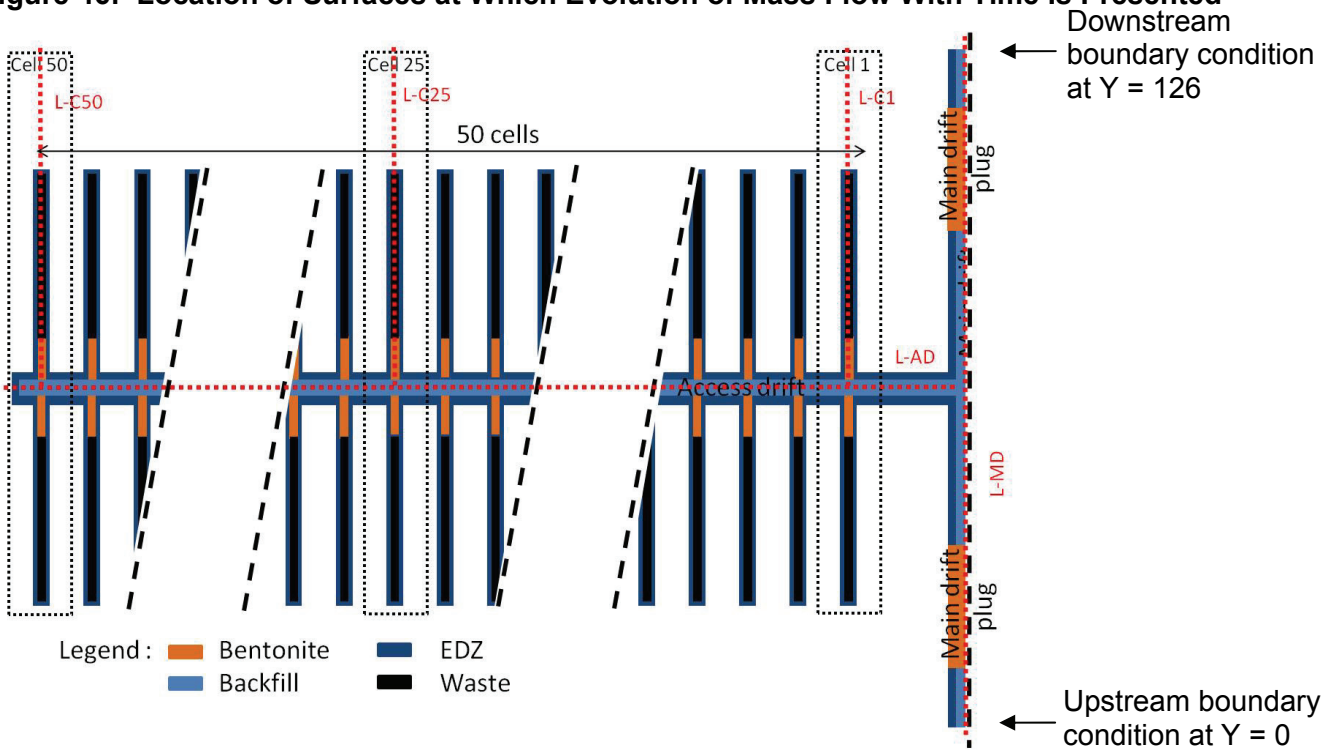

Figure duplicated from benchmark description in Appendix B.

Figure 47: Location of Lines at Which Evolution of Water Saturation and Pressures at Different Times Is Presented

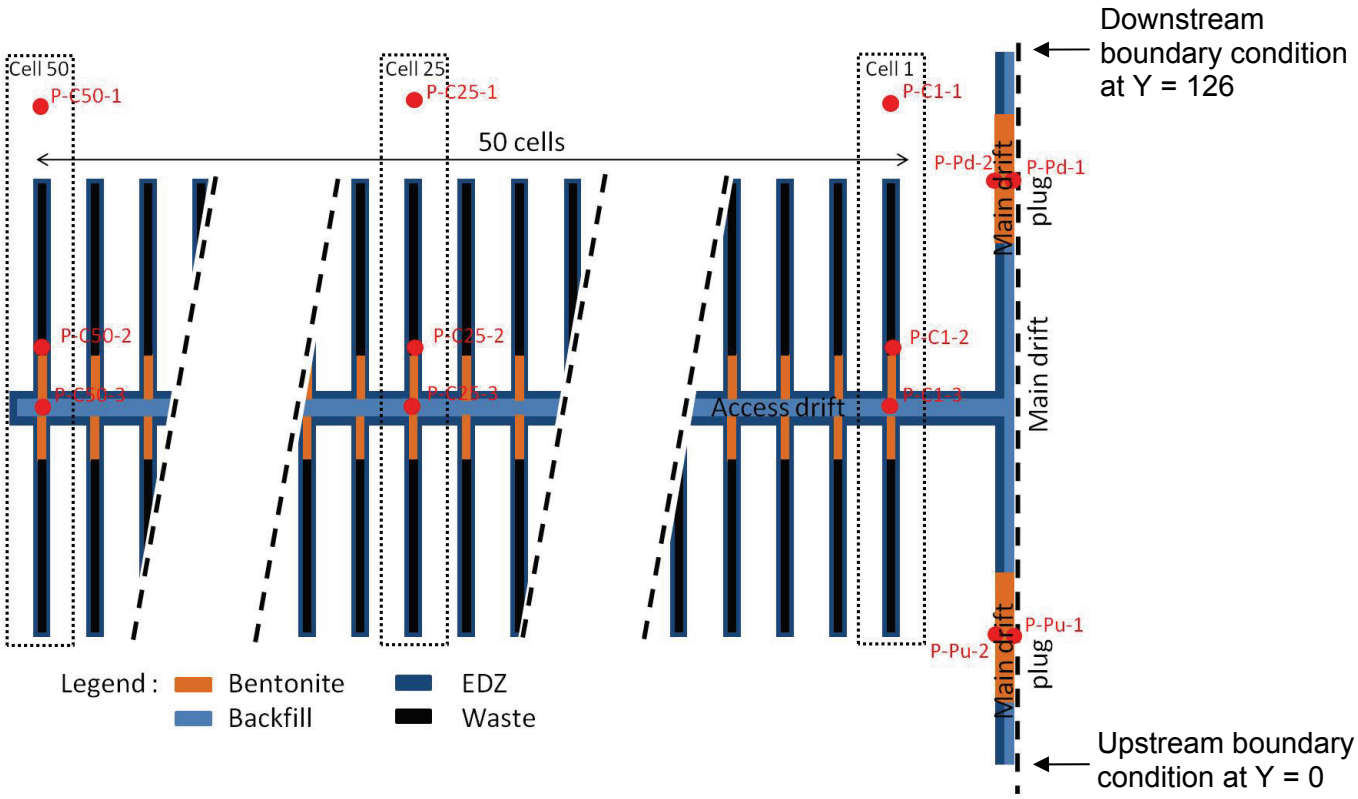

Figure duplicated from benchmark description in Appendix B.

Figure 48: Location of Points at Which Evolution of Water Saturation and Pressures with Time Is Presented

Immediately apparent at 1 year (see Figure 49) is the absence of gas in the cell interface and EDZ, despite the generation of a gas phase in the cells. This is a result of the dissolution of the gas initially present in the interface (less than 5% initial gas) and the negative water pressures, i.e., suction, in the cells (as a result of the initial gas pressure equal to 0.1 MPa) causing the immediate dissolution of any gas phase generated. As the cell water pressures increase, the generated gas remains in the gas phase, and the gas saturation increases above zero. Gas is still present in the drifts at 1 year due to the greater amount of initial gas in the drifts (approximately 30% initial gas).

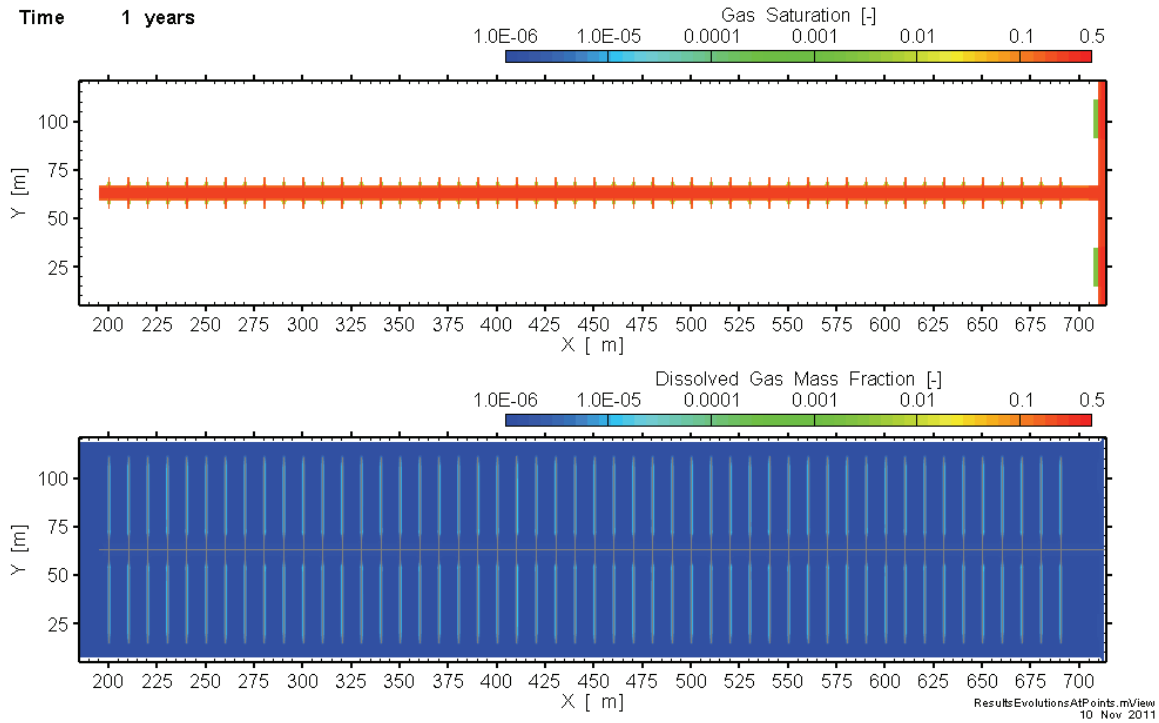

Figure 49: Gas Saturation and Dissolved Gas Mass Fraction at 1 Year, at a Plan Slice Through the Middle of the Repository

Over time, it is also apparent that the boundary conditions at the upper and lower ends of the main drift do not seem to correspond to conditions within the cells and access drift. Two processes are modelled by the main drift boundary condition (see gray line in Figure 50 and Figure 51 for the boundary condition):

(1) Between 1 and 1000 years, there is a drop in water saturation and water pressure, identical in both the upstream and downstream boundary conditions. Presumably, this is due to the bentonite plugs in the main drift, with their very high capillary pressures drawing water into the plugs during resaturation.

(2) Between 400 and 30 000 years, pressures upstream (Y=0) are slightly greater than downstream (Y=126). Note that the difference is so small, it is not apparent on the plot. Based on this pressure difference and the location of the module within the repository, it would be expected for water and gas to flow along the main drift from the upstream to the downstream boundary.

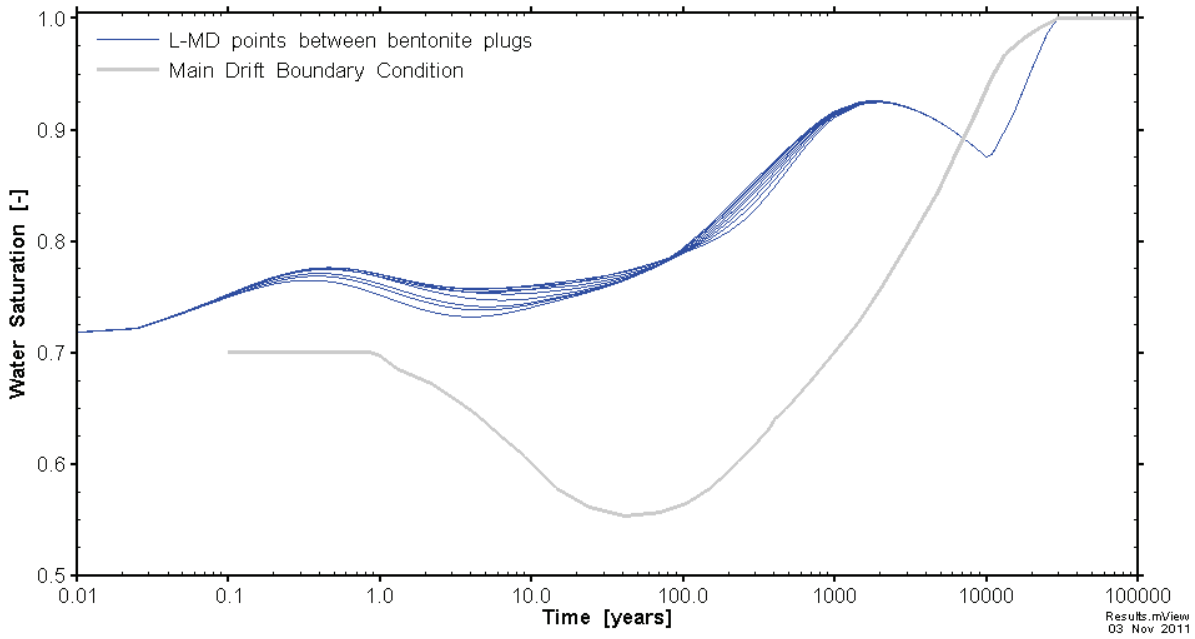

Figure 50: Water Saturation With Time at L-MD Points Between the Bentonite Plugs (Y= 35 to Y= 90), Compared to the Main Drift Boundary Condition

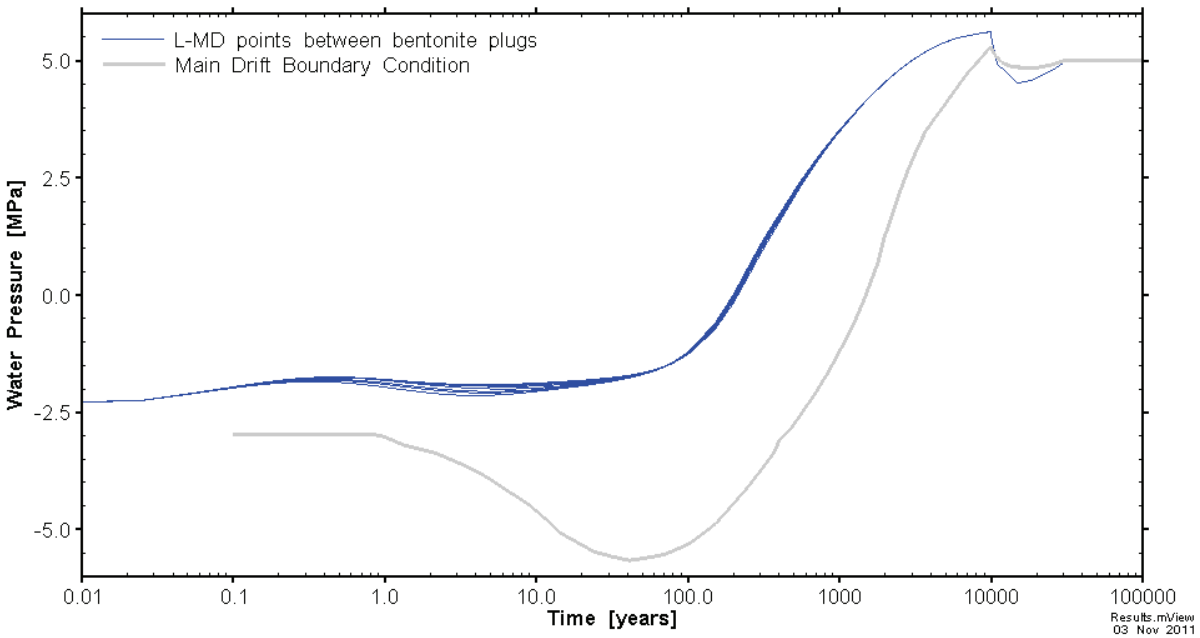

Figure 51: Water Pressure With Time at L-MD Points Between the Bentonite Plugs (Y= 35 to Y= 90), Compared to the Main Drift Boundary Condition

Water saturation and water pressure along the L-MD line (a line along the center of the main drift), shown in Figure 52, best illustrates the differences between the module main drift, defined as the main drift between the bentonite plugs (Y=35 to Y=90), and the main drift boundary conditions. Note that the low initial capillary and water pressures between Y=15 to Y=35, and between Y=90 and Y=110 are due to the bentonite plugs in the main drift. Two additional figures, Figure 50 and Figure 51, show water saturation and water pressure with time at all the module main drift points in the L-MD line between the bentonite plugs, compared to the main drift boundary condition. In the main drift, water saturates the drifts until approximately 0.5 years, when a small dip in water saturation of approximately 3% is observed, due to the bentonite drawing water as described above. Water saturations return to the same level as at 0.5 years by approximately 80 years. There is a small corresponding drop in water pressure of approximately 0.4 MPa. Generally, the model drift resaturates and water pressures equilibrate towards host rock pressures more rapidly than expressed by the boundary condition.

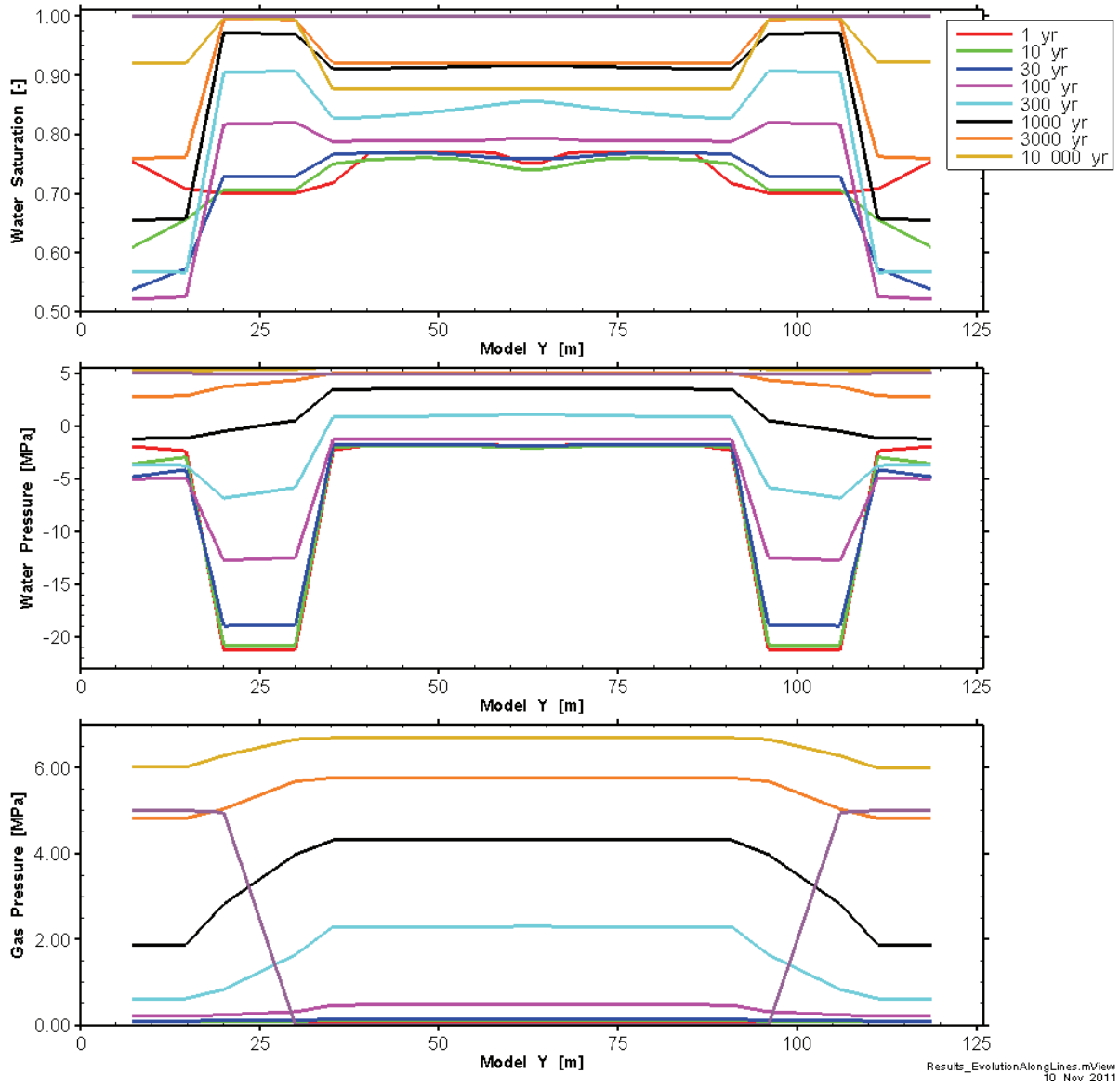

Figure 52: Evolution of Water Saturation, Water Pressure and Gas Pressure for Various Times Along the L-MD Line

This incongruence in the boundary condition causes gas and water from the module to flow towards both the upstream and downstream boundary conditions for the first 10 000 years, as shown by the F-P flows in Figure 53. After 10 000 years when gas generation ceases, water begins to flow in from the boundary conditions. As well, since prior to 10 000 years pressures at the boundary condition are considerably lower than the module, a strong pressure gradient develops between the ends of cell 1 and adjacent cells and the boundary condition, resulting in gas flow in these cells away from the access drift and towards the boundary condition (see gas saturations at 700 years in Figure 54). Once gas has penetrated the host rock, gas flows from the cells through the host rock towards the boundary condition.

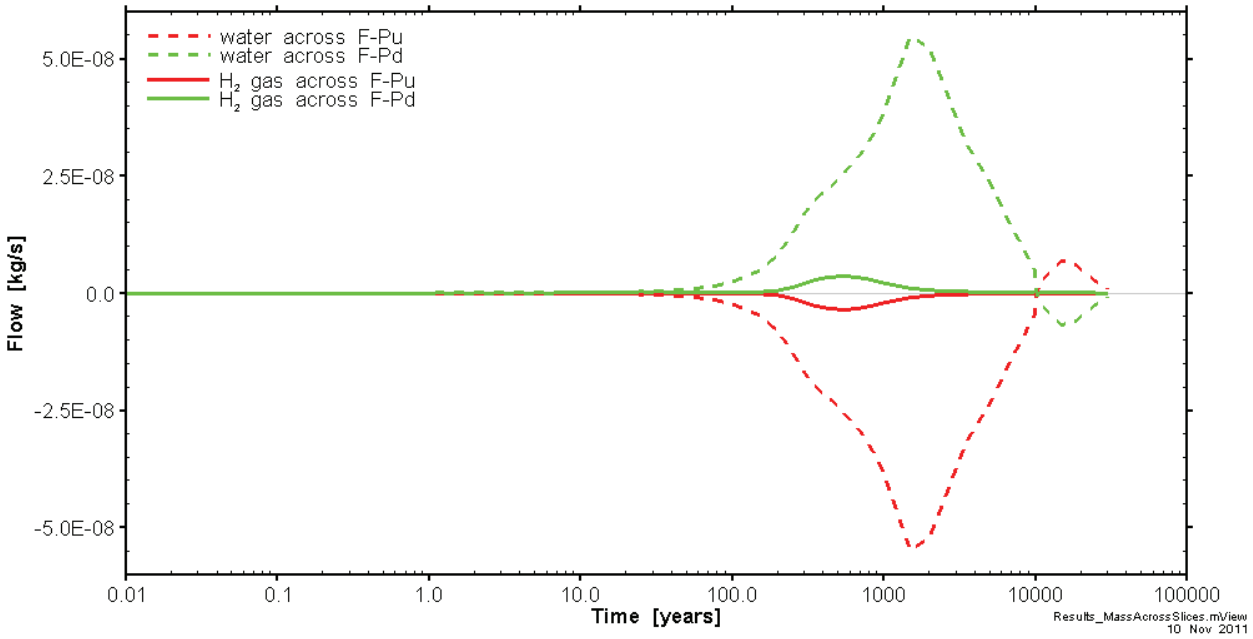

Figure 53: Evolution of Water and H2 Gas With Time Across F-P Surfaces

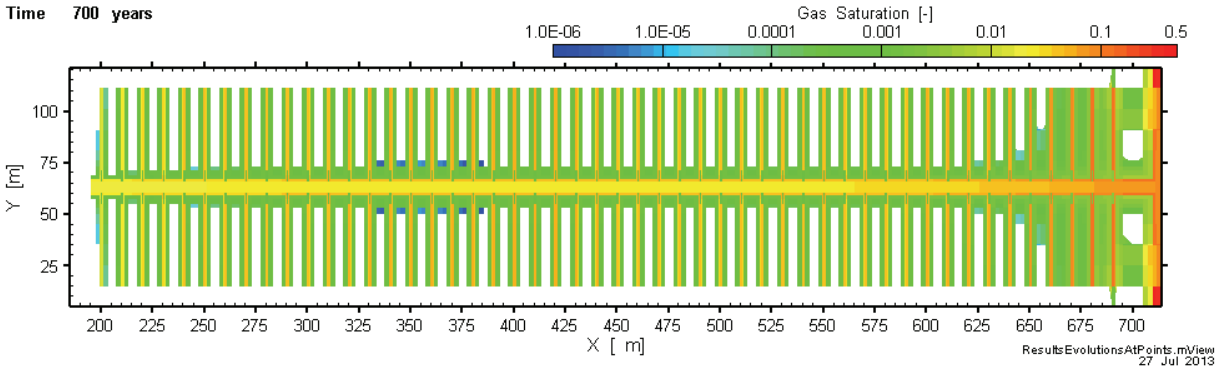

Figure 54: Plan View of Gas Saturations at 700 Years, Through the Middle of the Repository

Note that after 1000 years, water saturation begins to drop in the module (see Figure 50) due to gas generated in the repository flowing out to the main drift but impeded from flowing out of the main drift (through to the boundary conditions) by the bentonite blocks in the main drift. The decrease in module water saturation after 1000 years in Figure 50 is correctly not represented by the main drift boundary condition, due to the presence of the bentonite blocks preventing transmission of gas along the main drift.

For the first 1000 years, water and hydrogen gas generated within the cells travel towards the access drift, along the access drift and to the main drift. Water and gas flow across slices in the cells, access drift and main drift are shown in Figure 55 through Figure 58. Note the exception at Cell 1 (F-C1) in Figure 57, where at approximately 350 years the gas flow direction turns away from the access drift and towards the main drift boundary through the host rock. This is a consequence of the main drift boundary condition, as described above. Both water and gas flows divide in the main drift and flow towards both the upstream and downstream boundary conditions, as shown by F-Pu (upstream) and F-Pd (downstream) in Figure 56 and Figure 53. This is due to the difference between the boundary conditions and the equilibration of module water pressures (i.e., module pressures rise more rapidly than the prescribed boundary pressures in the main drift, due to equilibration of pressure in the module with the formation pressure, as explained above).

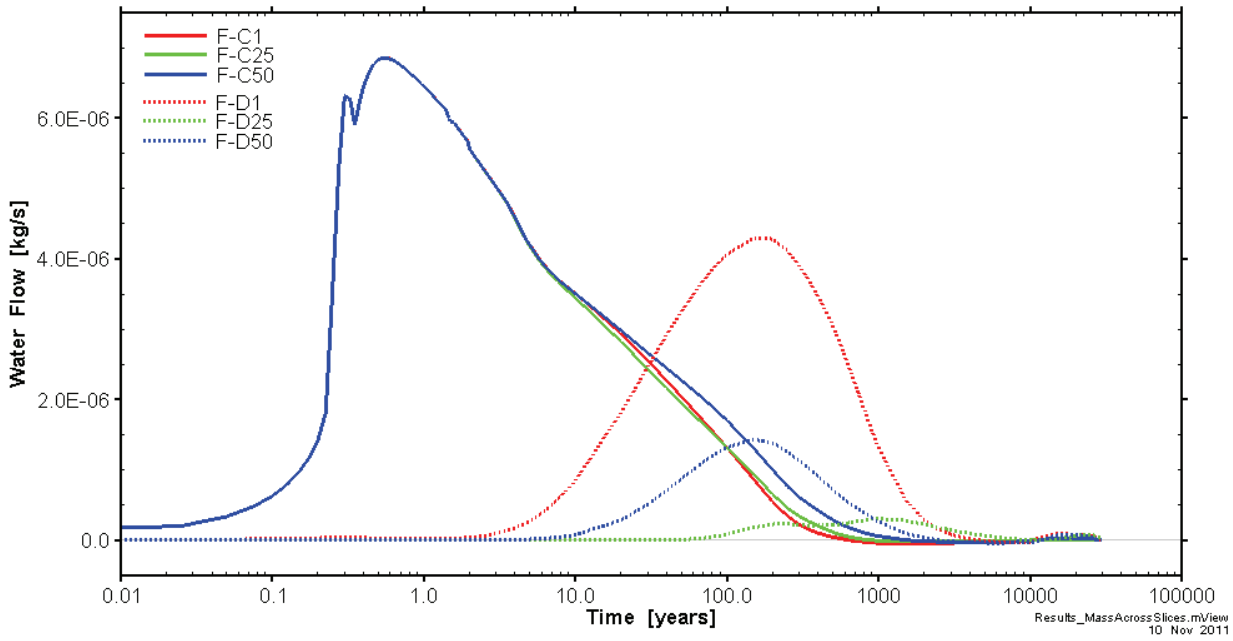

Figure 55: Evolution of Liquid Water With Time Across F-C (Cell) and F-D (Access Drift) Surfaces

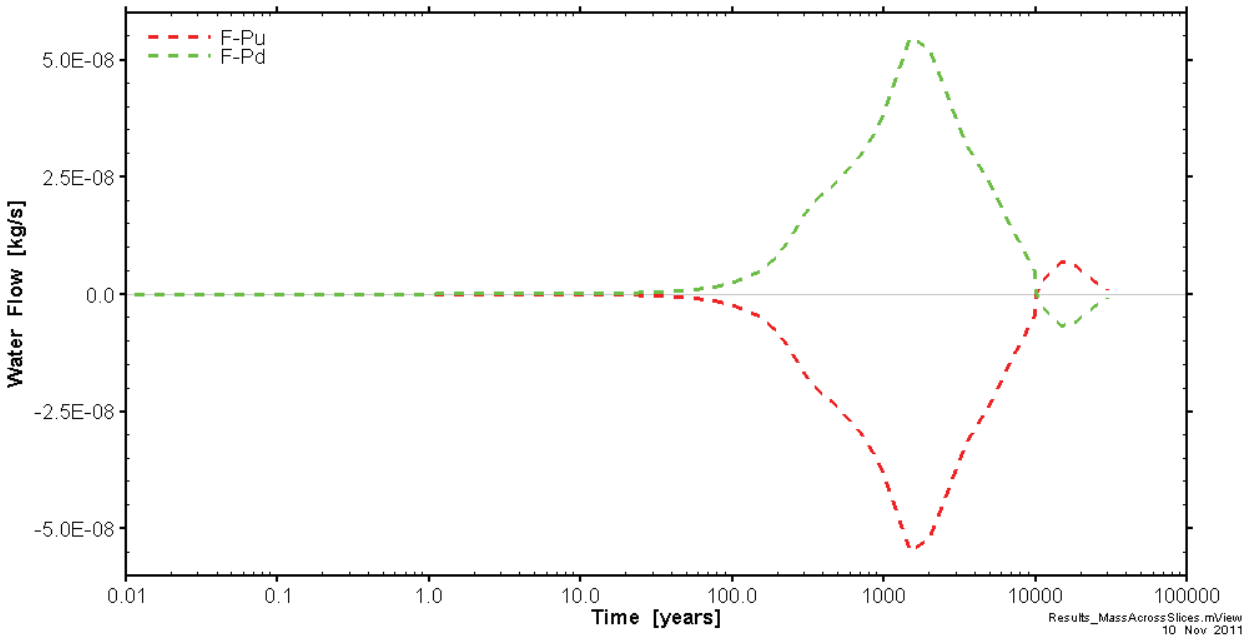

Figure 56: Evolution of Liquid Water With Time across F-P (Main Drift) Surfaces

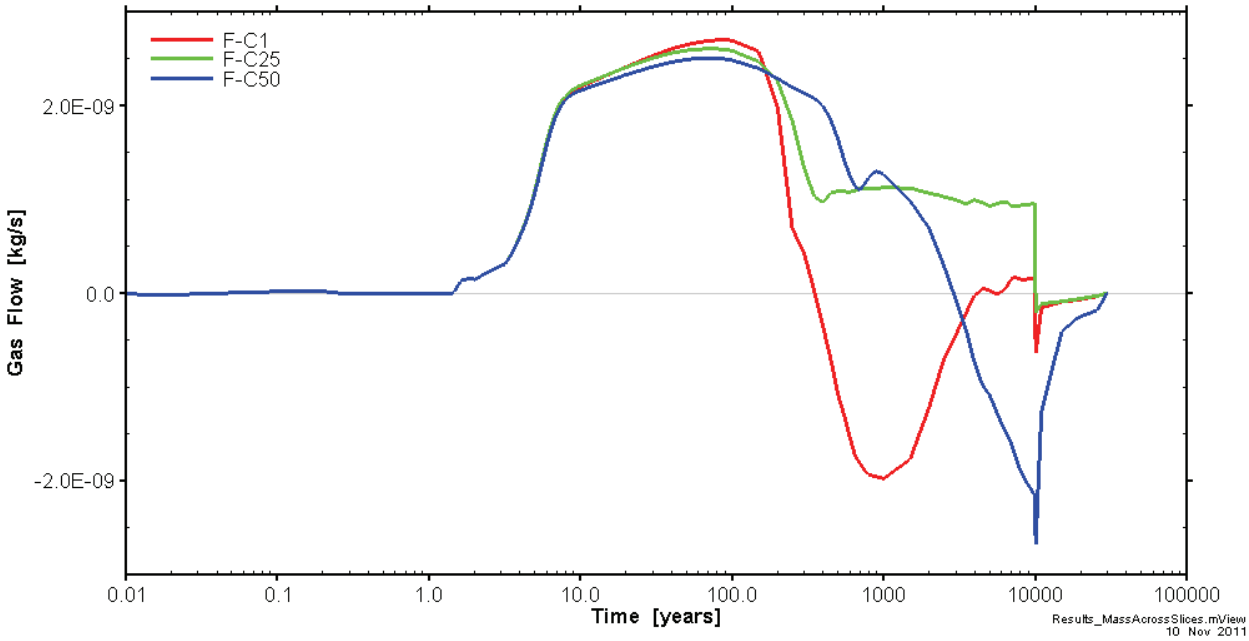

Figure 57: Evolution of Gas With Time Across F-C (Cell) Surfaces

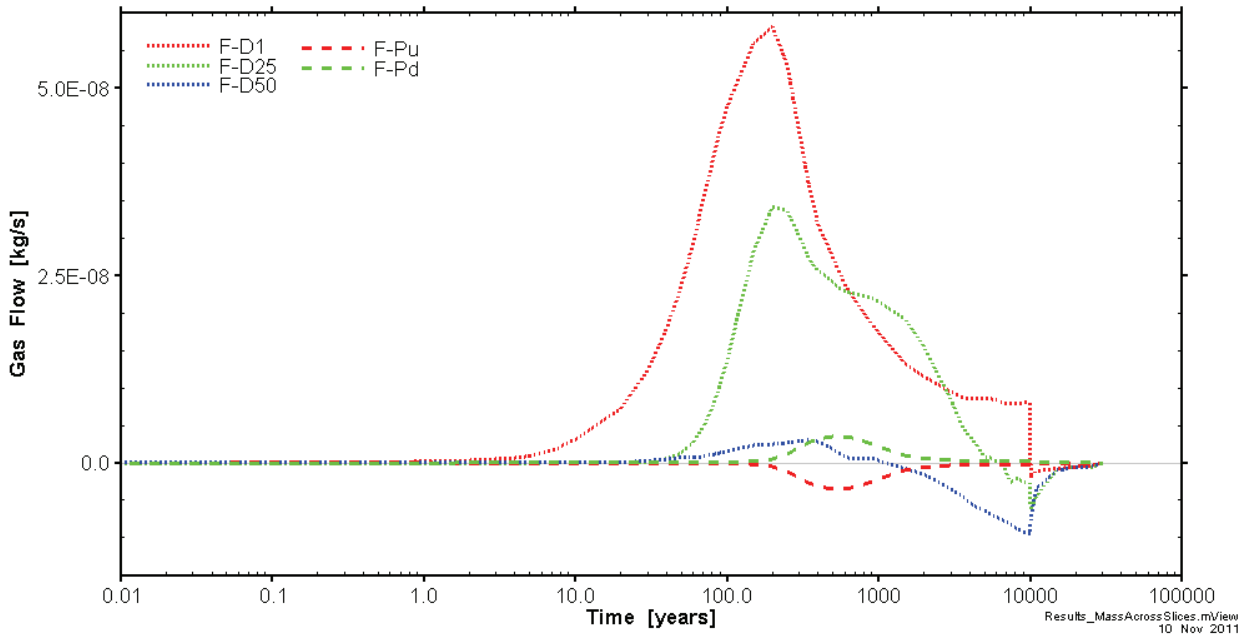

Figure 58: Evolution of Gas With Time Across F-D (Access Drift) and F-P (Main Drift) Surfaces

Gas flow in the access drift is least near Cell 50 (F-D50), farthest from the main drift, and greatest near Cell 1 (F-D1), closest to the main drift, as F-D1 has collected the gas from all the cells along the drift (Figure 58). The same pattern is not repeated for the water flows, as water flows in the access drift near the middle cell (F-D25) are the smallest flows (Figure 55). This somewhat odd pattern of water flows is due to the water pressure gradients along the access drift. Water pressures at all points in the system are shown in Figure 59, with water pressures in the access drift described here represented by the dark blue lines. There is very little difference in water pressure within the access drift between Cell 50 and Cell 25 until approximately 50 years, when water flows begin to increase at Cell 25. The water pressure difference remains small, as does the water flow at Cell 25, compared to the water pressure difference between Cell 1 and Cell 25. Water pressures equilibrate more quickly in the middle of the module and farthest from the main drift (short and long dashed red, green and blue lines in Figure 59), due to boundary condition effects close to the main drift, and results in low pressure gradients in the middle of the module. For cells farthest from the main drift, differences in water pressure between the module and the host rock along the whole length of Cell 50 result in greater water gradients and therefore greater water flows at Cell 50 (F-C50 after 20 years and F-D50).

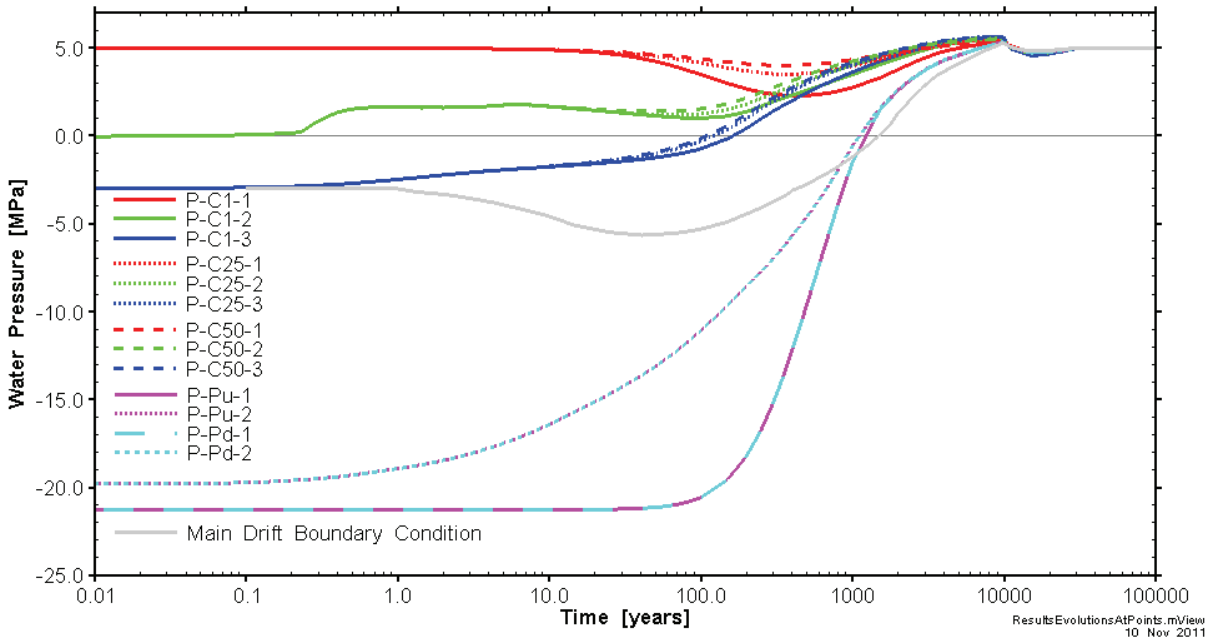

Figure 59: Water Pressures at All Output Points

Gas and water flow directions begin to change after 1000 years (Figure 55 to Figure 58), as gas and water pressures in the repository increase. Gas pressures increase due to gas generation and the impedance of gas transport out of the module by the bentonite seals in the main drift. Water pressures increase due to equilibration with the surrounding host rock. Water pressures at all output points are shown in Figure 59, and gas pressures in Figure 60. Around the time gas and water pressures at the cells reach adjacent host rock pressures of approximately 5 MPa, water and gas flows begin to reverse direction, and flow away from the access drift and the main drift, and into the host rock. This is evident in the gas flows at Cell 50 (F-C50 in Figure 57 and F-D50 in Figure 58) and Cell 25 (F-D25 in Figure 58). Water flows in all cells and the access drift at Cell 1 and Cell 50 are also slightly negative after 1000 years, although it is difficult to observe in Figure 55. Water flows in the access drift continue to flow into the main drift. Note that, as previously described, pressures in the middle of the module (i.e., Cell 25) are less variable than at the edge of the module (i.e., Cell 50). Consequently, flow changes occur earlier at Cell 50 than at Cell 25, and for gas flow out of the cells and water flow in the access drift, the flow direction does not change at all at Cell 25 (F-C25 in Figure 57).

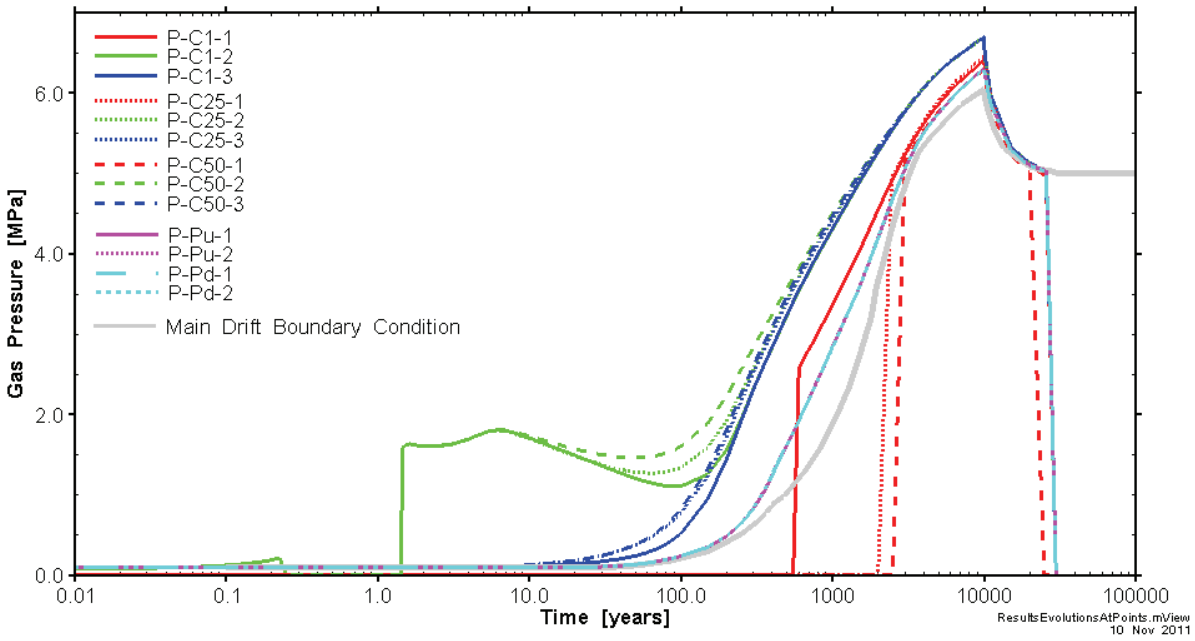

Figure 60: Gas Pressure at All Output points

There are some notable features of gas pressures in the cells (green lines for P-C1-2, P-C25-2 and P-C50-2 in Figure 60): the zero gas pressure around 1 year is due to zero gas saturations in the cells at that time; the relatively high gas pressure in the cells once the gas phase resumes in the cells at 1.5 years is due to the greater water pressures in the cells resulting from equilibration with the host rock while the cells were fully water saturated; the drop in gas pressure after 10 years is a result of the bentonite plugs at the end of each cell drawing water due to their high capillary pressures, with a corresponding drop in the gas pressure; and the delay in the drop in gas pressure is due to bentonite plugs preferentially sucking water from the adjacent host rock, until pressures in the host rock adjacent to the bentonite plugs decrease below pressures in the cells.

While the primary direction of gas flow before 1000 years is toward the main drift, some gas also travels outwards from the cells and drifts into the host rock. Starting close to the access drift, gas begins to migrate into the host rock by 100 years (see Figure 61). At 300 years (see Figure 62), gas migration into the host rock expanded along the cell away from the access drift, and at 1000 years (see Figure 63), gas penetrated all the host rock between cells for all cells except those farthest from the main drift. Near Cell 1 (closest to the main drift), boundary condition effects increased migration of gas into the host rock. For the remainder of cells, gas migration into the host rock occurred over a greater length of the cell (closest to the access drift) at cells near the middle and farthest from the main drift (i.e. cells between approximately X = 200 m to X = 525 m in Figure 62). This can be explained by the water pressures in the module: water pressures equilibrated more quickly in the middle of the module and farthest from the main drift as previously described, resulting in less water flowing into the cells, thus allowing gas to migrate outwards more easily. For cells farthest from the main drift, differences in water pressure between the module and the host rock along the whole length of Cell 50 resulted in sufficient water flow to delay gas flow into the host rock until approximately 3000 years (see Figure 64).

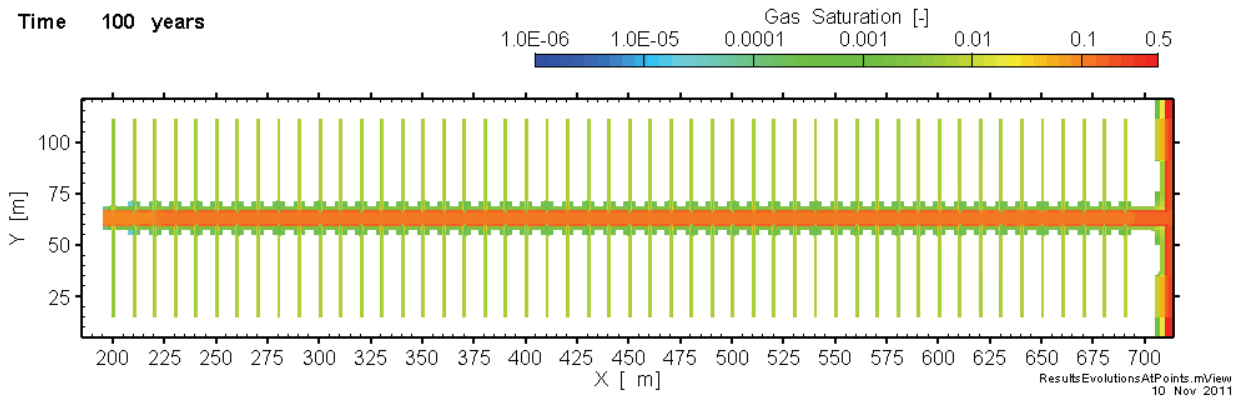

Figure 61: Gas Saturation and at 100 Years, at a Plan Slice Through the Middle of the Repository

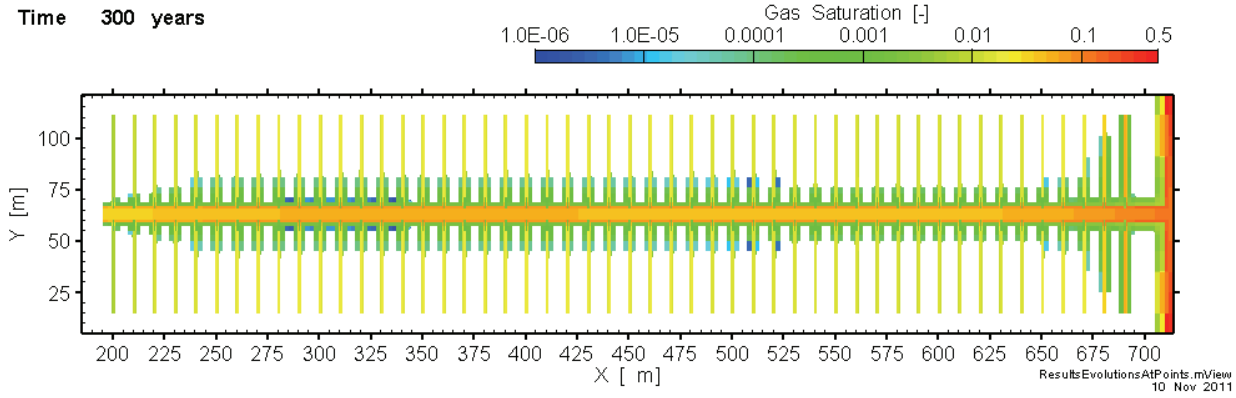

Figure 62: Gas Saturation and at 300 Years, at a Plan Slice Through the Middle of the Repository

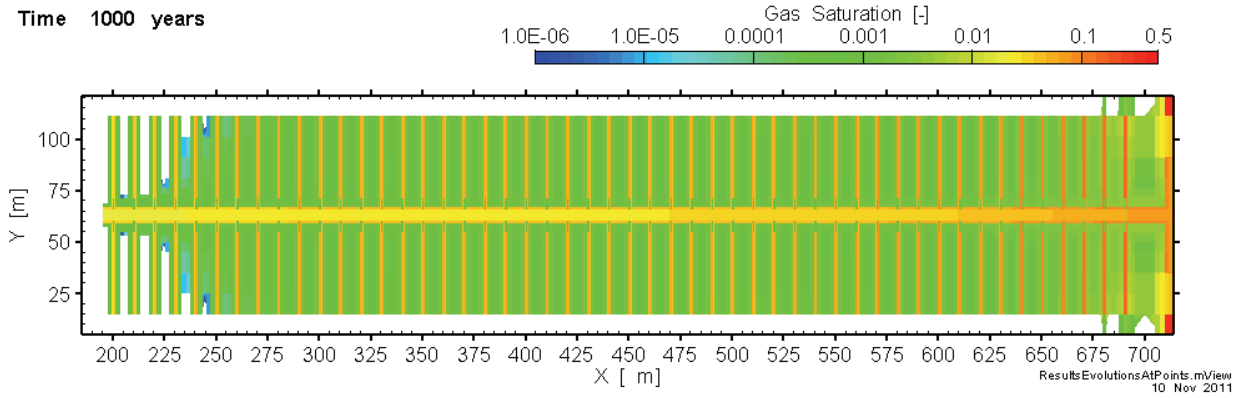

Figure 63: Gas Saturation and at 1000 Years, at a Plan Slice Through the Middle of the Repository

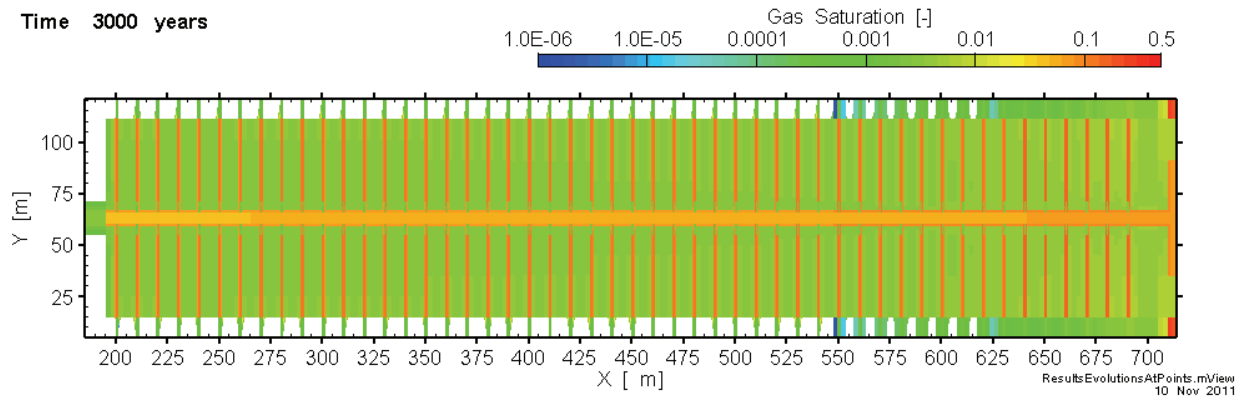

Figure 64: Gas Saturation and at 3000 Years, at a Plan Slice Through the Middle of the Repository

At 10 000 years, gas generation has ceased. Peak gas pressures of 6.7 MPa are observed within the cells and drifts at this time (see Figure 60). Gas saturations at this time are shown in Figure 65 in plan view, and Figure 66 at a vertical slice through the cells. Gas saturations have reached the Y boundary, and have migrated as far as 30 m out into the host rock away from the main drift in the X direction. Dissolved gas has migrated approximately 30 m farther than the gas phase, although this dissolved gas is at very low concentrations. In the vertical direction, gas saturations have migrated upwards approximately 50 m and downwards approximately 25 m. Dissolved gas has migrated within 15 m of the top and bottom boundaries.

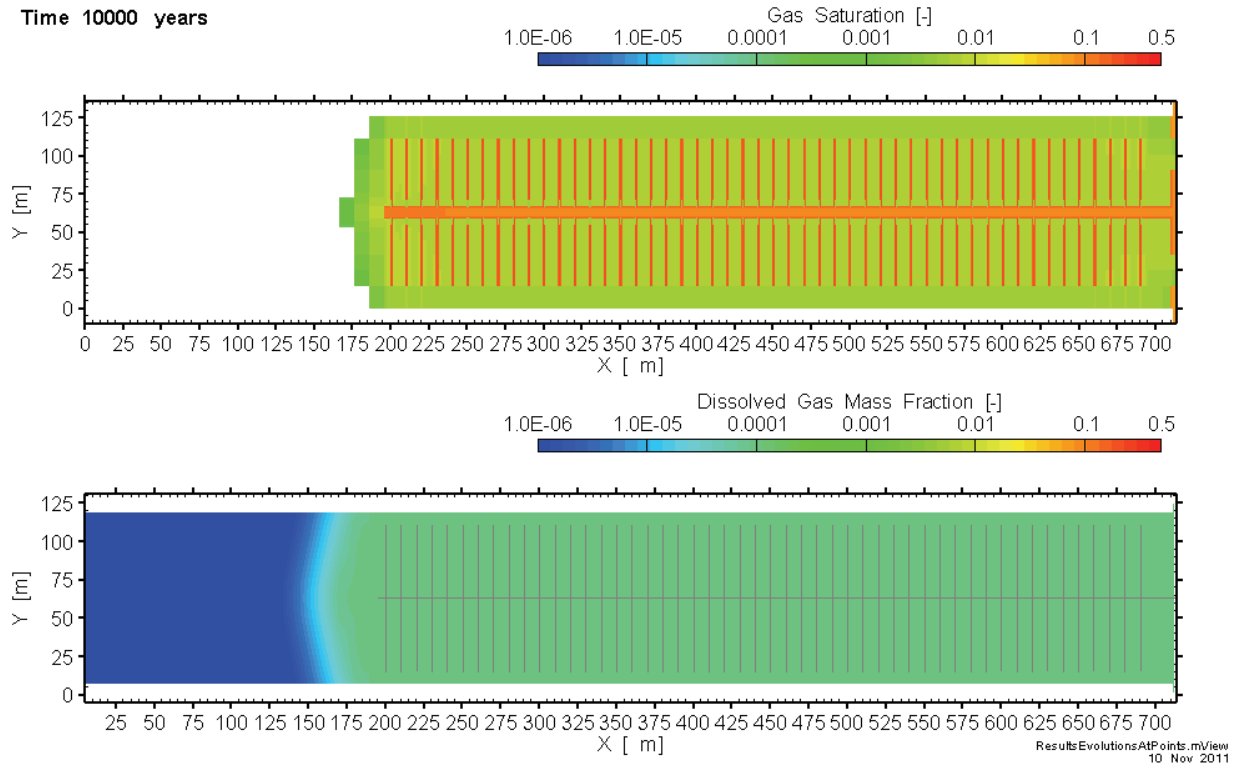

Figure 65: Gas Saturation and Dissolved Gas Mass Fraction at 10 000 Years, at a Plan Slice Through the Middle of the Repository

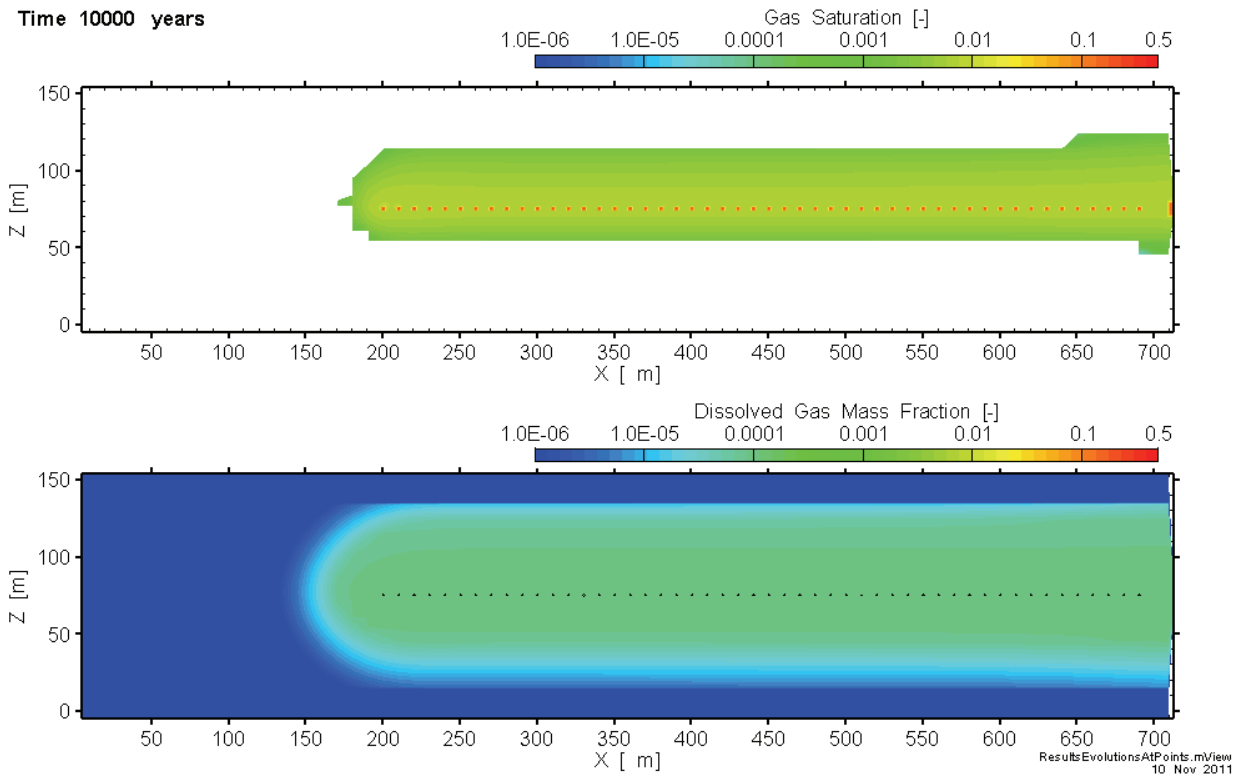

Note: Locations of cells are shown as black circles for clarity with dissolved gas mass fraction.

Figure 66: Gas Saturation and Dissolved Gas Mass Fraction at 10 000 Years, for a Vertical XZ Slice at Y = 72 (Just Above the Bentonite Plugs in the Cells)

After 10 000 years, gas generation stops and the gas phase present in the system dissolves. By 30 000 years, only a small amount of gas remains just above the repository (see Figure 67). The module has approximately 13 kg of initial mass and approximately 100 800 kg of mass is generated in the module. At the end of 30 000 years, only 0.001 kg remains in the gas phase, and 100 675 kg is present as dissolved gas. The difference exits the system from the main drift boundaries, both upstream and downstream (155 kg and 164 kg, respectively), primarily as free phase gas (99%). A negligible amount of dissolved gas exits the system from the top and bottom boundaries. A mass balance error of 0.2% was calculated, and it should be noted that this error includes error associated with the calculation of mass leaving across the main drift boundary conditions (which is limited by the time step output resolution).

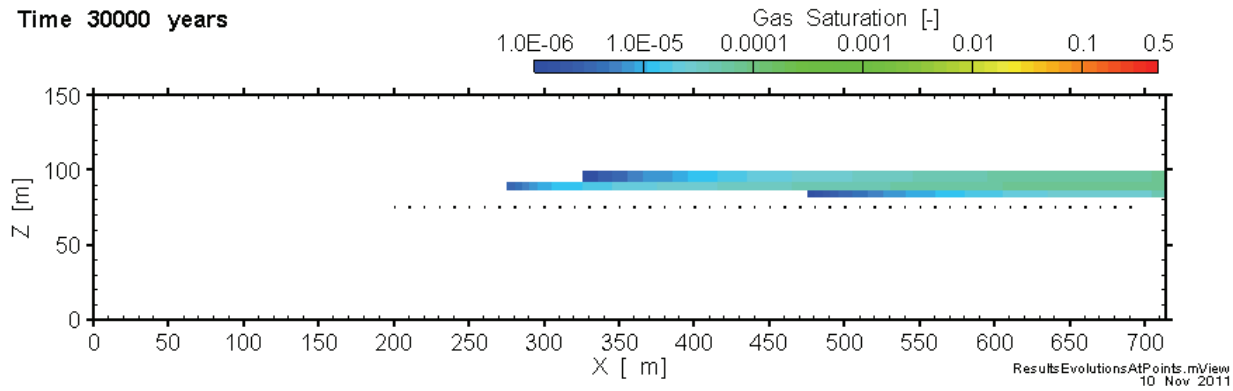

Note: Locations of cells are shown as black circles for clarity.

Figure 67: Gas Saturation at 30 000 Years, for a Vertical XZ Slice at Y = 72 (Just Above the Bentonite Plugs in the Cells)

In examining gas saturations in the different repository materials, it is not clear by 300 years which component of the repository system allows the most gas transport, although bentonite is obviously a barrier to gas transport (see Figure 68). In examining hydrogen gas flows by material across F-C slices, as shown in Figure 69, approximately half the total flow, a little more with time, is represented by the inner EDZ (upscaled interface material). The apparent minimal importance of the interface in the cells is likely due to the low permeability of the inner EDZ of the cell plugs, as the transmissivity of the inner EDZ of the plugs is equal to the transmissivity of the EDZ around the plug (1.2E-11 m^2/s). The transmissivity of the cell inner EDZ is greater than the EDZ (9.8E-8 m^2/s), but this is clearly limited by the transmissivity of the plug inner EDZ. This suggests that for the cells (including the plug), the interface plays a small role. The cell-scale model also concluded that the cell and plug interface was of minimal importance. An interesting sensitivity case would be removal of the cell and plug interfaces at the module-scale.

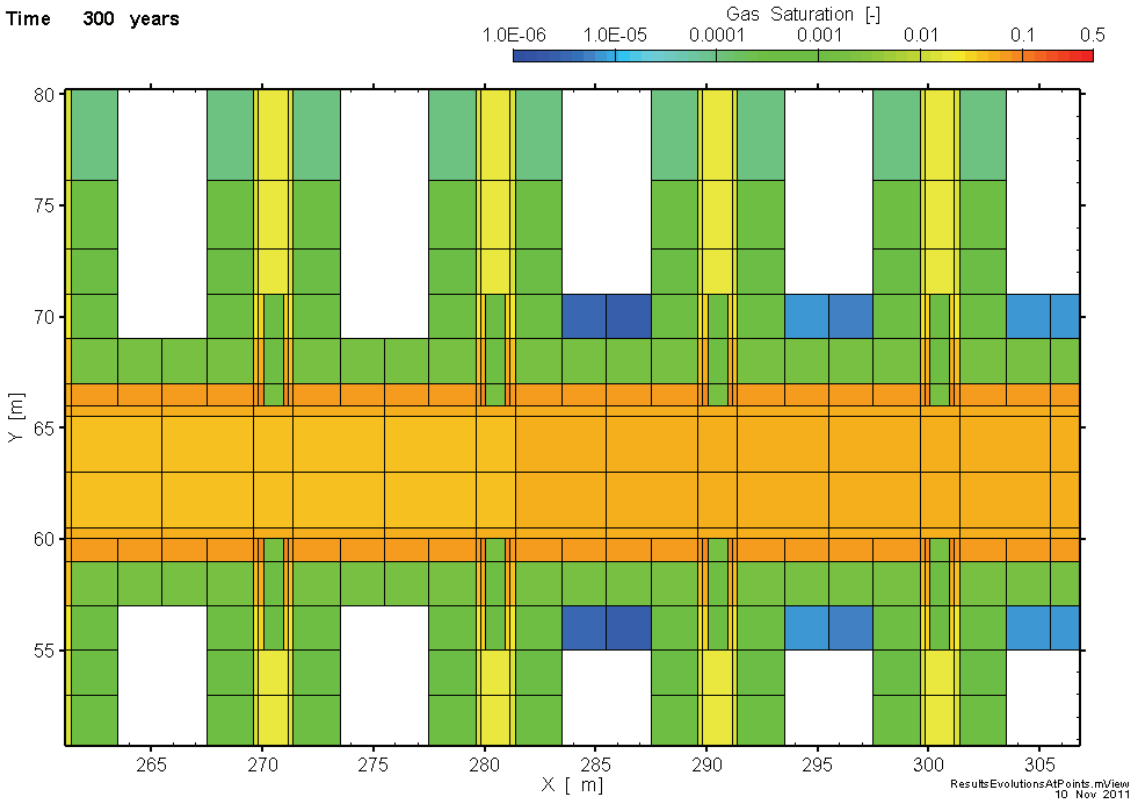

Note: Green blocks are either bentonite plugs at the end of cells, or host rock. White areas are areas with gas saturation less than 1E-6. Reminder that cell centers of upscaled interface and EDZ have modified block volumes similar to the adjacent EDZ blocks.

Figure 68: Gas Saturation at 300 Years, at a Detail of a Plan Slice Through the Middle of the Repository

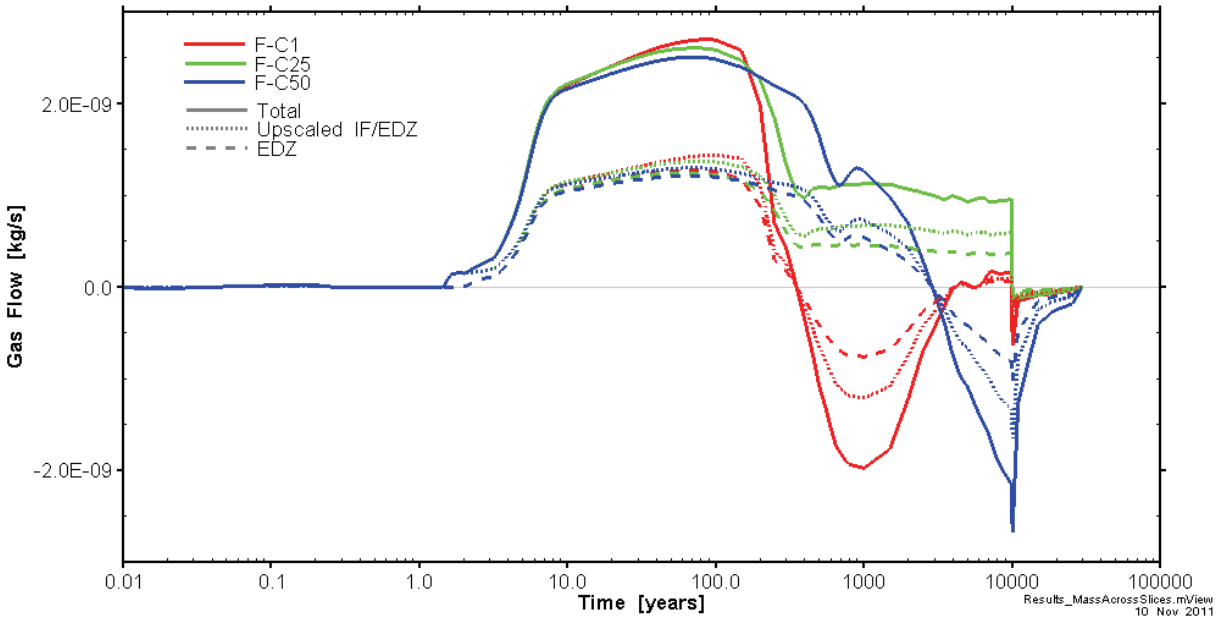

Figure 69: Hydrogen Gas Flow Across F-C Slices, Shown for Material Components in the Slice, Upscaled Interface (IF)/EDZ and EDZ

Across F-D slices, shown in Figure 70, the backfill has the greatest transmissivity of 2.5E-9 m^2/s, followed by the upscaled interface with a transmissivity of 3.4E-10 m^2/s and the EDZ with a transmissivity of 4.9E-11 m^2/s. While the backfill transmits the greatest portion of flow, the upscaled interface provides a significant contribution, with 36% of total peak flow at 350 years, while only representing 9% of the total cross-section area of the access drift (including EDZ).

In the F-P slices through the main drift plugs, shown in Figure 71, approximately three-quarters of gas flow occurs through the upscaled interface (combined with bentonite) with a transmissivity of 5.9E-13 m^2/s, and the remainder flows through the bentonite plug with a transmissivity of 2.9E-13 m^2/s.

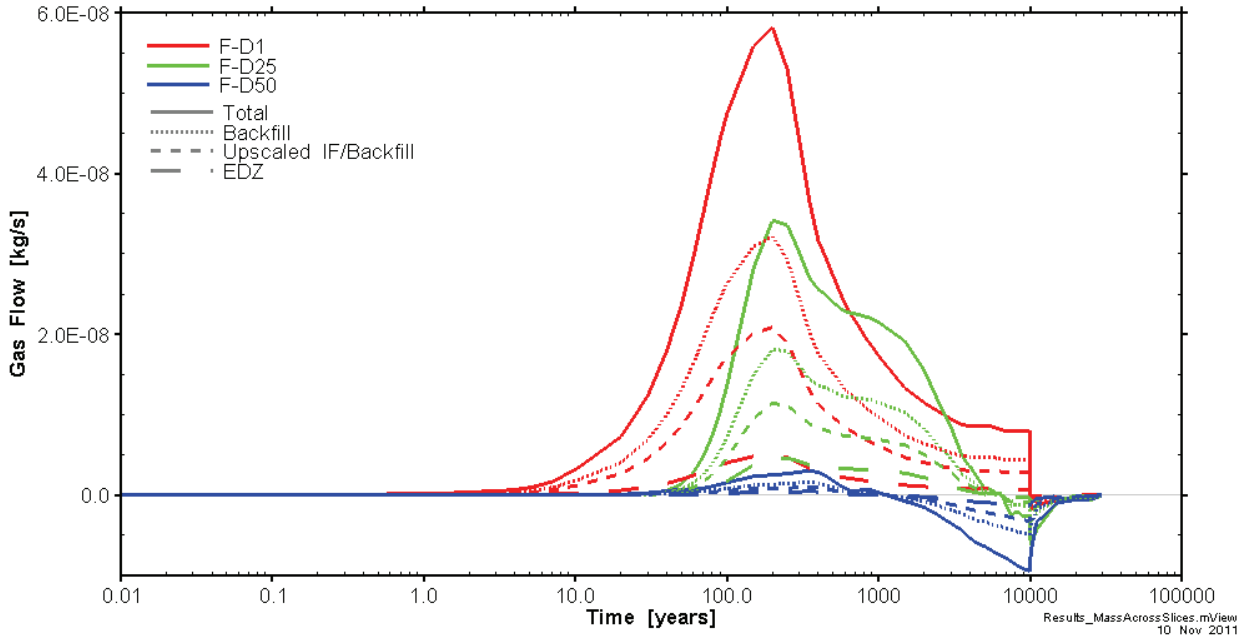

Figure 70: Hydrogen Gas Flow Across F-D Slices, Shown for Material Components in the Slice, Backfill, Upscaled Interface (IF)/Backfill and EDZ

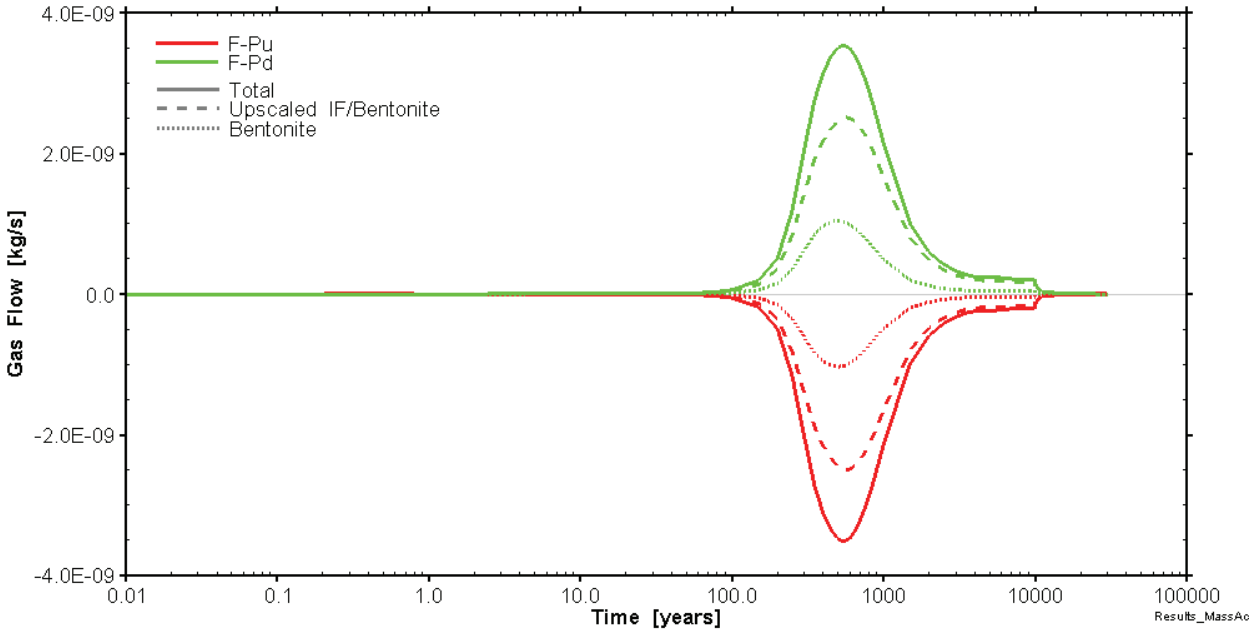

Figure 71: Hydrogen Gas Flow Across F-P Slices, Shown for Material Components in the Slice, Upscaled Interface (IF)/Bentonite and Bentonite.

5.2.2 Sensitivity Case – Alternative Parameters

A single sensitivity case with alternative upscaled parameters was simulated, as described in Section 5.1.4. This simulation is only complete to approximately 7000 years.

The alternative parameter case has slightly different parameters for the upscaled interface elements (Table 3). These upscaled interface elements have slightly anisotropic permeabilities due to the method used for upscaling permeability (average permeability for flows parallel to the interface and harmonic weighting for flows perpendicular to the interface); relative permeabilities equivalent to the material combined with the interface (EDZ, backfill or bentonite); and van Genuchten air entry pressures weighted by volume of the contributing material.

The change in parameters had little impact on the results, as shown by the water and gas flows in Figure 72 through Figure 75; the water saturations in Figure 76; and the water and gas pressures in Figure 77 and Figure 78. The greatest differences occur with water saturations within the cell (P-C1-2, P-C25-2, P-C50-2), with the alternative parameter set having greater water saturations after approximately 200 years, with a maximum difference of approximately 5%. This difference in cell water saturation does not seem to affect saturations, pressures or flows in the access drift.

The minimal differences between these two cases suggest that the first modelling attempt (the base case) is a sufficiently suitable representation of an upscaled interface.

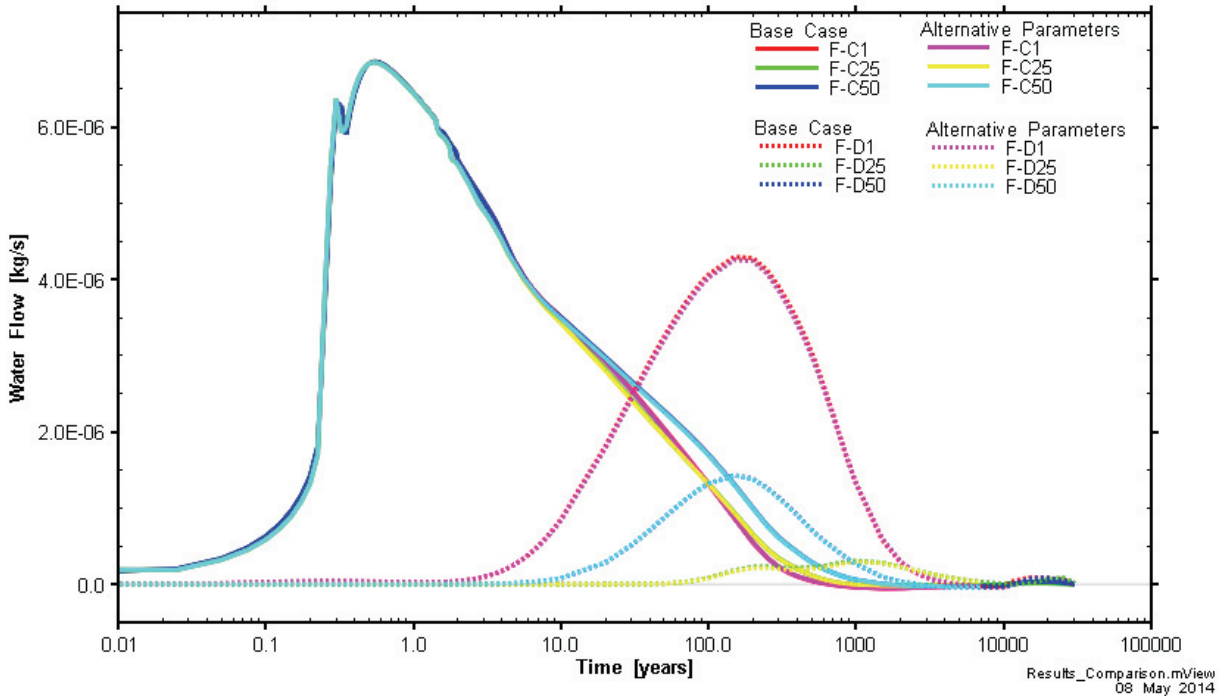

Figure 72: Comparison of Alternative Parameters to Base Case: Evolution of Liquid Water With Time Across F-C (Cell) and F-D (Access Drift) Surfaces

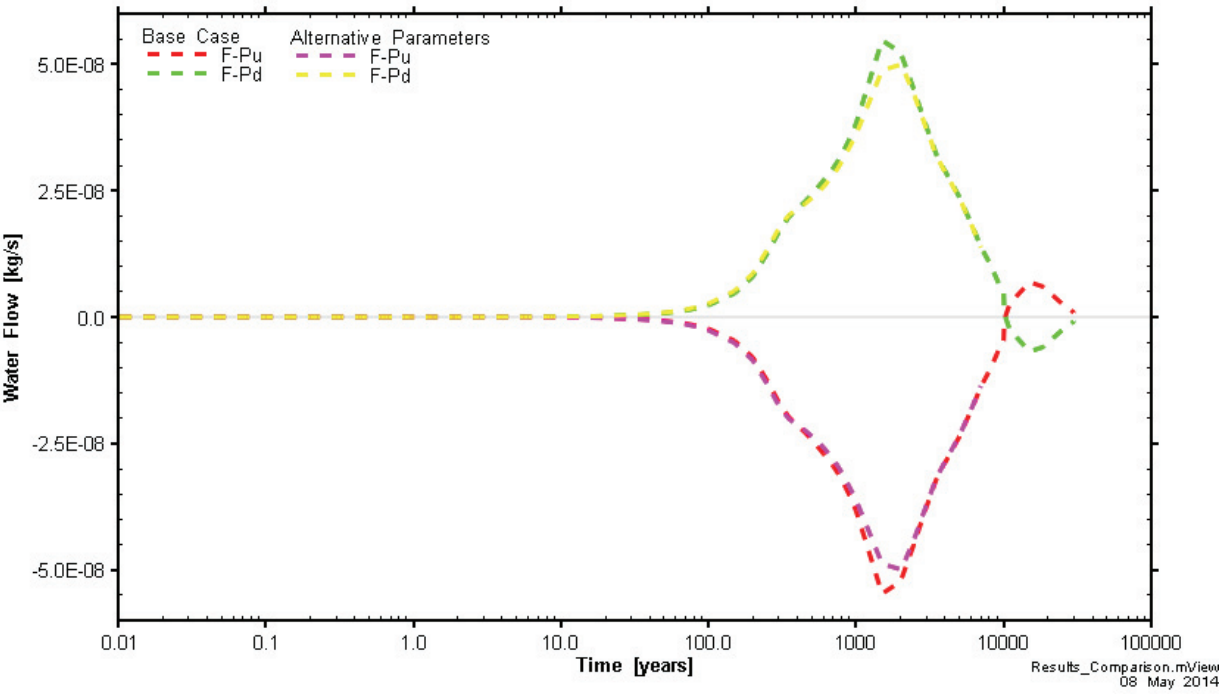

Figure 73: Comparison of Alternative Parameters to Base Case: Evolution of Liquid Water With Time Across F-P (Main Drift) Surfaces

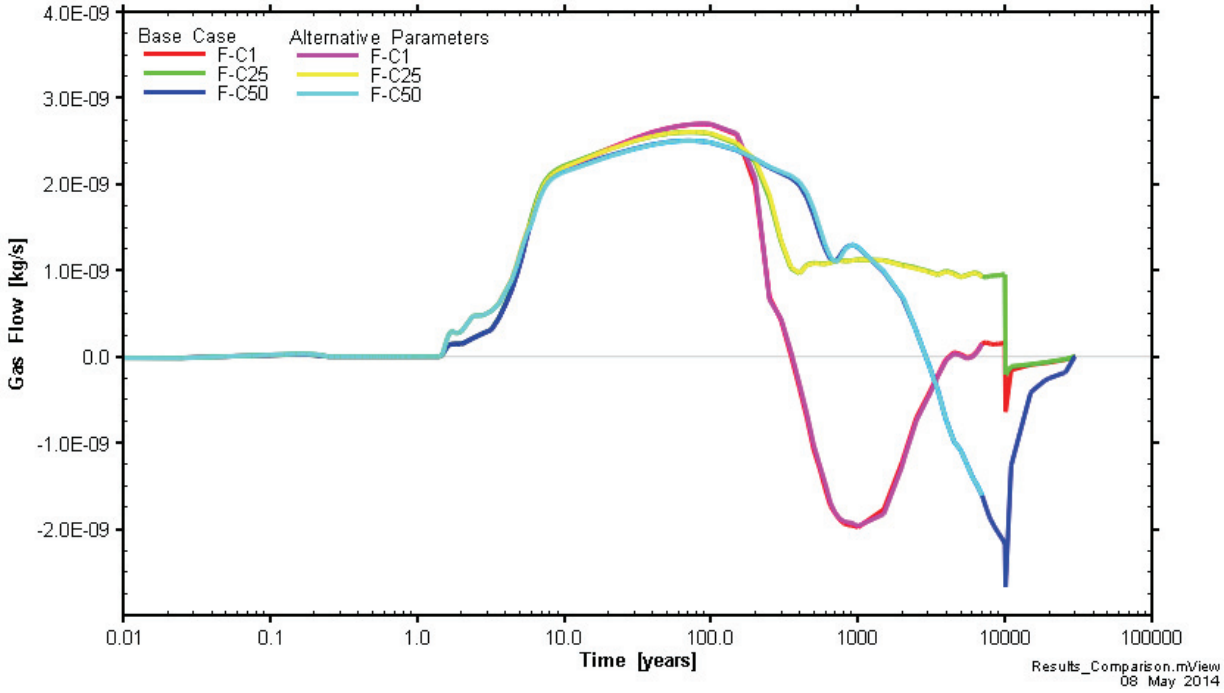

Figure 74: Comparison of Alternative Parameters to Base Case: Evolution of Hydrogen Gas With Time Across F-C (Cell) Surfaces

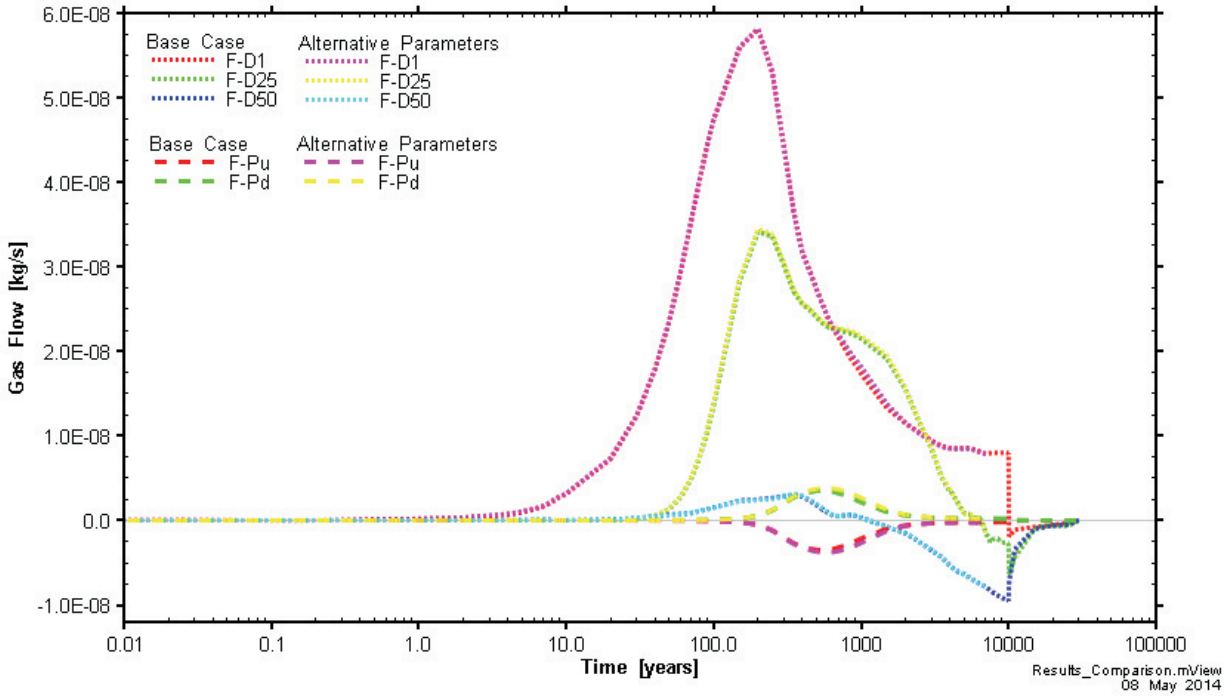

Figure 75: Comparison of Alternative Parameters to Base Case: Evolution of Hydrogen Gas With Time Across F-D (Access Drift) and F-P (Main Drift) Surfaces

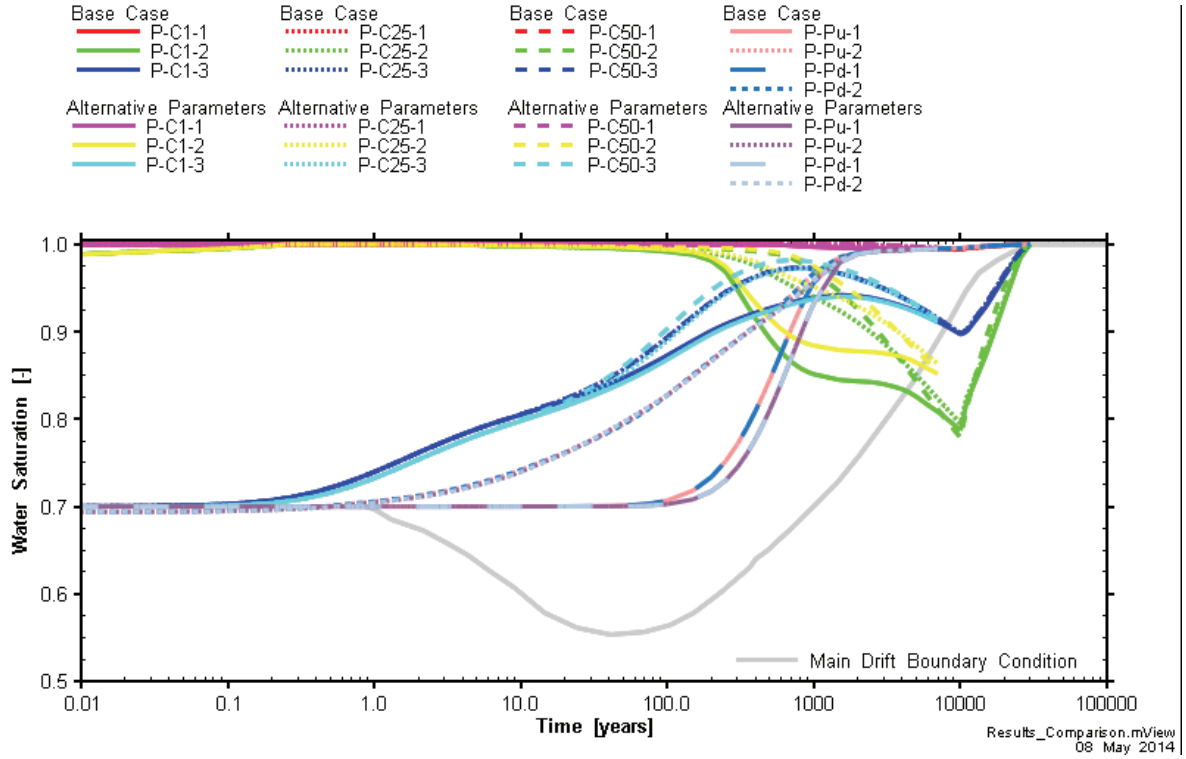

Figure 76: Comparison of Alternative Parameters to Base Case: Water Saturation at All Output Points

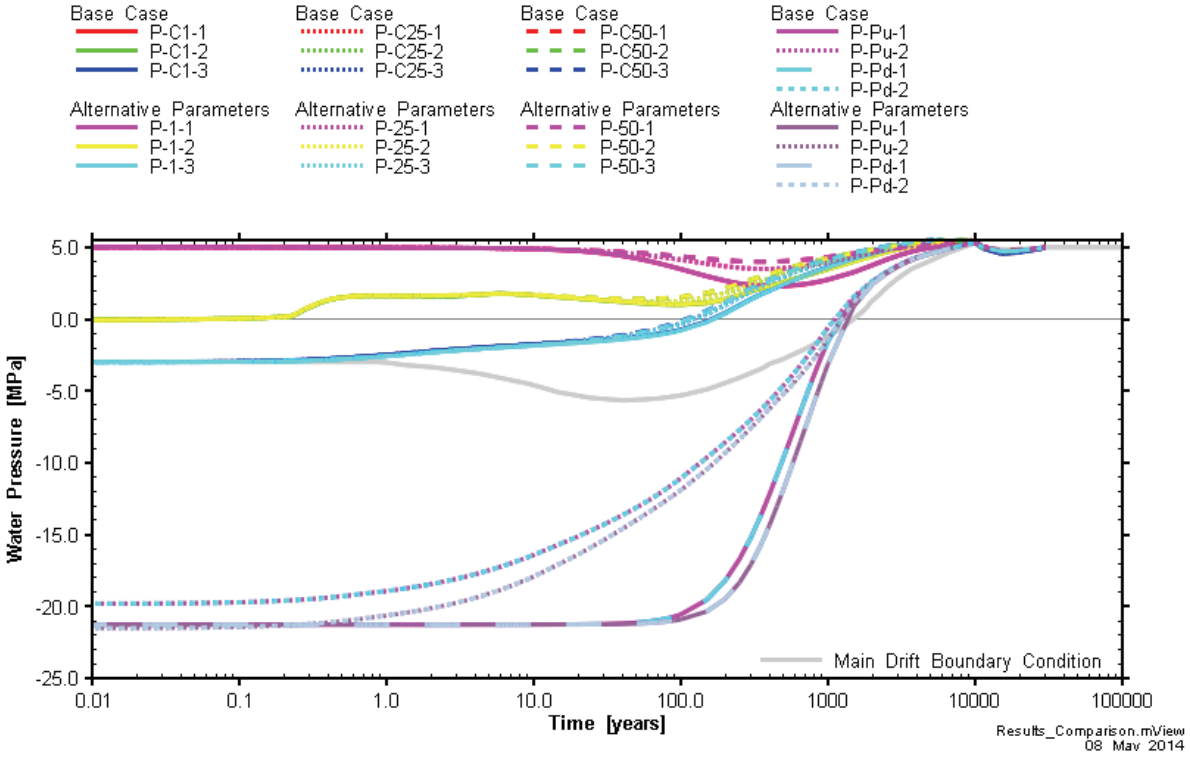

Figure 77: Comparison of Alternative Parameters to Base Case: Water Pressure at All Output Points

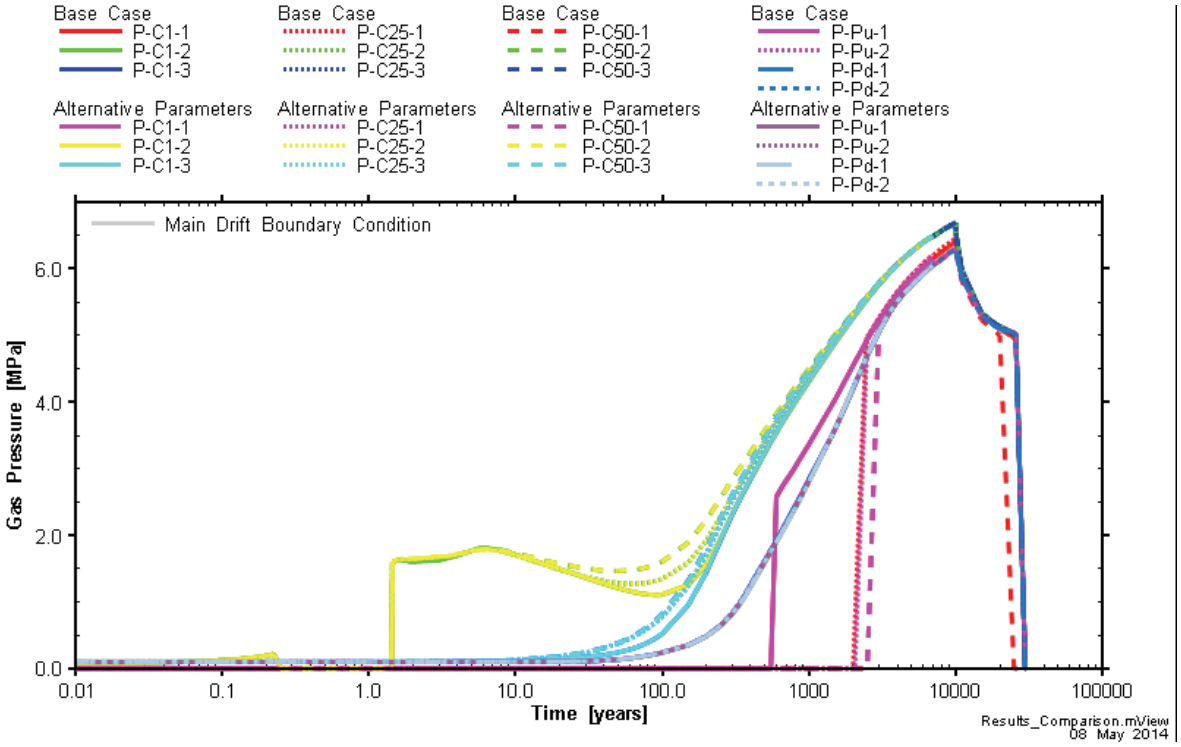

Figure 78: Comparison of Alternative Parameters to Base Case: Gas Pressure at All Output Points

5.2.3 Comparison of Key Results

Comparisons of base case model results with results obtained by other modelling groups are shown in Figure 79 through Figure 82.

In general, the results of the different modelling groups show similar trends, although magnitudes vary substantially. Peak gas pressures vary by as much as 1.5 MPa, peak water pressures by as much as 2.5 MPa. Gas and water flows are different by orders of magnitude.

Large differences in the models can sometimes be attributed to modelling and upscaling approaches. Based on information shared at modelling meetings, Quintessa included interfaces explicitly, whereas CNRS upscaled the interface and other components. Several of the output points (C25-2, C25-3, Pu-2 and Pd-2) are located within the interface, which accounts for large saturation and pressure differences at these points. LEI uses PetraSim, which does not allow the time-variable pressure and saturation boundary specified in the benchmark. Full details of these models are reported in the final FORGE report (Wendling et al. 2014b).

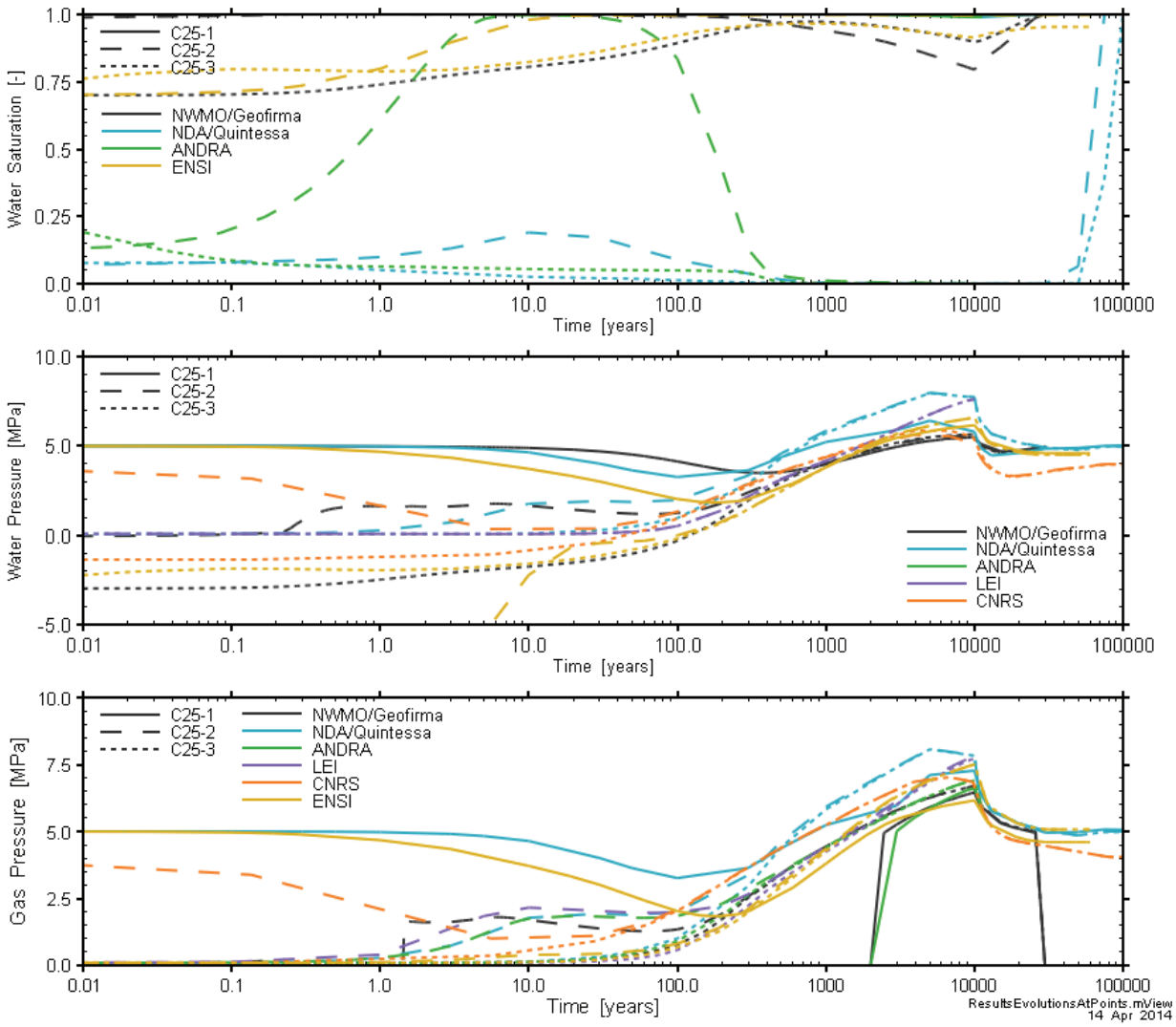

Note: C25-2 and C25-3 are located within the interface.

Figure 79: Module-Scale Comparison of Results Between Groups: Water Saturation, Water Pressure and Gas Pressure at Cell 25

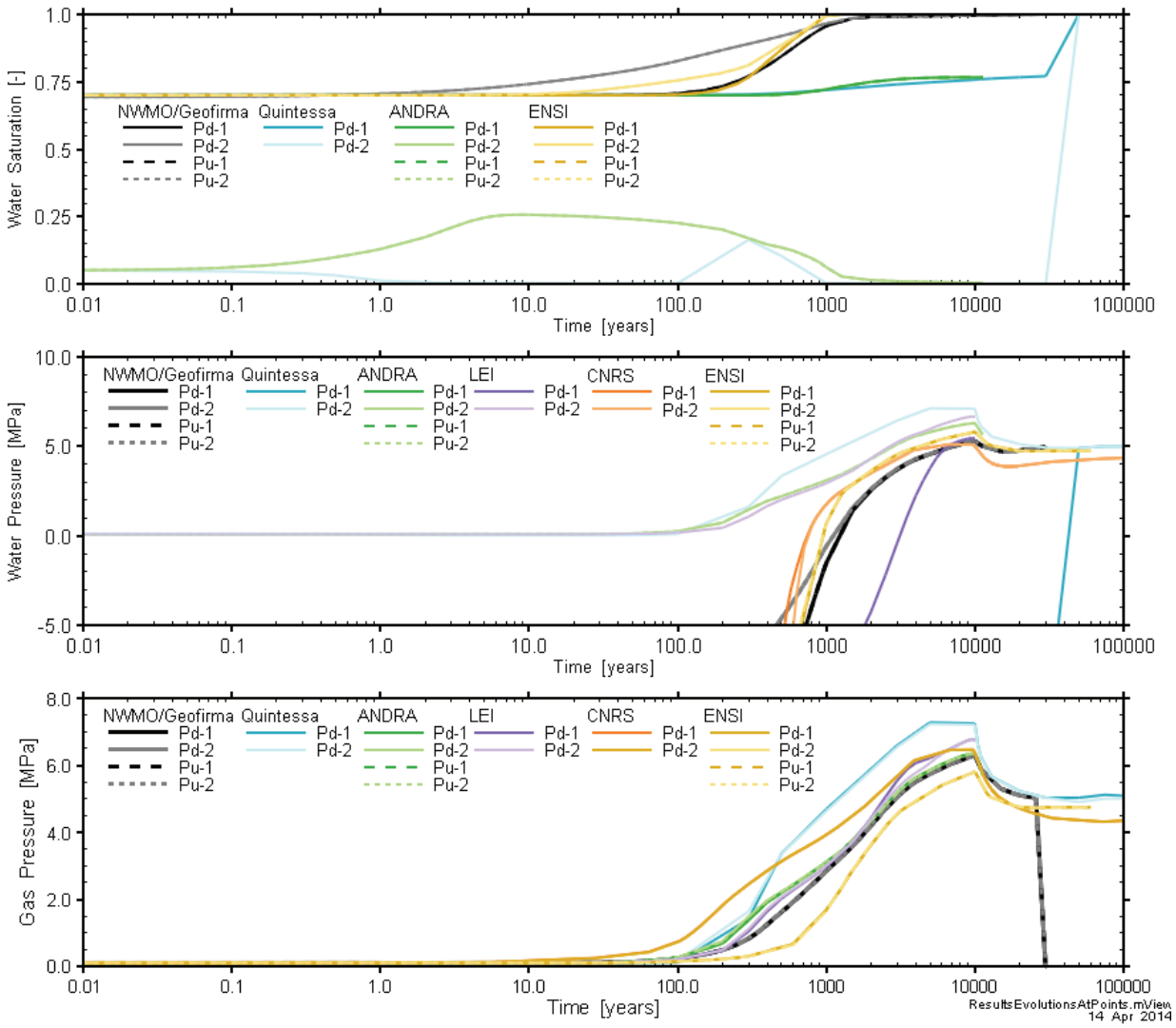

Note: Pd-2 and Pu-2 are located within the interface of the bentonite seal.

Figure 80: Module-Scale Comparison of Results Between Groups: Water Saturation, Water Pressure and Gas Pressure at the Bentonite Seals in the Main Drift

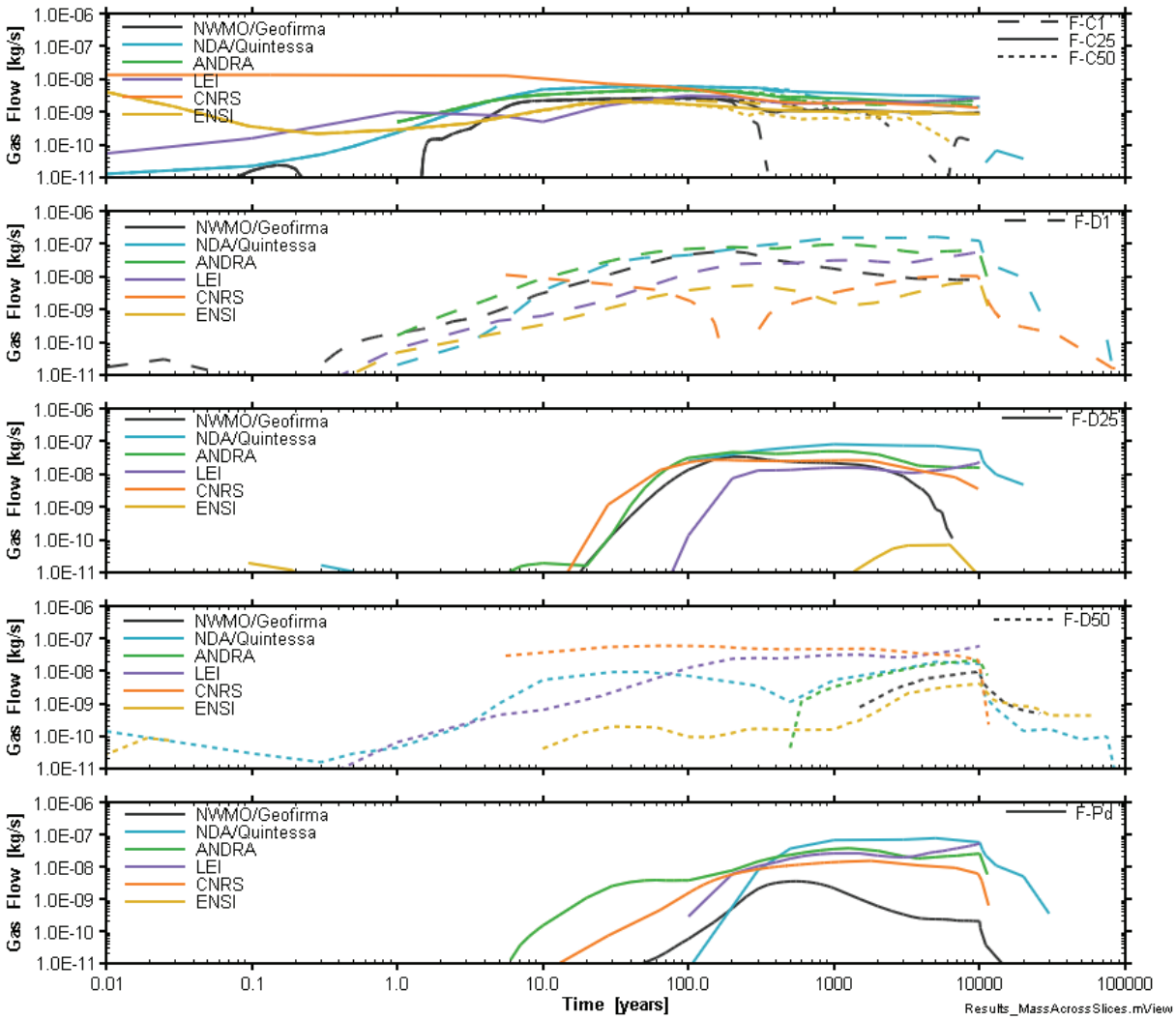

Figure 81: Module-Scale Comparison of Results Between Groups: Gas Flow in the Cells, Access Drift and Main Drift

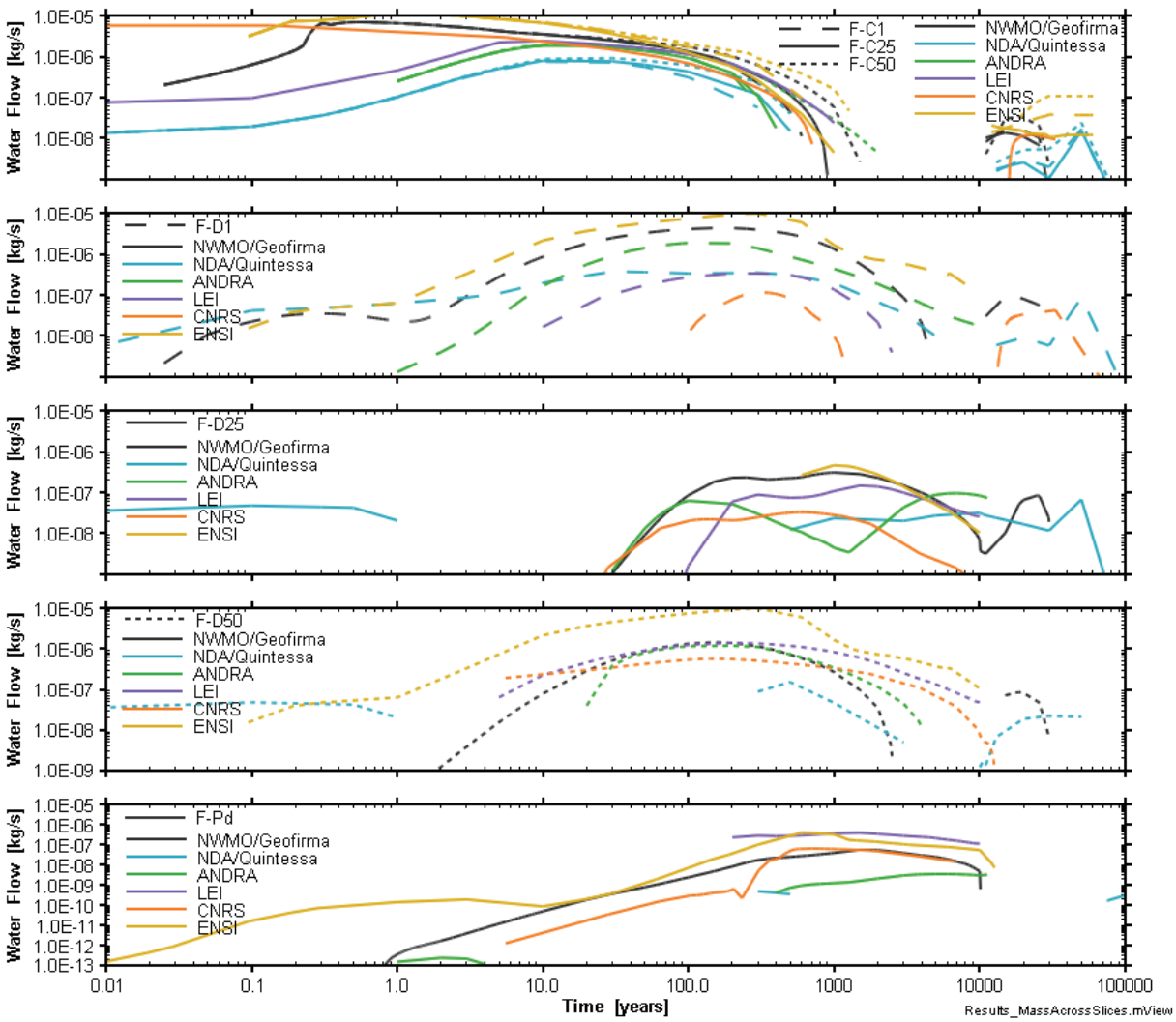

Figure 82: Module-Scale Comparison of Results Between Groups: Water Flow in the Cells, Access Drift and Main Drift

5.2.4 Summary

A 3D model of the module-scale benchmark was developed for WP1.2-2. The challenge in developing the module scale model was to assemble a grid discretization that adequately represented the module, while maintaining a tractable grid size. In order to obtain a working model, the interfaces were upscaled and several other simplifications were implemented, such as shifting the main drift bentonite plugs. Simulation results are available to 30 000 years.

Module behaviour and the applied boundary conditions in the main drift are not aligned. Water saturations and pressures in the module equilibrate with host rock pressures more quickly than specified in the boundary condition, and as a result, gas and water flows from the cells and access drift in the module to both the upstream and downstream main drift boundary conditions. As seen in the cell-scale results, the specified pressure and saturation boundary condition at the

drift is pivotal to model performance, and determines the magnitude and direction of gas flows. Despite the inconsistent boundary conditions, insights can be gained from this model.

Initially, gas migrates along the cells towards the access drift, and along the access drift towards the main drift. In addition to flowing through the access and main drift, gas also migrates into the host rock. Once pressures in the module begin to equilibrate with the host rock, changes in water and gas flow direction are seen in the cells and the access drift. Pressures in the middle of the module are less variable than at the edges, and consequently, water flows are smaller and water flow direction in the access drift and gas flow direction within the cell do not reverse as at the edges of the repository. Maximum gas pressures of 6.7 MPa are observed throughout the module cells and access drift at 10 000 years, the time at which gas generation stops. By 30 000 years, there is only a very small amount of hydrogen gas left in the system (0.001 kg), with the majority of generated gas present in a dissolved form (100 675 kg). A relatively small amount of hydrogen exits at both the upstream and downstream main drift boundary conditions (155 kg and 164 kg, respectively), primarily in the gas phase (99%).

Cell-scale modelling identified the EDZ as an important feature along cells, with the interface playing a relatively small role in terms of transporting gas, likely due in large part to the low conductivity of the cell bentonite plug interface. In the module-scale modelling and along the access drifts, the EDZ plays a less important role in gas transport, due the relatively high permeability of the backfill (5.0E-17 m^2) compared to the EDZ (5.0E-18 m^2). Along the bentonite plugs in the main drift, the interface (combined with bentonite at the outer edge of the plug) is important (no EDZ is present), with three-quarters of all gas flow occurring through the interface.

The impact of module-scale modelling simplifications was not examined, including the effect of discretization (notably the effect of rectangular cells and coarse discretization) and interface upscaling.

6. REPOSITORY-SCALE MODEL

6.1 MODELLING APPROACH

6.1.1 Grid

The repository scale domain is large and detailed. Consequently, the challenges of the model are incorporating small-scale details, such as the very thin interface between the cells or access drifts and the host rock, in a model of a tractable size. Two modelling approaches were taken:

(1) **Half-Domain**: A 3D grid was developed, representing one-half of the model domain. The grid was based on the grid developed for the module-scale. Figure 83 shows the model domain, with boundary conditions, cells and drifts. This approach, using multiple processor T2GGM-MP, has relatively slow run times.

(2) **Main-Drift**: A 3D grid representing the main drift and shaft (Figure 84). Input to the main drift from the module was based on output from the module-scale model. This modelling approach has some circularity as the main drift boundary conditions in the module-scale model are dependent on the repository-scale model results, while the module source input in the repository-scale model are dependent on the results of the module-scale model. However, this approach has quick run times, using single processor T2GGM. The circularity is addressed by ensuring that the discrepancy between pressures used as module scale boundary conditions and those pressures calculated using a module scale source term is minimized (by re-running both models with updated boundary conditions).

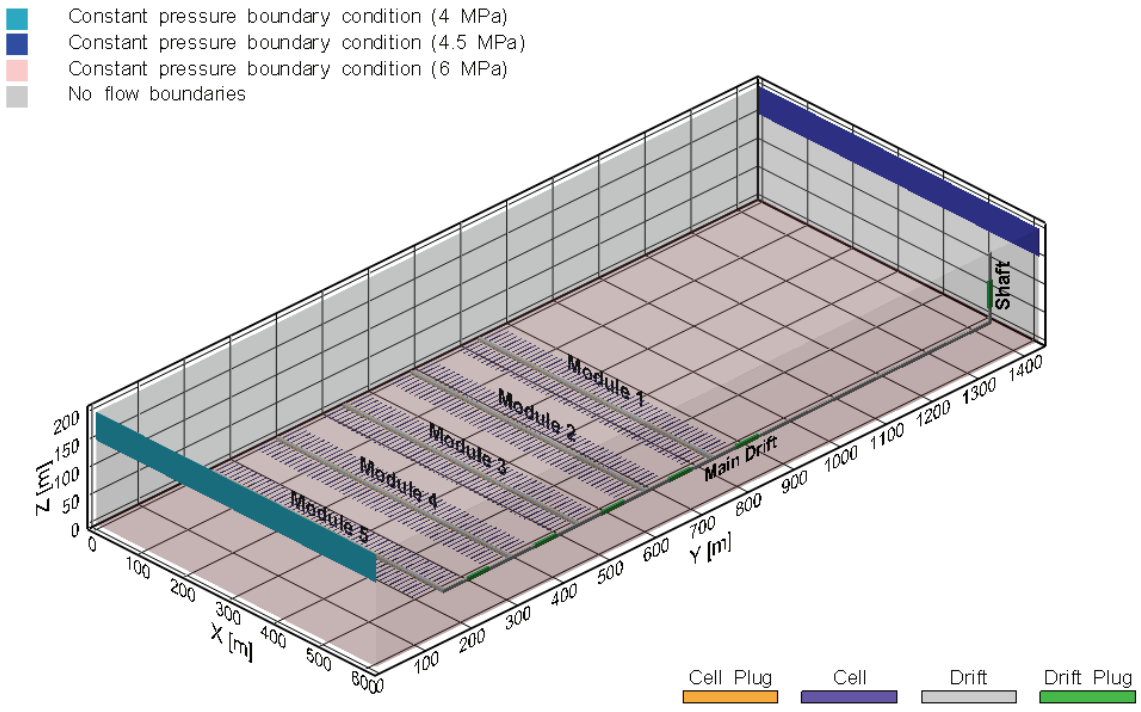

Figure 83: 3D Model Domain With Boundary Conditions, Cells and Drifts for Half-Domain Model

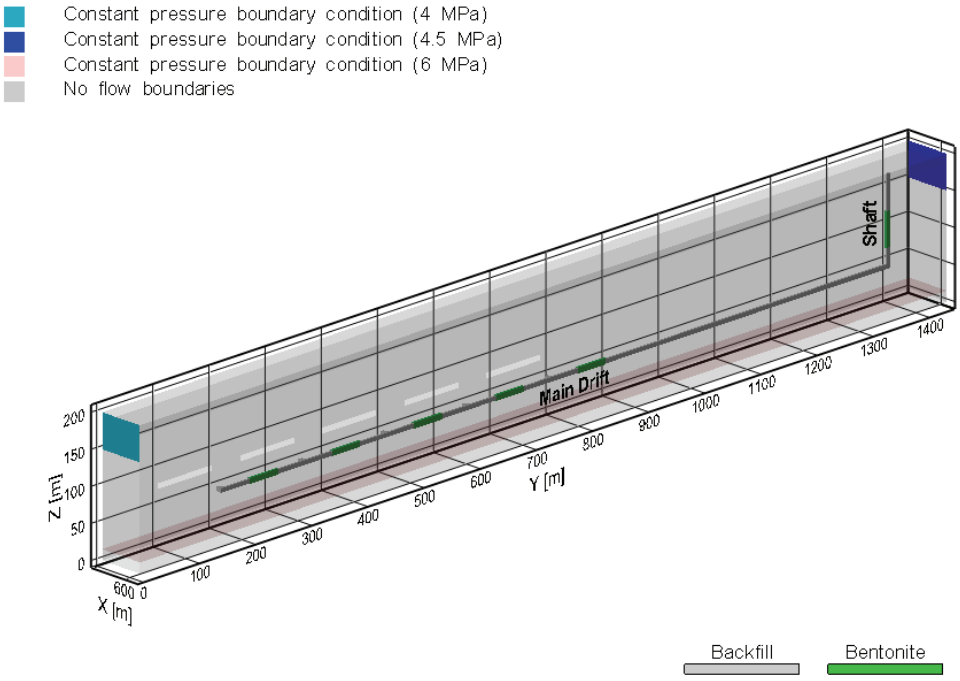

Note: White spaces represent location of modules.

Figure 84: 3D Model Domain With Boundary Conditions, Cells and Drifts for Main-Drift Model

6.1.1.1 Half-Domain

The greatest challenge in developing this grid was to obtain sufficient representation of the repository details, while maintaining a grid of tractable size. Similar problems were encountered in the module-scale model, which has a smaller domain with a similar level of detail. Building on the work of the module-scale modelling:

(1) The code was switched to T2GGM-MP. Module-scale modelling used standard T2GGM.
(2) The module-scale discretization was coarsened, and then expanded to include the full repository domain.

Consequently, the grid uses the same simplifications employed in the module scale models:

(1) The cells were represented as rectangular in cross-section, with equivalent cross-sectional areas to the circular cells defined in the benchmark. Using rectangular-shaped cells allows for significantly fewer grid elements, producing an overall grid of tractable size.

(2) Interface materials were combined with adjacent materials to provide tractable discretization. The details of the interface combinations are as follows:

a) The interface between the cell canisters and the EDZ was combined with the EDZ. The cell EDZ was divided into two components: (i) an inner EDZ which represents the combination of interface and EDZ, and (ii) an outer EDZ which represents the EDZ alone. The inner EDZ of the cells was represented as a single element in the middle of the cell. Block volumes and areas were adjusted to represent the actual volumes and areas of the inner EDZ surrounding the waste. The benchmark specifies the waste containers as impermeable to gas and water. Figure 85 shows a detailed cross-section of the discretization of a cell.

b) The interface between the cell plug and the EDZ was combined with the EDZ, creating and inner and outer EDZ as above. Figure 86 shows a detailed cross-section of the discretization of the cell plug.

c) The interface between the drift backfill and the EDZ was combined with the backfill in a 0.5 m width block on the edges of the drift (both access and main drifts). Figure 87 shows a plan-view of the discretization of the access and main drifts.

d) The interface between the main drift plug and the host rock was combined with the bentonite plug, also shown in Figure 87.

(3) EDZ and the interface at the end of the access drift furthest from the main drift were ignored. This omission is expected to be inconsequential, as gas and water are expected to flow towards the main drift.

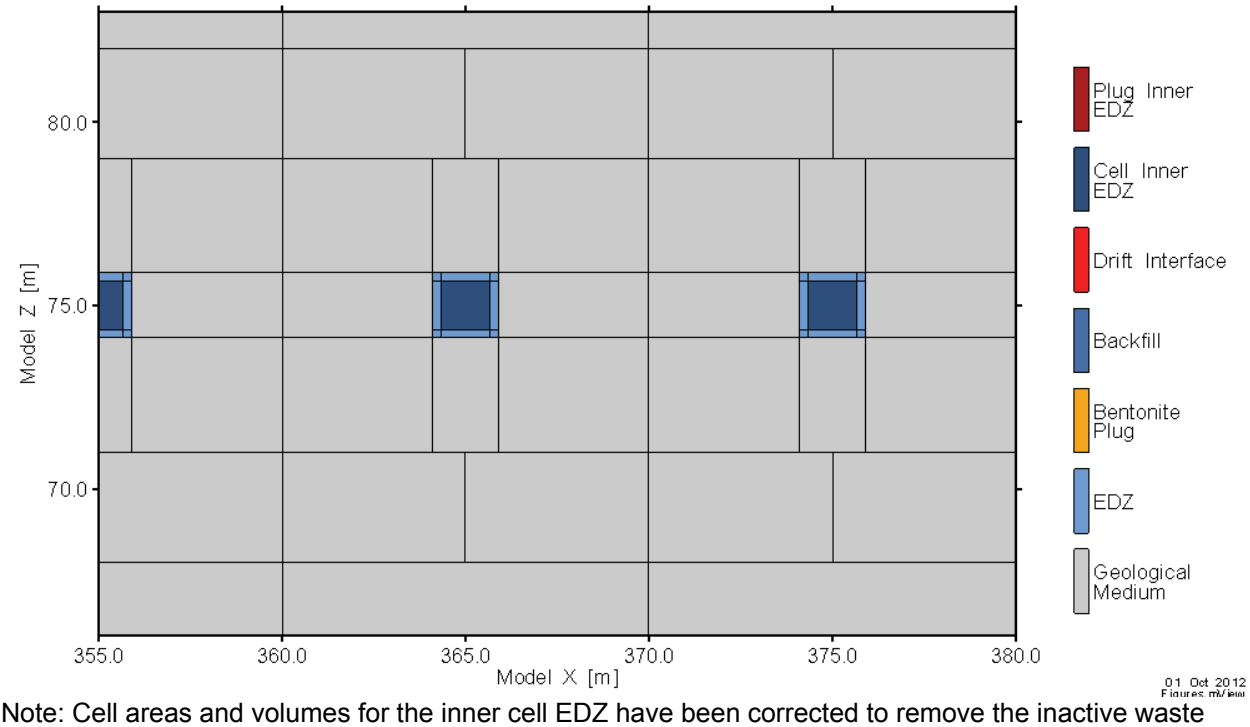

Note: Cell areas and volumes for the inner cell EDZ have been corrected to remove the inactive waste canisters, as described in the text.

Figure 85: Grid Discretization Detail: Cross-Section of a Cell

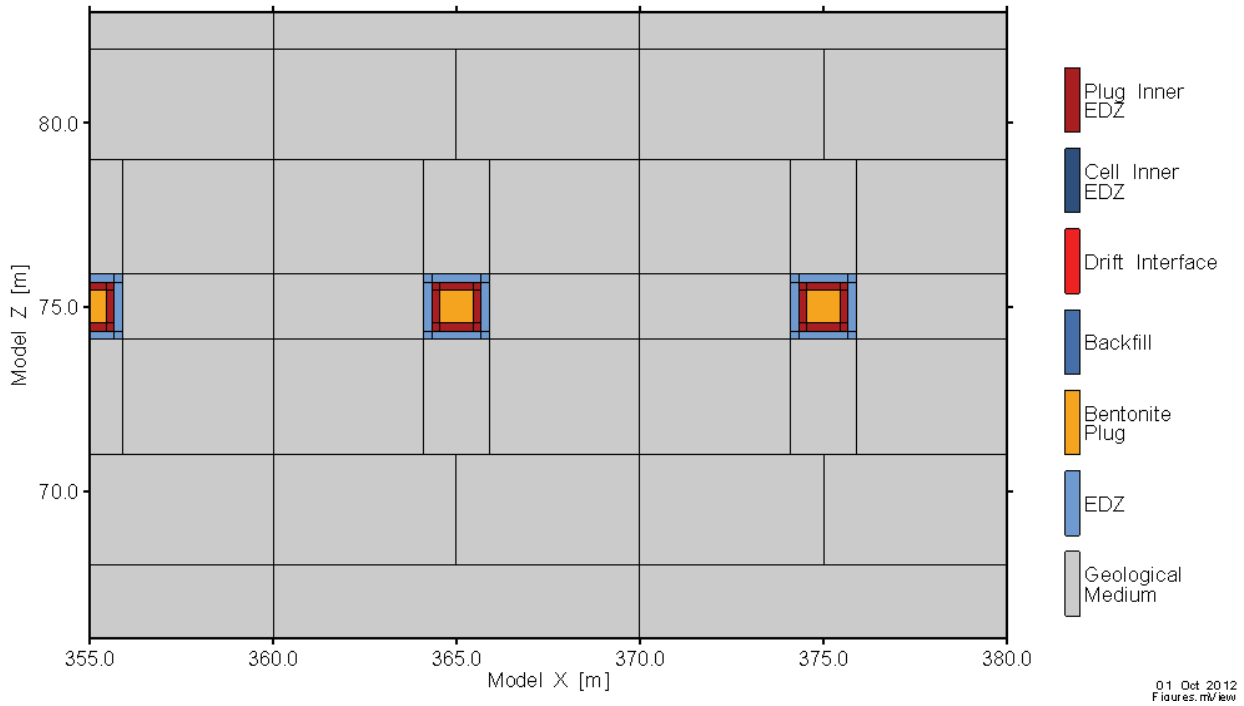

Figure 86: Grid Discretization Detail: Cross-Section of a Cell Plug

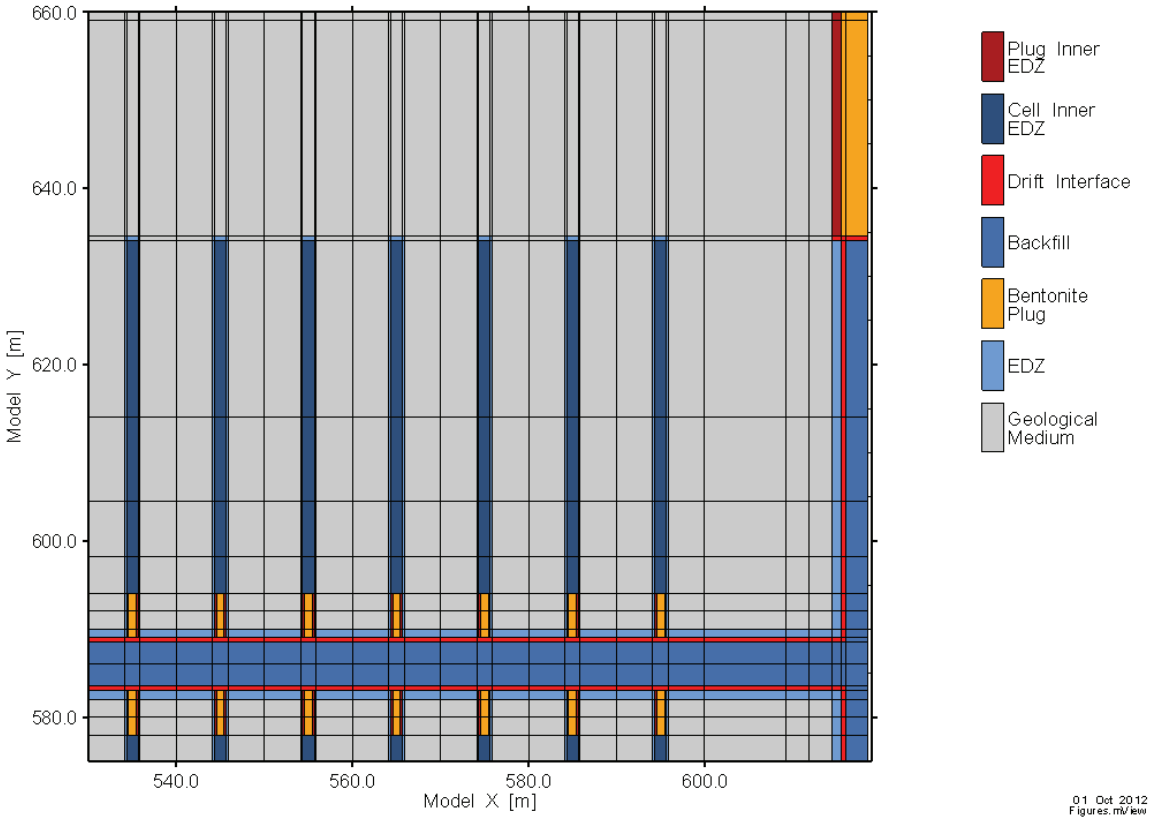

Figure 87: Grid Discretization Detail: Plan View of the Access and Main Drift

The resulting grid had 212 400 nodes and 706 549 connections. This is a very large grid for T2GGM-MP, with run times of approximately one week to reach 30 000 years, using 8 processors.

It should also be noted that the irregular grid of the final model does not strictly adhere to the TOUGH2 integral finite difference requirements; some nodal connections are not perpendicular to the connection area, resulting in shorter connection distances for these connections. The impact of these inaccuracies is expected to be small, and this has been confirmed at the cell-scale (see Section 4.1.1).

6.1.1.2 Main Drift

As the half-domain approach took some time to develop, debug and simulate, this simpler approach was developed. As an extension of the module-scale model, it contains the same simplification for interface upscaling as described for the half-domain model above. The cells were not explicitly modelled, with blocks within the module (at the edge of the model) removed from calculations. Gas and water input into the main drift (from the modules) were extracted from the module-scale model, with the assumption that the flow of gas into the main drift is the same for each module. As well, only positive flow (from the panel to the main drift) was considered. Small negative water flows (from the main drift to the panel) occur after 3000 years, and small negative gas flows occur after 10 000 years; these were ignored (i.e., gas or water input is set to zero). As these negative flows are very small relative to peak flow rates, the impact of their exclusion is expected to be minor. The module-scale model was rerun once, with boundary conditions extracted from the first repository-scale simulation.

The final grid had 2442 nodes and 6733 connections. Run times were less than 10 minutes.

6.1.2 Boundary Conditions, Initial Conditions and Sources

For both the half-domain and main drift models, boundary and initial conditions are identical. A constant pressure and zero gas saturation boundary condition was specified on the bottom of the model (Z= 0 m), at 6 MPa (Figure 83 and Figure 84). The top 50 m of the model (Z= 150 to 200 m) is an aquifer, with constant pressure and zero gas saturation boundary conditions specified at 4.5 MPa at Y = 1437 m (the edge of the model closest to the shaft) and 4.0 MPa at Y = 0 m. Initial conditions in the host rock and EDZ were based on steady-state pressures for a no-repository fully water saturated simulation, resulting in pressures of approximately 5 MPa at the repository horizon (Z = 75 m), and fully water saturated. In repository features, initial pressure is atmospheric and initial water saturation is 5% in the interfaces and 70% in the drift backfill and bentonite plugs.

Since the aquifer boundary condition is applied over a depth of 50 m, aquifer boundary condition include hydrostatic pressures assuming the bottom of the aquifer has the pressure values of 4.0 (at Y = 0 m) and 4.5 MPa (at Y = 1437 m) defined in the benchmark. Initially, the repository-scale model defined the aquifer boundary condition at the top of the aquifer. This difference resulted in a different direction of geosphere flows: when the boundary condition is defined at the bottom of the aquifer, geosphere flows are upwards, whereas when the boundary condition is at the top of the aquifer, geosphere flows are downwards. It was presumed, based on the pressure boundary conditions defined and a conservative flow field, that geosphere flows were intended to be upwards. Note that the difference has a very marginal effect on results: peak

hydrogen and dissolved hydrogen flows within the repository were less than 10% greater with downwards geosphere flows compared to the upwards geosphere flows of the model presented here. Note that since flows within the repository were greater for downwards geosphere flows, it is likely that flows into the EDZ/host rock were less for this upward flow field.

As the waste canisters were not included in the model, gas generation was specified at all inner EDZ nodes of the cell (properties a combination of interface and EDZ, as described below). The generation term was proportioned between nodes according to block volume of the generation node. The source term for the main drift model was derived from output at the module-scale model.

6.1.3 Deviations from the Benchmark Specification

Upscaling of parameters for the inner EDZ and other interface combinations uses the more conventional approach used in the module-scale sensitivity case, as follows:

- Scalar parameters, such as porosity, were calculated using a volumetric weighting approach (as in Equation 4 for the module-scale modelling).

- Tensor parameters, such as permeability, used an arithmetic average when component materials were layered parallel to the direction of the tensor and a harmonic average when component materials were layered perpendicular to the direction of the tensor.

- Van Genuchten shape parameter n was held constant (assumes relative permeability in the interface is the same as in the EDZ, backfill or bentonite), while the van Genuchten air entry pressure was calculated using the volumetric weighting approach of a scalar parameter. This is a similar method as used by NDA/Quintessa in the module-scale benchmark study. CNRS proposed an alternative method for upscaling van Genuchten parameters at the module-scale; however, this method resulted in greater capillary pressures at high water saturations than either contributing material.

Table 4 provides the final parameters for upscaled interface materials. Table 4 also contains the initial conditions within the upscaled interface materials. These initial conditions were determined in the same manner as a scalar parameter, weighted according to the relative volume of the contributing materials, and ignoring the benchmark specification where the interface at the bottom of a cell or drift is fully water saturated. Note that initial pressure conditions were not weighted: all materials with a partial saturation, including upscaled interface materials, were assigned a gas pressure of 0.1 MPa as defined by the benchmark for partially saturated materials.

Table 4: Parameters and Initial Conditions for Upscaled Interface Materials

	$K_{parallel}$ [m^2]	$K_{perpendicular}$ [m^2]	Porosity [-]	Pore Compressibility [Pa^{-1}]	Tortuosity [-]	S_{lr} [%]	S_{gr} [%]	n [-]	P_o [Pa]	Initial Water Saturation [%]
Inner cell EDZ	4.0E-14	5.2E-18	0.18	1.06E-09	0.28	0	0	1.5	1.44E+06	96.2
Inner cell plug EDZ	5.0E-18	5.0E-18	0.16	1.10E-09	0.28	0	0	1.5	1.44E+06	96.2
Main Drift Plug Interface	6.0E-20	1.0E-20	0.35	8.24E-10	0.06	0	0	1.6	1.58E+07	69.4
Drift Interface	5.1E-17	6.9E-17	0.40	2.06E-09	0.27	0	0	1.5	1.96E+06	68.7

6.2 MODELLING RESULTS

Model results for the half-domain model are presented, followed by results for the main-drift model, and how the main-drift model compares to the half-domain model.

Output points and slices presented below correspond to those defined in the benchmark (locations shown in Figure 88 through Figure 91). Note that in the subsequent figures showing gas saturation, white space indicates areas where gas saturations are below the legend threshold of 1E-6, often at zero gas saturation. For figures showing gas pressure, white areas indicate areas where there is no gas, and therefore no gas pressure.

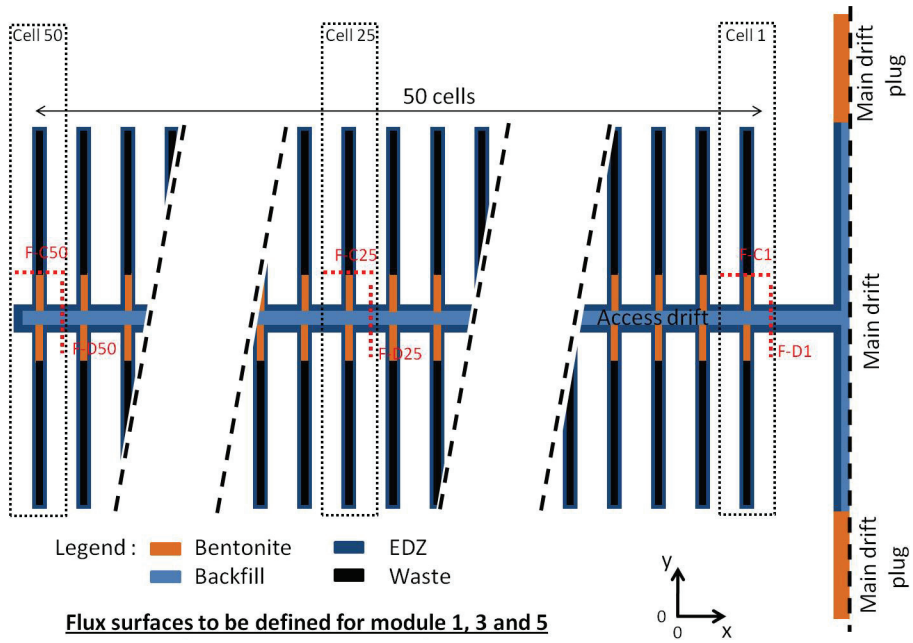

Note: Positive flow denotes flows along the cell (F-C) towards the access drift and along the access drift (F-D) towards the main drift. Figure duplicated from benchmark description in Appendix C.

Figure 88: Location of Surfaces at Which Evolution of Mass Flow With Time Is Presented for Modules 1, 3 and 5

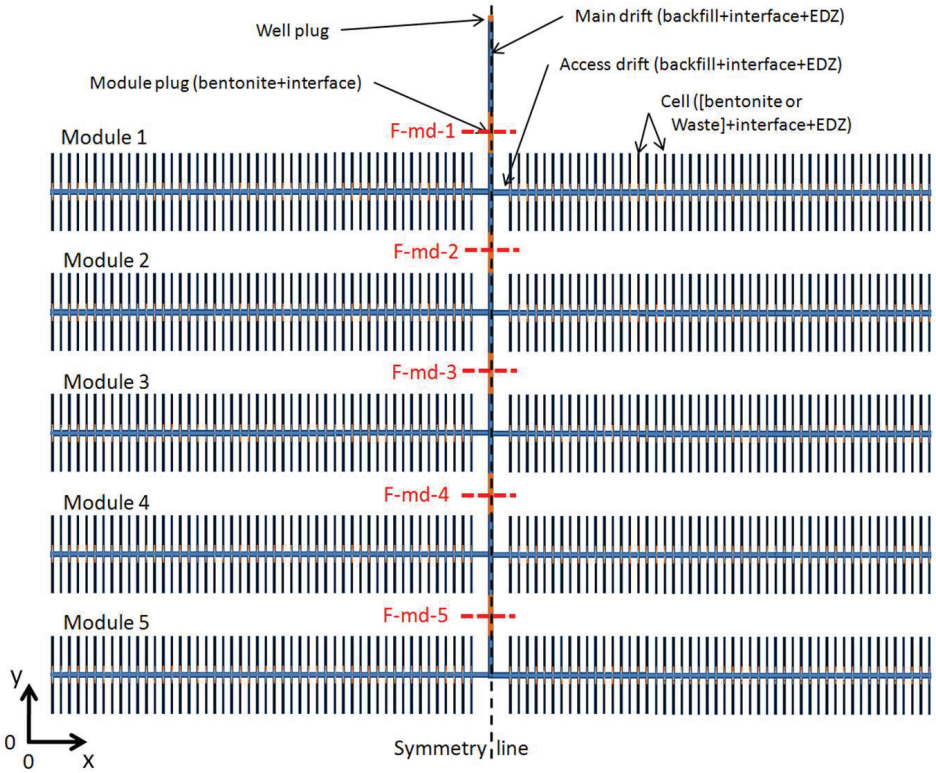

Note: Positive flow denotes flow along the main drift (F-MD, flow-main-drift) towards the shaft.
Figure duplicated from benchmark description in Appendix C.

Figure 89: Location of Surfaces at Which Evolution of Mass Flow With Time Is Presented Within the Main Drift

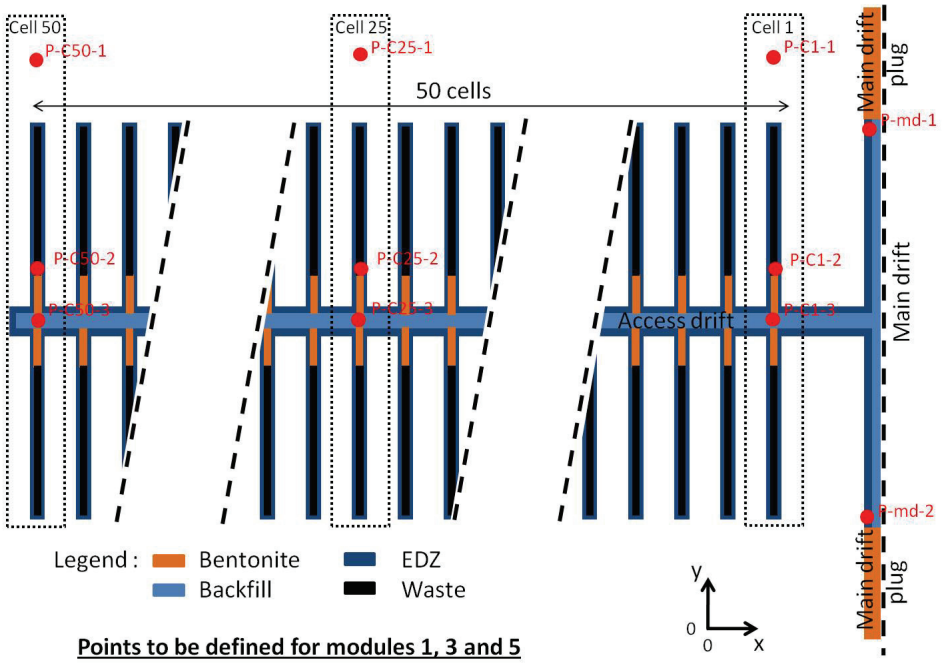

Figure duplicated from benchmark description in Appendix C.

Figure 90: Location of Points at Which Evolution of Water Saturation and Pressures With Time Is Presented for Modules 1, 3 and 5

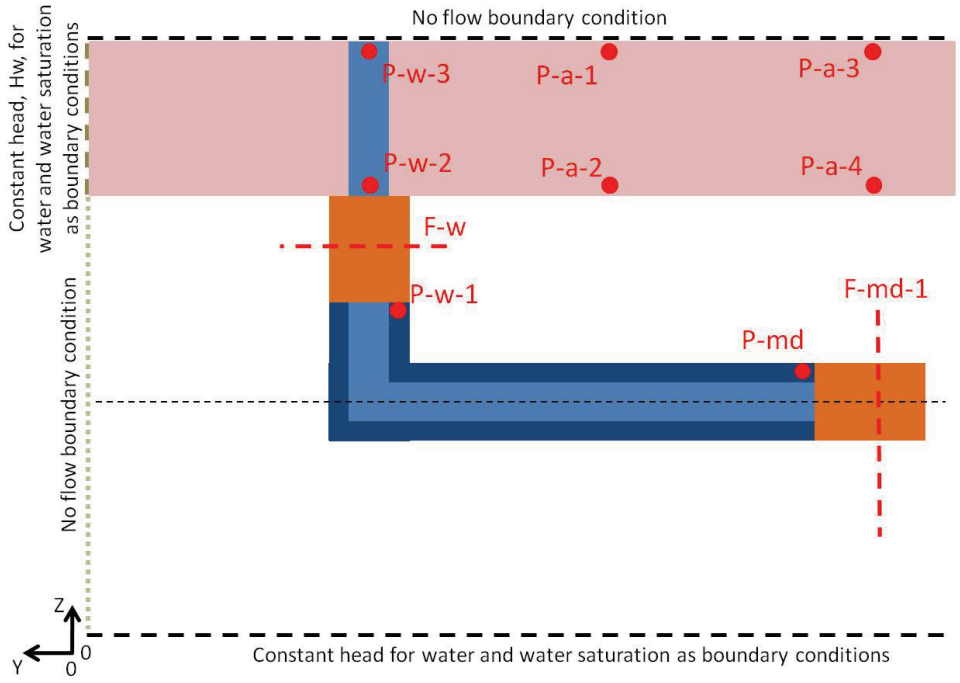

Figure duplicated from benchmark description in Appendix C.

Figure 91: Location of Points at Which Evolution of Water Saturation and Pressures With Time Is Presented for the Main Drift, Shaft and Aquifer

6.2.1 Half-Domain

Only a single module will be shown for the figures in most of this section, for visual simplification of these figures. To justify this simplified representation, the first set of figures show results at three modules (1, 3 and 5) to demonstrate the similarity between modules. Figure 92 shows the water saturation evolution in the modules. Results are similar for each module (note only module 1, 3 and 5 are shown). This similarity between module results extends to pressure results . Hydrogen and dissolved hydrogen gas flows in the modules, shown in Figure 93 and Figure 94, are also very similar between modules with some differences seen at module 5, close to the main drift. Due to the similarity between modules, the subsequent description of repository evolution will only show results for Module 3.

Gas flow in the modules is as expected, with gas flowing along cells and drifts towards the shaft, as demonstrated by the greatest gas flows at F-D1 (closest to the main drift), which is the accumulation of all the gas flows in the modules (Figure 93). After 1000 years, the behaviour is more complex, with little difference in gas flows between F-D25 and F-D1, due in part to the general reduction of gas flow out of the modules resulting from partial saturation of bentonite seals in the main drift. Dissolved gas flows exhibit more complex behaviour from the start of the simulation, due to more complex water gradients in the module (Figure 94). High water pressure gradients between the host rock and the module near cell 50 (farthest from main drift) result in greater dissolved gas flows at cell 50 than at cell 25 (middle of repository). High capillary pressures in the cell plugs results in high water flows (and therefore dissolved hydrogen flows) at all F-C slices.

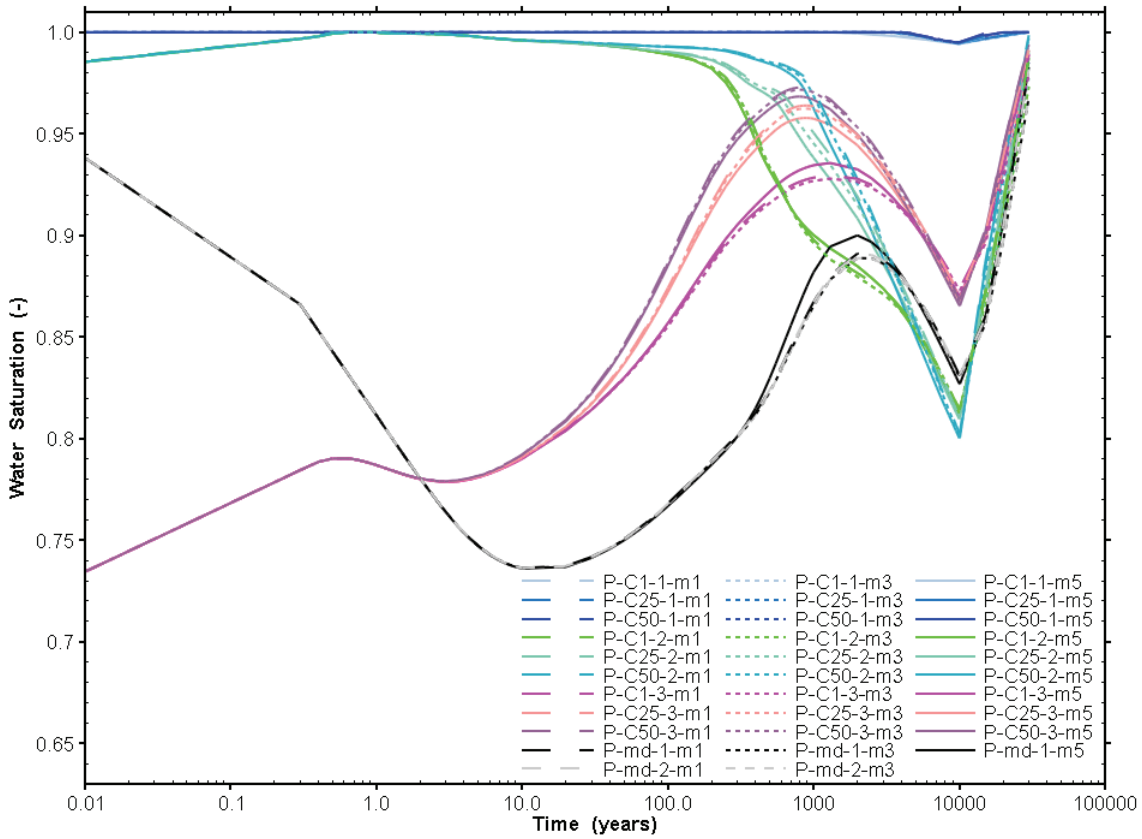

Figure 92: Water Saturation in Modules 1, 3 and 5

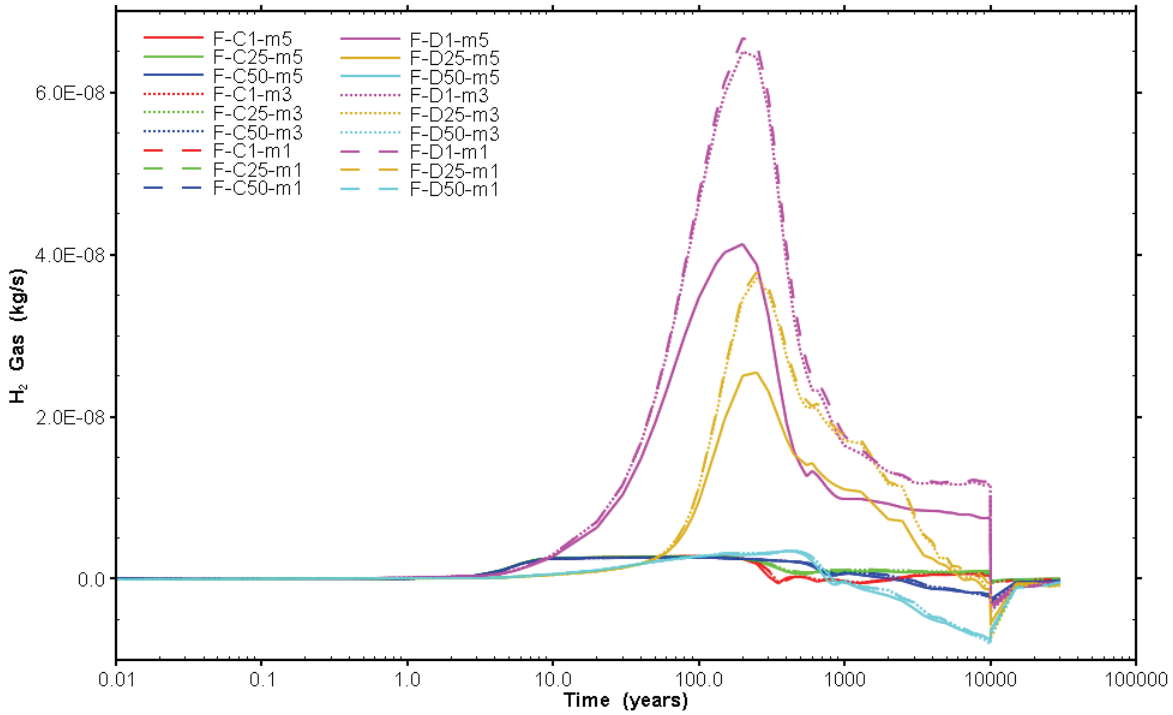

Figure 93: Hydrogen Gas Flows in Modules 1, 3 and 5

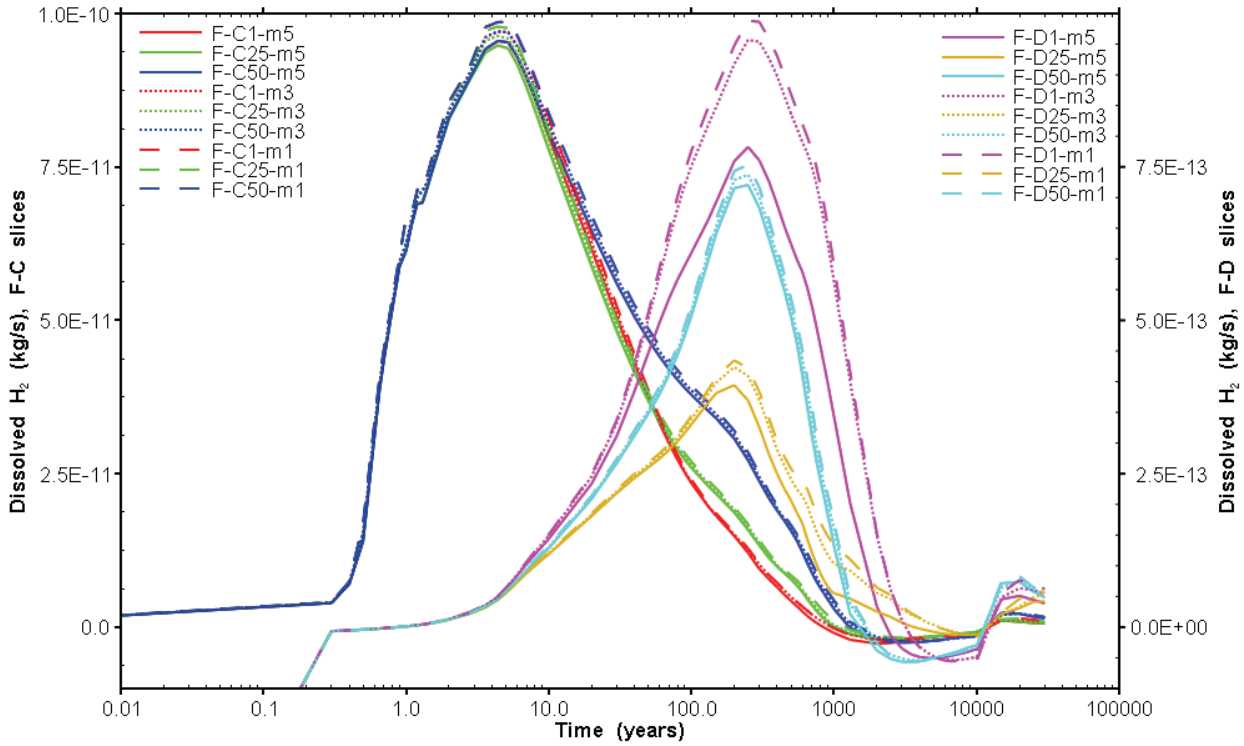

Note: F-C flows are plotted against the left axes, and F-D flows are plotted against the right axes.

Figure 94: Dissolved Hydrogen Gas Flows in Modules 1, 3 and 5

The water saturation, water pressure and gas pressure evolution in the repository and shaft are shown in Figure 95, Figure 96 and Figure 97 respectively. Additional points to those described above were added within the cell seal near P-C25-2-m3 (module 3, cell 25), as well as the main drift seal (note that seal results on either side of module 3 were indistinguishable). P-md1-m3, P-md and P-w-1 are located in the EDZ, which is initially fully water saturated.

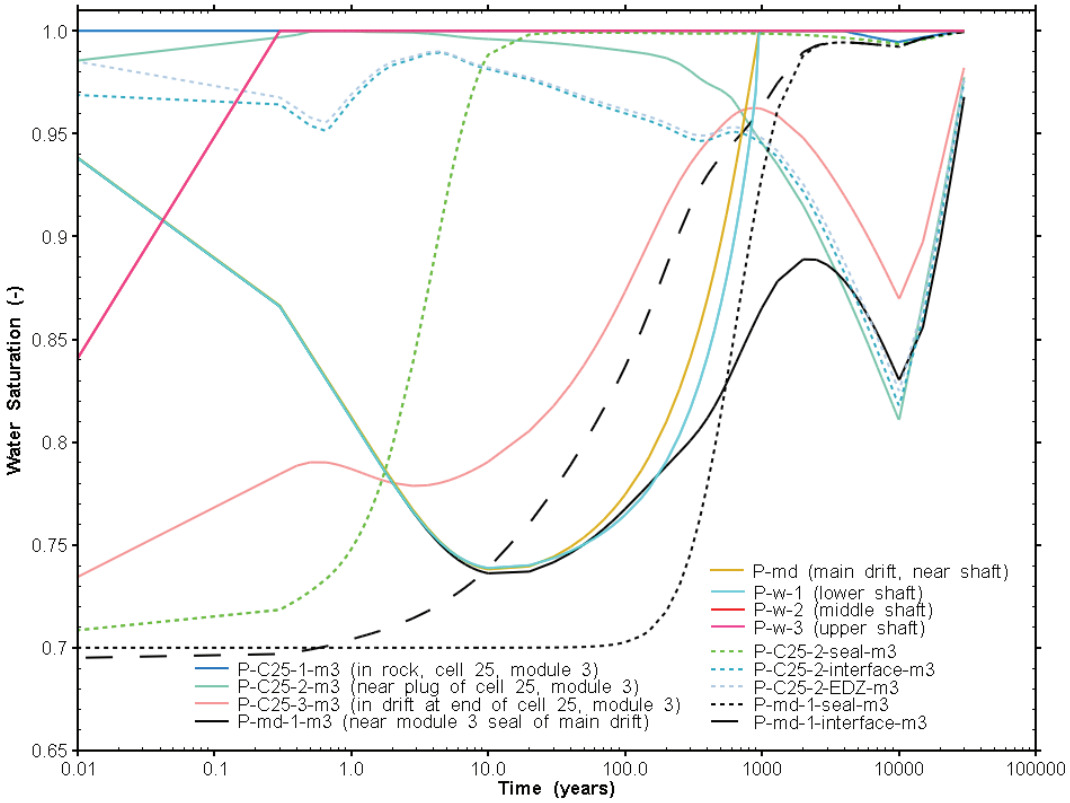

Note: P-w-2 and P-w-3 are identical.

Figure 95: Repository and Shaft Water Saturation Evolution

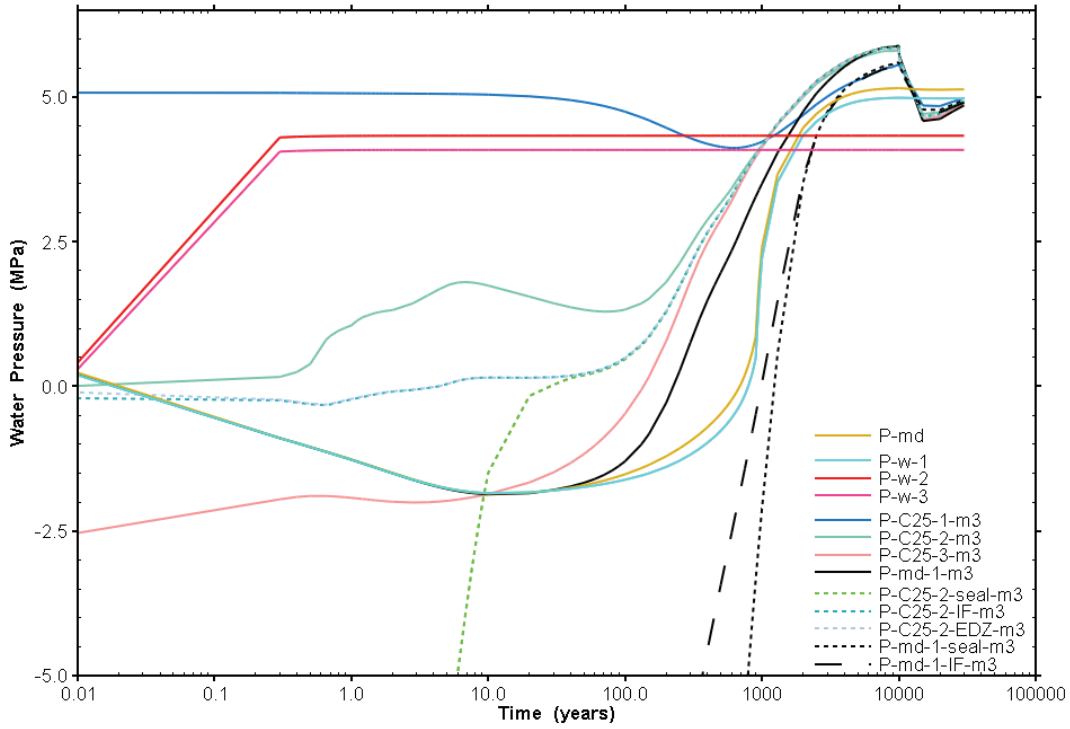

Figure 96: Repository and Shaft Water Pressure Evolution

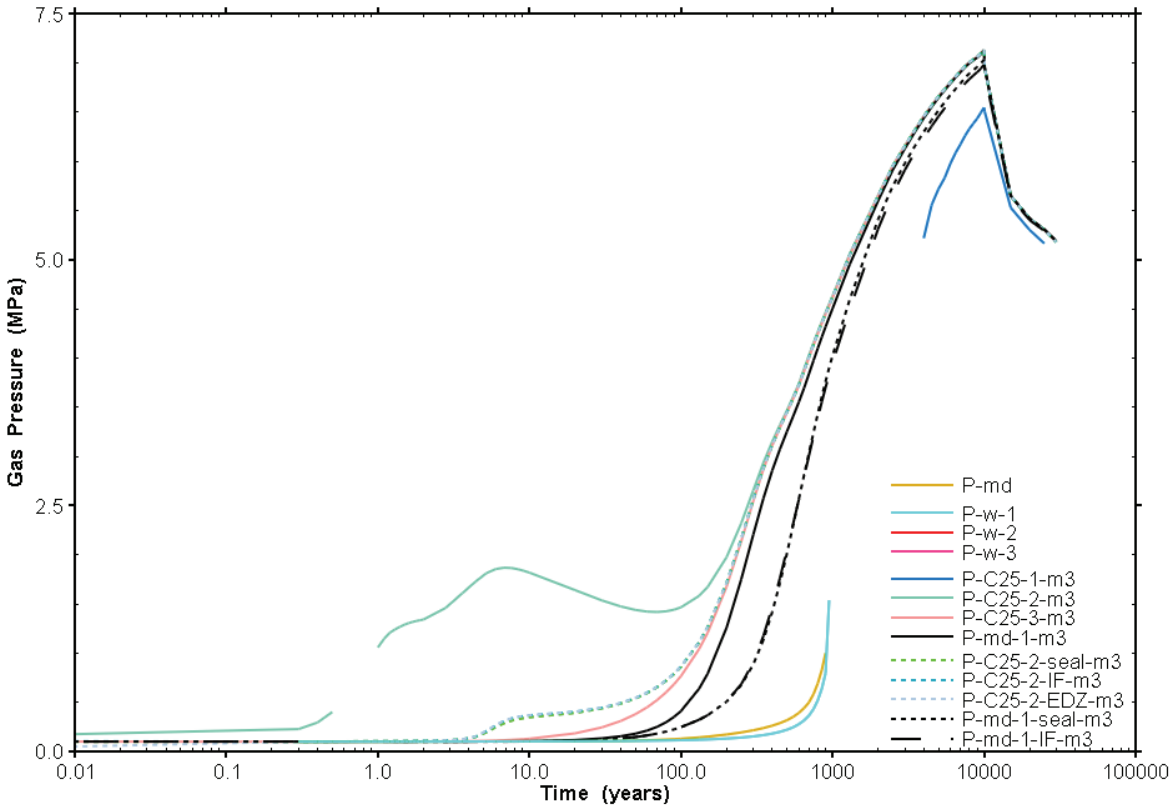

Figure 97: Repository and Shaft Gas Pressure Evolution

The cells go through a short period of full water saturation around 1 year (P-C25-2-m3, solid green line in Figure 95), as water inflow due to large pressure gradients (between host rock and initial atmospheric gas pressure in the repository) dissolves all generated gas. Prior to 10 years, the cells and access drifts saturate with water as the main drift and shaft desaturate due to equilibration of initial conditions. At P-C25-3-m3 (solid pink line) in the access drift, there is a small drop in water saturation and water pressure attributed to the increase in water saturation in the cell bentonite seals (P-C25-2-seal, dashed green line) resulting from high capillary pressures in bentonite.

By 20 years, the seal at the end of cell 25 (P-C25-seal-m3, dashed green line in Figure 95) is almost fully water saturated. The interface and EDZ surrounding the seal (P-C25-2-IF-m3, dashed blue line, and P-C25-2-EDZ-m2, dashed grey line) remains partially saturated, allowing gas to escape through to the access drift. The main drift seals (P-md-1-seal-m3, black short dashed line) and their interfaces (P-md-1-IF-m3, black long dashed line) become mostly water saturated around 2000 years, with a small amount of gas leaking through the seal. This small leakage of gas is quantified by the gas flows through the bentonite seals in the main drift, shown in Figure 98. The flow of gas through the main drift bentonite seals is greatest at module 5 and module 1, due to greater pressure gradients at the ends of the repository.

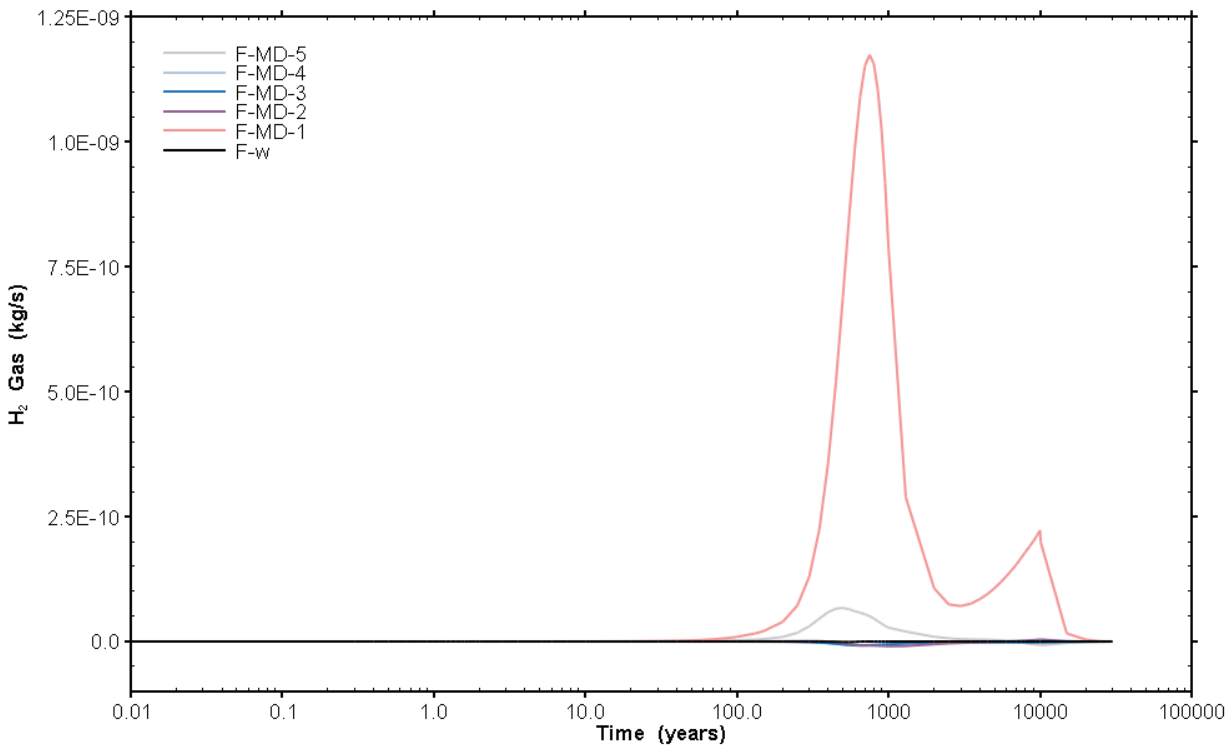

Figure 98: H_2 Gas Flow Through the Main Drift and Shaft

Between 1000 and 2000 years, as less gas escapes the system from the partially saturated seals and water pressures approach hydrostatic (5 MPa), gas production begins to steadily increase gas pressure and reduce water saturations in the cells, access drifts and main drifts (e.g. bump in the water saturation curve (Figure 95) in the access drift P-25-3-m3 (solid pink line) and main drift P-md-1-interface-m3 (solid black line)). Gas migrates into the host rock, with small reductions in water saturation apparent at P-C-25-1 (solid dark blue line) at about 5000 years (Figure 95). At 10 000 years, when gas generation ceases, peak gas pressures of 7.1 MPa are reached in the cells and drifts (Figure 97). Water saturation begins to increase throughout the repository until the repository is mostly water saturated at 30 000 years (Figure 95).

At the top of the shaft (above the seal), initial gas saturations are very quickly dissolved and the shaft remains fully water saturated for the remainder of the simulation (Figure 95). Below the shaft seal (P-w-1, cyan line), and along the main drift until the first repository seal (P-md, gold line), the shaft and main drift near the shaft becomes fully saturated with water at approximately 1000 years. Water pressures in the lower shaft and main drift near the shaft do not increase above hydrostatic pressure, reaching hydrostatic pressure at approximately 10 000 years (Figure 96).

Figure 99 shows hydrogen gas flows through the bentonite seal in the shaft, also indicating no flow of gas up the shaft. The small downward flow of gas prior to the saturation of the seal at 1000 years, is due to pressure gradients in the seal, shown at 650 years in Figure 100, with greater gas pressures at the top of the seal and the shaft above the seal already saturated (note that these gas flows are due to initial gases only). Also prior to saturation of the shaft at 1000 years, water flows in the shaft are primarily towards the bentonite seal as the seal saturates

(high capillary pressures in the bentonite draws water in from surrounding rock and shaft), as shown in Figure 100, and are therefore downwards for the particular slice through the bentonite seal shown in Figure 99. Dissolved gases flowing away from the shaft along the aquifer, as shown in Figure 101, are initial shaft gases (note that all gases in the model are hydrogen). After saturation of the bentonite seal at 1000 years, gas flow ceases and the flow of dissolved gas through the shaft is diminished, although this gas and dissolved gas flow is primarily still downwards - i.e., the gas and dissolved gases are representative of initial shaft gases migrating towards the repository. There is a relatively small amount of dissolved gas migrating upwards through the shaft starting at 7000 years, not discernible in Figure 99.

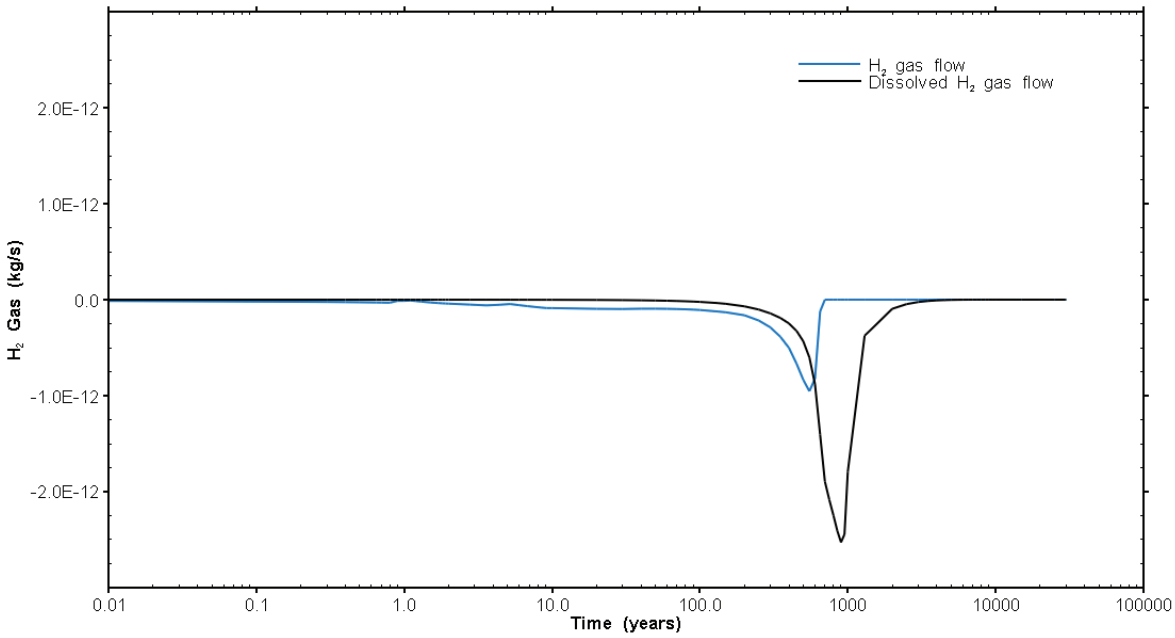

Note: Negative flows indicate downward flow.

Figure 99: Hydrogen and Dissolved Hydrogen Flows Through Bentonite Seal in the Shaft

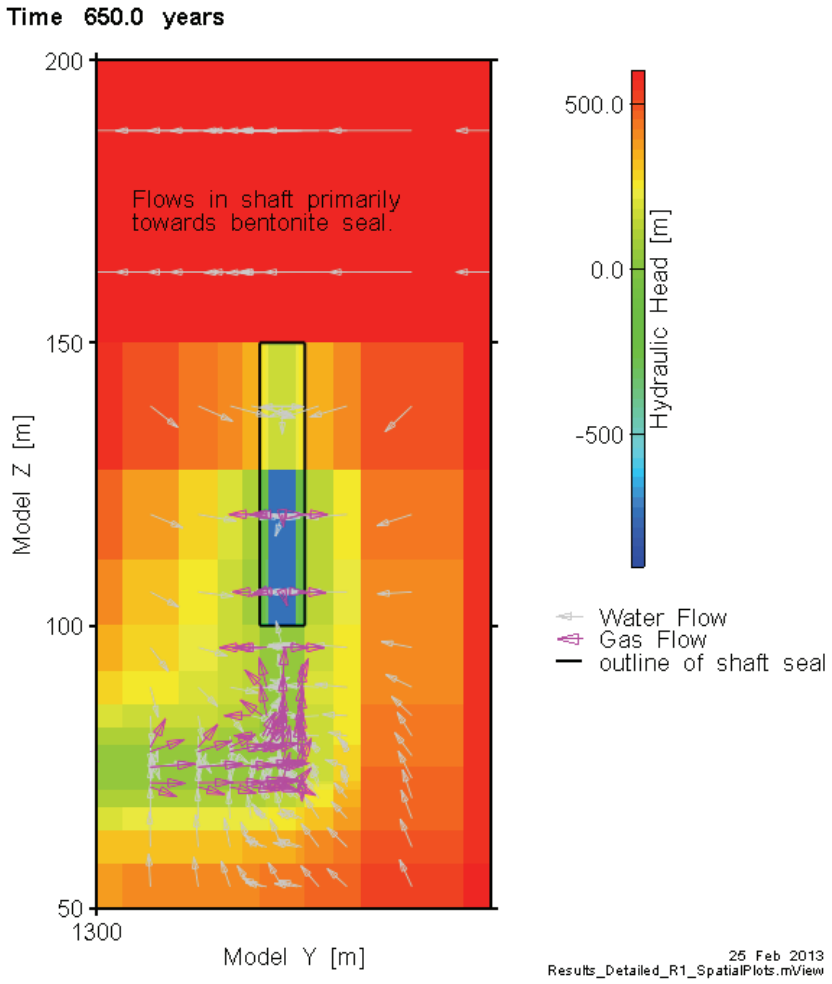

Figure 100: Vertical Slice of Gas and Water Flow in the Shaft at 650 Years

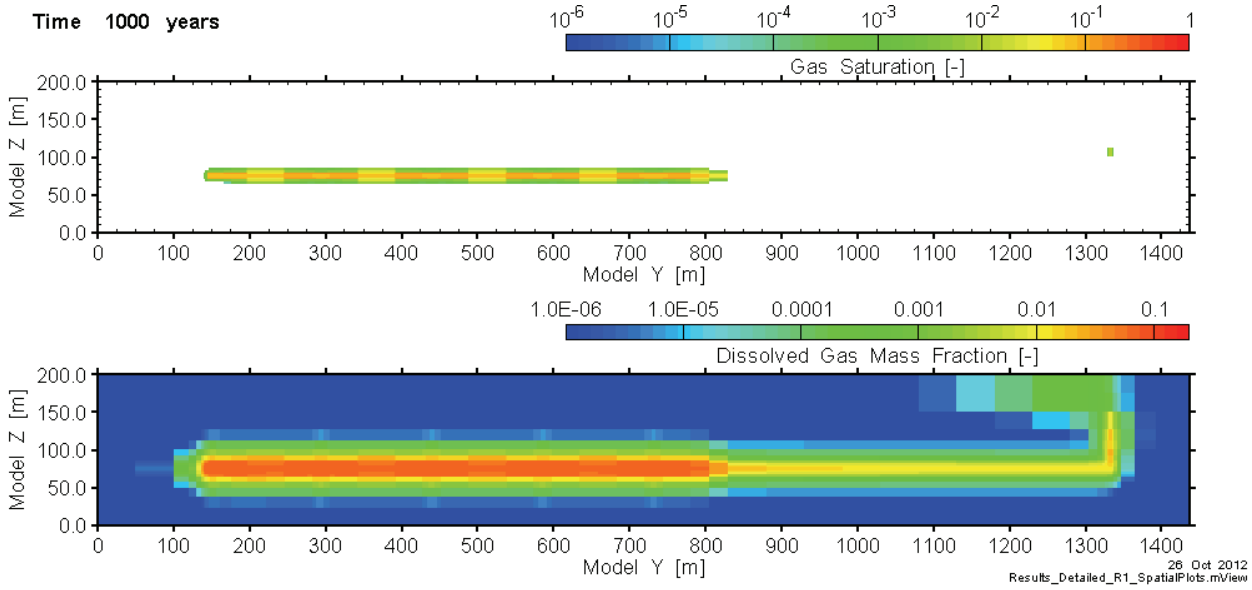

Figure 101: Gas and Dissolved Gas in a Vertical Slice Near the Shaft at 1000 Years

While gas does not migrate upwards through the shaft, it also does not migrate up through the host rock into the aquifer. All of the gas phase that migrates into the host rock dissolves in the water over time. Figure 102 shows gas saturations at 10 000 years along the main drift, and Figure 103 shows 3D gas saturations at various times, illustrating that the gas phase does not extend beyond approximately 35 m above the repository in the host rock. The primary pathway for generated gases to reach the aquifer is through dissolution and vertical migration of the dissolved gas in the host rock.

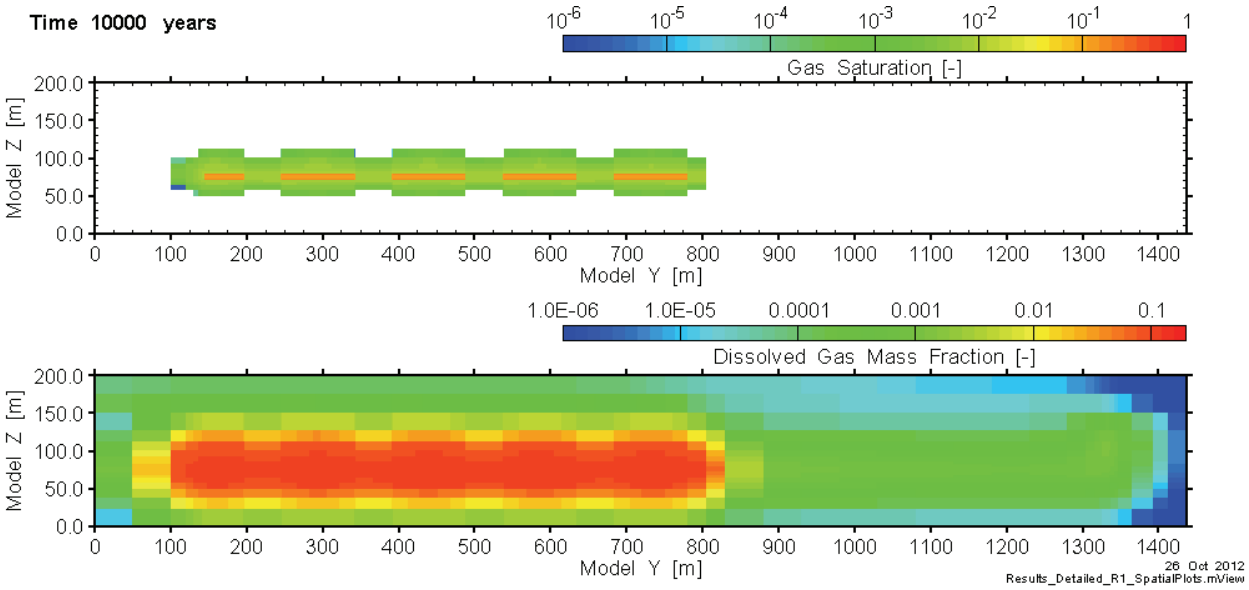

Figure 102: Gas and Dissolved Gas in a Vertical Slice Near the Shaft at 10 000 Years

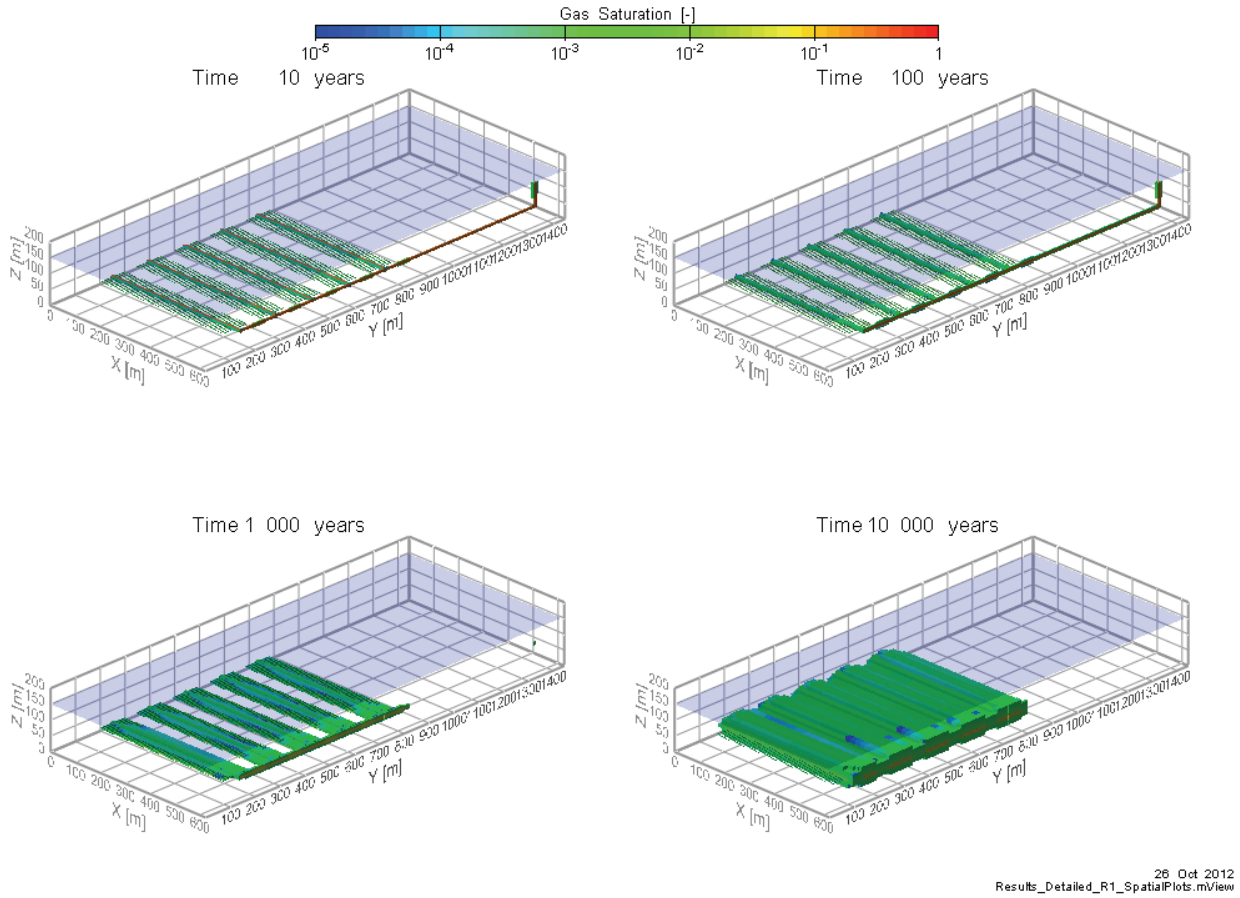

Note: The transparent blue plane delineates the bottom of the aquifer.

Figure 103: 3D Gas Saturations in the Repository at Various Times

6.2.2 Sensitivity Case: No Interface

A sensitivity case was simulated with the half-domain model to illustrate the effects of the interface. Properties for all elements which contained a combination of interface and an adjacent material were replaced with the properties for the adjacent material (e.g., EDZ for the inner EDZ). In the base case, the interface provides a permeable pathway with low capillary pressures. The exception is at the cell seal interface, where permeability is the same as the EDZ, but the interface has much lower capillary pressures (two orders of magnitude) and greater porosities. Compared to the Base Case, this simulation was numerically more stable and was able to use coarser convergence criteria. The resulting run time of 4.5 days is shorter than the one week run time of the Base Case, and improved run times may also be seen with coarser discretization (refined discretization was required in some cases to capture the upscaled interface elements).

From a repository water saturation and pressure perspective, the interfaces had minimal impact. Figure 104 and Figure 105 show the water saturation and gas pressure for the no interface case, compared to the base case half-domain model.

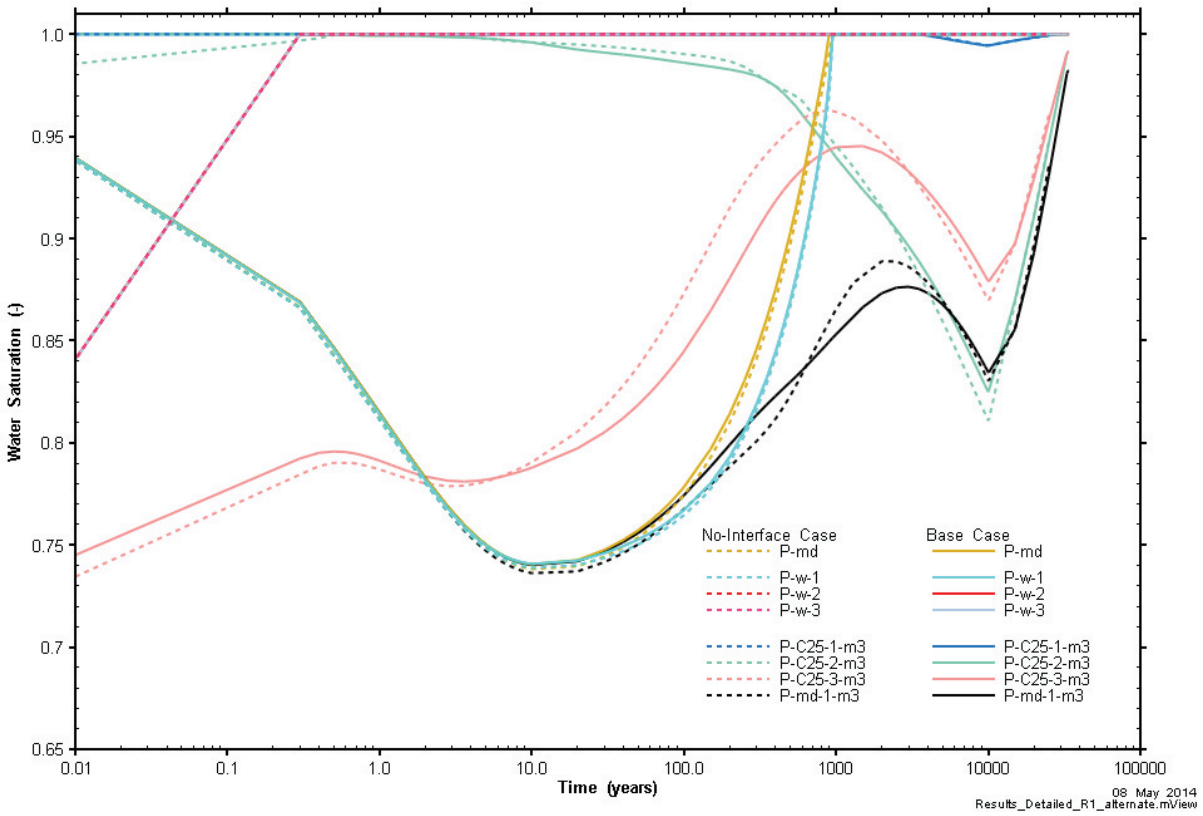

Figure 104: Water Saturation Comparison of Half-Domain Model With and Without Interfaces

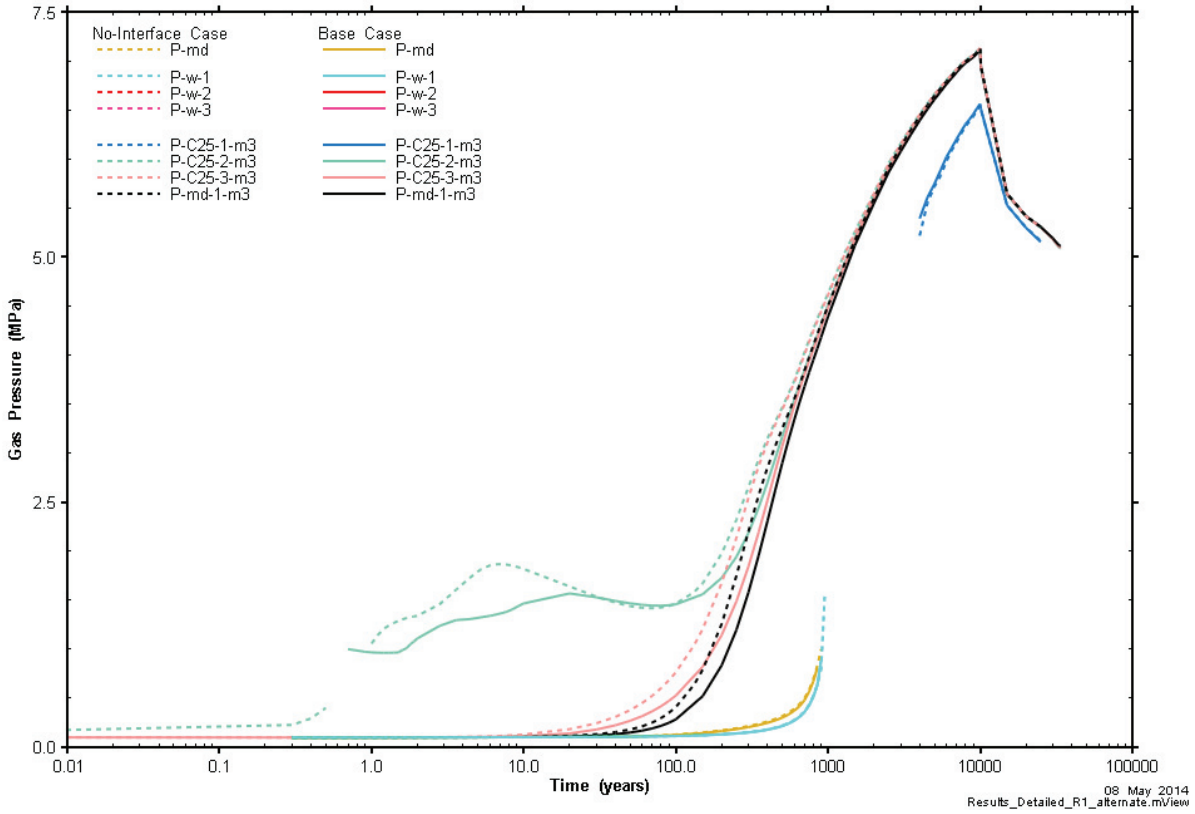

Figure 105: Gas Pressure Comparison of Half-Domain Model With and Without Interfaces

Gas and water flows in the cells, access drifts and main drifts were reduced in the no-interface case. Figure 106 shows gas flows and Figure 107 shows dissolved gas flows. Flow in the shaft is unchanged in that gas flows (F-w in Figure 106 are too small to be perceptible at this scale) and dissolved gas flows (F-w in Figure 107) are downwards. Note that flows in the access drift (F-D in Figure 106 and Figure 107) are greater than flows out of the cells (F-C in Figure 106 and Figure 107), due to the accumulation of flow out of all the cells. Flows in the main drift (F-MD in Figure 106 and Figure 107) are much reduced, due to the seals in the main drift (which is the location of these flow observations).

In the absence of gas or dissolved gas reaching surface through the shaft, the no-interface case provides a good representation of the saturation and pressures in the system, as well as the amount of dissolved gas reaching the aquifer. Figure 108 shows the amount of dissolved gas in the aquifer over time, for both the base and no-interface cases, showing that the amount of dissolved gas reaching the aquifer in each case is almost identical. This is perhaps not surprising since dissolved gas in the aquifer is a result of gas dissolving and diffusing into the host rock, rather than being transported along the repository cells and drifts containing the interfaces. In an alternative repository scenario where the shaft is an important pathway to surface, the no-interface case would likely underestimate gas and dissolved gas transport to surface.

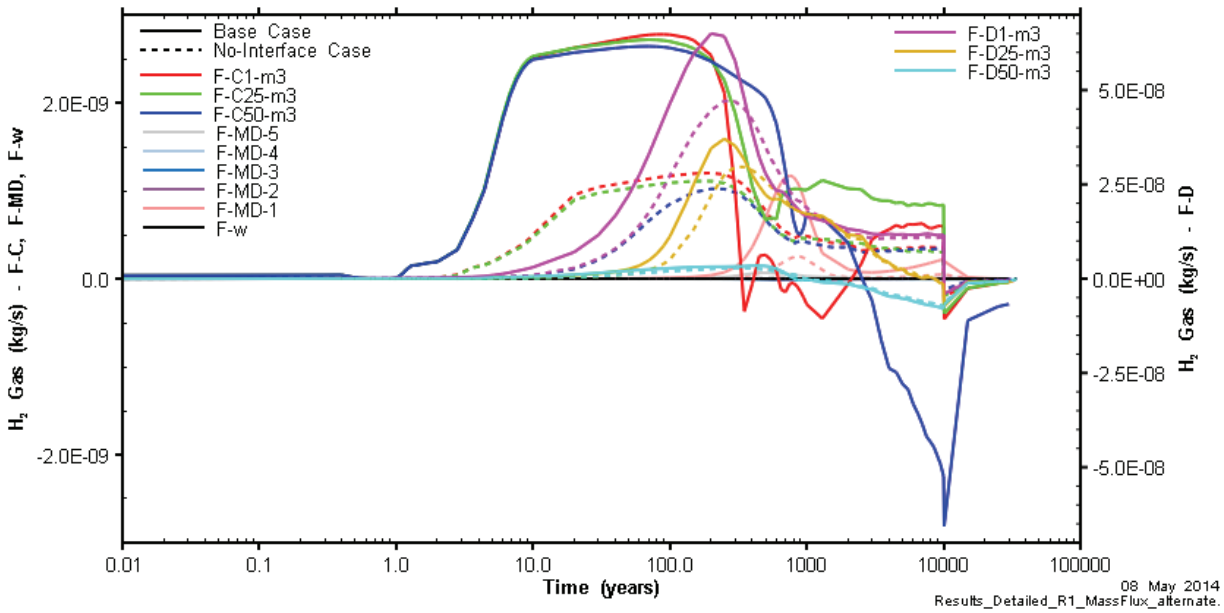

Note that F-D flows are plotted against the right axis and all other flows are plotted against the left axis.

Figure 106: Gas Flows at F-C, F-D, F-MD and F-w Slices for Both the Base and No-Interface Cases

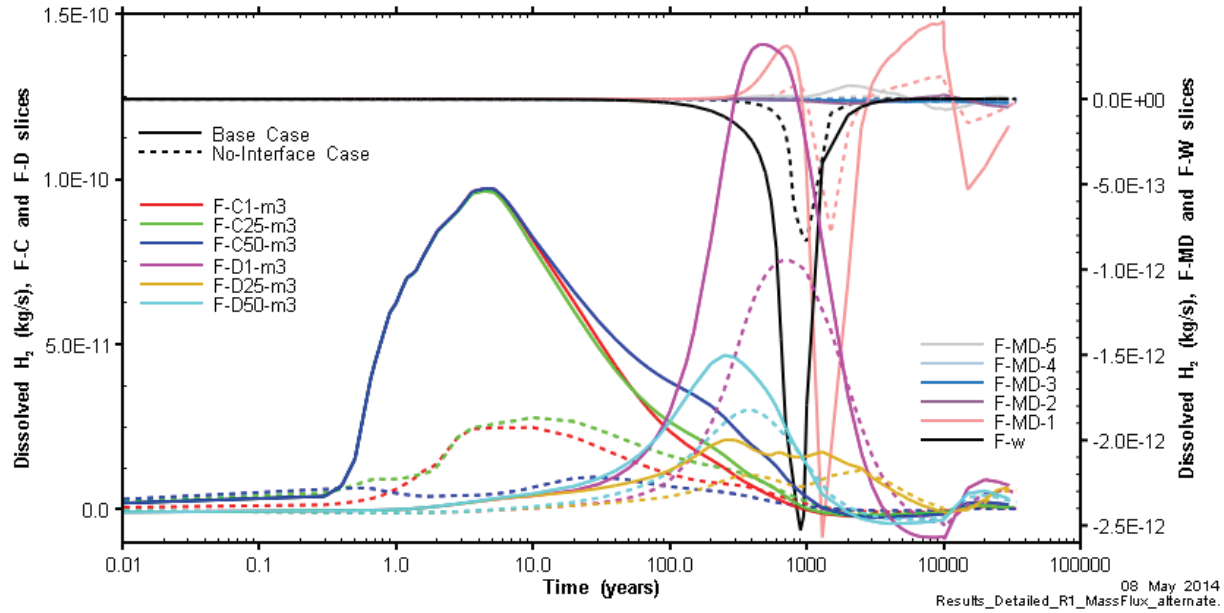

Note: F-C and F-D flows are plotted against the left axis and F-MD and F-w flows are plotted against the right axis.

Figure 107: Dissolved Gas Flows at F-C, F-D, F-MD and F-w Slices for Both the Base and No-Interface Cases

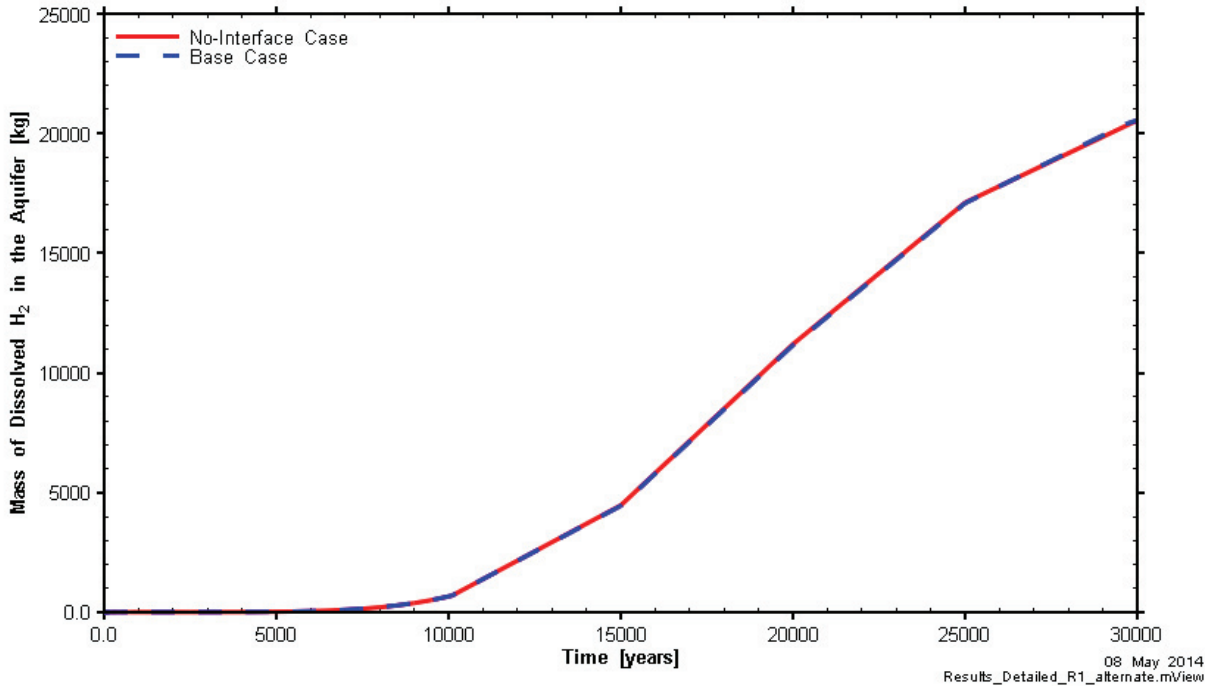

Figure 108: Mass of Dissolved Gas in the Aquifer Over the Course of the Simulation, for Both the Base and No-Interface Cases

6.2.3 Main Drift

The main drift model was created as a quick assessment of the repository scale. As such, it used the module-scale model to develop the inputs (note that boundary conditions were updated based on initial results of the main-drift model), which are the same for each module of the repository. While the output from the half-domain model could also be used, this model assesses the effectiveness of using a series of detailed small-scale models (such as the module-scale and main drift models) to represent the full-scale system. Figure 109 and Figure 110 compares the gas and water flow input into the main drift model (as output from the module-scale model) to the gas and water flows at the each module within the half-domain model. Generally, the shape of the curves is similar, with the main drift model inputs underestimating the peak gas flow, and overestimating the peak water flow of the half-domain model. The exception is the half-domain gas flows for module 5, which are less than the main drift model inputs (Figure 109). The main drift model input uses the same input for all modules, and consequently does not adequately represent gas flows at this end of the repository, farthest from the shaft.

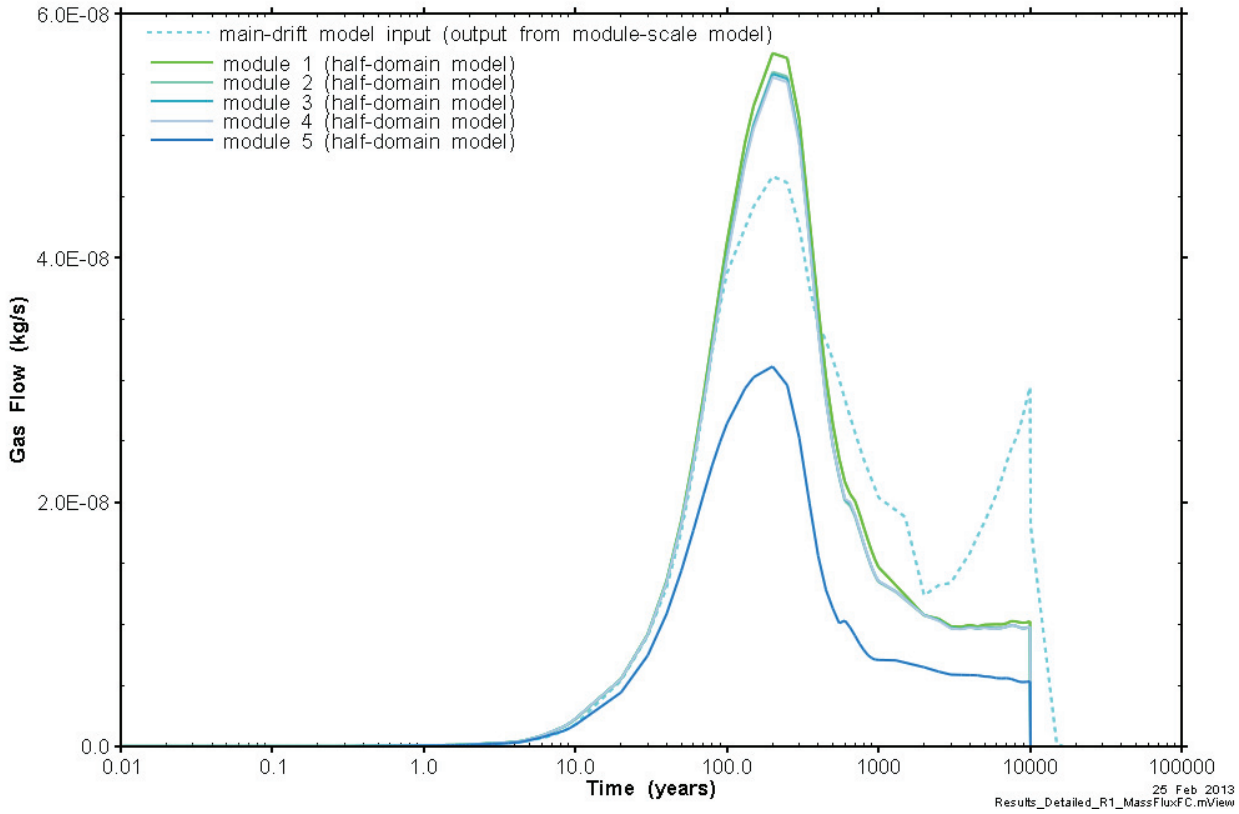

Figure 109: Gas Flow Comparison Between Main-Drift Model Input and Half-Domain Model Flows Out of Each Module

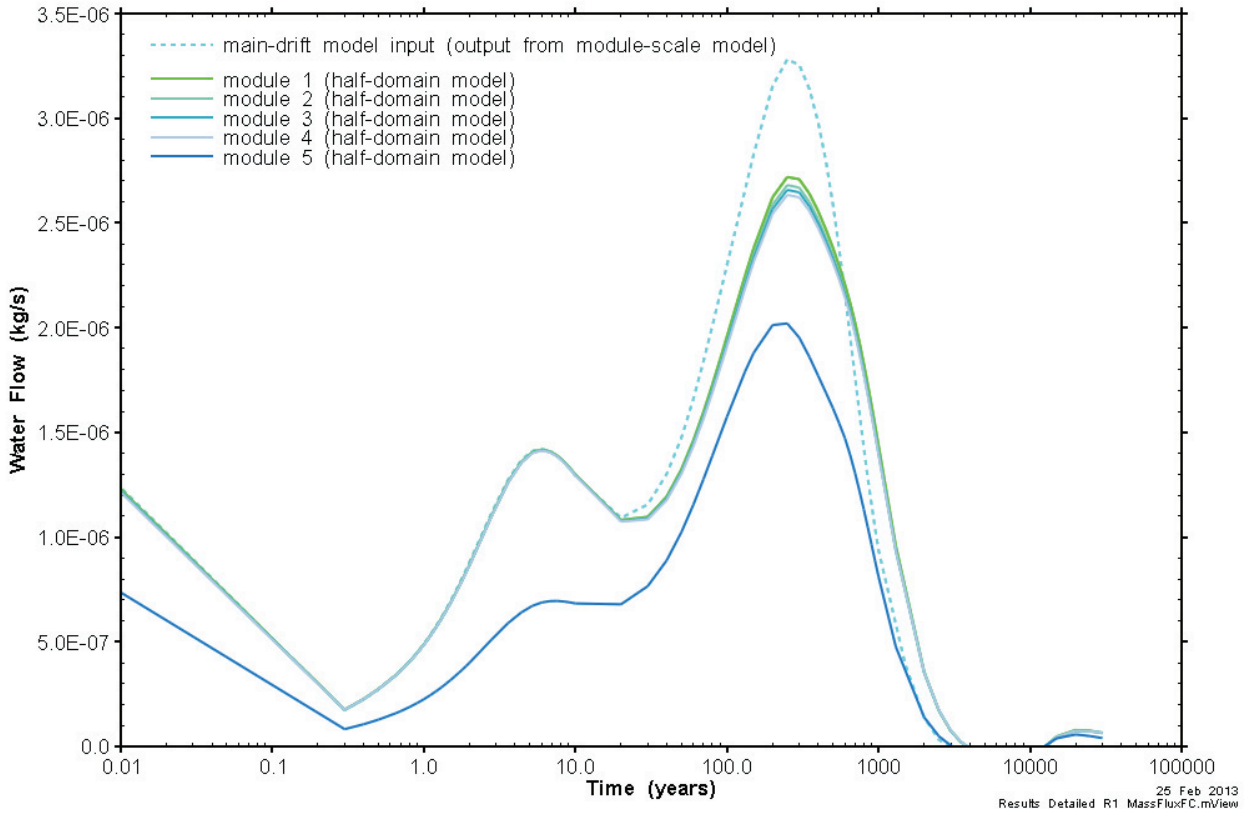

Figure 110: Water Flow Comparison Between Main-Drift Model Input and Half-Domain Repository Flows Out of Each Module

Despite these small differences in peak water and gas flow exiting the panels, the water saturation, water pressure and gas pressure evolution in the main drift and shaft are similar, as shown in Figure 111 through Figure 113. There are small differences in the peaks and timing of the saturation and pressure curves, although the trends of the curves are the same. Peak gas pressures are similar (in main drift near module 3), at 6.9 MPa for the main-drift model and 7.1 MPa for the half-domain model, and the drifts in both models are fully water saturated before 30 000 years.

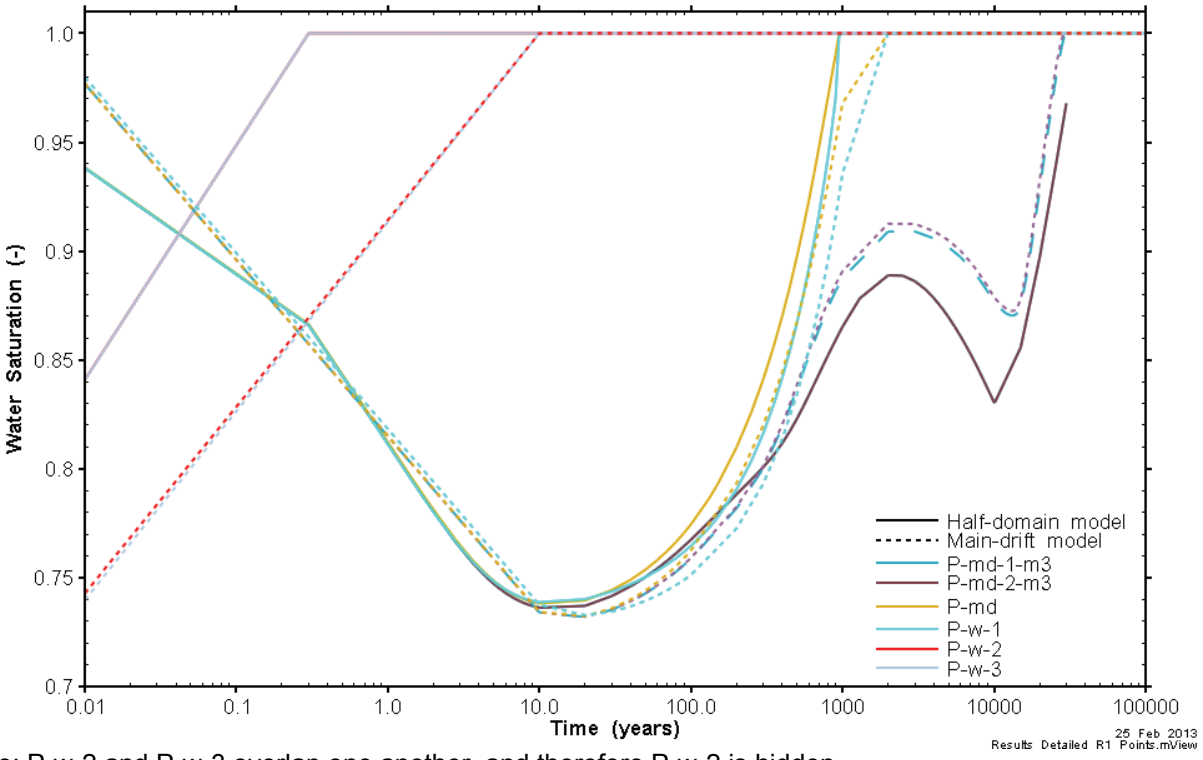

Note: P-w-2 and P-w-3 overlap one another, and therefore P-w-2 is hidden.

Figure 111: Water Saturation Comparison Between the Main-Drift and Half-Domain Models

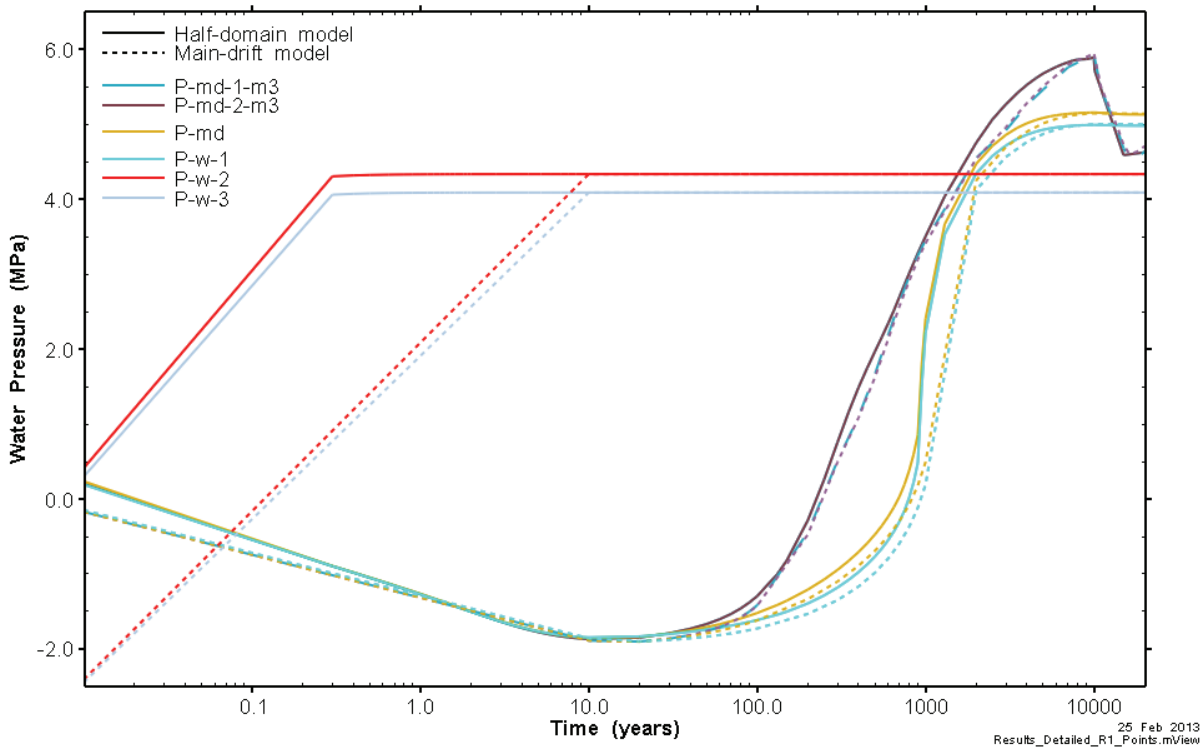

Figure 112: Water Pressure Comparison Between the Main-Drift and Half-Domain Models

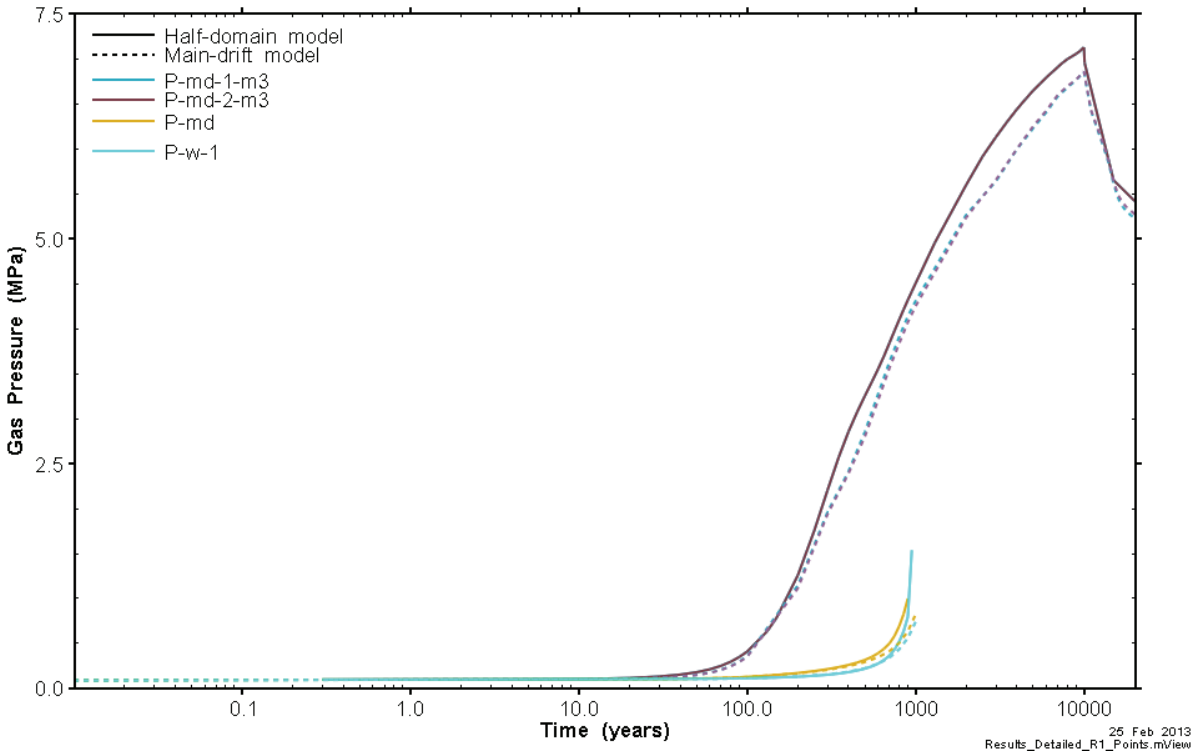

Figure 113: Gas Pressure Comparison Between the Main-Drift and Half-Domain Models

Figure 114 and Figure 115 compare hydrogen gas and dissolved hydrogen gas flows along the main drift in the main-drift and half-domain models. The main drift model generally overestimates gas flows and underestimates dissolved gas flows, which is in opposition to the discrepancies between the main drift source inputs and the half-domain model (Figure 109 and Figure 110). There are also greater discrepancies at module 5, which is not surprising given that this module differed from the other modules in the half-domain model, yet was treated to be similar to other modules in the main-drift model.

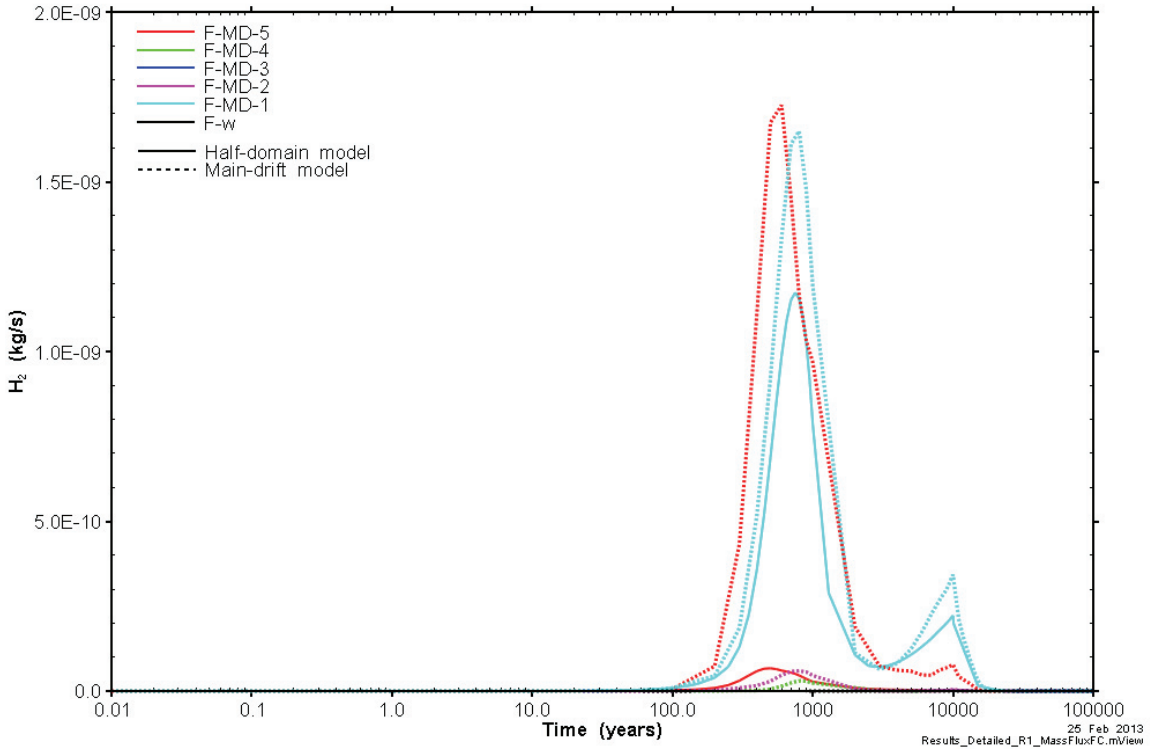

Figure 114: Comparison of H_2 Gas Flow Along Main Drift and Shaft Between Main-Drift and Half-Domain Models

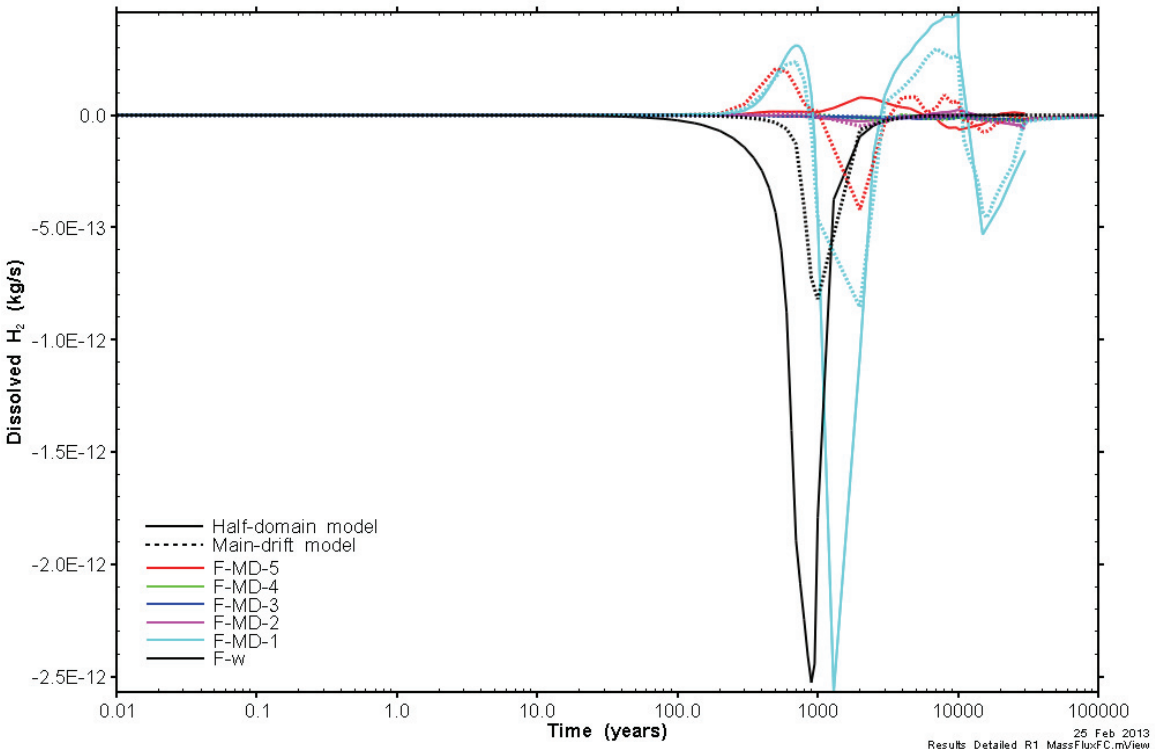

Figure 115: Comparison of Dissolved H_2 Gas Flow Along Main Drift and Shaft Between Main-Drift and Half-Domain Models

6.2.4 Comparison to Module-Scale Model

While the benchmark module-scale model had boundary conditions incongruous with the repository-scale model, it is still instructive to compare the two models: (1) to observe the effects of the incorrect module-scale boundary conditions (as previously discussed, the module-scale boundary conditions did not equilibrate with the host rock as quickly as the module), and (2) to observe any effects of the nested model approach. Where appropriate, results from the module-scale model with improved boundary conditions based on the repository-scale model, executed in support of the main-drift model, are included in the comparison. This simulation includes parameters consistent with the repository-scale model, which is equivalent to the alternative upscaled parameter set of the module-scale model. Section 5.2.2 provides a module-scale comparison between the base case module-scale parameter set and the alternative parameter set.

Figure 116, Figure 117 and Figure 118 show water saturation, gas pressure and water pressure for the module-scale model, updated module-scale model and repository-scale model. Repository-scale model results are extracted from module 3. Results are very similar between models. Maximum gas pressure differs, with 6.7 MPa at the module-scale, 7.1 MPa at the repository-scale and 7.3 MPa for the updated module-scale model.

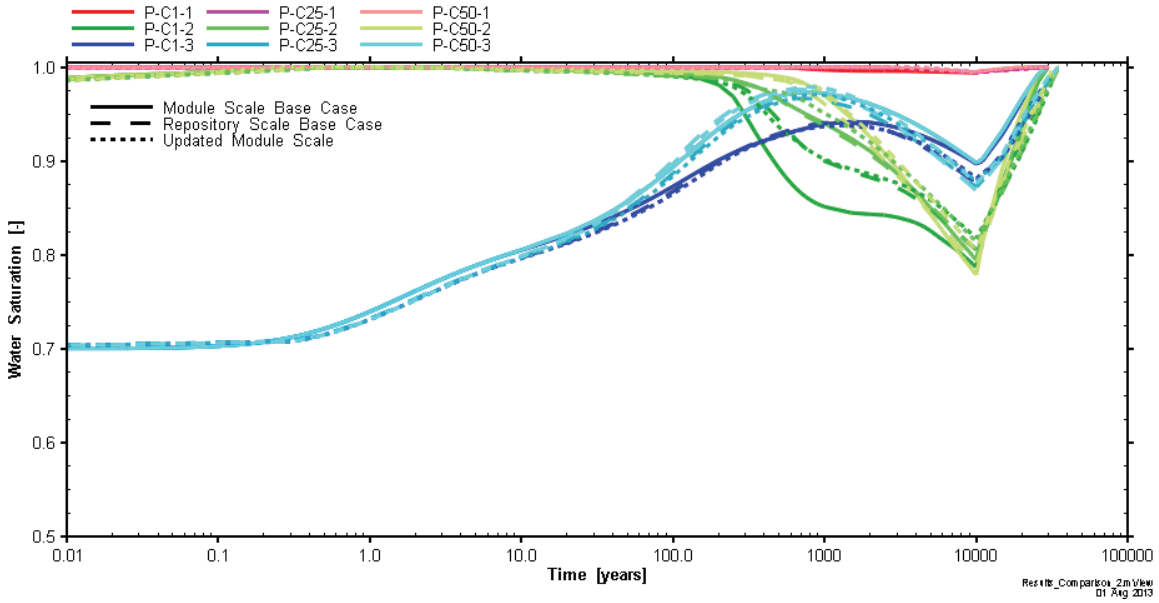

Figure 116: Water Saturation at Module Output Points for the Module-Scale and Repository-Scale (Module 3) Models

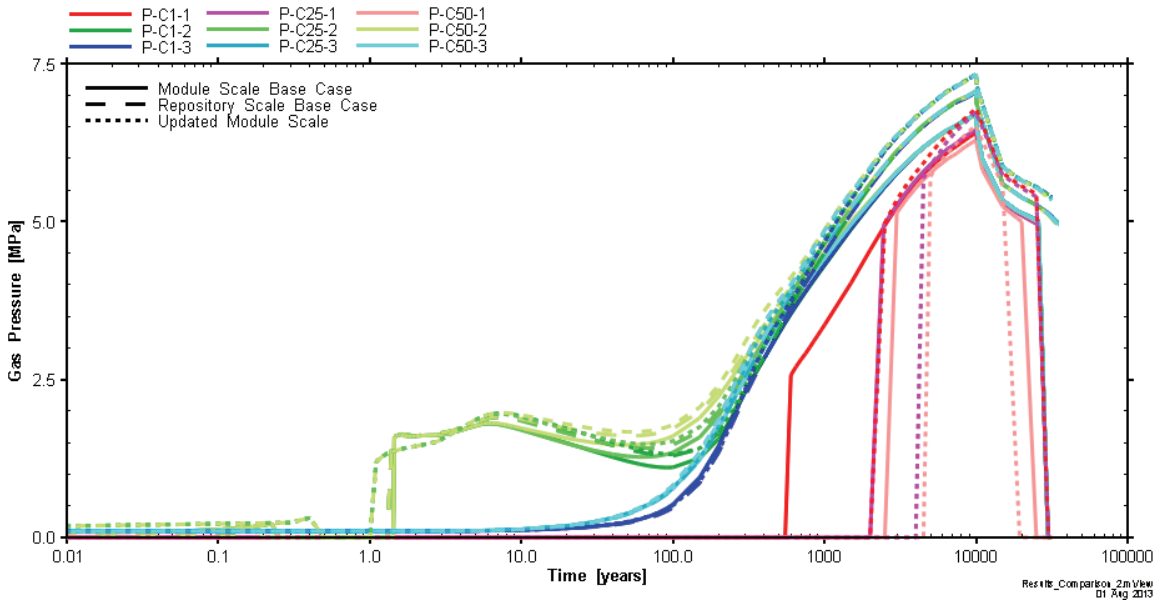

Figure 117: Gas Pressure at Module Output Points for the Module-Scale and Repository-Scale (Module 3) Models

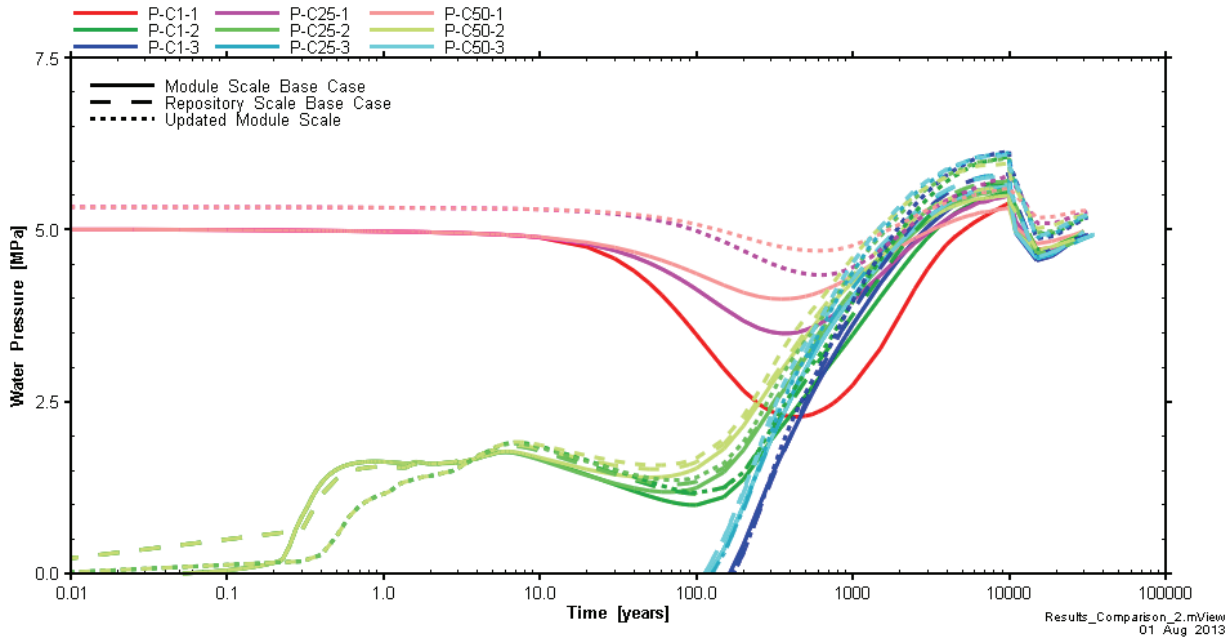

Figure 118: Water Pressure at Module Output Points for the Module-Scale and Repository-Scale (Module 3) Models

Figure 119 and Figure 120 compare hydrogen gas and water flow between the models at slices along the access drift (FD). In general, there is a good comparison between all models, suggesting that the module-scale model, even with inaccurate main drift boundary conditions, provides a good representation of the module behaviour. It also suggests that the bentonite seals in the drift provide a strong driver for flow in the repository, regardless of the boundary condition on the other side of the bentonite seal. One feature that is different between the cases is the hydrogen gas flows at FD-1 in the access drift for the updated module-scale model, where a secondary peak forms after 1000 years and terminates when gas generation ceases at 10 000 years. This secondary peak is similar to the flow trends observed in the main drift of the repository scale model (see Figure 114), at modules 1 and 5. This similarity between the main drift flows and the updated module-scale model flows suggests that the boundary condition for the updated module-scale model has notable effects on results, highlighting a potential weakness of nested models. An iterative approach to the boundary condition may improve congruence between the module and repository scale models.

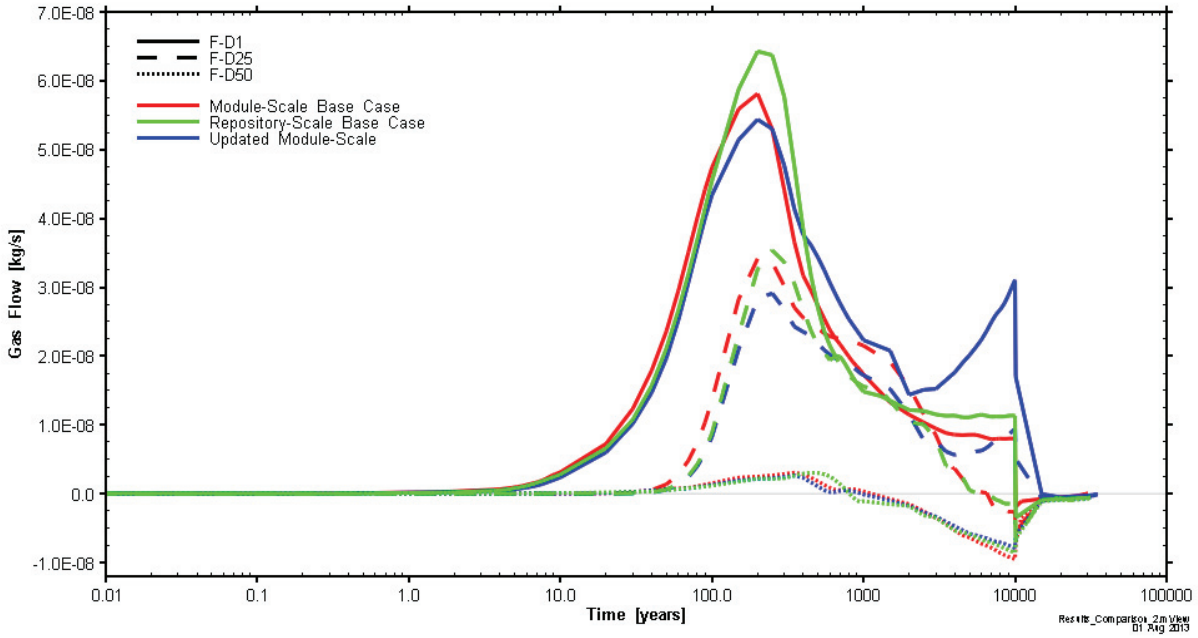

Figure 119: Hydrogen Gas Flows at FD Slices for the Module-Scale and Repository-Scale Models

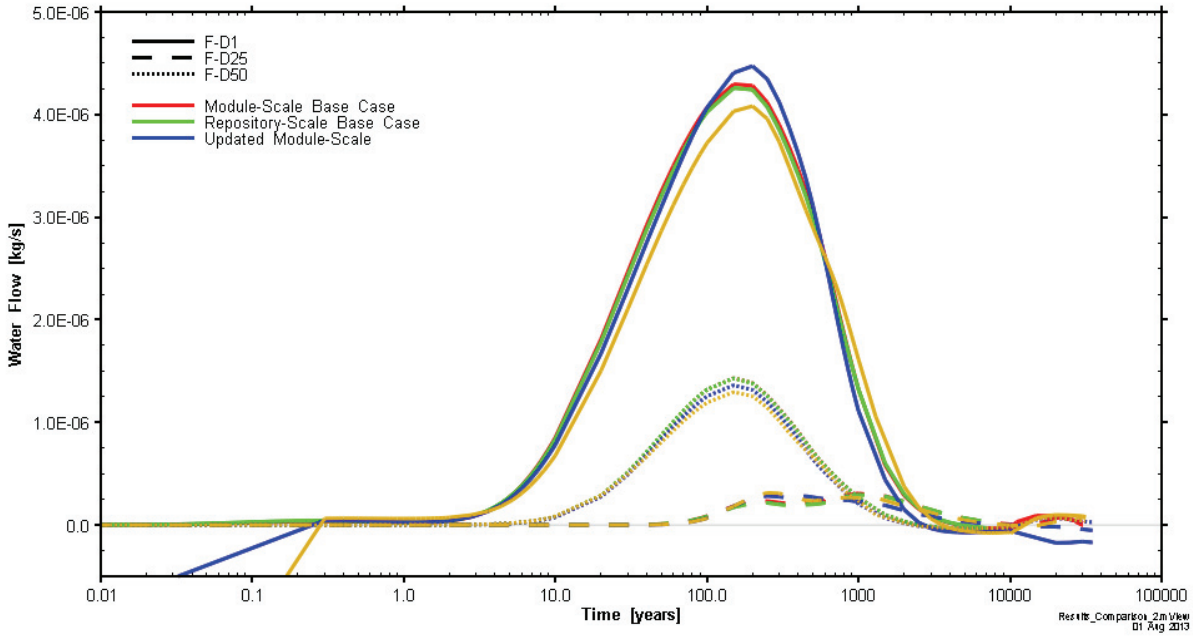

Figure 120: Water Flows at FD Slices for the Module-Scale and Repository-Scale Models

6.2.5 Comparison of Key Results

This section compares key results of the half-domain model to results produced by two other teams contributing to the FORGE benchmark studies, NDA/Quintessa and ANDRA. Other FORGE teams have not produced repository-scale results.

Both NDA/Quintessa and ANDRA included the interface explicitly. They also assumed that a single cell changes little across or between modules, by using calculations at a single cell to represent a number of cells across the module. Further details are published in the final FORGE benchmarking report (Wendling et al. 2014c)

Figure 121 compares gas pressures from the half-domain model to results obtained from NDA/Quintessa and ANDRA. Results from NDA/Quintessa appear to include water pressures when no gas is present (e.g. P-w-2). Figure 122 compares liquid pressures. The trend in pressures compares well between groups; however, higher peak pressures are obtained by both teams. The peak gas pressure is 8.9 MPa from NDA/Quintessa, 7.6 MPa from ANDRA and 7.1 MPa from NWMO/Geofirma. The peak water pressure is 7.5 MPa from both NDA/Quintessa and ANDRA, and 5.8 MPa from NWMO/Geofirma.

Gas and water flow results are shown in Figure 123 through Figure 126. General trends compare well with NDA/Quintessa and ANDRA. For some locations, ANDRA gas and water flows are substantially higher than either NDA/Quintessa or NWMO/Geofirma. In particular, NDA/Quintessa and ANDRA's results in the shaft correspond to the results presented here: no gas flows up the shaft (Figure 125), and water flow is also downwards (Figure 126), suggesting transport of dissolved gas up the shaft is limited to diffusion.

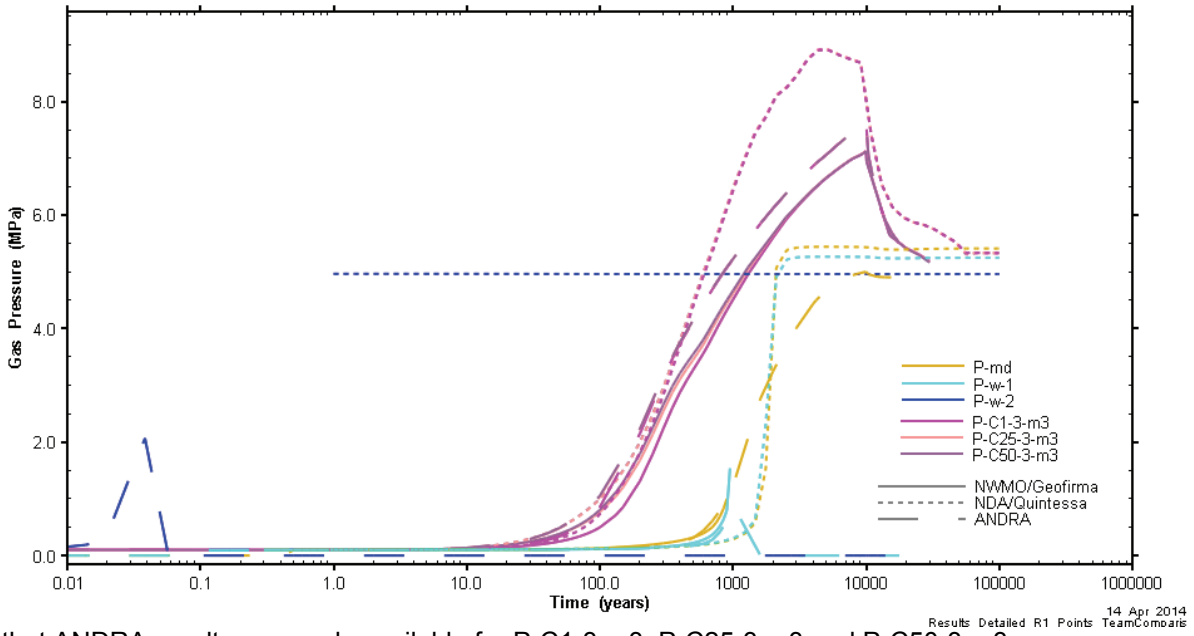

Note that ANDRA results were only available for P-C1-3-m3, P-C25-3-m3 and P-C50-3-m3.

Figure 121: Gas Pressure Comparison to NDA/Quintessa and ANDRA Results

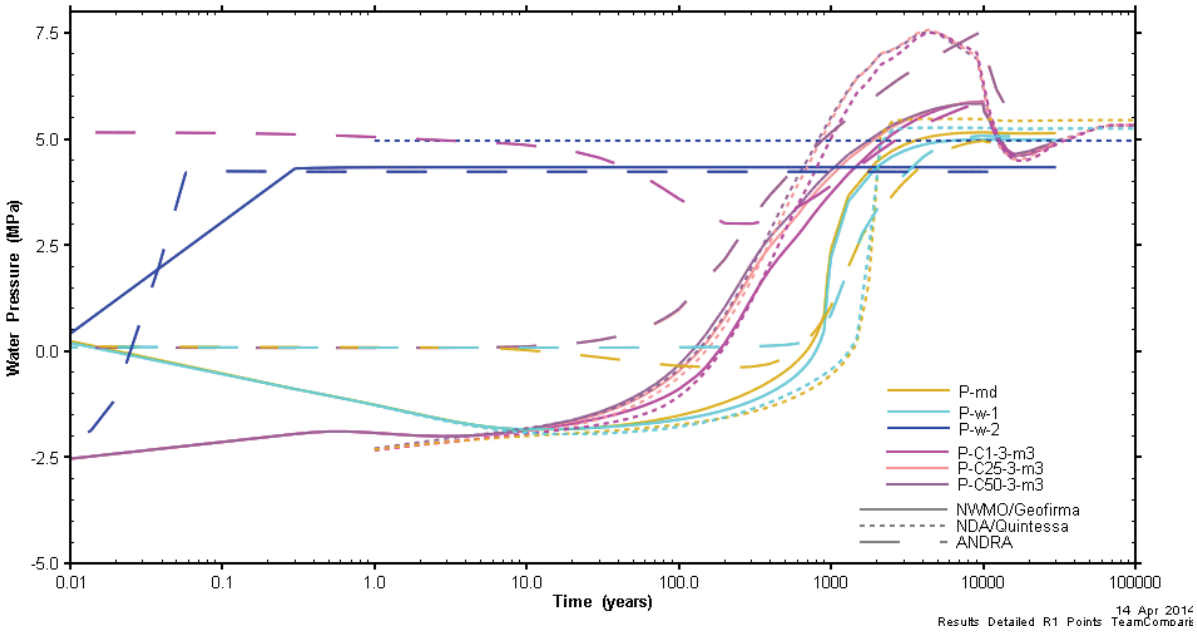

Figure 122: Water Pressure Comparison to NDA/Quintessa and ANDRA Results

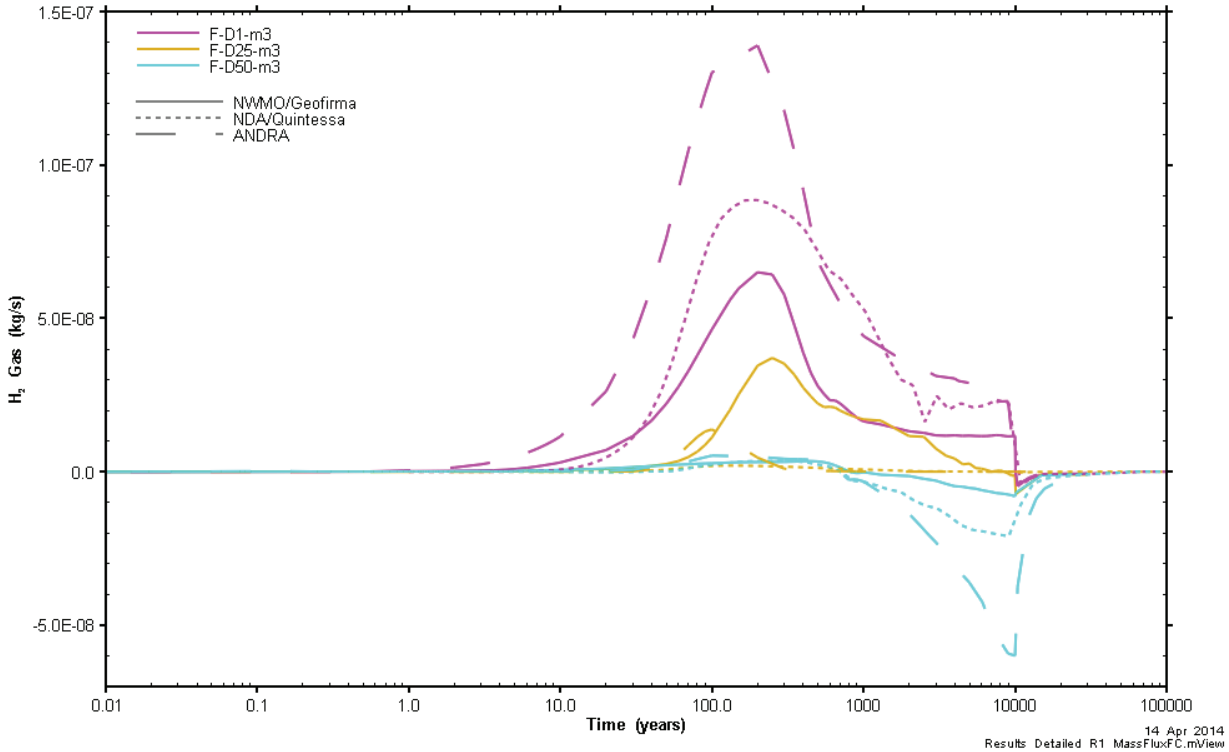

Figure 123: Gas Flow Comparison in the Access Drift of Module 3 to NDA/Quintessa and ANDRA Results

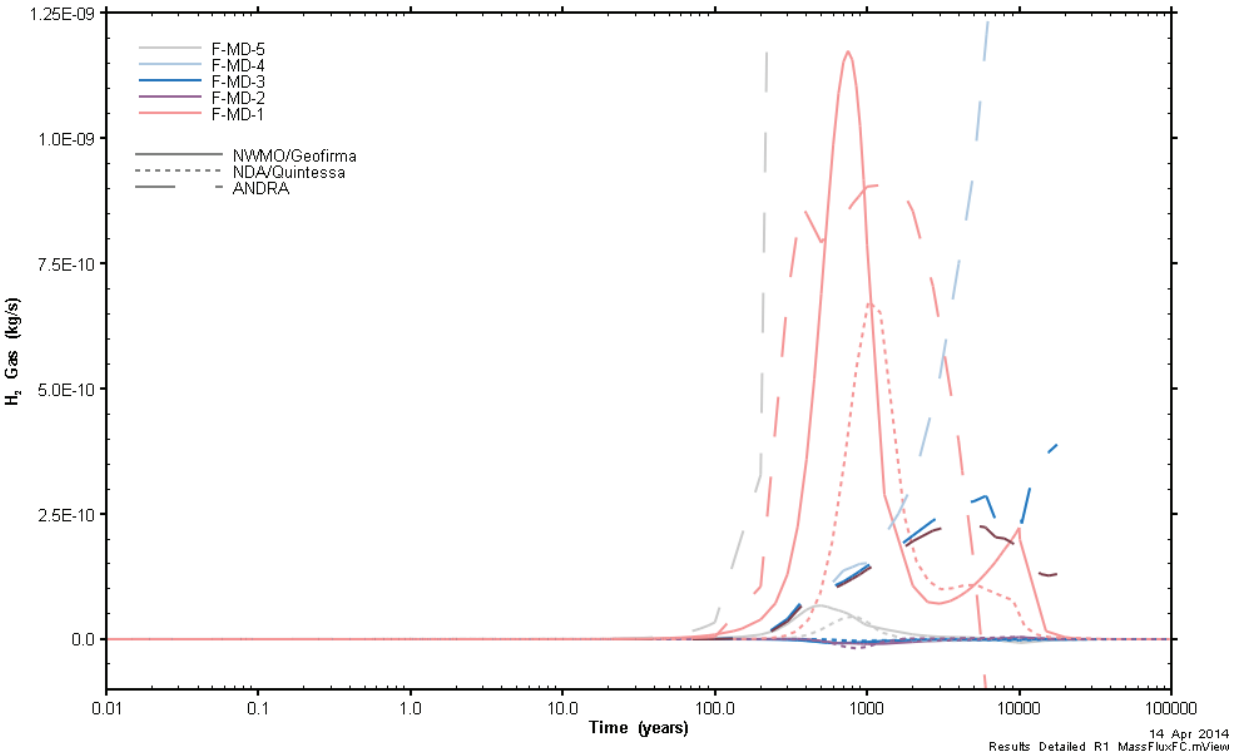

Figure 124: Gas Flow Comparison in the Main Drift to NDA/Quintessa Results

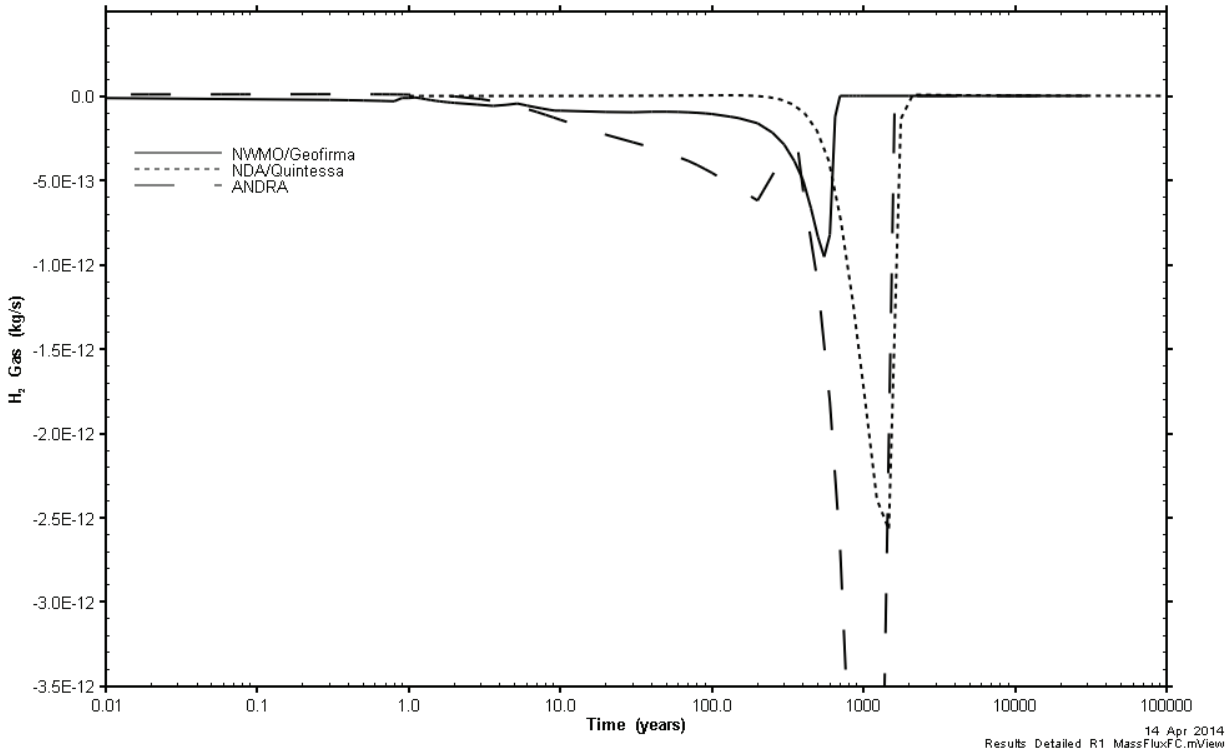

Figure 125: Gas Flow Comparison in Shaft to NDA/Quintessa Results

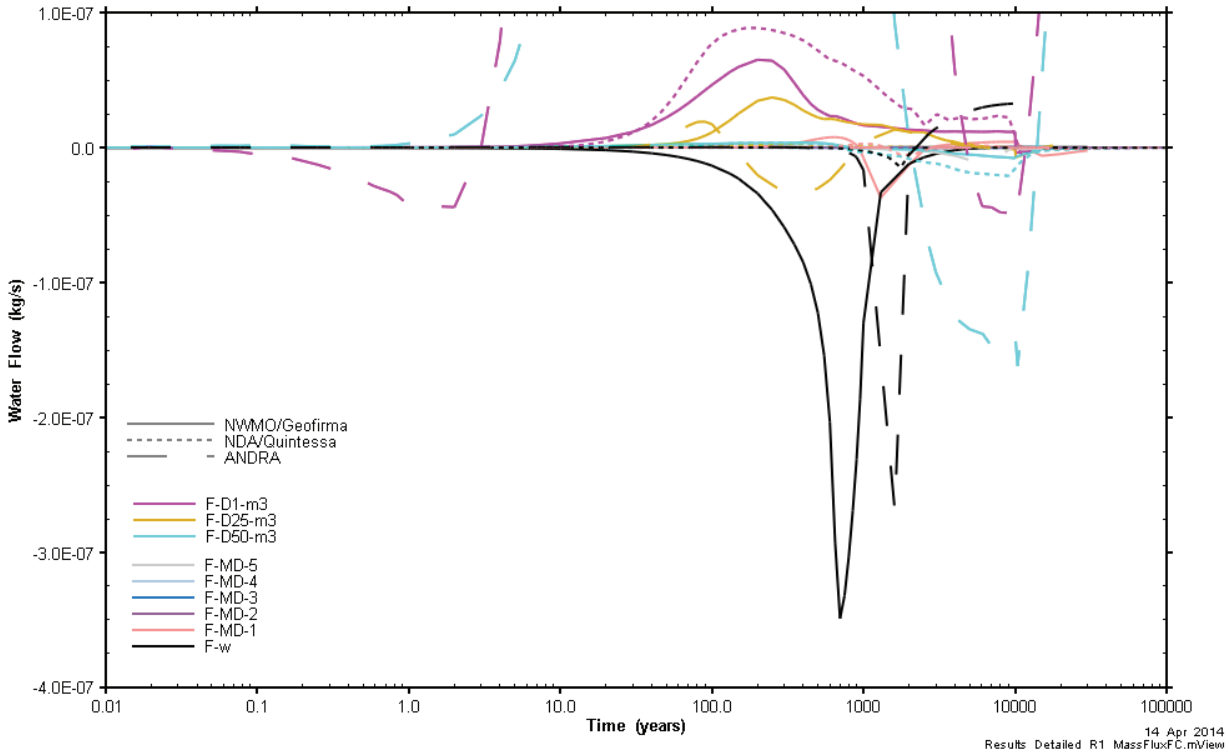

Figure 126: Water Flow Comparison to NDA/Quintessa and ANDRA Results

6.2.6 Summary

The challenge in developing the repository scale model was defining a grid discretization that adequately represented the module, while maintaining a tractable grid size. Two models were developed (1) a half-domain model, and (2) a main drift model, which used output from the module-scale model as a source term input to the main drift. For both models, interfaces were upscaled. The half-domain model took approximately 1 week to complete to 30 000 years, and the main drift model completes to 100 000 years in under 10 minutes.

The maximum gas pressure in the repository develops once the seals in the main drift have mostly saturated, limiting flow of gas out of the system. Characterization of the seals, their capacity for resaturation (capillary pressure curves, particularly at the saturated end of the curve) and the presence of an interface or EDZ surrounding these seals will significantly affect the maximum pressure in the repository. The presence of interfaces, albeit upscaled interfaces, had minimal impact on repository pressures and saturations, as evidenced by the sensitivity case with no-interfaces.

Gas transport occurs along main drifts and shafts, and into the host rock. No free gas enters the aquifer or passes the bentonite seal in the shaft during the simulation. Dissolved gas does reach the aquifer, by means of diffusion through the host rock. No dissolved gas is transported up the shaft. Characterization of diffusion in the host rock is clearly important to determine the amount of gas reaching the aquifer at surface.

The main drift model provided a very quick assessment of the performance of the main drift and shaft of the repository. For this benchmark repository, this model provides a reasonable estimate of repository saturations and pressures, but overestimates gas flow and underestimates water flows in the main drift. While the main-drift model inputs underestimates gas flows into the main drift, the main-drift model overestimates gas flows along the main drift. The current main drift model is an incomplete assessment of this upscaling approach, using a somewhat cumbersome module-scale model. A more comprehensive development of a set of scaled models (cell through repository, with linked boundary conditions) may provide sufficient assessment of a full-scale repository, with fewer differences between flow results. While a half-domain model may still be desired to ensure validity of the set of connected models, the quick run times of the nested model approach would allow for an enhanced sensitivity analysis.

In addition to the half-domain and main drift models, a no-interface sensitivity case was simulated. The no-interface case provided an excellent representation of the repository evolution, including saturations, pressures and dissolved gas at surface, with some improvement in numeric stability. With a different repository system, which had some transport up the shaft, a no-interface case would be expected to underestimate gas and dissolved gas flows up the shaft. The limited impact of interfaces may in part be due to the low permeabilities of the interface at the seals, particularly the cell seal which has the same permeability as the EDZ (but lower air-entry pressures and higher porosities).

Two model uncertainties were not examined by this set of models: the impact of an explicit interface, and the effect of coarse discretization. Cell-scale modelling found that the interface had minimal impact on results, unless the EDZ permeability was low relative to the interface. The no-interface case supports these results; however, it should be noted that the no-interface case suggests that flows along the drifts and shaft are underestimated, which would be important in a scenario where the shaft was an important pathway for gas and dissolved gas

transport. Different model discretizations have not been examined directly, and would be best examined using a small-scale model such as the main-drift model.

7. DISCUSSION

Benchmark modelling provides an excellent opportunity to evaluate and validate various modelling approaches. The FORGE modelling work as is stands provides excellent validation of T2GGM modelling through comparison with results produced by the other modelling groups. The variability in results between modelling groups provides a sense of the range of responses possible due to different modelling approaches and assumptions. It also underscores the importance of assessing the modelling approach: for example, through inclusion of a detailed model such as the half-domain repository-scale model to validate a simplified model such as the main drift repository-scale model.

Several modelling issues were not fully examined in this project, in particular model discretization and interface upscaling. For the repository-scale model, a very coarse discretization was used to obtain a model of tractable size. Both the module-scale and repository-scale models used interface upscaling, but the effects of this upscaling were only evaluated fully with the cell-scale model.

The benchmark modelling also examined, to a limited extent, the sensitivities of the model to the interface, EDZ, two-phase flow relationships and diffusion. However, these sensitivities may differ for a different geosphere and different sealing material properties, which may result in conclusions different from those reached for the FORGE benchmark study.

Several issues related to the benchmark definition should be considered when interpreting results. The benchmark defines only interfaces (no EDZ) surrounding the bentonite plugs in the main drift. This is likely conservative for gas pressures, as gas pressures increase once the bentonite plugs become water-saturated and prevent flow along the drift. However, it is likely non-conservative from the perspective of gas, dissolved gas, or dissolved radionuclides migrating along the main drift and up the shaft. As well, only two-phase flow is considered. It is generally acknowledged that other gas migration processes, such as dilation, may occur in saturated bentonite materials at sufficiently high pressures. Gas flow by dilatant mechanisms could potentially occur along interfaces between bentonite seals and tunnel walls, potentially resulting in higher permeability of these interfaces.

8. CONCLUSIONS

For the FORGE benchmark modelling study, two-phase flow gas transport modelling was conducted at three scales: cell, module and repository. At all three scales, model results compared well to those produced by other modelling groups.

For the FORGE benchmark geosphere and repository design, the repository design was effective at minimizing gas flow out of the repository, even with interfaces surrounding bentonite seals (note there is no EDZ surrounding the bentonite seals in the drifts or shaft). Maximum pressure at the repository-scale was 7.1 MPa. Lower maximum pressures were observed in the cell and module scale models; however, boundary conditions were integral to defining maximum pressures and flows in these models. As the cell-scale and module-scale models were developed before the repository-scale model, the boundary conditions in these models were estimated (by the benchmark definition), and consequently results between models cannot be directly compared.

Important model sensitivities include:

- the characterization of the seals, both in their capacity for resaturation (two-phase flow curves, particularly at the saturated end of the curve) and in the presence of an EDZ around these seals; and
- the dissolved gas diffusion coefficient, as dissolution and diffusion of dissolved gas was the only transport pathway to the aquifer at the repository-scale. At the cell-scale, an increase in the dissolved gas diffusion coefficient resulted in dissolution and diffusion of gas into the host rock, rather than advective flow out of the cell.

ACKNOWLEDGEMENTS

The author wishes to acknowledge the other modelling groups in the FORGE benchmark study, whose data was used in this report for comparison purposes, and also provided feedback for the work as it progressed. The author also wishes to acknowledge Jacques Wendling, who coordinated the collection and distribution of the data for all the modelling groups.

REFERENCES

Pruess, K., C. Oldenburg and G. Moridis. 1999. TOUGH2 User's Guide, Version 2.0. Lawrence Berkeley National Laboratory LBNL-43134. Berkeley, USA.

Suckling, P., J. Avis, N. Calder, P. Humphreys, F. King and R. Walsh. 2012. T2GGM Version 3.1: Gas Generation and Transport Code. Quintessa Ltd. and Geofirma Engineering Ltd. report for the Nuclear Waste Management Organization NWMO TR-2012-23 R000. Toronto, Canada.

Wendling, J., L. Yu, E. Treille, M. Dymitrowska, D. Pellegrini, E. Ahusborde, M. Jurak, B. Amaziane, F. Caro, A. Genty, P. Poskas, D. Justinavicius, M. Sentis, S. Norris, A. Bond, H. Leung and N. Calder. 2014a. Final Report on Benchmark Studies on Repository-Scale Numerical Simulations of Gas Migration Part 1: Cell Scale Benchmark. FORGE Deliverable D1.6-R, Euratom 7th Framework Project: FORGE 2014.

Wendling, J., E. Treille, M. Dymitrowska, D. Pellegrini, E. Ahusborde, M. Jurak, B. Amaziane, F. Caro, A. Genty, P. Poskas, D. Justinavicius, M. Sentis, S. Norris, A. Bond, H. Leung and N. Calder. 2014b. Final Report on Benchmark Studies on Repository-Scale Numerical Simulations of Gas Migration Part 2: Module Scale Benchmark. FORGE Deliverable D1.6-R, Euratom 7th Framework Project: FORGE 2014.

Wendling, J., E. Treille, S. Norris, A. Bond, H. Leung and N. Calder. 2014c. Final Report on Benchmark Studies on Repository-Scale Numerical Simulations of Gas Migration Part 3: Repository Scale Benchmark. FORGE Deliverable D1.6-R, Euratom 7th Framework Project: FORGE 2014.

APPENDIX A: FORGE WP1.2 CELL-SCALE BENCHMARK

CONTENTS

Page

LIST OF TABLES

LIST OF FIGURES

A.1 CONTEXT AND OBJECTIVES

From WP1 participants point of view, the aim of the benchmark should less be a comparison of numerical codes then an exercise trying to answer some precise questions in a PA logic (for example, which could be the relative role of the EDZ, interfaces, backfill in the migration of gas at storage scale?). This clearly includes numerical considerations, but they are a mean and not an objective.

One of the difficulties is to find a common playground for all participants, which allows bringing some add-on for each one. After discussion, a general agreement was that the reference exercise will be as generic as possible (without targeting precisely on national concepts) and to propose sensitivity analyses making it possible to cover national specificities. What is aimed is more to feel how the systems react and why they can react differently rather than an inter-comparison of codes. A second agreement was that, although the final aim of the benchmark studies is to represent repository-scale simulations, the first exercise should be rather simple and at cell scale.

In this context, one of the major problems in representing gas transfers in a repository for radioactive waste is to model simultaneously all gas sources (generally located in the disposal cells) and the transfer pathways constituted by the network of interfaces, plugs and undergrounds drift.

A.2 REFERENCE TEST CASE

The objective of this first test case is to simulate the gas production and migration in a disposal cell and a portion of the drift (Figure A-1).

The calculation domain is axisymetric. In the direction of the cell axis, the extension takes into account the length of the cell, the distance between the bottom of two adjacent cells in this direction and the radius of the access drift (Figure A-2 and Table A-1). The radius of the axisymetric domain is a compromise between the inter-cell distance along the access drift and the thickness of the geological layer.

A gas-production term is provided for the disposal cell. It is imposed on the external surface of the cylinder that represents schematically the canisters. The cell is constituted of a material impermeable to both water and gas, and is not explicitly represented in the model (the external surface of the canister is a no flux boundary). The materials to be taken into account in that simulation include the EDZ of both the cell and the access drift, the cell plug, the backfill of the access drift and the geological medium. Moreover the interface between the cell and the cell EDZ should be represented (general retention behaviour similar to a sand), taking into account a different behaviour whether the interface is facing the bentonite plug (same permeability as EDZ) or the canisters (same permeability as a sand).

The aim of this test case is to better understand the mechanisms of the gas migration (transport, diffusion and dissolution) at the cell scale and in particular to analyze the effect of the presence of different material and interfaces on such mechanisms.

For this first exercise, isothermal hypothesis at 20°C were considered, even in the sensitivity analysis.

The main constraints of the case are to give a detailed representation of all the elements of the proposed problem and to maintain compatible calculation times with the simulation tools while complying with the physics of the problem. Moreover special attention should be paid at the effect of the size and form of the mesh on the results of the simulation.

The simulations should be performed using a full physical model (multiphase Darcy's law, with interaction between each phase: dissolution/evaporation and diffusion), a consistent example can be found in "A.5 ANNEX 1: MATHEMATICAL MODEL PROPOSED FOR THE EXERCISE".

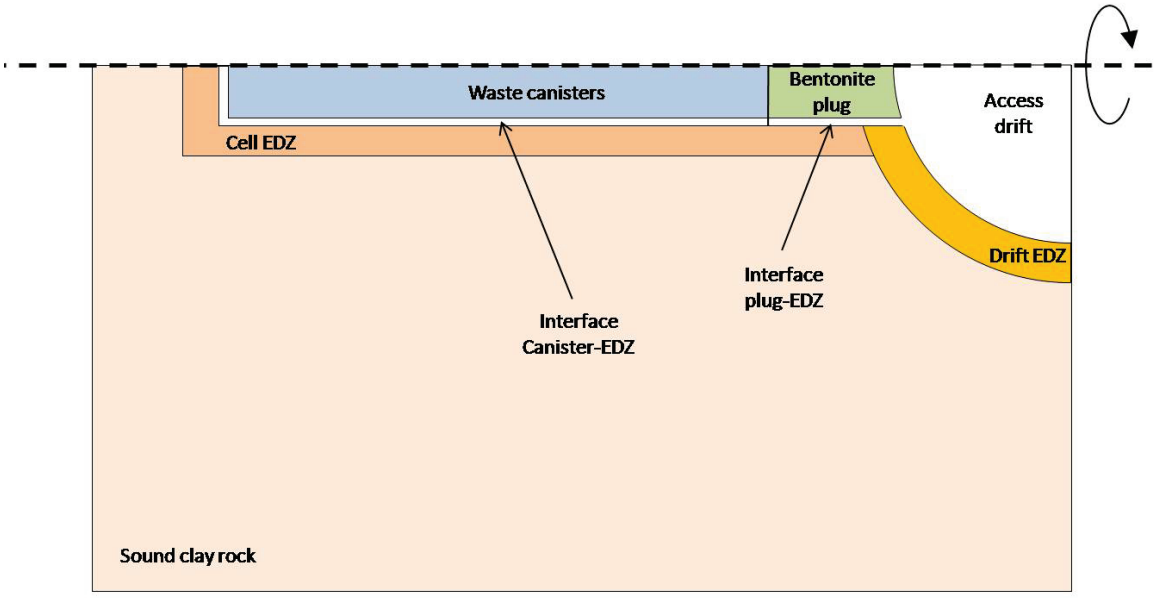

Figure A-1: Representation of the Axisymetric Calculation Domain

A.2.1 GEOMETRY

The canister and the plug share the same circular section.

The section of the access drifts is circular. Disposal cell is positioned at half-height in the access drift.

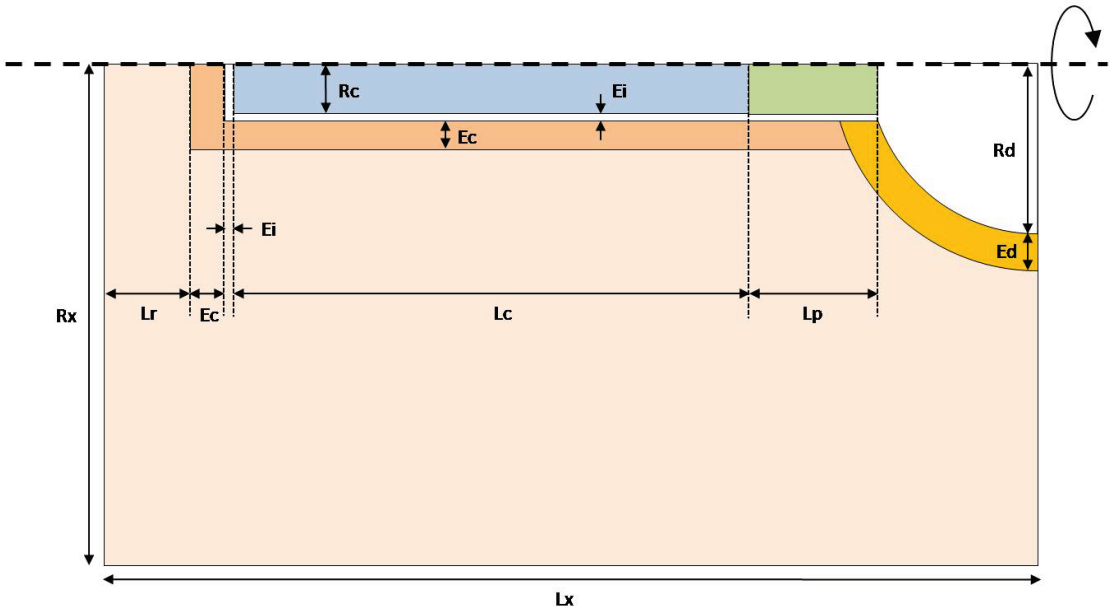

Figure A-2: Dimensions in the Calculation Domain

Table A-1: Size of Items in the Calculation Domain

Name of Parameter	Parameter	Value
Length of the domain (cell axis direction)	Lx	60 m
Radius of the domain	Rx	20 m
Radius of access drift	Rd	3 m
Thickness of the access drift EDZ	Ed	1 m
Length of the plug	Lp	5 m
Length of the canister zone	Lc	40 m
Thickness of the cell EDZ	Ec	0.5 m
Plug and canisters radius	Rc	0.5 m
Thickness of the interface	Ei	0.01 m
Distance between end of cell EDZ and boundary	Lr	11.5 m

A.2.2 PHYSICAL PARAMETERS

Physical parameters at 20°C are shown in Table A-2 (for this first exercise, all calculations are isotherm and temperature is set at 20°C throughout the simulation period).

Table A-2: Physical Characteristics of Materials

Parameter (at 20°C)	Materials		
	Interface facing plug	Interface facing canister	Backfill (access drift)
K_v [m^2]	$5.0\ 10^{-18}$	$1.0\ 10^{-12}$	$5.0\ 10^{-17}$
K_h [m^2]	$1.0\ 10^{-17}$	Kv=Kh	
Porosity [%]	30	100	40
Specific storage coefficient [m^{-1}]	$4.6\ 10^{-6}$	$4.6\ 10^{-6}$	$1.0\ 10^{-5}$
Two-phase flow parameters			
S_{gr} [%]	0	0	0
S_{wr} [%]	0	0	0
Van Genuchten parameters			
n [-]	4	4	1.5
P_r [Pa]	10^4	10^4	$2\ 10^6$
τ (Tortuosity)	1	1	2

Parameter (at 20°C)	Materials		
	Bentonite plug	EDZ	Geologial Medium
K_v [m^2]	$1.0\ 10^{-20}$	$5.0\ 10^{-18}$	$5.0\ 10^{-21}$
K_h [m^2]	Kv=Kh	$1.0\ 10^{-17}$	$1.0\ 10^{-20}$
Porosity [%]	35	15	15
Specific storage coefficient [m^{-1}]	$4.4\ 10^{-6}$	$2.3\ 10^{-6}$	$2.3\ 10^{-6}$
Two-phase flow parameters			
S_{gr} [%]	0	0	0
S_{wr} [%]	0	0	0
Van Genuchten parameters			
n [-]	1.6	1.5	1.5
P_r [Pa]	$1.6\ 10^7$	$1.5\ 10^6$	$1.5\ 10^7$
τ (Tortuosity)	4.5	2	2

- ***Viscosity of the gas mixture:***

The viscosity of the gas mixture (water vapour + hydrogen) can be estimated by a classical Wilke approximation or by a simplified formula as follows:

$$\mu_g = \frac{1}{\frac{X^g_{H_2}}{\mu^g_{H_2}} + \frac{X^g_{wvap}}{\mu^g_{wvap}}} \text{ with } \qquad \mu^g_{H_2}(T = 293K) = 9\,10^{-6}\,Pa.s \qquad \mu^g_{wvap}(T = 293K) = 10^{-5}\,Pa.s$$

- ***Diffusion coefficient of dissolved H_2 in water:***

$$D_{H_2/water} = 1.57\ 10^{-14}\,\frac{T}{\mu_{water}(T)} \qquad (m^2.s^{-1})$$

- ***Diffusion coefficient of gaseous H_2 in water vapour:***
(T_0=293 K and at P_0=1.0·10^5 Pa: D_0=9.5·10^{-5} m^2.s^{-1})

$$D^g_{H_2-H_2O} = D_0\left(\frac{P_0}{P}\right)\left(\frac{T}{T_0}\right)^{1.75} \qquad (m^2.s^{-1})$$

- ***Diffusion coefficient of dissolved H_2 in the water of the porous medium:***

$$D^w_{H_2} = S_w\left(\frac{\omega}{\tau^2}\right)D_{H_2/eau}$$

- ***Diffusion coefficient of dissolved H_2 in the binary H_2/water-vapour mixture of the porous medium:***

$$D^g_{H_2/vap} = (1 - S_w)\left(\frac{\omega}{\tau^2}\right)D^g_{H_2-H_2O}$$

- ***Solubility of hydrogen in water:*** $H_{H_2}(T = 293K) = 7.610^{-6}\ mol.Pa^{-1}.m^{-3}$

Note: Temperature in diffusion models is stated in Kelvin.

A.2.3 INITIAL CONDITIONS

Water saturation:
- in the geological medium is equal to 100%;
- in the cell and drift EDZ is equal to 100%
- in the interface (facing canister and plug) equal to 5%;
- in the bentonite plug is equal to 70%;
- in the backfill of the access drifts is equal to 70%.

Pressure:

- In the water-saturated materials at 100%, the water and gas pressure are equals to the value at radial outer boundary (respectively 5 MPa and 0.1 MPa; see boundary limits);
- In partially-saturated materials, the gas pressure is equal to 1 atmosphere. The water pressure is deduced from the gas pressure and the saturation by applying Van Genuchten models associated with each material.

A.2.4 BOUNDARY CONDITIONS

Figure A-3 is a schematic representation of the boundary conditions to be used.

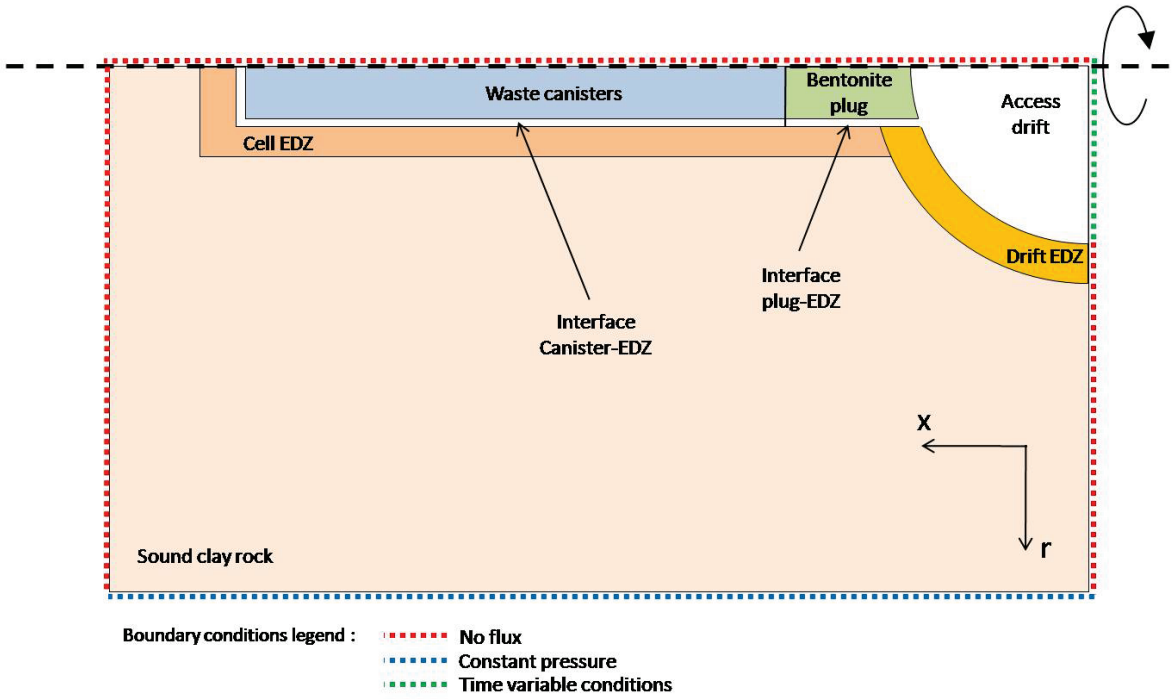

Figure A-3: Schematic Representation of the Boundary Conditions

- **Conditions at the outer radius of the calculation domain:**

$$P_w(x,r=20,t)=5.0\,10^6\,Pa \quad S_w(x,r=20,t)=1 \qquad P_g(x,r=20,t)=1.0\,10^5\ Pa \quad x\in[0,60],\ t\in[0,t_{fin}]$$

As gaseous phase is not expressed, the gas pressure corresponds also to a concentration via Henry's law (see "A.5 ANNEX 1: MATHEMATICAL MODEL PROPOSED FOR THE EXERCISE" for details).

- **Conditions at the centre (r=0) of the calculation domain:**

$$Flux_w(x,r=0,t)=0 \qquad Flux_g(x,r=0,t)=0 \qquad x\in[0,60] \quad t\in[0,t_{fin}]$$

- **Conditions on the lateral side, x=60 of the calculation domain:**

$$Flux_w(x=60,r,t)=0 \qquad Flux_g(x=60,r,t)=0 \qquad r\in[0,20] \qquad t\in[0,t_{fin}]$$

- **Conditions on the lateral side, x=0 of the calculation domain:**

$$Flux_w(x=0,r>3,t)=0 \qquad Flux_g(x=0,r>3,t)=0 \qquad r\in]3,20] \qquad t\in[0,t_{fin}]$$

For r ≤ 3, the boundary conditions are variable in time for water and gas. The representation of these variations can be found in Figure A-4.

The boundary conditions represented in Figure A-4 are extrapolated from a study made by Andra at a module scale (several hundred of cells). The hypothesis used in this study are a bit different from the one assigned here (especially, the generation term for hydrogen is more complex), but the general behaviour should be the same.

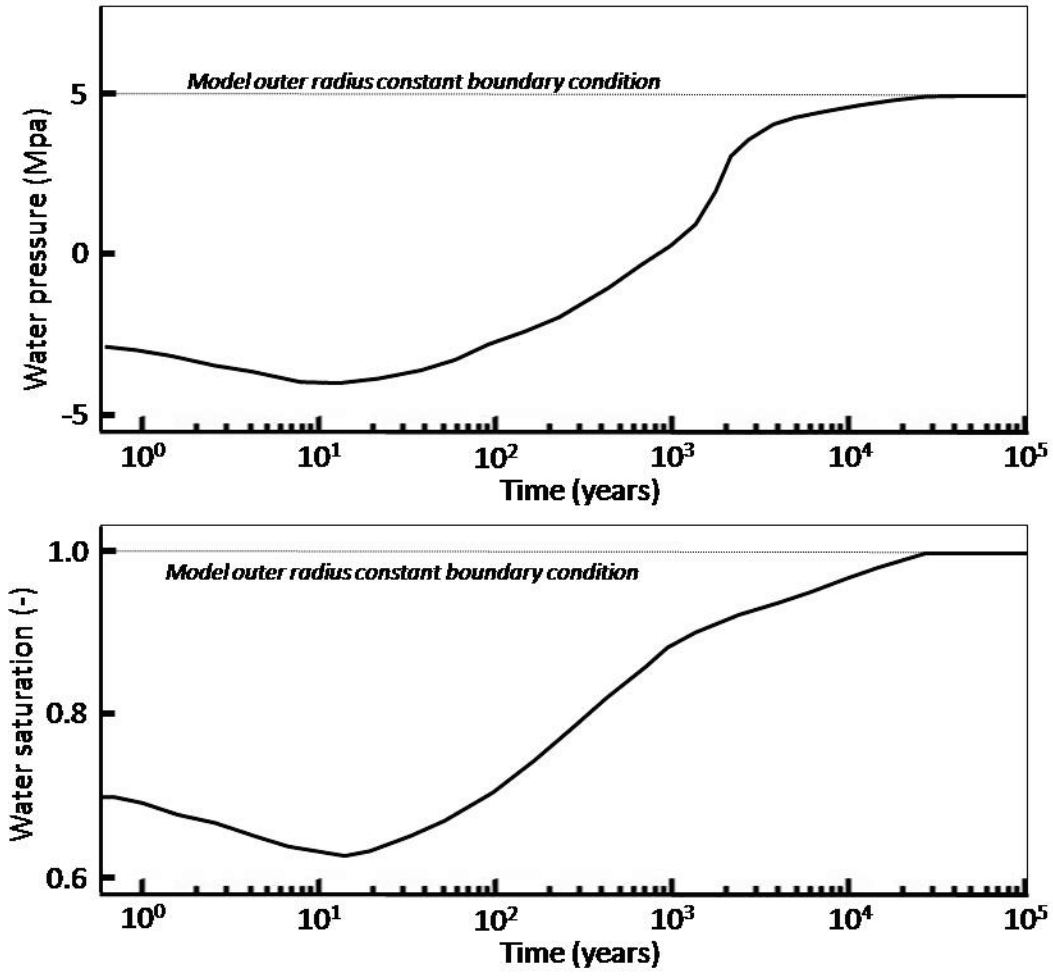

Figure A-4: Time Variable Boundary Conditions to be Used in the Drift

A.2.5 PRODUCTION TERM FOR HYDROGEN

The hydrogen-production term is to be distributed over the external surface of the cell, as follows:

- for 0 < t ≤ 10000 years, $Q^{g}_{H_2} = 100\ mol/year/cell$ $Q^{w}_{H_2} = 0$
- for t > 10000 years $Q^{g}_{H_2} = 0\ mol/year/cell$ $Q^{w}_{H_2} = 0$

A.2.6 SIMULATION PERIOD

The simulation will be performed between moment $t_0=0$ and moment t_{fin}=100 000 years.

A.3 SENSITIVITY ANALYSIS

For this first exercise, the sensitivity analysis is concentrated around uncertainties concerning the EDZ, the host rock permeability and the diffusion of H_2 in porous media.

A.3.1 SENSITIVITY 1

The evolution of the EDZ intrinsic permeability with time is not well known; some data however show a reduction of permeability with time down to values similar to those of the undisturbed rock. Concerning the evolution with time of the retention and relative permeability curve of the EDZ, no consistent data are available.

For this sensitivity analysis, everything else being equal to the reference case, EDZ intrinsic permeability (for both drift and cell) is supposed equal to undisturbed rock permeability

A.3.2 SENSITIVITY 2

Depending of the type of clay rock, Mualem / Van Genuchten curve is not always the best choice for relative permeability of the host rock and EDZ. For certain data a power law fits quite well the measures.

For this sensitivity analysis, everything else being equal to the reference case, relative permeability curve for water and gas of undisturbed host rock and EDZ (for both drift and cell) is supposed to follow saturation at the power 3:

$$K^{w}_{r} = S^{3}_{w} \qquad K^{g}_{r} = S^{3}_{g} = (1 - S_{w})^{3}$$

- K^{w}_{r}: Relative permeability for water (-)

- K_r^g : Relative permeability for the total gas phase (-)
- S_w : saturation for water (-)
- S_g : saturation for the total gas phase (-)

A.3.3 SENSITIVITY 3

Uncertainties for the diffusion coefficient of dissolved hydrogen in porous media is quite high and this parameter can have a real impact on the percentage of H_2 turning effectively to gas. For this sensitivity analysis, everything else being equal to the reference case, the diffusion coefficient of dissolved hydrogen under water saturated conditions will be multiplied by 10 for all simulated porous media.

A.4 OUTPUT RESULTS

The output will be the same for the reference case and the sensitivity cases.

A.4.1 EVOLUTION WITH TIME OF FLUXES THROUGH SURFACES

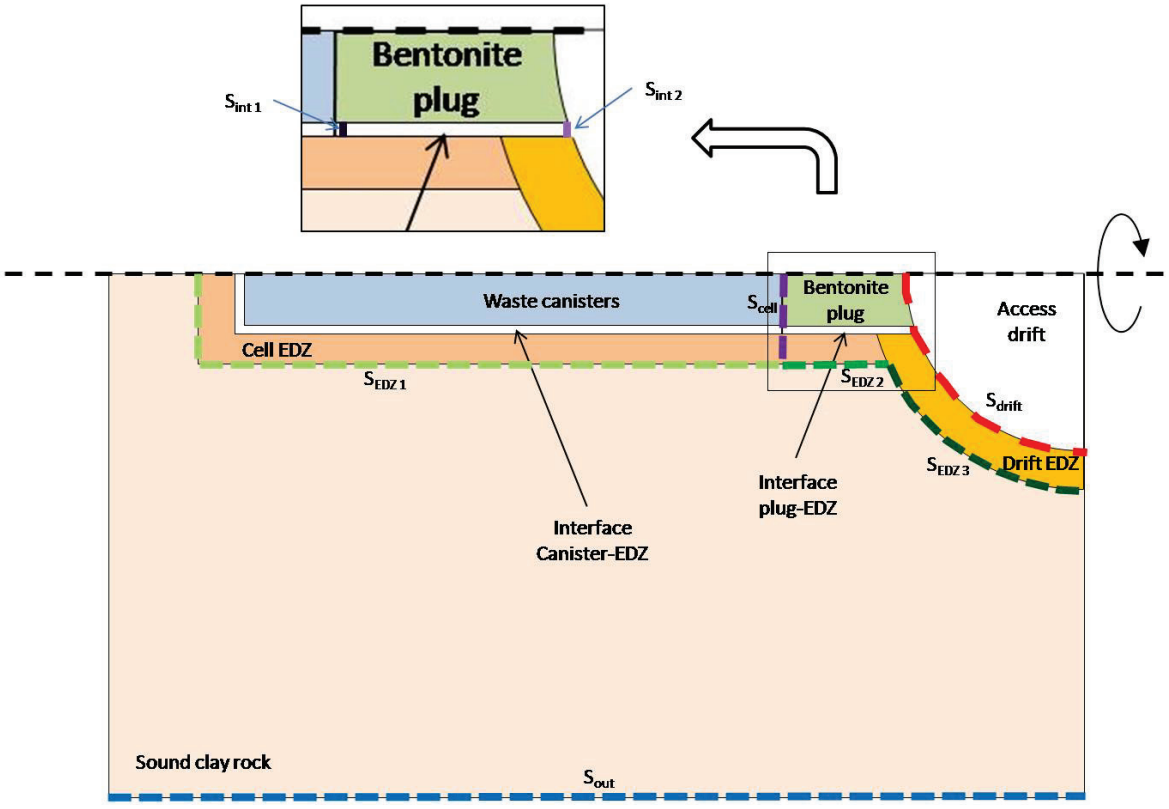

Figure A-5: Schematic Representation of the Surfaces Through Which Fluxes Will Be Calculated

Type of fluxes:

- Liquid water flux
- Water vapor
- Gaseous H_2
- Dissolved H_2

Type of surfaces:

- Outer boundary of the model at r=20 m (S_{out} in Figure A-5), fluxes counted positively out of the model.
- Drift wall (S_{drift} in Figure A-5), fluxes counted positively toward the drift.
- Outside surface of the EDZ, separated in 3 sections (see Figure A-5): S_{EDZ1} (around canister), S_{EDZ2} (around plug), S_{EDZ3} (drift EDZ). Fluxes counted positively out of the EDZ toward the undisturbed rock.
- Inner cell surfaces (see Figure A-5): Scell (section including interface and EDZ at canister-plug junction), Sint1 (interface at canister-plug junction), Sint2 (interface at the drift wall). Fluxes counted positively toward the drift.

A.4.2 EVOLUTION WITH TIME ALONG LINES

Evolution with time of:

- Water saturation
- Water pressure
- Gas pressure (in the gas phase when it exists)
- Dissolved H_2 pseudo-pressure (see Henry's law in "A.5 ANNEX 1: MATHEMATICAL MODEL PROPOSED FOR THE EXERCISE" for details)
- Capillary pressure

Type of lines

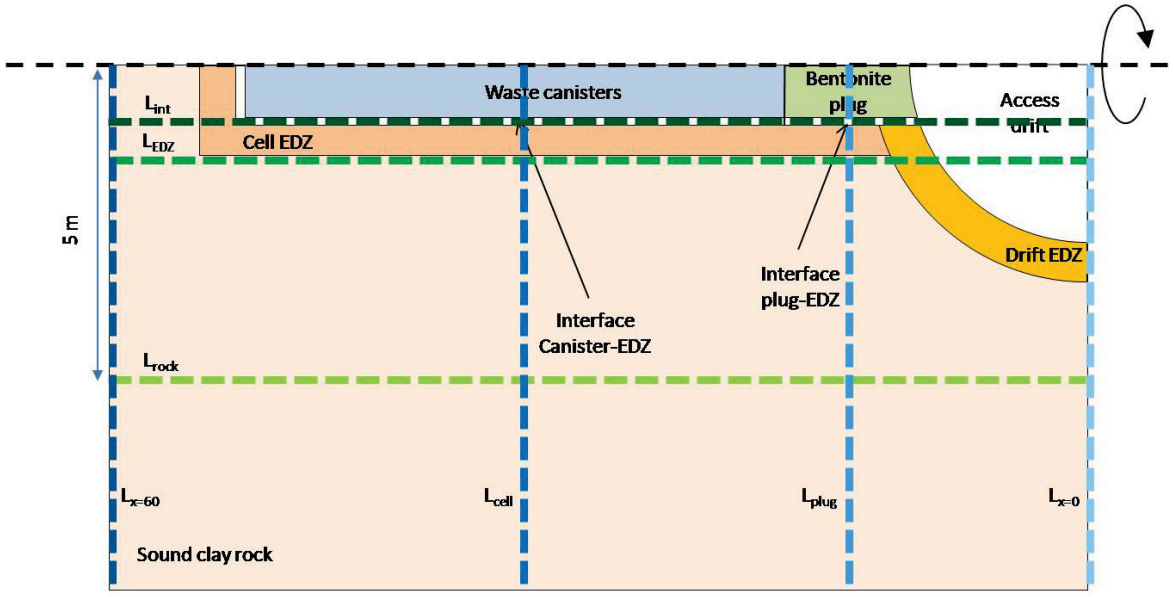

Figure A-6: Schematic Representation of the Lines Along Which Results Should Be Given

- Lines at constant radius (see Figure A-6): L_{int} (passes through the interface), L_{EDZ} (just outside the cell EDZ), L_{rock} (inside the rock at a 5 m radius)
- Lines at constant x (see Figure A-6): $L_{x=0}$ and $L_{x=60}$ (boundaries of the model), L_{plug} (in the middle of the plug), L_{cell} (in the middle of the canister)

A.4.3 EVOLUTION WITH TIME AT GIVEN POINTS

Evolution with time of:

- Water saturation
- Water pressure
- Gas pressure (in the gas phase when it exists)
- Dissolved H_2 pseudo-pressure (see Henry's law in "A.5 ANNEX 1: MATHEMATICAL MODEL PROPOSED FOR THE EXERCISE" for details)
- Capillary pressure

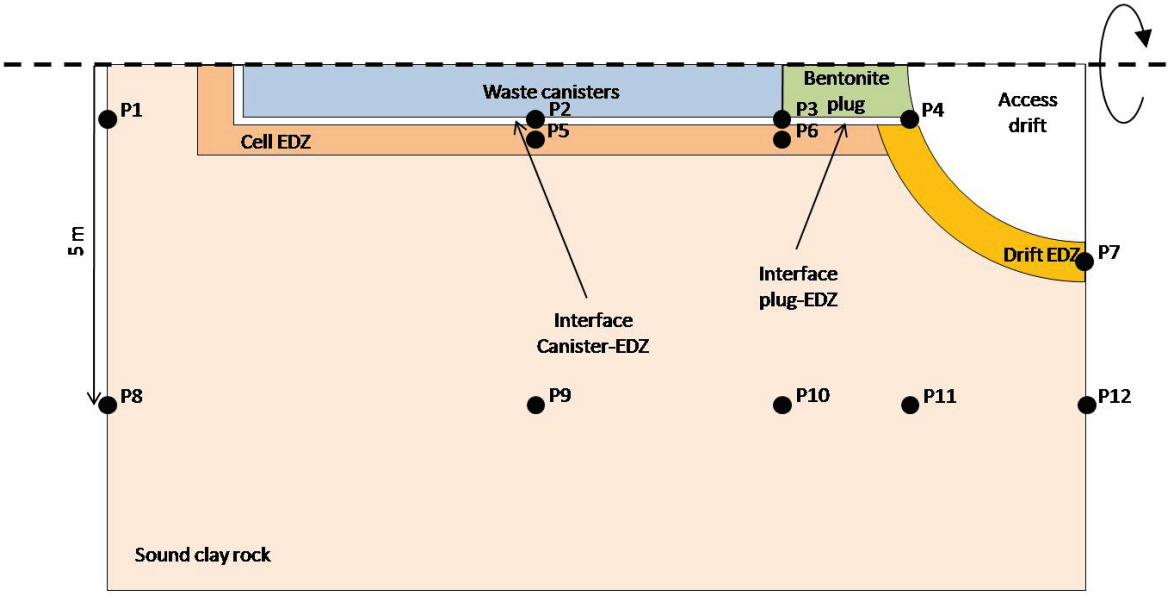

Figure A-7: Schematic Representation of the Point Where Results Should Be Given

Type of points:

- Points 1 to 4, at the same radius as the centre of the interface (see Figure A-7): P1 and P4 (at the boundaries), P2 (in the middle of the canister), P3 (in the middle of the plug)
- Points 5 and 6, at the same radius as the centre of the cell EDZ (see Figure A-7): P5 (in the middle of the canister), P6 (in the middle of the plug)
- Point 7 (see Figure A-7) in the middle of the drift EDZ on the x=0 boundary
- Points 8 to 12, at a 5 m radius (see Figure A-7): P8 and P12 (at the boundaries), P9 (at the same x as the middle of the canister), P10 (at the same x as the middle of the plug), P11 (at the same x as the intersection of the drift and the interface)

A.5 ANNEX 1: MATHEMATICAL MODEL PROPOSED FOR THE EXERCISE

The capillary pressure is defined as the difference between gas pressure and water pressure:

$$P_C = P_g - P_w \quad (1)$$

- P_c: capillary pressure (Pa)
- P_g: total pressure of the gas phase (Pa)
- P_w: water pressure (Pa)

The dependence between water and gas saturation in each porous media is expressed by:

$$S_g + S_W = 1 \quad \text{with} \quad S_g = \frac{V_g}{V_p} \text{ and } S_w = \frac{V_w}{V_p}$$

- S_g: gas saturation (-)
- S_w: water saturation (-)
- V_g: gas volume (m^3)
- V_w: water volume (m^3)
- V_p: pore volume (m^3)

Van Genuchten model is used to express capillary pressure function of the effective saturation in a given porous media:

$$S_{we} = \frac{S_w - S_{wr}}{1 - S_{wr} - S_{gr}} \quad (2)$$

$$S_{we} = \frac{1}{\left[1 + \left(\frac{P_c}{P_r}\right)^n\right]^m} \quad (3)$$

- S_{we}: Effective water saturation (-)
- S_{wr}: residual water saturation (-)
- P_r: reference pressure for Van Genuchten law (Pa). Generally the value for this coefficient is higher than the gas entry pressure for a given porous media
- n, m: coefficient for Van Genuchten law. We have $m = 1 - \frac{1}{n}$

The relative permeability for water is expressed by integrating the Mualem prediction model in the Van Genuchten capillarity model:

$$k_r^w = \sqrt{S_{we}}\left[1 - \left(1 - S_{we}^{1/m}\right)^m\right]^2 \quad (4)$$

- k_r^w : relative permeability for water (-)

The relative permeability for gas is expressed similarly:

$$k_r^g = \sqrt{1 - S_{we}}\left[1 - S_{we}^{1/m}\right]^{2m} \quad (5)$$

- k_r^g : relative permeability for gas (-)

The water and gas movement in a porous media is represented by the mass conservation law and the energy conservation law (reduced to the generalized Darcy law):

$$U_w = -\frac{k k_r^w(S_w)}{\mu_w}(\nabla P_w + \rho_w g \nabla z) \quad (6)$$

$$U_g = -\frac{k k_r^g(S_g)}{\mu_g}(\nabla P_g + \rho_g g \nabla z) \quad (7)$$

- K: intrinsic permeability of the porous media (m^2)
- μ_g: viscosity of the total gas phase ($kg.s^{-1}.m^{-1}$)
- μ_w: viscosity of water ($kg.s^{-1}.m^{-1}$)
- ρ_g: volumetric mass of the total gas phase ($kg.m^{-3}$)
- ρ_w: volumetric mass of water ($kg.m^{-3}$)
- g: gravity ($m.s^{-2}$)
- z: altitude (m)

$$\rho_w(P_w) = \rho_{atm} \exp\left[S_s(P_w - P_{atm})\right] \quad (8)$$

- ρ_{atm}: volumetric mass of water at atmospheric pressure ($kg.m^{-3}$)
- P_{atm}: atmospheric pressure (Pa)
- S_s: specific storage (Pa^{-1})

Equation of conservation for water:

$$\frac{\partial(\rho_w \omega S_w)}{\partial t} + \nabla(\rho_w U_w) = Q^w \quad (9)$$

- U_g: Darcy velocity for the gas phase ($m.s^{-1}$)
- U_w: Darcy velocity for water ($m.s^{-1}$)
- ω: porosity (-)
- Q^w: consumption/production of water ($kg.m^{-3}.s^{-1}$)

Equation of conservation for the total gas phase:

$$\frac{\partial(\rho_g \omega S_g)}{\partial t} + \nabla(\rho_g U_g) = Q^g \quad (10)$$

- Q^g : consumption/production for the total gas phase (kg.m^{-3}.s^{-1})

The mass fraction of gaseous hydrogen is expressed as:

$$X_{H_2}^g = \frac{\rho_{H_2}^g}{\rho_g} \tag{11}$$

With $\rho_{H_2}^g = \frac{m_{H_2}^g}{V_g}$ and $\rho_g = \frac{m^g}{V_g}$

- $X_{H_2}^g$ is the mass fraction of hydrogen in the total gas phase (-)
- $m_{H_2}^g$ is the hydrogen mass in the gas phase (kg)
- m^g is the total mass of the gas phase (kg)
- $\rho_{H_2}^g$ is the volumetric mass of gaseous hydrogen in the gas phase (kg.m^{-3})

Mass conservation law for gaseous hydrogen:

$$\frac{\partial}{\partial t}(\omega S_g \rho_g X_{H_2}^g) + \nabla(\rho_g X_{H_2}^g U_g - J_{H_2}^g) + \Omega_{H_2}^{g/l} = Q_{H_2}^g \tag{12}$$

- $\Omega_{H_2}^{g/l}$ is the exchange term from the gaseous phase to the liquid phase for H_2 (kg.m^{-3}.s^{-1})
- $Q_{H_2}^g$ is the consumption/production term for gaseous hydrogen (kg.m^{-3}.s^{-1})
- $J_{H_2}^g$ is the diffusive term for gaseous hydrogen (kg.m^{-2}.s^{-1})

Diffusive flux for a binary mixture of gas (H_2 and water vapor) can be expressed by Kick law:

$$J_{H_2}^g = \rho_g D_{H_2 vap}^g \nabla X_{H_2}^g \tag{13}$$

- $D_{H_2 vap}^g$ is the diffusion coefficient for gaseous hydrogen in water vapor (m^2.s^{-1})

The mass fraction of dissolved hydrogen is expressed as:

$$X_{H_2}^w = \frac{\rho_{H_2}^w}{\rho_w} \tag{14}$$

With $\rho_{H_2}^w = \frac{m_{H_2}^w}{V_w}$ and $\rho_w = \frac{m^w}{V_w}$

- $X_{H_2}^w$ is the mass fraction of dissolved hydrogen (-)
- $m_{H_2}^w$ is the dissolved hydrogen mass (kg)
- m^w is the total mass of the liquid phase (kg)

- $\rho_{H_2}^w$ is the volumetric mass of dissolved hydrogen in the liquid phase (kg.m^{-3})

Mass conservation law for dissolved hydrogen is expressed as:

$$\frac{\partial}{\partial t}(\omega S_w \rho_w X_{H_2}^w) + \nabla(\rho_w X_{H_2}^w U_w - J_{H_2}^w) + \Omega_{H_2}^{l/g} = Q_{H_2}^w \quad (15)$$

- $\Omega_{H_2}^{l/g}$ is the exchange term from the liquid phase to the gas phase for H_2 (kg.m^{-3}.s^{-1})
- $Q_{H_2}^w$ is the consumption/production term for dissolved hydrogen (kg.m^{-3}.s^{-1})
- $J_{H_2}^w$ is the diffusive term for dissolved hydrogen (kg.m^{-2}.s^{-1})

The exchange terms from between liquid and gaseous phase are linked by the following relation:

$$\Omega_{H_2}^{l/g} = -\Omega_{H_2}^{g/l} \quad (16)$$

Diffusive flux for dissolved hydrogen can be expressed by Kick law:

$$J_{H_2}^w = \rho_w D_{H_2 vap}^w \nabla X_{H_2}^w \quad (17)$$

- $D_{H_2 vap}^w$ is the diffusion coefficient for dissolved hydrogen in water vapor (m^2.s^{-1})

Part of the gas will be dissolved in the pore water. The solubility limit for the gas depends mainly on thermodynamic conditions and can be expressed by Henry's law:

$$C_{H_2}^w = H_{H_2}(T) P_{H_2}^g \quad (18)$$

Where $C_{H_2}^w = \frac{X_{H_2}^w \rho_w}{M_{H_2}}$

- $C_{H_2}^w$ is the maximum concentration of hydrogen in water (mol.m^{-3})
- H_{H_2} is the constant of Henry's law for hydrogen (mol.m^{-3}.Pa^{-1})
- $P_{H_2}^g$ is the partial pressure of hydrogen in the total gaseous phase (Pa)
- M_{H_2} is the molar mass for hydrogen (kg.mol^{-1})

The relation between partial pressure of each gas present in the total gas phase and total gas pressure is given by Dalton law that writes for a binary mixture (H_2 and water vapor):

$$P_g = P_{H_2}^g + P_{wvap}^g \quad (19)$$

- P_{wvap}^g is the partial pressure of water vapor in the total gas phase (Pa)

Each of the gas is supposed perfect:

$$P_{H_2}^g = \frac{\rho_{H_2}^g}{M_{H_2}} RT \text{ and } P_{wvap}^g = \frac{\rho_{wvap}^g}{M_{wvap}} RT \quad (20,21)$$

For the gas mixture this writes:

$$P_g = \frac{\rho_g}{M_g} RT \quad (22)$$

- M_g: molar mass for the total gaseous phase (H_2 + water vapor) ($kg.mol^{-1}$)
- R: constant of the perfect gas ($J.mol^{-1}.K^{-1}$) : R = 8.314 $J.mol^{-1}.K^{-1}$
- T: temperature (°K)

Saturation pressure for water vapor is only depending on temperature and can by expressed by:

$$\log_{10}(P_{sat}) = 2.786 + 0.031514T_c - 1.2373x10^{-4}T_c^{\,2} + 4.2267x10^{-7}T_c^{\,3} - 8.1308x10^{-10}T_c^{\,4} \quad (23)$$

- P_{sat}: saturation pressure for water vapor (Pa)
- T_c: Temperature (°C)

Kelvin law is giving a relation between saturation pressure for water vapor, effective pressure for water vapor and capillary pressure:

$$P_{wvap}^g(T, S_w) = \exp\left(\frac{M_w P_c(S_w)}{\rho_w RT}\right) P_{sat}(T) \quad (24)$$

APPENDIX B: FORGE WP1.2 MODULE-SCALE BENCHMARK

CONTENTS

LIST OF TABLES

LIST OF FIGURES

B.1 CONTEXT AND OBJECTIVES

From WP1 participants point of view, the aim of the benchmark should less be a comparison of numerical codes then an exercise trying to answer some precise questions in a PA logic (for example, which could be the relative role of the EDZ, interfaces, backfill in the migration of gas at storage scale?). This clearly includes numerical considerations, but they are a mean and not an objective.

One of the difficulties is to find a common playground for all participants, which allows bringing some add-on for each one. After discussion, a general agreement was that the reference exercise will be as generic as possible (without targeting precisely on national concepts) and to propose sensitivity analyses making it possible to cover national specificities. What is aimed is more to feel how the systems react and why they can react differently rather than an inter-comparison of codes.

A second agreement was that, although the final aim of the benchmark studies is to represent repository-scale simulations, the first exercise should be rather simple and at cell scale. This first step was done during 2009 and first part of 2010. Results are showing a significant role of interfaces between plug and argillite and a transfer dominated at this scale by convection toward the drifts, radial diffusion being of secondary order.

Representing the transfer of gas at a larger scale including drifts and several tens of cells is then worthwhile. In this context, one of the major problems in representing gas transfers in a repository for radioactive waste is to model simultaneously all gas sources (generally located in the disposal cells) and the transfer pathways constituted by the network of interfaces, plugs and undergrounds drifts.

This document contains the specifications for such an exercise.

B.2 BENCHMARK GENERAL SPECIFICATION AT MODULE SCALE

One of the major difficulties in the representation of gas transfer in a repository is to take into account simultaneously all the sources terms (generally located inside the storage cells) and to represent at the same time the transfer network constituted by the different drifts and cells.

For this exercise we assume a repository having a simple architecture (see Figure B-1). This architecture is more or less representative of some general concepts for HLW repository zones but without any national specificity. The main features are:

- Subdivision of the all repository into several modules linked by a main drift;
- All the modules are equal and contains an access drift serving 50 cells on each side;
- All modules are separated from their neighbors by a drift seal.

This test case is limited to a portion of such a repository containing an access drift serving a number of cells (see Figure B-1). This portion is called a module (a drift serving two rows of vitrified HLW cells containing each 50 cells, see Figure B-2).

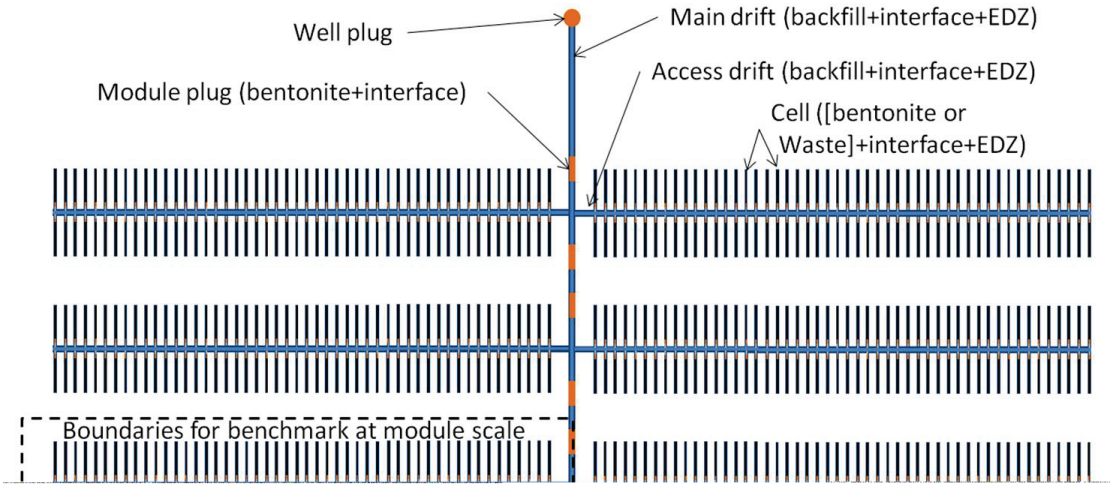

Figure B-1: Schematic Representation of a Repository for HLW

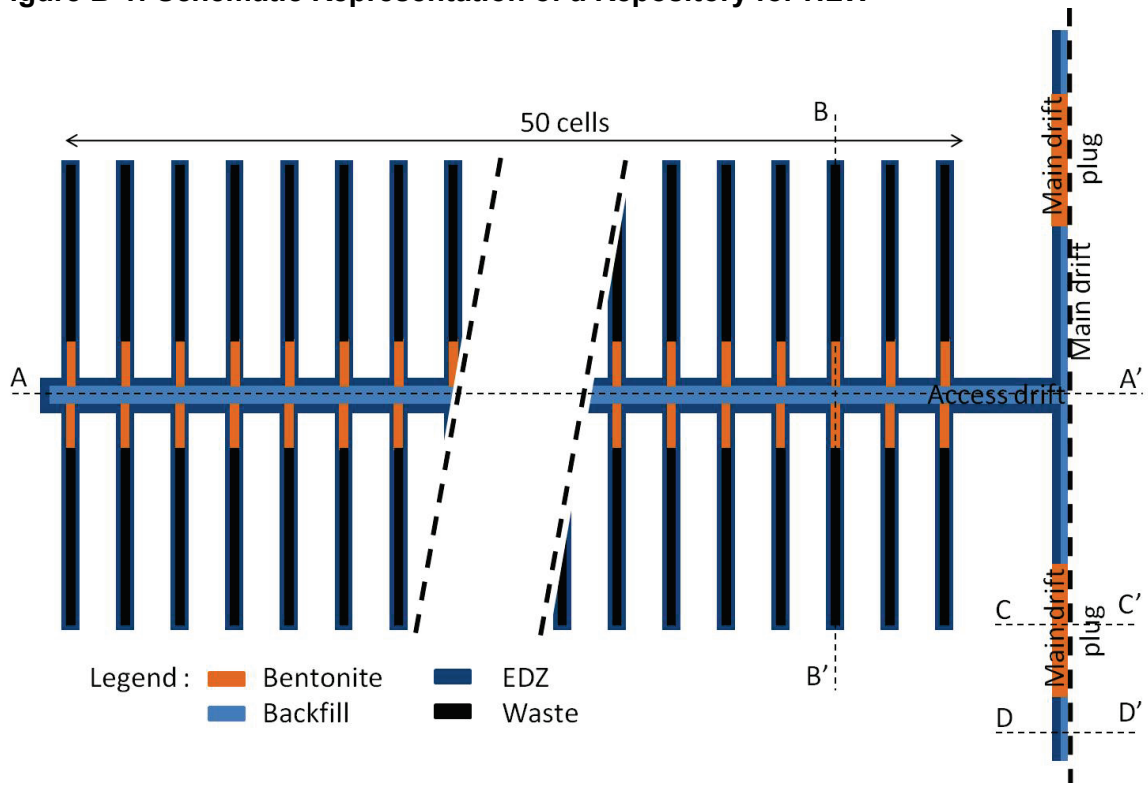

Figure B-2: Schematic Representation of the Module to be Simulated and Definition of the A-A', B-B', C-C' and D-D' Cross Sections

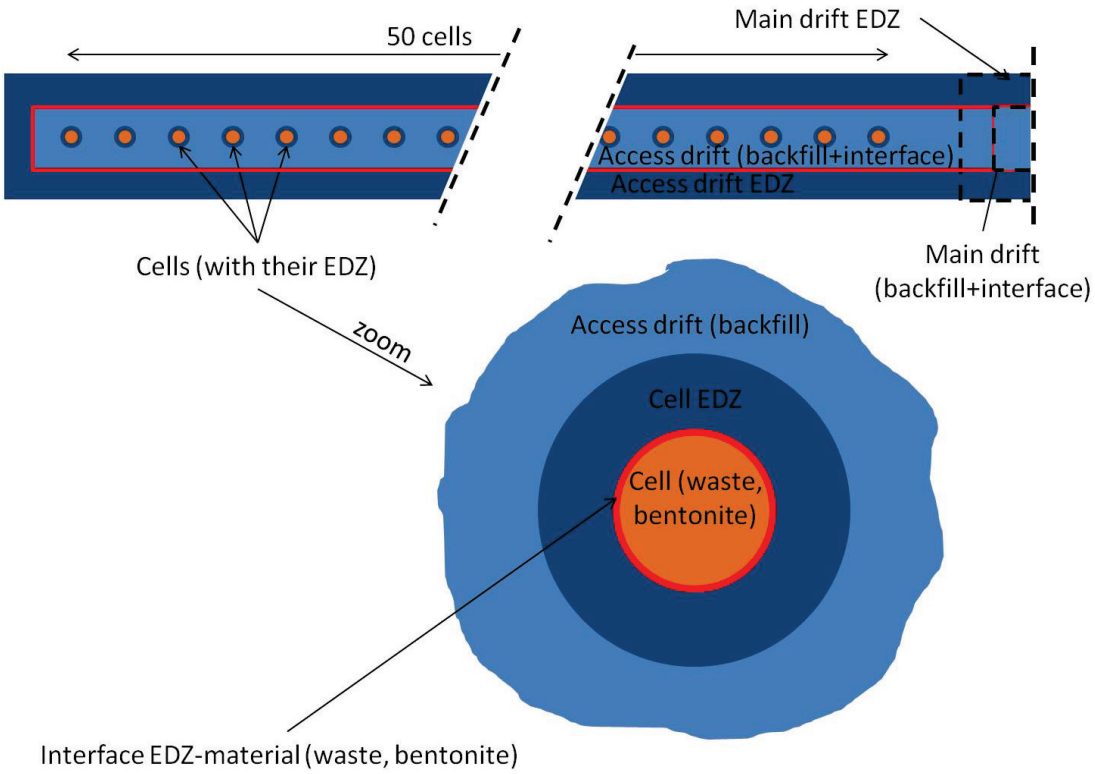

Figure B-3: Schematic Representation of the A-A' Vertical Cross Section (See Figure B-2 for Definition)

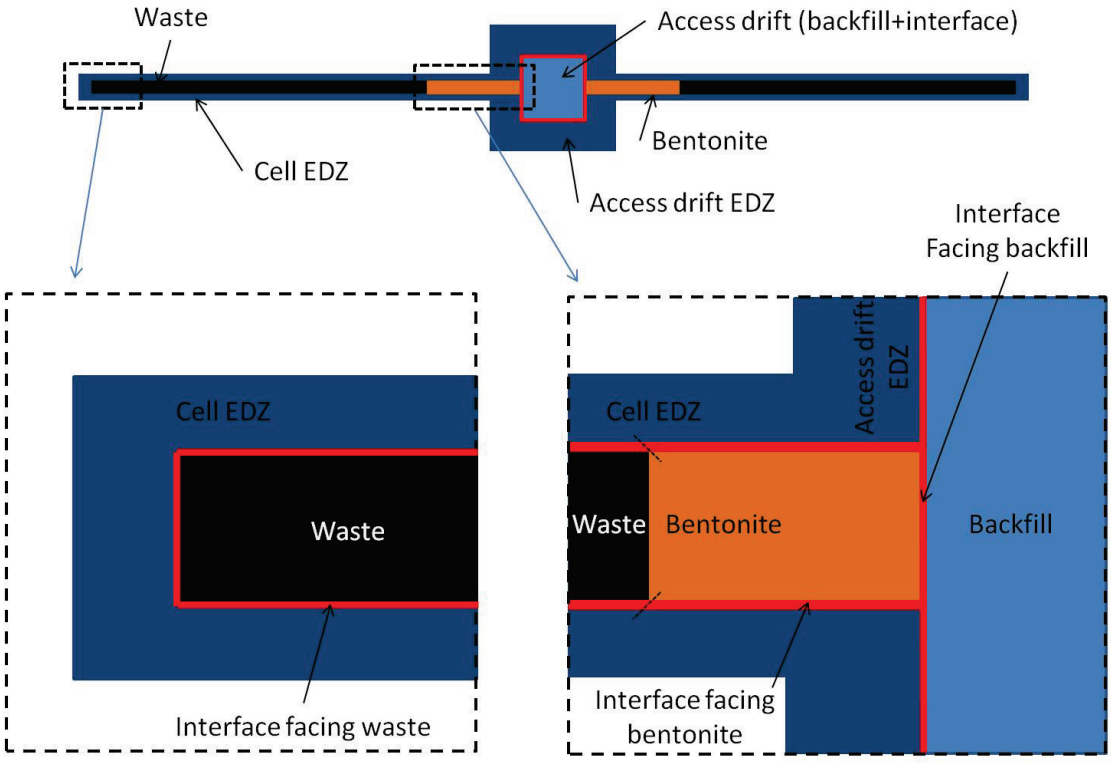

Figure B-4: Schematic Representation of the B-B' Vertical Cross Section (See Figure B-2 for Definition)

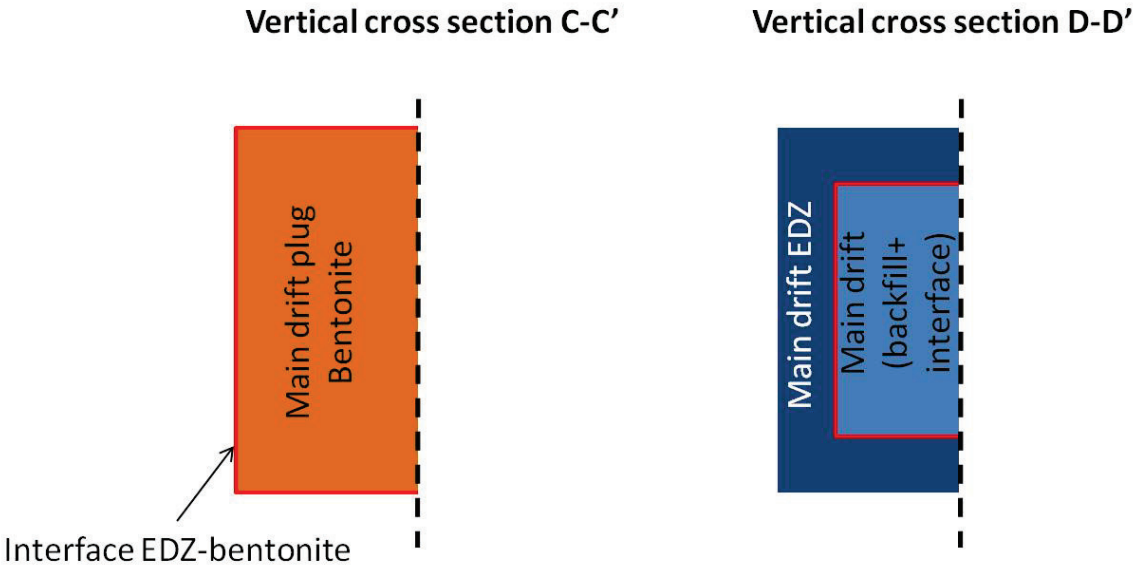

Figure B-5: Schematic Representation of Vertical Cross Section C-C' and D-D' (See Figure B-2 for Definitions)

More details on the domain to be simulated are given in Figure B-2, Figure B-3, Figure B-4 and Figure B-6.

The calculation domain is 3D and includes the full extension of the argillite layer (150 m). In the horizontal plane, the extension is determined by the axial distance between each cell and their length. A common gas production term is given for each cell. It is imposed on the external cylinder representing schematically the cell. The materials to take into account in this simulation are argillite (natural medium), EDZ (Excavation Damaged Zone), EDZ-material interface (material can be bentonite or backfill depending on the position), bentonite (cells and drift plug) and backfill of the drift. The waste itself is supposed to be impermeable to gas and water and is not explicitly represented.

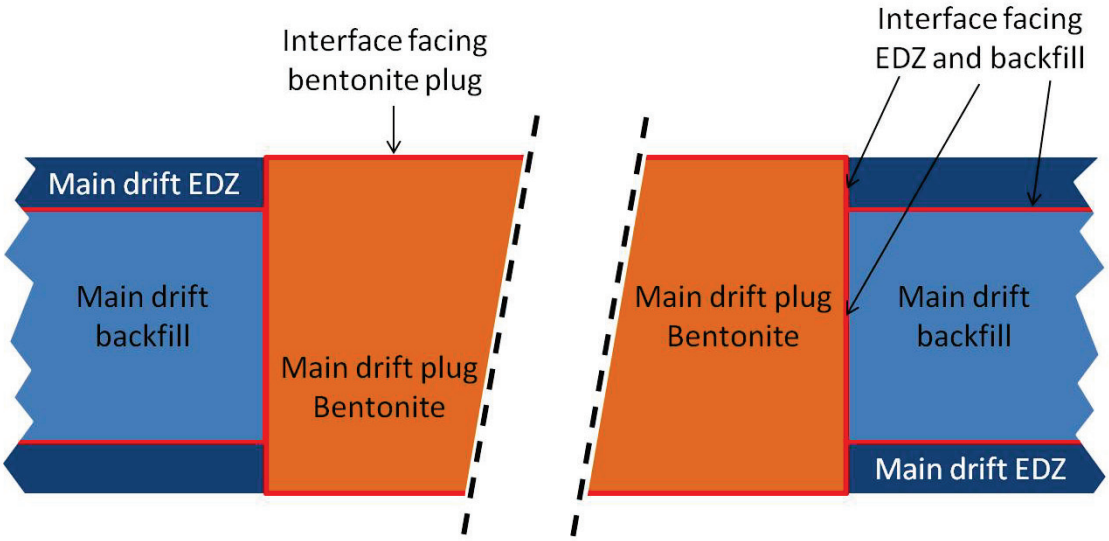

Figure B-6: Schematic Representation of the Main Drift Plugs and Backfills Interfaces

In the cell the EDZ is not overcut at bentonite plug emplacement (see Figure B-3), but in the drift it is (see Figure B-5). The bentonite-argillite interface is present around all types of plugs. The interface is in fact present around all “drift/cell filling material” and can have different physical characteristics depending on the material (waste, backfill, bentonite) (see Table B-2).

The main objective of this simulation is to understand how gas is moving from a cell toward a drift and finally toward a drift plugs (is convection still the main process at this scale, which part of the gas generated inside the cells is moving across the drift plugs, what is the characteristic time for this transfer, what pressure can be achieved, …).

However, a secondary objective is to study the different methods (homogenization, domain decomposition, high performance calculation, …) used by the different teams to achieve this simulation taking into account all the physics described below and restraining the computation time and/or the mesh size to something manageable.

Note that all characteristics already defined in the first exercise at cell scale are the same for this exercise at module scale.

B.3 DETAILED DESCRIPTION OF THE TEST CASE

B.3.1 GEOMETRY

For the cells, waste and bentonite plugs have the same circular sections. Sections of the access drift and main drift are squared and identical. Cells are positioned at mid height of the access drift and at mid height of the whole calculation domain (argillite layer). There are 50 cells on each side of the access drift.

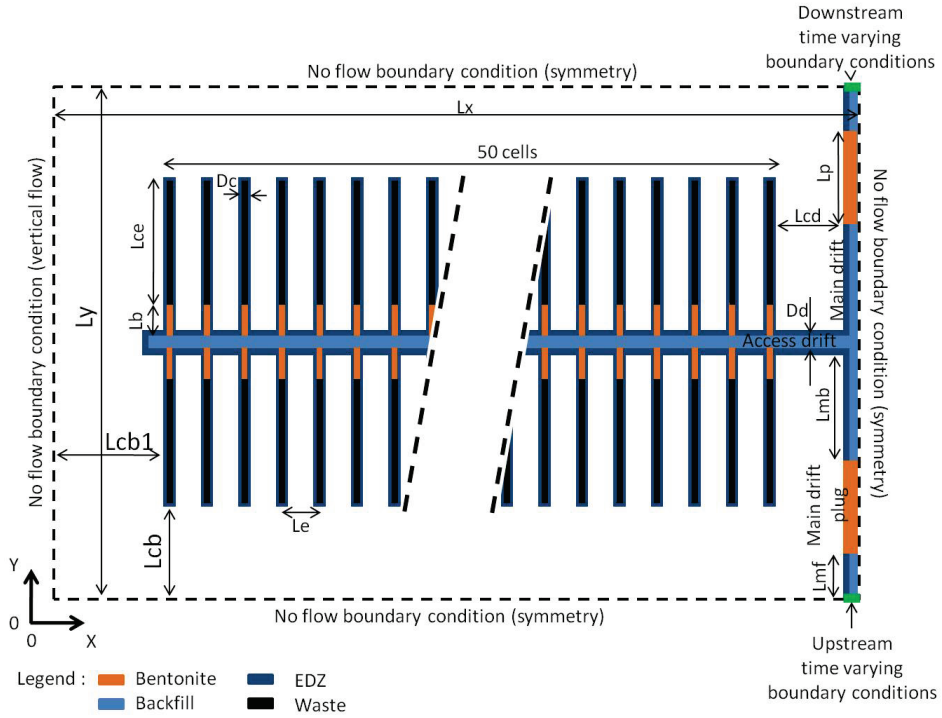

Figure B-7: Horizontal Dimensions and Boundary Conditions

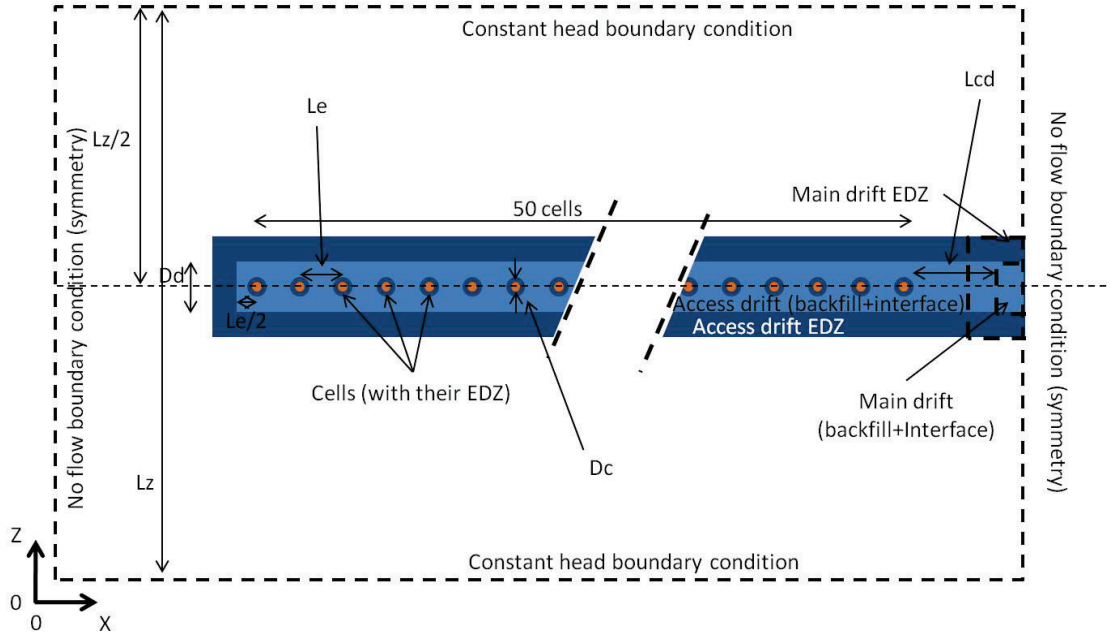

Figure B-8: Vertical Dimensions and Boundary Conditions on Cross Section A-A'

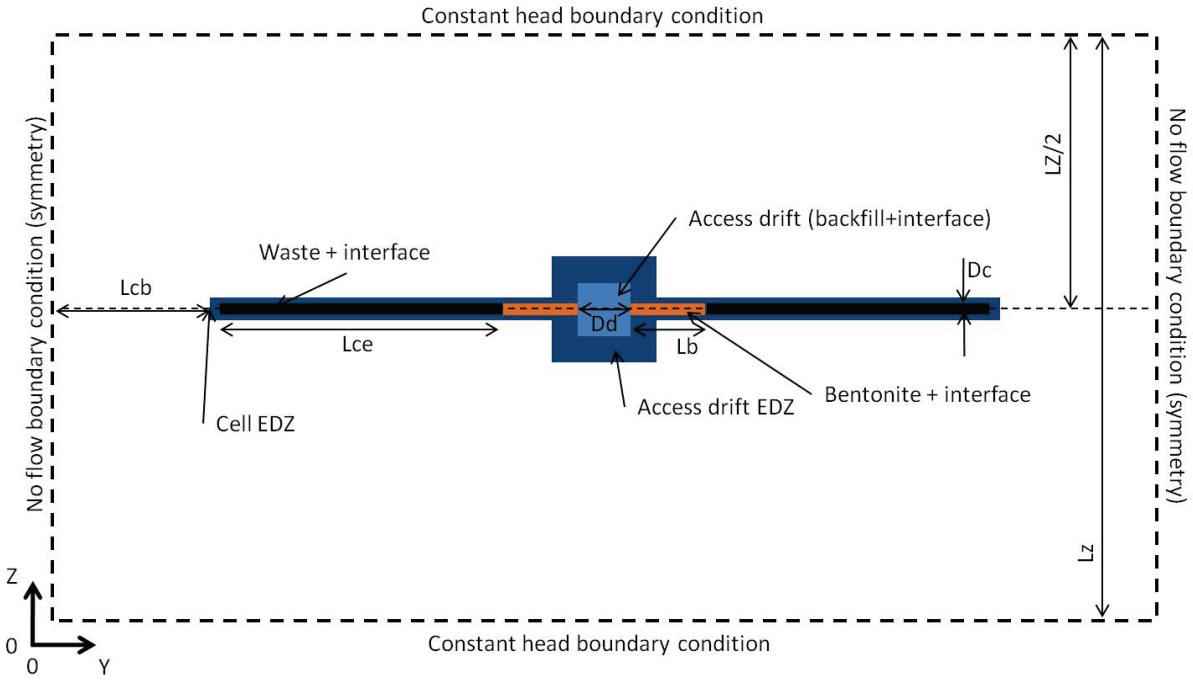

Figure B-9: Vertical Dimensions and Boundary Conditions on Cross Section B-B'

Table B-1: Dimensions Relative to the Simulated Domain

Parameter Description	Name	Value
X total extension of the simulation domain	Lx	714 m
Y total extension of the simulation domain	Ly	126 m
Z total extension of the simulation domain	Lz	150 m
Distance between cell end (with interface, without EDZ) and the boundary in the Y direction	Lcb	15 m
Distance between outer wall of the last cell (#50 - with interface, without EDZ) and the boundary in the X direction	Lcb1	200 m
Length of the bentonite plug in the cell (without interface)	Lb	5 m
Length of "waste zone" in the cell (with interface)	Lce	40 m
Distance between axes of two adjacent cells	Le	10 m
Cell diameter (with interface, without EDZ)	Dc	1 m
Access and main drifts side length (with interface, without EDZ)	Dd	6 m
Length of the bentonite plug in the main drift (without interface)	Lp	20 m
Distance between outer wall of the access drift (with interface, without EDZ) and end (without interface) of the main drift plug	Lmb	30 m
Distance between end without interface) of the main drift plug and external boundary	Lmf	10 m
Distance between outer wall of the main drift (with interdface, without EDZ) and outer wall of the first cell (with interface, without EDZ)	Lcd	20 m
Extension of interface (between waste-argillite, backfill-argillite and bentonite-argillite). Not mentioned in the figures	wi	1 cm
Extension of cell EDZ. Not mentioned in the figures	Cedz	0.5 m
Extension of access drift and main drift EDZ. Not mentioned in the figures	Dedz	1 m

B.3.2 BOUNDARY CONDITIONS

See also Figure B-7 to Figure B-9

$x \in [0, x_{\max}], y \in [0, y_{\max}], z \in [0, z_{\max}], t \in [0, t_{end}]$

with $x_{\max}$ =714 m, $y_{\max}$ =126 m, $z_{\max}$ =150 m, t_{end} =100000 years

Conditions on the top and bottom of the simulation domain:

$P_w(x, y, z = z\min, t) = 6\,10^6\,Pa \quad S_w(x, y, z = z\min, t) = 1 \quad X^w_{H_2} = 0$

$P_w(x, y, z = z\max, t) = 4\,10^6\,Pa \quad S_w(x, y, z = z\max, t) = 1 \quad X^w_{H_2} = 0$

When gaseous phase is not present, the gas pressure corresponds also to a concentration via Henry's law (see mathematical model for details).

Conditions on the vertical sides of the simulation domain:

$$Flux_w(x=0,y,z,t)=0 \qquad Flux_g(x=0,y,z,t)=0$$
$$Flux_w(x=x_{\max},y,z,t)=0 \qquad Flux_g(x=x_{\max},y,z,t)=0$$
$$for \quad y\in[0,y_{\max}],z\in[0,z_{\max}],t\in[0,t_{end}]$$

$$Flux_w(x,y=0,z,t)=0 \qquad Flux_g(x,y=0,z,t)=0$$
$$Flux_w(x,y=y_{\max},z,t)=0 \qquad Flux_g(x,y=y_{\max},z,t)=0$$
$$for \quad x\in\left[0,x_{\max}-\frac{Dd}{2}\right], \quad z\in[0,z_{\max}], \quad t\in[0,t_{end}]$$

$$Flux_w(x,y=0,z,t)=0 \qquad Flux_g(x,y=0,z,t)=0$$
$$Flux_w(x,y=y_{\max},z,t)=0 \qquad Flux_g(x,y=y_{\max},z,t)=0$$
$$for \quad x\in\left[x_{\max}-\frac{Dd}{2},x_{\max}\right], \quad z\in\left[\frac{z_{\max}+Dd}{2},z_{\max}\right], \quad t\in[0,t_{end}]$$
$$and \quad x\in\left[x_{\max}-\frac{Dd}{2},x_{\max}\right], \quad z\in\left[0,\frac{z_{\max}-Dd}{2}\right], \quad t\in[0,t_{end}]$$
$$and \quad x\in\left[0,x_{\max}-\frac{Dd}{2}\right], \quad z\in[0,z_{\max}], \quad t\in[0,t_{end}]$$

At intersection between main drift and outer limits of the model:

y=0 or y= $y_{\max}$ and

$$x\in\left[x_{\max}-\frac{Dd}{2},x_{\max}\right], \quad z\in\left[\frac{z_{\max}-Dd}{2},\frac{z_{\max}+Dd}{2}\right]$$

The boundary conditions are time varying, on both sides of the model: there is a small amount of gas flowing from one side of the model to the other one inside the main drift. A graphical representation of the time varying water pressure and gas pressure is presented in Figure B-10 and Figure B-11.

These boundary conditions have been determined using a simulation at the global repository scale and modified to cope with this benchmark definition. For example the gas source term applied in the whole storage simulation is not the same as the one used up to now in the FORGE WP1.2 benchmark and boundary conditions have been modified so that the gas peak occurs at the end of the source term. This is also why on the boundary of the simulation domain there is a part of backfill: the data available was on backfill pressures and saturation, not on bentonite.

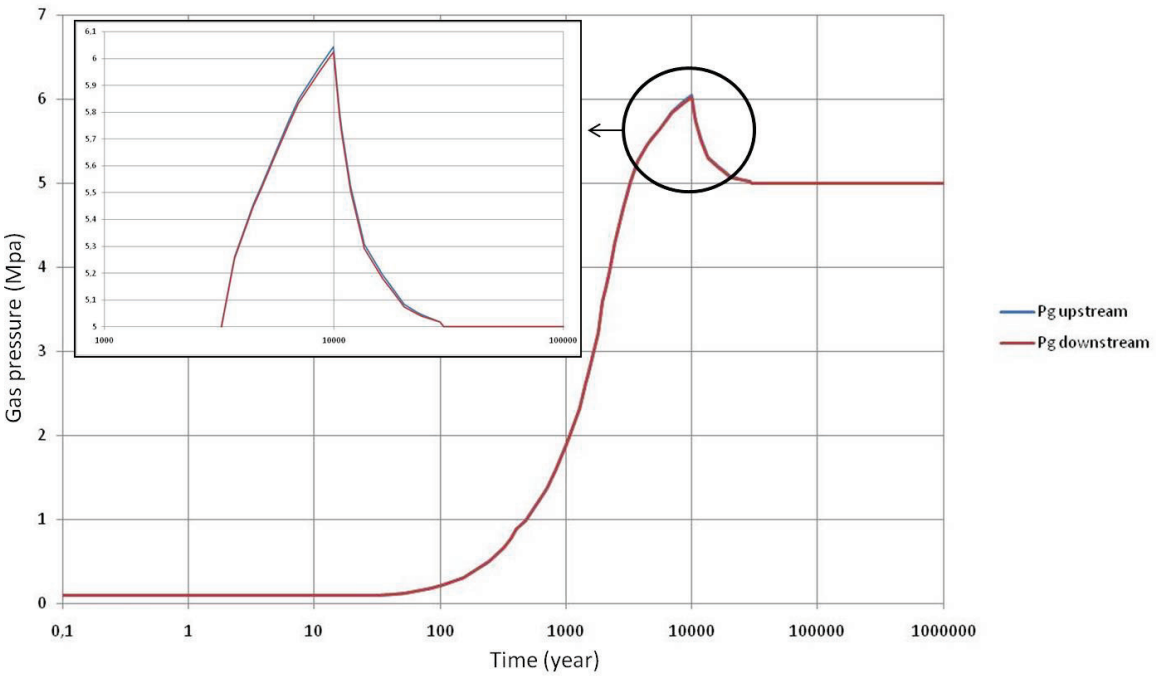

Figure B-10: Gas Pressure Time Varying Boundary Conditions on the Backfill of the Main Drift

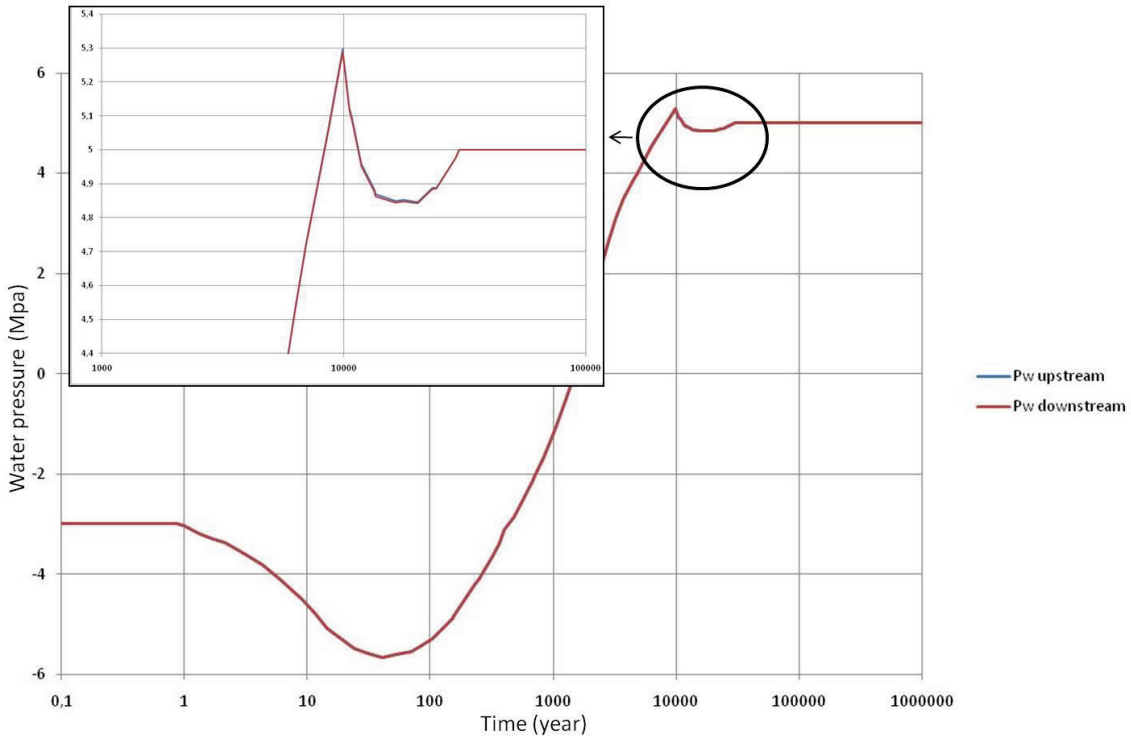

Figure B-11: Water Pressure Time Varying Boundary Condition

As fluxes of water and or gas are very small from upstream part to downstream part of the simulation domain, the differences in terms of gas and water pressure for the time varying boundary conditions are quite small (only several meters of water at the peak).

B.3.3 PHYSICAL PARAMETERS

The values of the different physical parameters needed for this simulation are given in the following table. The simulation is supposed to be isothermal at 20°C (293°K) during all the calculation.

Note: The gravity is taken into account for this 3D simulation.

Table B-2: Values for Physical Parameters

Parameter (at 20°C)	Materials		
	Interface facing plug (cf.*)	**Interface facing waste**	**Interface facing backfill and edz**
K [m^2]	$5.0\ 10^{-18}$	$1.0\ 10^{-12}$	$1.0\ 10^{-15}$
Porosity [%]	30	100	40
Specific storage coefficient [m^{-1}]	$4.6\ 10^{-6}$	$4.6\ 10^{-6}$	$4.6\ 10^{-6}$
Two-phase flow parameters			
S_{gr} [%]	0	0	0
S_{wr} [%]	0	0	0
Van Genuchten parameters			
n [-]	4	4	4
P_r [Pa]	10^4	10^4	10^4
τ (Tortuosity)	1	1	1

Parameter (at 20°C)	Materials			
	Backfills	**Bentonite plugs**	**EDZ**	**Geological medium**
K [m^2]	$5.0\ 10^{-17}$	$1.0\ 10^{-20}$	$5.0\ 10^{-18}$	$1.0\ 10^{-20}$
Porosity [%]	40	35	15	15
Specific storage coefficient [m^{-1}]	$1.0\ 10^{-5}$	$4.4\ 10^{-6}$	$2.3\ 10^{-6}$	$2.3\ 10^{-6}$
Two-phase flow parameters				
S_{gr} [%]	0	0	0	0
S_{wr} [%]	0	0	0	0
Van Genuchten parameters				
n [-]	1.5	1.6	1.5	1.5
P_r [Pa]	$2\ 10^6$	$1.6\ 10^7$	$1.5\ 10^6$	$1.5\ 10^7$
τ (Tortuosity)	2	4.5	2	2

* For all the bentonite plugs (cells and main drift): interface facing plug: only in the radial (perpendicular to the axis) direction (not in the longitudinal direction). See Figure B-4 and Figure B-6).

- ***Viscosity of the gas mixture:***

The viscosity of the gas mixture (water vapour + hydrogen) can be estimated by a classical Wilke approximation or by a simplified formula as follows:

$$\mu_g = \frac{1}{\frac{X^g_{H_2}}{\mu^g_{H_2}} + \frac{X^g_{wvap}}{\mu^g_{wvap}}} \text{ with } \qquad \mu^g_{H_2}(T = 293K) = 9\,10^{-6}\,Pa.s \qquad \mu^g_{wvap}(T = 293K) = 10^{-5}\,Pa.s$$

- ***Diffusion coefficient of dissolved H_2 in water:***

$$D_{H_2/water} = 1.57\ 10^{-14}\,\frac{T}{\mu_{water}(T)} \qquad (m^2.s^{-1})$$

- ***Diffusion coefficient of gaseous H_2 in water vapour:***
(T_0=293 K and at $P_0=1.0\cdot10^5$ Pa: $D_0=9.5\cdot10^{-5}$ m^2/s)

$$D^g_{H_2-H_2O} = D_0\left(\frac{P_0}{P}\right)\left(\frac{T}{T_0}\right)^{1.75} \qquad (m^2.s^{-1})$$

- ***Diffusion coefficient of dissolved H_2 in the water of the porous medium:***

$$D^w_{H_2} = S_w\left(\frac{\omega}{\tau^2}\right)D_{H_2/eau}$$

- ***Diffusion coefficient of dissolved H_2 in the binary H_2/water-vapour mixture of the porous medium:***

$$D^g_{H_2/vap} = (1 - S_w)\left(\frac{\omega}{\tau^2}\right)D^g_{H_2-H_2O}$$

- ***Solubility of hydrogen in water:*** $H_{H_2}(T = 293K) = 7.610^{-6}\ mol.Pa^{-1}.m^{-3}$

Note: Temperature in diffusion models is expressed in Kelvin.

B.3.4 INITIAL CONDITIONS

Water saturation:

- in the geological medium is equal to 100%;
- in the cells and drifts EDZ is equal to 100%;
- in the bentonite plugs is equal to 70%;
- in the backfill of the main drift and of the access drift is equal to 70%;
- in the interfaces is equal to 5%.

Pressure:

- In the fully initially water-saturated materials, the water pressure is linearly distributed between values at upper and lower boundary (see Boundary limits);
- In partially-saturated materials at initial time, the gas pressure is equal to 0.1 MPa (~1 atmosphere). The water pressure is deduced from the gas pressure and the saturation by applying Van Genuchten models associated with each material.

B.3.5 PRODUCTION TERM FOR HYDROGEN

The hydrogen-production term is to be distributed over the whole external surface (radial and lateral) of all the wastes, as follows:

- for 0 < t ≤ 10000 years, $Q^{g}_{H_2} = 100\ mol/year/cell$ $Q^{w}_{H_2} = 0$
- for t > 10000 years $Q^{g}_{H_2} = 0\ mol/year/cell$ $Q^{w}_{H_2} = 0$

B.3.6 SIMULATION PERIOD

The simulation will be performed between t_0=*0* and t_{end} =100.000 years.

B.4 OUTPUT RESULTS

For all output results, times will be expressed in years, pressures will be expressed in MPa, mass flows will be expressed in kg s^{-1}.

B.4.1 EVOLUTION WITH TIME OF MASS FLOWS ACROSS SURFACES

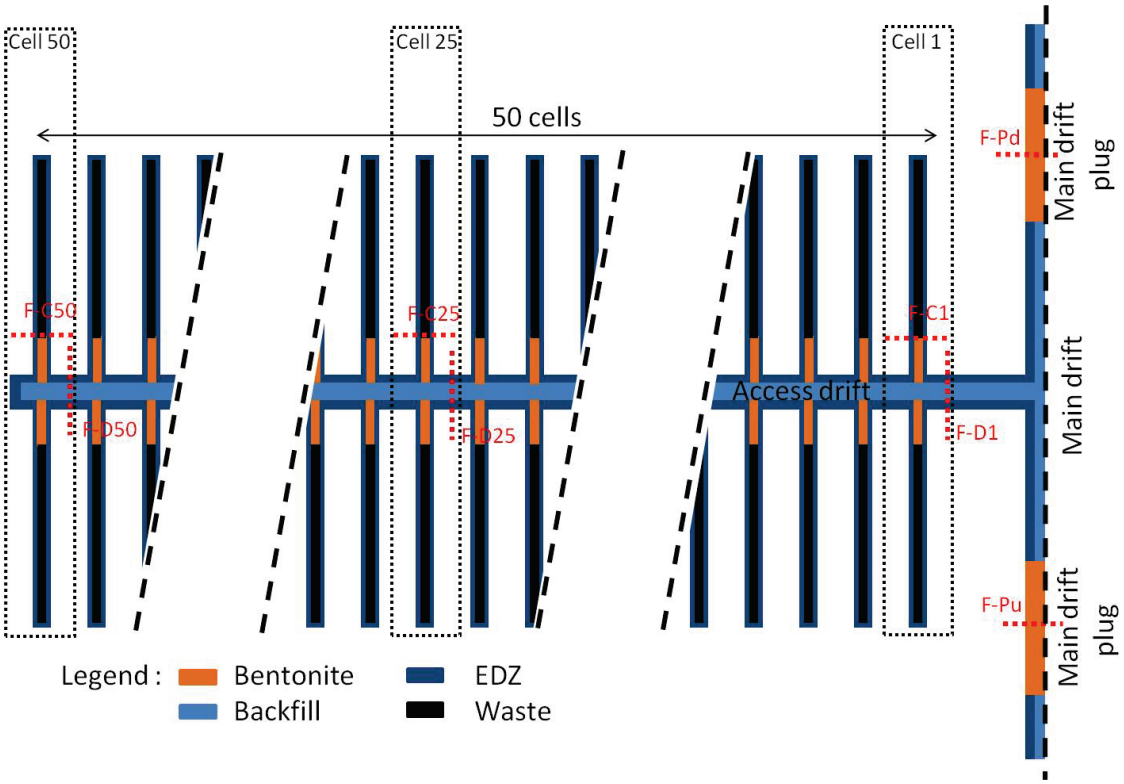

Figure B-12: Schematic Representation of the Surfaces Across Which Flows Will Be Calculated

Type of mass flows: total flows, diffusive flows and advective flows for the following components/phases:

- Liquid water
- Water vapor
- Gaseous H_2
- Dissolved H_2

Type of surfaces:

- For each of cells 50, 25 and 1 (see Figure B-12 for their locations), flows in the cell interface and the cell EDZ, across the following surface: vertical plane passing through the end (close to the wastes) of the cell bentonite plug. Corresponding to surfaces F-C50, F-C25 and F-C1 on Figure B-12;
  Mathematical description of the surfaces: y=71 m; 0.49 m < radius from the cells axis < 1 m;
- For each of cells 50, 25 and 1, flows in the access drift backfill, access drift interface and access drift EDZ, across the following surface: vertical plane 5 m away – downstream - from the cell axis. Corresponding to surfaces F-D50, F-D25 and F-D1 on Figure B-12;
  Mathematical description of the surfaces: 59 m < y < 67 m; 146 m < z < 154 m; x=695.5 m for cell 1; x=445.5 m for cell 25, x=205.5 m for cell 50;
- Flows in the main drift plugs and main drift interfaces (as shown in Figure B-5, cross section C-C') across the following surface: vertical planes passing through the middle of

the plug; flows are computed separately for upstream and downstream main drift plugs. Corresponding to surfaces F-Pu and F-Pd on Figure B-12
Mathematical description of the surfaces: y=20 m or y=106 m; 711 m < x < 714 m; 72 m < z < 78 m;

- Global water flow across the upper and lower boundaries of the whole simulation domain (not presented on Figure B-12). Flows are computed separately for upper and lower boundaries;
- Global hydrogen flow across the upper and lower boundaries of the whole simulation domain (not presented on Figure B-12). Flows are computed separately for upper and lower boundaries.

B.4.2 EVOLUTION ALONG LINES AT DIFFERENT TIMES

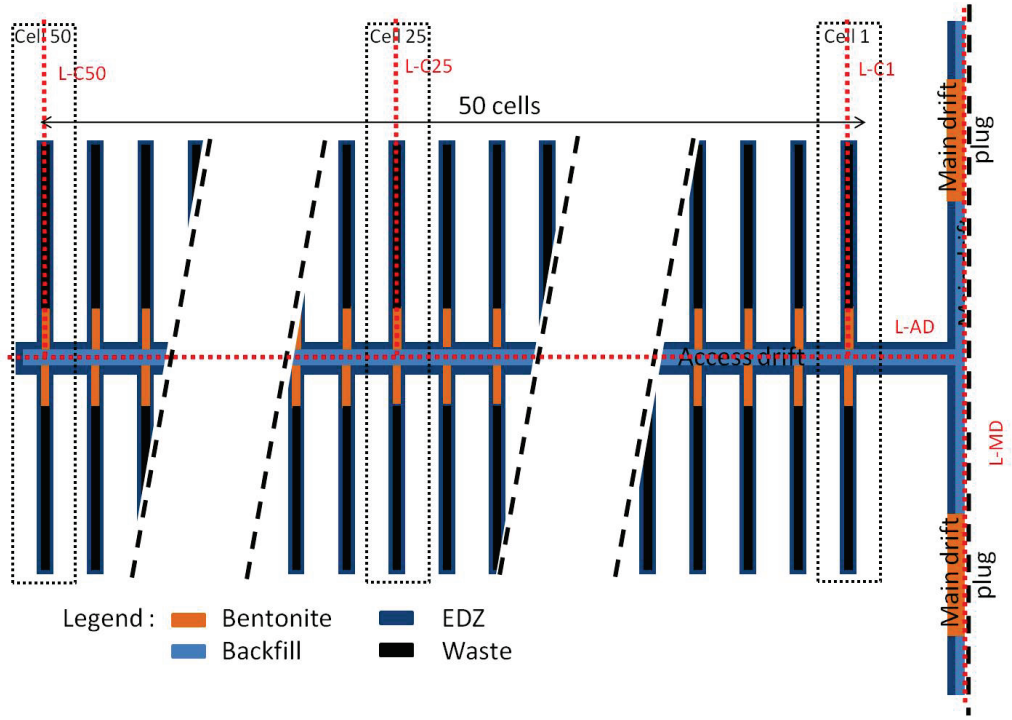

Figure B-13: Schematic Representation of the Lines on Which Results Should Be Given

Evolution along lines of:

- Water saturation
- Water pressure
- Gas pressure (in the gas phase when it exists)
- Dissolved H_2 pseudo-pressure (see Henry's law, equations (18) and (18'), in § 0 for details)
- Capillary pressure

Times to be used (years):
1, 3, 10, 30, 100, 300, 1 000, 3 000, 10 000, 30 000, 100 000

Types of lines:

- For cells 50, 25 and 1 (respectively line L-C50, L-C25 and L-C1 on Figure B-13): lines parallel to the axis of the cell, in the interface – upper part - between waste (or bentonite) and EDZ, and going from the outer boundary to the EDZ of the access drift
  Mathematical description of the lines: 66 m < y < 126 m; z=75.495 m;
  x=690.5 m for cell 1; x=440.5 m for cell 25, x=200.5 m for cell 50;
- Line parallel to the axis of the access drift, in the interface – upper part - between backfill and EDZ of the access drift, and going from the end of the access drift to the EDZ of the main drift (L-AD on Figure B-13
  Mathematical description of the line: 194 m < x < 711 m; y=63 m; z=77.995 m;
- Line parallel to the axis of the main drift, in the interface – upper part - between backfill (or bentonite) and EDZ of the main drift, and going from the upstream boundary to the downstream boundary (crossing the whole simulation domain (L-MD on Figure B-13);
  Mathematical description of the line: x=714 m; 0 < y <126 m; z=77.995 m.

B.4.3 EVOLUTION WITH TIME AT GIVEN POINTS

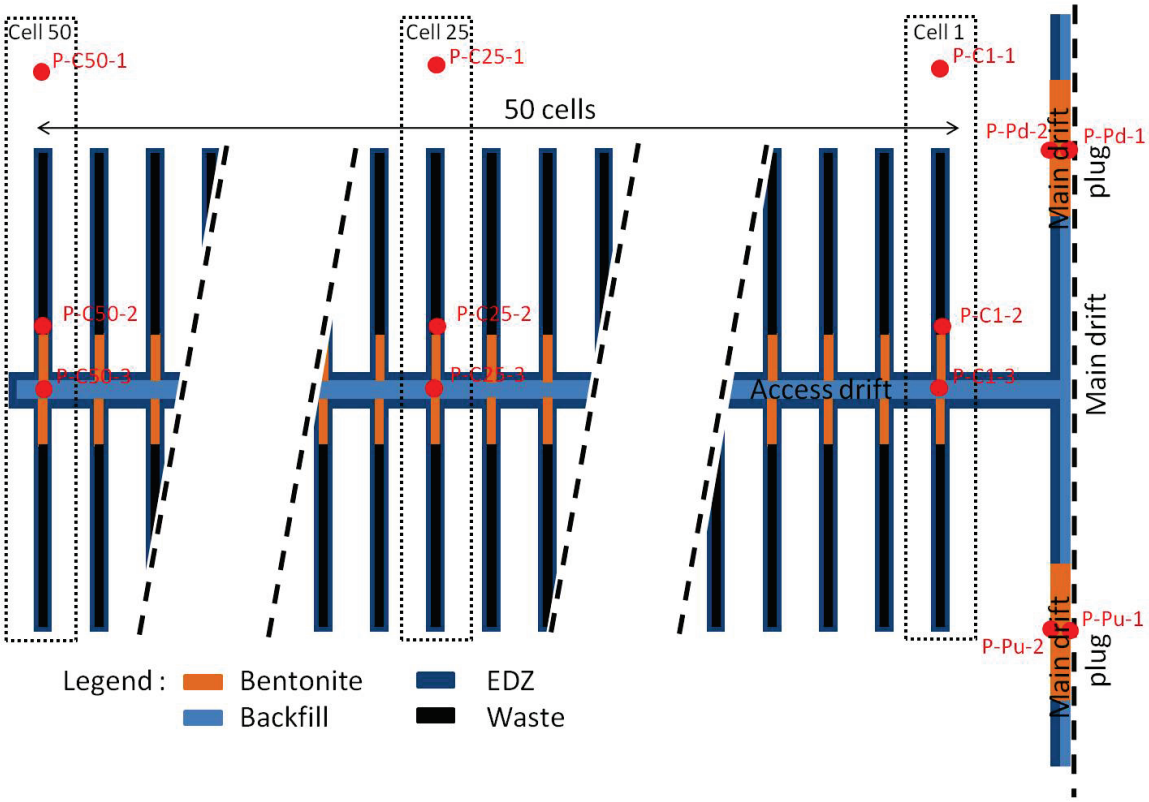

Figure B-14: Schematic Representation of the Points Where Results Should Be Given

Evolution with time of:

- Water saturation
- Water pressure
- Gas pressure (in the gas phase when it exists)
- Dissolved H_2 pseudo-pressure (see Henry's law, equations (18) and (18'), in § 0 for details)
- Capillary pressure

Type of points:

- For cell 50 (see Figure B-14):
  - Point P-C50-1: point whose horizontal coordinates are along the axis of the cell, 5 m away from the end of the cell (with interface, without EDZ);
    coordinates: x=200.5 m; y=116 m; z=75.495 m (this point is along line L-C50)
  - Point P-C50-2: point situated in the interface between waste and EDZ (upper part) as close as possible to the bentonite plug;
    coordinates: x=200.5 m; y=71.005 m; z=75.495 m (this point is along line L-C50);
  - Point P-C50-3: point situated in the interface between access drift and EDZ (upper part); horizontal coordinates are those of the intersection axes of cell 50 and access drift;
    coordinates: x=200.5 m; y=63 m; z=77.995 m (this point is along line L-AD)

- Same types of point as for cell 50 but for cell 25 (points P-C25-1, P-C25-2, P-C25-3) and cell 1 (points (P-C1-1, P-C1-2, P-C1-3); see Figure B-14;
  P-C25-1: coordinates: x=440.5 m; y=116 m; z=75.495 m (point along line L-C25);
  P-C25-2: coordinates: x=440.5 m; y=71.005 m; z=75.495 m (point along line L-C25);
  P-C25-3: coordinates: x=440.5 m; y=63 m; z=77.995 m (point along line L-AD);
  P-C1-1: coordinates: x=690.5 m; y=116 m; z=75.495 m (point along line L-C1);
  P-C1-2: coordinates: x=690.5 m; y=71.005 m; z=75.495 m (point along line L-C1);
  P-C1-3: coordinates: x=690.5 m; y=63 m; z=77.995 m (point along line L-AD).

- For upstream plug (see Figure B-14):
  - Point P-Pu1: situated at the middle of the length and on the axis of the plug (in the middle of the bentonite); horizontal coordinates: x=714 m; y=20 m; z=75 m;
  - Point P-Pu-2: situated at the middle of the length of the plug and in the interface between bentonite and EDZ; horizontal coordinates: x=711.005 m; y=20 m; a=75 m;
  - Same points as for upstream plug, but in the downstream plug (points P-Pd-1 and P-Pd-2, see Figure B-14).
    P-Pd-1: horizontal coordinates: x=714 m; y=106 m; z=75 m;
    P-Pd2: horizontal coordinates: x=711.005 m; y=106 m; z=75 m.

B.5 MATHEMATICAL MODEL PROPOSED FOR THE EXERCISE

Remark: This model is the same as the one proposed in the first part of the benchmark at cell scale.

The capillary pressure is defined as the difference between gas pressure and water pressure:

$$P_C = P_g - P_w \qquad (1)$$

- P_c: capillary pressure (Pa)
- P_g: total pressure of the gas phase(Pa)
- P_w: water pressure (Pa)

The dependence between water and gas saturation in each porous medium is expressed by:

$$S_g + S_W = 1 \quad \text{with} \quad S_g = \frac{V_g}{V_p} \text{ and } S_w = \frac{V_w}{V_p}$$

- S_g: gas saturation (-)
- S_w: water saturation (-)
- V_g: gas volume (m^3)
- V_w: water volume (m^3)
- V_p: pore volume (m^3)

Van Genuchten model is used to express capillary pressure function of the effective saturation in a given porous medium:

$$S_{we} = \frac{S_w - S_{wr}}{1 - S_{wr} - S_{gr}} \quad (2)$$

$$S_{we} = \frac{1}{\left[1 + \left(\frac{P_c}{P_r}\right)^n\right]^m} \quad (3)$$

- S_{we}: effective water saturation (-)
- S_{wr}: residual water saturation (-)
- P_r: reference pressure for Van genuchten law (Pa). Generally the value for this coefficient is higher than the gas entry pressure for a given porous medium
- n, m: coefficients for Van Genuchten law. We have $m = 1 - \frac{1}{n}$

The relative permeability for water is expressed by integrating the Mualem prediction model in the Van Genuchten capillarity model:

$$k_r^w = \sqrt{S_{we}}\left[1 - \left(1 - S_{we}^{1/m}\right)^m\right]^2 \quad (4)$$

- k_r^w : relative permeability for water (-)

The relative permeability for gas is expressed similarly:

$$k_r^g = \sqrt{1 - S_{we}}\left[1 - S_{we}^{1/m}\right]^{2m} \quad (5)$$

- k_r^g : relative permeability for gas (-)

The water and gas movement in a porous medium is represented by the mass conservation law and the energy conservation law (reduced to the generalized Darcy law):

$$U_w = -\frac{k k_r^w(S_w)}{\mu_w}(\nabla P_w + \rho_w g \nabla z) \quad (6)$$

$$U_g = -\frac{k k_r^g(S_g)}{\mu_g}(\nabla P_g + \rho_g g \nabla z) \quad (7)$$

- K: intrinsic permeability of the porous medium (m^2)
- μ_g: viscosity of the total gas phase ($kg.s^{-1}.m^{-1}$)
- μ_w: viscosity of water ($kg.s^{-1}.m^{-1)}$
- ρ: volumetric mass of the total gas phase ($kg.m^{-3}$)
- ρ_w: volumetric mass of water ($kg.m^{-3}$)

$$\rho_w(P_w) = \rho_{atm} \exp\left[S_s(P_w - P_{atm})\right] \quad (8)$$

- ρ_{atm}: volumetric mass of water at atmospheric pressure ($kg.m^{-3}$)
- P_{atm}: atmospheric pressure (Pa)
- S_s: specific storage (Pa^{-1})
- g: gravity ($m.s^{-2}$)

- z: altitude (m)
- U_g: Darcy velocity for the gas phase ($m.s^{-1}$)
- U_w: Darcy velocity for water ($m.s^{-1}$)

Equation of conservation for water:

$$\frac{\partial(\rho_w \omega S_w)}{\partial t} + \nabla(\rho_w U_w) = Q^w \quad (9)$$

- ω: porosity (-)
- Q^w: consumption/production of water ($kg.m^{-3}.s^{-1}$)

Equation of conservation for the total gas phase:

$$\frac{\partial(\rho_g \omega S_g)}{\partial t} + \nabla(\rho_g U_g) = Q^g \quad (10)$$

- Q^g: consumption/production for the total gas phase ($kg.m^{-3}.s^{-1}$)

The mass fraction of gaseous hydrogen is expressed as:

$$X^g_{H_2} = \frac{\rho^g_{H_2}}{\rho_g} \quad (11)$$

With $\rho^g_{H_2} = \frac{m^g_{H_2}}{V_g}$ and $\rho_g = \frac{m^g}{V_g}$

- $X^g_{H_2}$ is the mass fraction of hydrogen in the total gas phase (-)
- $m^g_{H_2}$ is the hydrogen mass in the gas phase (kg)
- m^g is the total mass of the gas phase (kg)
- $\rho^g_{H_2}$ is the volumetric mass of gaseous hydrogen in the gas phase ($kg.m^{-3}$)

Mass conservation law for gaseous hydrogen:

$$\frac{\partial}{\partial t}(\omega S_g \rho_g X^g_{H_2}) + \nabla(\rho_g X^g_{H_2} U_g - J^g_{H_2}) + \Omega^{g/l}_{H_2} = Q^g_{H_2} \quad (12)$$

- $\Omega^{g/l}_{H_2}$ is the exchange term from the gaseous phase to the liquid phase for H_2 ($kg.m^{-3}.s^{-1}$)
- $Q^g_{H_2}$ is the consumption/production term for gaseous hydrogen ($kg.m^{-3}.s^{-1}$)
- $J^g_{H_2}$ is the diffusive term for gaseous hydrogen ($kg.m^{-2}.s^{-1}$)

Diffusive flux for a binary mixture of gas (H_2 and water vapor) can be expressed by Fick's law:

$$J^g_{H_2} = \rho_g D^g_{H_2 vap} \nabla X^g_{H_2} \quad (13)$$

- $D^g_{H_2 vap}$ is the diffusion coefficient for gaseous hydrogen in water vapor ($m^2.s^{-1}$)

The mass fraction of dissolved hydrogen is expressed as:

$$X_{H_2}^w = \frac{\rho_{H_2}^w}{\rho_w} \quad (14)$$

With $\rho_{H_2}^w = \frac{m_{H_2}^w}{V_w}$ and $\rho_w = \frac{m^w}{V_w}$

- $X_{H_2}^w$ is the mass fraction of dissolved hydrogen (-)
- $m_{H_2}^w$ is the dissolved hydrogen mass (kg)
- m^w is the total mass of the liquid phase (kg)
- $\rho_{H_2}^w$ is the volumetric mass of dissolved hydrogen in the liquid phase (kg.m^{-3})

Mass conservation law for dissolved hydrogen is expressed as:

$$\frac{\partial}{\partial t}(\omega S_w \rho_w X_{H_2}^w) + \nabla(\rho_w X_{H_2}^w U_w - J_{H_2}^w) + \Omega_{H_2}^{l/g} = Q_{H_2}^w \quad (15)$$

- $\Omega_{H_2}^{l/g}$ is the exchange term from the liquid phase to the gas phase for H_2 (kg.m^{-3}.s^{-1})
- $Q_{H_2}^w$ is the consumption/production term for dissolved hydrogen (kg.m^{-3}.s^{-1})
- $J_{H_2}^w$ is the diffusive term for dissolved hydrogen (kg.m^{-2}.s^{-1})

The exchange terms from between liquid and gaseous phase are linked by the following relation:

$$\Omega_{H_2}^{l/g} = -\Omega_{H_2}^{g/l} \quad (16)$$

Diffusive flux for dissolved hydrogen can be expressed by Fick's law:

$$J_{H_2}^w = \rho_w D_{H_2 vap}^w \nabla X_{H_2}^w \quad (17)$$

- $D_{H_2 vap}^w$ is the diffusion coefficient for dissolved hydrogen in water vapor (m^2.s^{-1})

Part of the gas will be dissolved in the pore water. The solubility limit for the gas depend mainly on thermodynamic conditions and can be expressed by Henry's law:

$$C_{H_2}^w = H_{H_2}(T) P_{H_2}^g \quad (18)$$

Where $C_{H_2}^w = \frac{X_{H_2}^w \rho_w}{M_{H_2}}$

- $C_{H_2}^w$ is the maximum concentration of hydrogen in water (mol.m^{-3})
- H_{H_2} is the constant of Henry's law for hydrogen (mol.m^{-3}.Pa^{-1})
- $P_{H_2}^g$ is the partial pressure of hydrogen in the total gaseous phase (Pa)

- M_{H_2} is the molar mass for hydrogen (kg.mol^{-1})

***Remark**: given the actual hydrogen concentration in water, $C'^{w}_{H_2}$, it is possible to define a "pseudo pressure" of the dissolved hydrogen, $P'^{g}_{H_2}$, by inversion of Henry's law:*

$$P'^{g}_{H_2} = \frac{C'^{w}_{H_2}}{H_{H_2}(T)} \qquad (18)$$

The relation between partial pressure of each gas present in the total gas phase and total gas pressure is given by Dalton law that writes for a binary mixture (H_2 and water vapor):

$$P_g = P^g_{H_2} + P^g_{wvap} \qquad (19)$$

- P^g_{wvap} is the partial pressure of water vapor in the total gas phase (Pa)

Each of the gases is supposed perfect:

$$P^g_{H_2} = \frac{\rho^g_{H_2}}{M_{H_2}} RT \text{ and } P^g_{wvap} = \frac{\rho^g_{wvap}}{M_{wvap}} RT \qquad (20,21)$$

For the gas mixture this writes:

$$P_g = \frac{\rho_g}{M_g} RT \qquad (22)$$

- Mg: molar mass for the total gaseous phase (H_2 + water vapor) (kg.mol^{-1})
- R: constant of the perfect gas (J.mol^{-1}.K^{-1}): R = 8.314 J.mol^{-1}.K^{-1}
- T: temperature (°K)

Saturation pressure for water vapor is only depending on temperature and can by expressed by:

$$\log_{10}(P_{sat}) = 2.786 + 0.031514T_c - 1.2373x10^{-4}T_c^{\,2} + 4.2267x10^{-7}T_c^{\,3} - 8.1308x10^{-10}T_c^{\,4} \qquad (23)$$

- Psat: saturation pressure for water vapor (Pa)
- Tc: Temperature (°C)

Kelvin's law is giving a relation between saturation pressure for water vapor, effective pressure for water vapor and capillary pressure:

$$P^g_{wvap}(T, S_w) = \exp\left(\frac{M_w P_c(S_{w)}}{\rho_w RT}\right) P_{sat}(T) \qquad (24)$$